

University of Southampton Research Repository  
ePrints Soton

Copyright © and Moral Rights for this thesis are retained by the author and/or other copyright owners. A copy can be downloaded for personal non-commercial research or study, without prior permission or charge. This thesis cannot be reproduced or quoted extensively from without first obtaining permission in writing from the copyright holder/s. The content must not be changed in any way or sold commercially in any format or medium without the formal permission of the copyright holders.

When referring to this work, full bibliographic details including the author, title, awarding institution and date of the thesis must be given e.g.

AUTHOR (year of submission) "Full thesis title", University of Southampton, name of the University School or Department, PhD Thesis, pagination

**UNIVERSITY OF SOUTHAMPTON**  
**FACULTY OF ENGINEERING, SCIENCE AND MATHEMATICS**  
**School of Electronics and Computer Science**

**Thermal Bubble Behaviour in Liquid Nitrogen under Electric Fields**

by

**Ping Wang**

Thesis for the degree of Doctor of Philosophy

October 2008

UNIVERSITY OF SOUTHAMPTON

ABSTRACT

FACULTY OF ENGINEERING, SCIENCE AND MATHEMATICS  
SCHOOL OF ELECTRONICS AND COMPUTER SCIENCE

Doctor of Philosophy

THERMAL BUBBLE BEHAVIOUR IN LIQUID NITROGEN UNDER ELECTRIC  
FIELDS

by Ping Wang

This thesis describes thermally induced bubble behaviour changes in liquid nitrogen ( $\text{LN}_2$ ) under electric fields. Cryogenic liquids such as  $\text{LN}_2$  have been used not only as the coolant but also as the electrical insulator in superconducting and cryogenic apparatus. However, bubbles are easily formed in these liquids by even moderate heating because of a narrow liquid temperature range and low boiling point. Bubbles are considered to be one of the factors causing a reduction of the electrical insulation level. Consequently, bubble behaviour in electric fields is of great interest primarily in the study of prebreakdown and breakdown phenomena in the presence of thermally induced bubbles. In addition, a bubble can appear and its behaviour changes in a fluid under the influence of an electric field, and this is the main reason for boiling heat transfer enhancement which is related to thermal stability and heat transfer efficiency.

Studies including single bubble behaviour and bubble column behaviour as well as boiling heat transfer enhancement due to changes in bubble behaviour under electric fields using different electrodes have been completed. Free thermal bubble motion and related characteristics in  $\text{LN}_2$  under a conductor-plane electrode have been experimentally studied. A model for bubble motion in this non-uniform electric field has been developed and is described. Compared with theoretical results, the experimental measurements are in good agreement. An experimental study into the behaviour of thermal bubbles between two plane-plane inclined electrodes has been completed. Using a stainless steel mesh-to-plane electrode system, experimental investigations have been carried out to study the effect of uniform dc electric fields on the behaviour of a single thermal bubble in  $\text{LN}_2$ . Bubble characteristics such as bubble growth, deformation and bubble departure frequency have been experimentally evaluated. Finally, the electric field effects on boiling heat transfer of  $\text{LN}_2$  have been experimentally assessed. The obtained data is applicable to the design of  $\text{LN}_2$  cooled high temperature superconductor power apparatus for both coolant and electrical insulation issues.

# Contents

<b>Abstract</b> .....	i
<b>Contents</b> .....	ii
<b>List of Figures</b> .....	vi
<b>List of Tables</b> .....	xi
<b>Declaration of authorship</b> .....	xii
<b>Acknowledgements</b> .....	xiii
<b>Nomenclature</b> .....	xiv
<b>Chapter 1 Introduction</b> .....	1
1.1 Superconductivity.....	1
1.2 Liquid nitrogen and its properties .....	2
1.2.1 Liquid nitrogen .....	3
1.2.2 Physical properties.....	4
1.2.3 Electrical and thermal properties.....	4
1.2.4 Breakdown voltage .....	5
1.3 Study motivation .....	7
1.4 Aims and objectives .....	10
1.5 Contents of this thesis.....	11
1.6 Summary .....	12
<b>Chapter 2 Literature Review</b> .....	13
2.1 Introduction.....	13
2.2 Electrical insulation .....	13
2.2.1 Bubble generation mechanisms .....	14
2.2.2 Thermal bubble behaviour under uniform fields.....	14
2.2.3 V-t characteristics and breakdown mechanism .....	18
2.2.4 Thermal bubble behaviour under non-uniform fields.....	20
2.3 Thermal/cryogenic stability and heat transfer efficiency .....	21
2.3.1 Boiling phenomena .....	21
2.3.2 Pool boiling .....	21
2.3.3 Heat transfer into liquid nitrogen .....	24
2.3.4 Boiling curves of liquid nitrogen and its critical heat flux .....	24

2.4	Electrohydrodynamic (EHD) principles .....	25
2.4.1	EHD phenomena .....	25
2.4.2	The EHD technique of heat transfer .....	28
2.4.3	EHD mechanism.....	28
2.4.4	Phase change processes.....	31
2.4.5	Mechanism of EHD Enhancement boiling heat transfer .....	32
2.5	Summary .....	36
<b>Chapter 3</b>	<b>Thermal Bubble in a Non-uniform Electric Field: Conductor-Plane Electrode System.....</b>	<b>37</b>
3.1	Introduction.....	37
3.2	Theoretical study of bubble behaviour .....	38
3.2.1	Modelling of bubble motion.....	38
3.2.2	Simulation of electric field distribution .....	39
3.2.3	Electric field force analysis .....	39
3.2.4	Equations of bubble motion .....	41
3.2.5	Theoretical results.....	45
3.3	Experimental study of bubble behaviour.....	48
3.3.1	Experiment setup and procedure .....	48
3.3.2	Experimental results and discussion.....	49
3.4	Summary .....	57
<b>Chapter 4</b>	<b>Thermal Bubbles in a Non-uniform Electric Field: Plane-Plane Inclined Electrode System .....</b>	<b>59</b>
4.1	Introduction.....	59
4.2	Electrode system and experimental apparatus .....	60
4.3	Experimental results and analysis .....	61
4.3.1	Observation of bubble behaviour .....	61
4.3.2	Theoretical analysis of the bubble's behaviour.....	65
4.4	Summary .....	68
<b>Chapter 5</b>	<b>The Effect of Uniform Electric Field Distribution on the Behaviour of Thermally Induced Bubbles in Liquid Nitrogen .....</b>	<b>70</b>
5.1	Introduction.....	70
5.2	Experimental setup and procedure .....	71
5.3	Electric field distribution and electric force acting on the bubble .....	72
5.3.1	The electric field distribution around a bubble .....	72

5.3.2	Electric force acting on the bubble .....	75
5.4	Experimental results and discussion.....	78
5.4.1	Image processing .....	78
5.4.2	Thermal bubble growth and departure on the grounded electrode.....	78
5.4.3	Bubble deformation on the grounded electrode .....	81
5.4.4	Polarity effect .....	82
5.4.5	Comparison with previous research results.....	83
5.5	Summary .....	86
<b>Chapter 6</b>	<b>The Effect of Electric Field on Boiling Heat Transfer of Liquid Nitrogen</b>	<b>87</b>
6.1	Introduction.....	87
6.2	Experimental setup and procedures.....	89
6.2.1	Experiment apparatus .....	89
6.2.2	Electrode design and arrangement.....	90
6.2.3	Heat transfer and temperature measurement system .....	93
6.2.4	Visual observation .....	94
6.2.5	Experimental procedure .....	95
6.2.6	Data processing and uncertainties analysis.....	96
6.3	FEA model, simulation results and analysis.....	98
6.3.1	The heat transfer model and its input parameters.....	98
6.3.2	Simulation results and analysis .....	99
6.4	Experimental results and discussion.....	104
6.4.1	Time to cool process .....	104
6.4.2	Zero-field heat transfer and typical images.....	105
6.4.3	Effect of electric field on the ONB .....	107
6.4.4	Effect of electric field on the boiling hysteresis.....	110
6.4.5	Effect of electric field on nucleate boiling curves.....	116
6.4.6	Effect of electric field on the critical heat flux.....	124
6.5	Summary .....	127
<b>Chapter 7</b>	<b>Conclusions and Further work.....</b>	<b>128</b>
7.1	Conclusions.....	128
7.2	Further work.....	132
<b>Appendices</b>	<b>.....</b>	<b>134</b>
A	Electrical connection .....	134

B	Force analysis for thickness of the copper cap.....	137
C	Indium soldering of electrodes.....	139
D	Data sheet of liquid nitrogen from BOC Gases .....	141
E	List of publications from this research.....	143
<b>References</b>	.....	<b>144</b>

# List of Figures

Figure 1.1 History of superconductors, increases in critical temperature (vertical axis, in Kelvin) [2] .....	3
Figure 1.2 Breakdown voltages of uniform or nearly uniform field gaps as a function of gap length in LN <sub>2</sub> [11].....	5
Figure 1.3 Breakdown strength of porcelain, cryogenic liquids, and vacuum insulation under d.c. voltage stress in a uniform field [12].....	6
Figure 1.4 Breakdown voltage as a function of spacing in nitrogen vapour (Paschen's curve) close to the normal boiling point [12].....	7
Figure 2.1 Schematic diagram of experimental setup and a pair of parallel electrode system [11] .....	15
Figure 2.2 Sequential stages of bubble deformation in liquid nitrogen with applied voltage, d=1mm [11].....	15
Figure 2.3 Breakdown voltage as a function of heater power, d=1mm [11] .....	16
Figure 2.4 Vapour structure in the presence of dc uniform electric field [18].....	16
Figure 2.5 Comparison of bubble shapes under ac and dc electric fields [26] .....	17
Figure 2.6 Summary of breakdown mechanism by ramped voltage in cryogenic liquid in the presence of nucleate boiling [18] .....	19
Figure 2.7 V-t curves of liquid nitrogen with different voltages [28]. Waveform of applied voltages: (I) 1.2/80 $\mu$ s, (II) 2.0/5.5ms, (III) 10/30 ms, (IV) 115/415 ms and (V) ramped voltage of ~2 kV/s slope.....	19
Figure 2.8 Typical pool boiling curve [39] .....	22
Figure 2.9 Typical pool boiling curve for liquid nitrogen [60] .....	26
Figure 2.10 Experimental nucleate and film pool boiling of nitrogen at 1 atm [61]....	26
Figure 3.1 Electrode system and coordinates for analysis of bubble motion.....	38
Figure 3.2 Electric field distribution on a conductor-plane electrode. ....	39
Figure 3.3 The function f(x) and linear approximations over the region 0.002≤x≤0.016 .....	44
Figure 3.4 Bubble stream trajectories for six voltage values (25, 30, 35, 40, 45, 50 kV from top to bottom in each figure), Nitrogen bubble in LN <sub>2</sub> ( $R= 0.6$ mm on the basis of our preliminary experiments) .....	46

Figure 3.5 Bubble stream trajectories for five different release points under the same voltage value of 35 kV. Nitrogen bubble in LN <sub>2</sub> ( $R= 0.6$ mm and $v_{yi} = 0.22$ m·s <sup>-1</sup> on the basis of preliminary experiments) .....	48
Figure 3.6 Schematic diagram of the experiment.....	49
Figure 3.7 Bubble behaviour under positive voltage.....	50
Figure 3.8 Bubble behaviour under negative voltage .....	51
Figure 3.9 The conductor-plane electrode area map .....	52
Figure 3.10 Comparison of half area bubble percentage under negative and positive polarity (Areas A and C).....	53
Figure 3.11 Bubble collision height as a function of voltage and comparison with theoretically modelled values.....	54
Figure 3.12 Comparison of minimum bubble collision height for theoretical and experimental results ( $x_i=5$ mm for theory calculation) .....	55
Figure 3.13 Bubbles collision percentage as a function of voltage .....	56
Figure 3.14 Comparison of the magnitude of gradient force and buoyancy applied to a bubble (here V=50 kV, R=0.6 mm).....	56
Figure 3.15 Histogram of bubble-plane collisions data (the interval is 10 mm, 2 groups of experimental data for each voltage situation) .....	57
Figure 4.1 Plane-plane inclined non-uniform field electrode system. The angle between the electrodes is 21° .....	60
Figure 4.2 Bubble behaviour under plane-to-plane non-uniform negative fields (for Type 1 electrode arrangement).....	62
Figure 4.3 Comparison of bubble behaviour with different voltages for two kinds of electrode arrangements .....	63
Figure 4.4 Bubble behaviour under plane-to-plane non-uniform positive fields (for Type 1 electrode arrangement).....	64
Figure 4.5 Electric field strength along centre line, bottom to top (a-a' with reference to Figure 4.7) .....	65
Figure 4.6 Electric field strength of the horizontal direction across the top of electrodes (b-b' with reference to Figure 4.7) .....	66
Figure 4.7 The centre line position and the horizontal position across the top of electrodes.....	66
Figure 4.8 The sketch of plane-plane inclined electrode for non-uniform electric field calculation .....	68

Figure 4.9 Comparison of buoyancy with gradient force applied to a bubble .....	68
Figure 5.1 Schematic diagram of the experiment.....	71
Figure 5.2 Potential contours around a bubble attached to grounded electrode (numbers close to potential lines corresponds to voltage in kV. bubble radius R=0.5mm, applied voltage V=30kV, $\epsilon_l=1.432$ , $\epsilon_g=1$ ) .....	73
Figure 5.3 Distribution of the electric field around the bubble .....	73
Figure 5.4 Distribution of the electric field in position A of Figure 5.3.....	74
Figure 5.5 Distribution of the electric field in position B of Figure 5.3 .....	74
Figure 5.6 Distribution of the electric field in position C of Figure 5.3 .....	75
Figure 5.7 Horizontal and vertical components of the electric stresses acting on the bubble.....	77
Figure 5.8 Bubble sliding phenomenon along the grounded electrode due to unbalanced horizontal forces acting on the bubble. Applied voltage is 50kV, camera speed is 1000fps. The frame number is included under each image. ....	77
Figure 5.9 Image processing for a bubble at point of detachment .....	79
Figure 5.10 Bubble growth in the absence and presence of the electric field (V=0kV, 30kV, 40kV and 50kV for (a)-(d)), the camera speed is 5000fps .....	80
Figure 5.11 Bubble departure frequency as a function of applied voltage and electric field .....	80
Figure 5.12 Normalized bubble departure volume versus applied voltage and electric field .....	81
Figure 5.13 Experimental images of bubbles before departure recorded at 5000fps at different voltages .....	81
Figure 5.14 Bubble deformation versus applied voltage and electric field .....	82
Figure 5.15 Experimental images of bubbles before departure recorded at 5000fps at different negative voltages .....	83
Figure 5.16 Comparison of experimental data on bubble departure frequency as a function of electric field strength for two experiments.....	84
Figure 5.17 Comparison of experimental data on bubble departure volume as a function of electric field strength for two experiments .....	85
Figure 5.18 Comparison of experimental data on bubble aspect ratio as a function of electric field strength for two experiments.....	85
Figure 6.1 Schematic diagram of experimental setup for LN <sub>2</sub> boiling heat transfer study .....	89

Figure 6.2 A photograph of the whole experimental apparatus .....	90
Figure 6.3 Electrode arrangement .....	91
Figure 6.4 Cross section of the grounded electrode (unit in mm). ....	92
Figure 6.5 The copper block and brass tube.....	93
Figure 6.6 Schematic diagram of temperature measurement system .....	94
Figure 6.7 A photograph of boiling of liquid nitrogen .....	95
Figure 6.8 A sample to calculate the heating surface temperature.....	97
Figure 6.9 The 2-D axial symmetric copper block electrode FEA model.....	99
Figure 6.10 The 2-D axial symmetric surface plot, continuous plot of temperatures (input power is 100 W and outer boundary temperature is 77 K).....	100
Figure 6.11 A close-up view of the electrode temperature contour .....	100
Figure 6.12 Temperature along the central axis, bottom to top .....	101
Figure 6.13 Heat flux in the upper region of the copper block electrode (Q=100 W, $T_{out}=77$ K).....	103
Figure 6.14 Heat flux along the top surface of the electrode .....	103
Figure 6.15 Time to cool for the electrode.....	104
Figure 6.16 Heat flux as a function of surface superheat at zero-field conditions.....	105
Figure 6.17 Typical images of three heat transfer regimes.....	106
Figure 6.18 Temperature drop of 3 pt100s at onset of nucleate boiling .....	108
Figure 6.19 Electric field effect on ONB. (a) negative, (b) positive .....	109
Figure 6.20 Two kinds of hysteresis phenomenon [75].....	110
Figure 6.21 First hysteresis of liquid nitrogen under high voltage.....	112
Figure 6.22 Hysteresis phenomenon: (a) 0kV, (b) +10kV (c) +20kV, (d) +30kV.....	115
Figure 6.23 Nucleate boiling curve under different negative voltages.....	117
Figure 6.24 Nucleate boiling curve under different positive voltages.....	118
Figure 6.25 Heat transfer coefficients ratio versus applied voltage .....	119
Figure 6.26 Heat transfer coefficient, $h$ , vs heat flux, $q$ .....	119
Figure 6.27 Heat transfer coefficient, $h$ , vs surface superheat, $\Delta T$ .....	120
Figure 6.28 Nucleate boiling heat transfer mechanisms [75].....	121
Figure 6.29 Comparison the heat transfer coefficients ratio of LN <sub>2</sub> to those of other three fluids with similar heat flux conditions under electric fields (a, b, c from [75], d this study). .....	123
Figure 6.30 Temperature rise of the Pt100s at the onset of film boiling .....	124
Figure 6.31 Critical heat flux, $q_{CHF}$ , as a function of the voltage.....	125

Figure 6.32 $q_{\text{CHF}}(V)/ q_{\text{CHF}}(0)$ versus applied voltage .....	126
Figure A.1 General assembly schematic showing electrical components .....	134
Figure A.2 Electrical feed through connections within the $\text{LN}_2$ cryostat.....	135
Figure A.3 Connection 3 Pt100s to the PC card terminal (TBX-68).....	136
Figure B.1 A plate subjected to uniform pressure [119].....	137
Figure B.2 The maximum deflection as a function of the plate thickness.....	138
Figure C.1 Joints of the electrode (indium solder for joint 1 and 2, lead solder for 3 and 4) .....	139

# List of Tables

Table 1.1 The physical properties of nitrogen.....	4
Table 1.2 LN <sub>2</sub> electrical and thermal properties.....	4
Table 2.1 Electrical properties of liquids boiling at 1 atm.....	34
Table 3.1 Experimental electrode arrangement parameters .....	38
Table 4.1 Parameters for the two electrode types.....	61
Table 5.1 The comparison of parameters for the two experiments .....	84
Table 6.2 Electrical properties of the other three working fluids and LN <sub>2</sub> .....	123

# Declaration of authorship

I, ..... **PING WANG**..... [please print name]

declare that the thesis entitled [enter title]

## **Thermal Bubble Behaviour in Liquid Nitrogen under Electric Fields**

.....  
and the work presented in the thesis are both my own, and have been generated by me as the result of my own original research. I confirm that:

- this work was done wholly or mainly while in candidature for a research degree at this University;
- where any part of this thesis has previously been submitted for a degree or any other qualification at this University or any other institution, this has been clearly stated;
- where I have consulted the published work of others, this is always clearly attributed;
- where I have quoted from the work of others, the source is always given. With the exception of such quotations, this thesis is entirely my own work;
- I have acknowledged all main sources of help;
- where the thesis is based on work done by myself jointly with others, I have made clear exactly what was done by others and what I have contributed myself;
- parts of this work have been published as: see Appendix E

**Signed:** .....

**Date:**.....

# Acknowledgements

My acknowledgement must go to my supervisors Dr.Paul Lewin and Dr.George Chen for their professional advice and encouragement in every part of this work without which the completion of this work would not be possible. My gratitude must also go to the School of Electronics and Computer Science for granting me an opportunity to do research in the Tony Davies High Voltage Laboratory and University of Southampton for supporting my study by awarding me the University Scholarship.

I wish to express my thanks to all my colleagues in the high voltage group for their assistance and support. In particular, to Dr. David Swaffield for his great help in choices of research interests and valuable discussions and suggestions, Mr.Neil Palmer, Mr.Mike Smith and Mr Brian Rogers for their technical assistance in experimental equipment building and repairing.

Finally I would like to thank my family for their love and support throughout the duration of my study in the UK.

# Nomenclature

## *Abbreviations*

<b>Symbol</b>	<b>Meaning</b>
ac	Alternating current
dc	Direct current
CHF	Critical heat flux
EHD	Electrohydrodynamic
FEA	Finite element analysis
fps	Frames per second
HTS	High temperature superconductor
HV	High voltage
LN <sub>2</sub>	Liquid nitrogen
LH <sub>e</sub>	Liquid helium
LTS	Low temperature superconductor
ONB	Onset of nucleate boiling
PD	Partial discharge
p.u.	Per unit
SC	Superconducting
SQUID	Superconducting quantum interference device
V-t	Breakdown voltage versus time to breakdown

## *Notation*

<b>Symbol</b>	<b>Meaning</b>	<b>Units</b>
A	area	m <sup>2</sup>
B <sub>o</sub>	bond number	
E	electric stress	V·m <sup>-1</sup>
E <sub>0</sub>	uniform electric stress	V·m <sup>-1</sup>
F <sub>g</sub>	gradient force	N
F <sub>B</sub>	buoyancy	N
F <sub>D</sub>	drag face	N
F <sub>e</sub>	effective electric field force	N

$h$	heat transfer coefficient	$\text{W}\cdot\text{m}^{-2}\cdot\text{K}^{-1}$
$I$	current	A
$k$	thermal conductivity	$\text{W}\cdot\text{m}^{-1}\cdot\text{K}^{-1}$
$L$	distance between conductor and plane	m
$L_c$	latent heat of vaporization of LN <sub>2</sub>	$\text{kJ}\cdot\text{kg}^{-1}$
$M_{\text{eff}}$	bubble effective mass	kg
$q$	heat flux	$\text{W}\cdot\text{m}^{-2}$
$Q$	power	W
$r$	bubble position	m
$r$	equivalent radius of deformed bubble	m
$R$	bubble radius	m
$R_w$	conductor radius	m
$t$	time	s
$T$	temperature	K
$T_{\text{sat}}$	saturation temperature	K
$T_w$	heat transfer surface temperature	K
$u$	growth velocity of bubble	$\text{m}\cdot\text{s}^{-1}$
$V$	voltage	V
$\Delta T$	wall superheat	K
$f_e$	body force per unit volume	$\text{N}\cdot\text{m}^{-3}$
$f_{sn}$	normal electric stress	$\text{N}\cdot\text{m}^{-2}$
$x_i$	bubble initial location	m
$q_v$	free charge density	$\text{C}\cdot\text{m}^{-3}$
$q_s$	surface charge density	$\text{C}\cdot\text{m}^{-2}$
$\theta$	angular coordinate	°
$\theta_p$	angle of both plane electrodes	°
$\epsilon$	dielectric permittivity	$\text{F}\cdot\text{m}^{-1}$
$\epsilon_0$	vacuum dielectric permittivity( $8.85\times 10^{-12}$ )	$\text{F}\cdot\text{m}^{-1}$
$\tau_c$	characteristic time	s
$\tau_e$	relaxation time	s
$\rho$	density	$\text{kg}\cdot\text{m}^{-3}$
$\mu$	dynamic viscosity of liquid nitrogen	$\text{kg}\cdot\text{m}^{-1}\cdot\text{s}^{-1}$
$v$	bubble vector velocity	$\text{m}\cdot\text{s}^{-1}$

$\lambda_e$	electrical conductivity	$\Omega^{-1} \cdot m^{-1}$
$\sigma$	surface tension	$kg \cdot s^{-2}$
$\sigma(E)$	apparent surface tension	$kg \cdot s^{-2}$
$\delta$	vapour film thickness	m
$\lambda_d$	most dangerous wavelength	m
$g$	gravitational acceleration ( $9.8 \text{ m}\cdot\text{s}^{-2}$ )	$\text{m}\cdot\text{s}^{-2}$

*Subscripts*

<b>Symbol</b>	<b>Meaning</b>
l	liquid
g	gas
v	vapour
i	initial
x	horizontal component
y	vertical component
z	horizontal component
cu	copper
in	input
out	output
sat	saturation

# Chapter 1

## Introduction

### 1.1 Superconductivity

Dutch physicist Heike Kamerlingh Onnes first observed superconductivity in 1911 when he cooled mercury to 4.15K and observed that the electrical resistance suddenly dropped to zero (i.e. it became superconducting) [1]. In Onnes' time, superconductors were only simple metals like mercury, lead, bismuth etc. working at the very low temperature of liquid helium. Onnes also observed that normal conduction characteristics could be restored in the presence of a strong magnetic field. For his research in this area, he won a Nobel Prize in 1913. In 1933, the property of superconductor-perfect diamagnetism was discovered (the Meissner effect) by Walter Meissner and Robert Ochsenfeld. This effect shows a superconducting material will repel a magnetic field, and it is so strong that a magnet can actually be levitated over a superconductive material. In subsequent decades, other superconducting metals, alloys and compounds have been discovered and developed. For example, the Rutherford Appleton Laboratory in the UK developed high-energy particle-accelerator electromagnets made of copper-clad niobium-titanium (NbTi) in the 1960s [1].

There are two widely-accepted theoretical explanations of superconductivity. The first one is BCS theory. It was proposed by American physicists John Bardeen, Leon Cooper, and John Schrieffer in 1957. This theory suggests the formation of so-called ‘Cooper pairs’, and fully explains superconductivity at temperatures close to absolute

zero for elements and simple alloys. However, it does not account well for high temperature superconduction, which is still not fully understood. Another significant theory, known today as the ‘Josephson effect’, was advanced by Brian D.Josephson in 1962. He predicted electrical current would flow between two superconducting materials even if there was a non-superconductor or insulator placed between them. This tunneling phenomenon was later confirmed and has been applied to electronic devices such as the SQUID, an instrument capable of detecting quiet weak magnetic fields.

In 1986, researchers at an IBM laboratory in Switzerland first discovered that some perovskite ceramic materials were superconductors at a temperature of about 35 Kelvin. This was a breakthrough discovery in the field of superconductivity. Soon, compound materials were found that would superconduct above 77 K, this made it possible to use liquid nitrogen as the refrigerant. Correspondingly, these materials were called high temperature superconductors. There are three advantages in using liquid nitrogen instead of liquid helium, firstly and also most importantly, liquid nitrogen is relatively cheaper to produce; secondly, 77 K is far easier to obtain and maintain rather than the 4.2 K required for liquid helium; thirdly, liquid nitrogen has a much greater heat capacity to keep things cold than does liquid helium.

Remarkable advances have been made in theoretical and experimental research on superconductors and new materials were found in quick succession. Figure 1.1 shows a history of discovery of superconductors, it was noted that a sharp climb in critical-temperature since high temperature superconductor (HTS) discoveries in 1986 [2]. Though a plateau occurs in the past few years, a new world record for critical temperature  $T_c$  of 150K may well be, for the compound  $\text{InSnBa}_4\text{Tm}_4\text{Cu}_6\text{O}_{18}$  filed by Superconductors.ORG in 2006 [3].

## 1.2 Liquid nitrogen and its properties

Cryogenic liquids such as liquid nitrogen and liquid helium have been used not only as the coolant but also as the electrical insulator in superconducting apparatus [4].

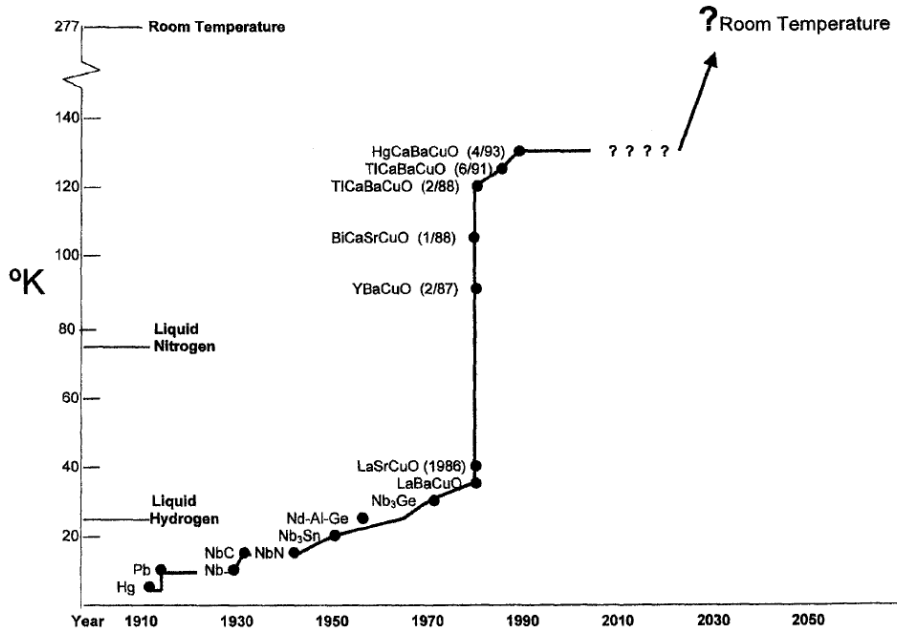


Figure 1.1 History of superconductors, increases in critical temperature (vertical axis, in Kelvin) [2]

### 1.2.1 Liquid nitrogen

Liquid nitrogen ( $\text{LN}_2$ ) is inert, colourless, odourless, non-corrosive, nonflammable, and an extremely cold liquid [5]. As the liquid changes to gas at ambient temperature and pressure, the expansion ratio is approximately 700:1; the cold gas accumulates at low levels due to its greater density than air.  $\text{LN}_2$  is produced industrially in large quantities by distillation from liquid air at reasonable cost, its ability to maintain a very low temperature (normal boiling temperature of 77 K) makes it extremely useful in a wide range of applications including:

- ◆ the immersion, freezing and transportation of food products
- ◆ the preservation of bodies, reproductive cells (sperm and egg), and biological samples and materials
- ◆ in the study of cryogenics
- ◆ for demonstrations in science education
- ◆ in dermatology for removing unsightly or potentially malignant skin lesions, e.g., warts, actinic keratosis, etc

In cryogenic liquids,  $\text{LN}_2$  with a normal boiling temperature of 77 K is the most interesting fluid in the domain of the high critical temperature superconductors. Simultaneously, it can also act as electrically insulating liquid whose dielectric strength

of non-boiling state has been found to be several hundred kV/cm (approximately 300kV/cm) in small scale short term experiments [4]. There are two other advantages of LN<sub>2</sub> as an insulator. One is no pollution, it may be directly disposed back to air after the end of equipment life without additional expenditure; another one is no fire risk due to its chemical inactivity.

A peculiarity of liquid nitrogen is the easy formation of vapour bubbles due to its narrow liquid temperature range and low latent heat of vaporization.

### 1.2.2 Physical properties

The physical properties of LN<sub>2</sub> are listed in Table 1.1 [5, 6]:

Table 1.1 The physical properties of nitrogen

Molecular weight	28.01
Boiling point @ 1atm	77.36 K
Melting point @ 1atm	66.15 K
Critical point	126.21 K
Critical pressure	33.5 atm
Density, liquid phase	824 kg·m <sup>-3</sup>
Density, gas phase	4.59 kg·m <sup>-3</sup>
Viscosity, liquid phase	$1.65 \times 10^{-4}$ kg·m <sup>-1</sup> ·s <sup>-1</sup>
Expansion ratio, liquid to gas	1:694

### 1.2.3 Electrical and thermal properties

LN<sub>2</sub>'s electrical and thermal properties are listed in Table 1.2 [7, 8], as follows:

Table 1.2 LN<sub>2</sub> electrical and thermal properties

Dielectric permittivity, liquid phase	1.432
Dielectric permittivity, gas phase	≈1.00
Electrical resistivity	$> 1 \times 10^{16}$ Ω·m
Thermal conductivity	0.14 W·m <sup>-1</sup> ·K <sup>-1</sup>
Specific heat capacity	2.04 kJ·kg <sup>-1</sup> ·K <sup>-1</sup>
Latent heat of vaporization	199.1 kJ·kg <sup>-1</sup>
Surface tension	$8.8 \times 10^{-3}$ kg·s <sup>-2</sup>

## 1.2.4 Breakdown voltage

$\text{LN}_2$  has a high dielectric strength, comparable to dielectric liquids at room temperature especially when hydrostatic pressure is applied to suppress bubble nucleation.  $\text{LN}_2$  breakdown data displays volume and area effects [9, 10] and is dependant on other parameters including purity, electrode material and surface condition. However, an approximate relation can be determined according to the following field conditions.

### 1.2.4.1 Uniform or nearly uniform field

In order to give available data for the insulation design of superconducting or cryoresistive apparatus, the breakdown voltages of uniform or nearly uniform field gaps in  $\text{LN}_2$  by many researchers are summarized as a function of the gap length, Figure 1.2 [11]. With reference to Figure 1.2, the data denoted as 'ac' indicates the peak values of ac breakdown voltage. The lower envelope of summarized data is expressed approximately to be (electrode spacing  $d$  in mm;  $V_B$  in kV)

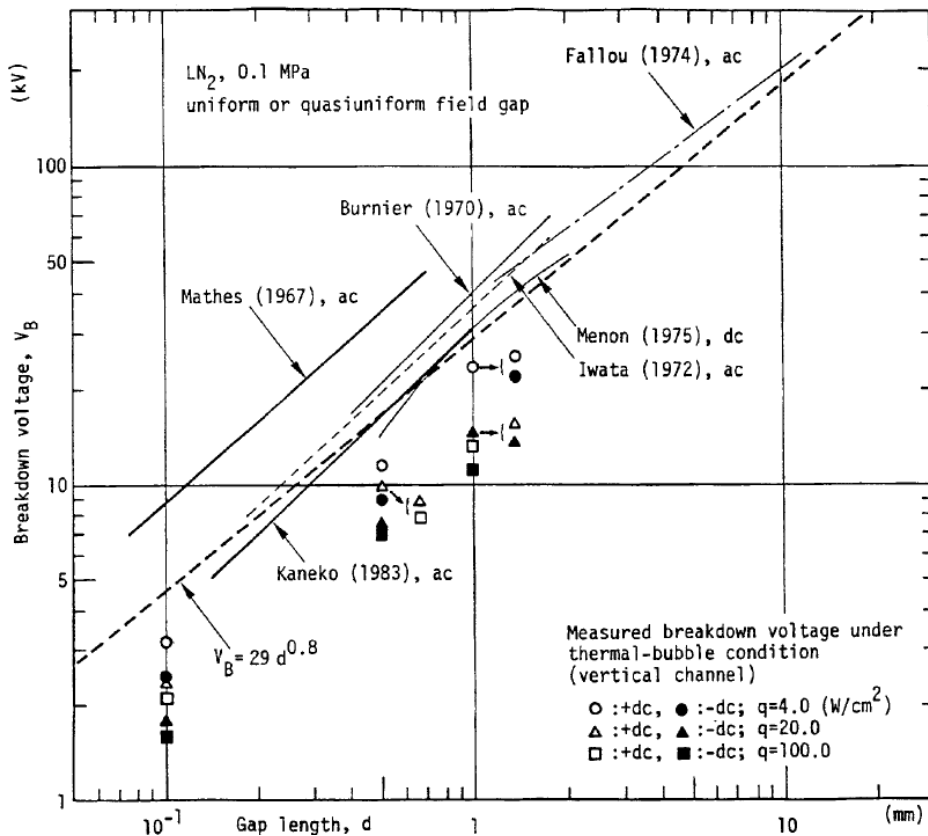


Figure 1.2 Breakdown voltages of uniform or nearly uniform field gaps as a function of gap length in  $\text{LN}_2$  [11].

$$V_B = 29d^{0.8} \quad (1.1)$$

for commercial liquid nitrogen, as illustrated by broken thick lines in Figure 1.2. Of course, the dielectric strength of liquids is never purely a function of the material, its ‘intrinsic strength’ is fictitious but it can be taken as a kind of asymptotic approximation [12].

Figure 1.3 shows a survey of near-uniform field breakdown strength of various insulators in applications. It may help to classify commercial-grade cryogenic liquids such as LN<sub>2</sub> in comparison to common high voltage insulators. It may be noted that LN<sub>2</sub> has a higher breakdown voltage than conventional transformer oil.

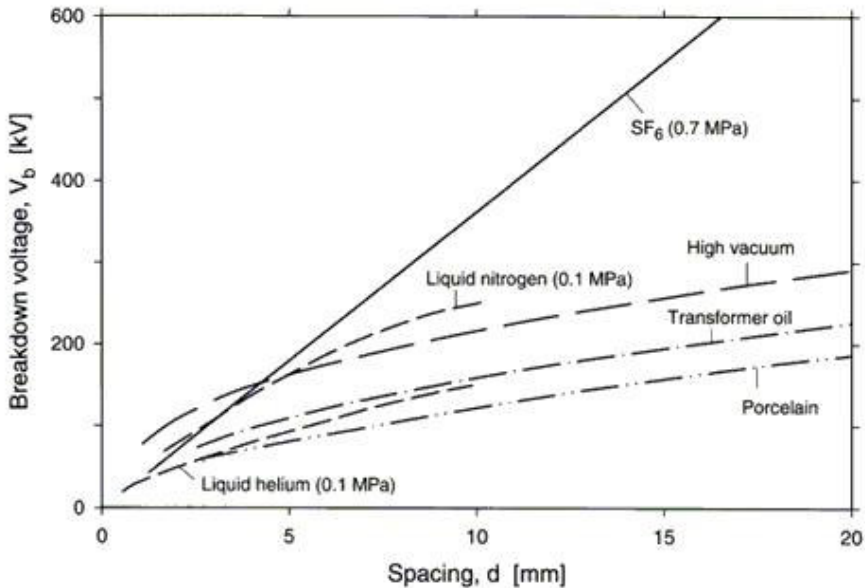


Figure 1.3 Breakdown strength of porcelain, cryogenic liquids, and vacuum insulation under d.c. voltage stress in a uniform field [12].

#### 1.2.4.2 Gas nitrogen breakdown voltage close to the normal boiling point

LN<sub>2</sub> may be inhomogeneous when gas bubbles appear. Any electric field strength is enhanced within the nitrogen bubble from its bulk value by an order of 1.432/1. This effect must be considered, especially as vaporization is easy to create with cryogenic liquids. Figure 1.4 shows the breakdown voltage vs. spacing in nitrogen vapour close to the normal boiling point [12]. It looks similar to the nitrogen Paschen curve under the situation of saturated vapour density.

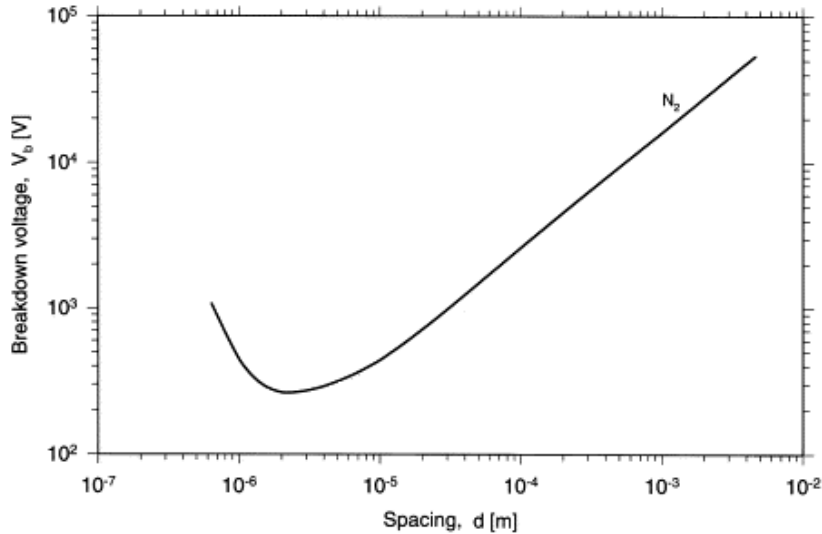


Figure 1.4 Breakdown voltage as a function of spacing in nitrogen vapour (Paschen's curve) close to the normal boiling point [12]

#### 1.2.4.3 Non-uniform field

Highly non-uniform fields are not very favourable for high withstand voltages in cryogenic liquids. Point electrode gap configurations should be suppressed in practice. For a point to plane configuration (spacing  $d$  in mm;  $V_b$  in kV)

$$V_B = 18d^{0.26} \quad (1.2)$$

has been found to indicate breakdown in normal boiling LN<sub>2</sub> [12]. This formula may be relevant for spacings of less than 10 mm. Corona can arise before breakdown, especially when stressing the gap using an a.c. voltage [12].

### 1.3 Study motivation

Application of superconductivity in power equipment has been discussed since the early seventies. It is well known that the superconductor exhibits no resistance or losses when a steady current of electricity flows through it. Based on this point, electricity transmission without losses offers enormous benefits for the electric power industry. In addition, because of its efficiency and high capacity, superconductor technology has the potential to increase stability and reliability of the electric grid. It also can create environmental benefits by reducing pollution and eliminate the use of certain toxic materials. It is also favoured for its high capacity to size ratio ("power density") to

supply built-up areas or where overhead lines are not possible/desirable. Especially for HTS, reduced cooling costs make it more affordable than other superconductor alternatives. So, although HTS technology is still in the research and development phase, it offers many promising applications [13]:

- ◆ Transmission lines
- ◆ Electric motors
- ◆ Generators
- ◆ Transformers
- ◆ Compensators
- ◆ Fault current limiters
- ◆ Energy storage devices

Furthermore, electrical power applications based upon HTS are now being designed and tested in many countries such as Europe, Japan and the USA due to government and industry partnerships, only a few years after the discovery of HTS. A ‘road map’ of HTS power applications to go into the real world has been described by O.Tsukamoto [14]. He pointed out some applications such as HTS cables to supply low voltage dc power to a large number of computer servers in internet data centres may be early achievements prior to final targets. Generally, these applications offer many practical benefits to the resident electrical system [15]:

- ◆ Increased energy efficiency;
- ◆ Reduced equipment size;
- ◆ Reduced negative environmental impact;
- ◆ Increased stability and reliability;
- ◆ Flexible transmission and distribution;

but quantifying them needs realistic analysis. These benefits have a common focus: lower electricity costs, improved environmental quality and more competitive products for a global market.

To ensure the feasibility of the introduction of superconductivity into electric power systems, the reliability of the electrical insulation must be incorporated in the design from the beginning of the development of any superconducting power equipment [16]. The electrical insulation system of the superconducting power apparatus is generally placed in a pool of cryogenic liquid coolant. Helium and nitrogen are

excellent insulating fluids for classical low temperature superconductors (LTS) and HTS, respectively [4, 12]. Cryogenic insulation systems are often a complex composite, not only because electrical stress has to be controlled safely but also because thermal and mechanical requirements must also be satisfied [17]. Any failure can result in a catastrophic event. The reliable dielectric performance of a cryogenic liquid is of course the key point for any power application. Moreover, superconducting power apparatus also has properties that may influence dielectric performance. For example, quench phenomena are inevitable in some designs and the dielectric strength is significantly reduced if the coolant vaporizes due to the Joule heat at the quenched part of the superconductor [18]. These factors must be taken into account in the insulation design, and also considered in high voltage tests to ensure the reliability of the designed electrical insulation.

A peculiarity of cryogenic liquids is the easy formation of vapour bubbles caused by mechanical, thermal or electrical factors. Thermal bubbles are very common in cryogenic liquids. For example, thermal bubbles are produced in the case of external heat input into the liquid. It is known that bubbles generated thermally in the liquid coolant of superconducting and cryoresistive apparatus are one of the factors causing a reduction of the electrical breakdown voltage of the apparatus [11]. Bubbles and density fluctuations can affect the dielectric strength considerably, especially in equipment such as fault current limiters where vaporizing of a liquid is an inherent function. The design of the insulation system must take account of a scenario with extended vapour regions. Experiments show high pressure may prevent this shortcoming to some extent but it is restricted to specific arrangements and cooling cycles [4]. In addition, in superconducting (SC) apparatus, boiling due to a local hot spot on conductors by quench also will become the most important bubble formation mechanism from the viewpoint of electrical insulation design. Even with the most careful design of SC apparatus, the possibility of a local hot spot occurring is not zero. In particular, a quench initiated in an SC coil by a hot spot will not only cause bubble formation but also create a high voltage drop across the coil layer and might cause a voltage breakdown. Some studies on the bubble-triggered breakdown have been investigated with simulated quench conditions and real dynamic quench conditions [18]. It was noted that the characteristics of bubble-triggered breakdown voltage depend

mainly on electrode configuration, applied voltage, ambient pressure and heat transfer rate on the electrode surface.

In addition, it is also necessary to study the dynamic boiling phenomenon with or without electric fields, caused by an increasing heat input in cryogenic liquids such as LN<sub>2</sub> to generate source data for cooling stability and safety design of large-scale superconducting systems. The current characteristics of HTS equipment determine that the question of thermal stability and thermal control play a crucial role in the design of all HTS equipment [19, 20]. For example, a superconducting a.c. magnet produces heat due to a.c. loss in its windings and other electrically conductive structure materials, and the heat must be removed. Thus, heat transfer into the LN<sub>2</sub> is an aspect of great interest. In other words, the heat transfer characteristics between the surface of superconductors and LN<sub>2</sub> are very important.

It is well known that the electrohydrodynamic (EHD) enhancement technique is one of the most promising methods among various active techniques in boiling heat transfer applications. The effect of an electric field on heat transfer of LN<sub>2</sub> has not been systematically studied. Therefore, there is the necessity for experimental investigation into the EHD effect on boiling heat transfer in liquid nitrogen. The concept of enhanced boiling heat transfer by using an electric field is also one of the methods used to increase the heat transfer coefficient in cryogenic cooling systems. Especially, in the cases of small scale and compact designs, effective heat transfer enhancement techniques should be considered because the heat needed to be removed per unit area will be increased.

## 1.4 Aims and objectives

Based on the study motivation discussed above, this study has the following objectives: Firstly, to observe bubble behaviour changes under non-uniform or uniform electric field and understand and explain these changes, and then give a guide or method or concept for actual question solution in real superconductor power applications. Secondly, to investigate the heat transfer characteristics of LN<sub>2</sub> under an electric field, this may help the design of the LN<sub>2</sub> related components for HTS device cooling and also provide an initial perspective on the possible improvements for cryogenic cooling of HTS equipment.

## 1.5 Contents of this thesis

In Chapter 1, the basic knowledge and concepts on superconductivity and some properties of LN<sub>2</sub> are described. Initial study motivation and aims and objectives for this study are given. Chapter 2 presents a literature review of the bubble behaviour under electric fields in liquid nitrogen, focusing on electrical insulation and thermal stability aspects. The EHD phenomena and mechanism on enhancement boiling heat transfer are described and explained. The LN<sub>2</sub> boiling curve is also reviewed, with special interest in determining the maximum heat transfer flux of LN<sub>2</sub> from previous published research. Chapter 3 describes an experimental study into the influence of a non-uniform electric field on bubble motion and behaviour in liquid nitrogen. The electric field effect on bubble motion as it rises due to buoyancy within applied dc electric fields is quantitatively investigated using a conductor-plane gap. Thermal bubble motion and bubble collision with the plane electrode processes are observed in these experiments. In addition, a model based on analysis of the forces acting on the bubble has been developed. This set of differential equations describes the motion of a spherical bubble in the conductor-plane gap with voltage, and can be solved numerically to determine bubble trajectory. Chapter 4 investigates an experimental study of the behaviour of thermally nucleated bubbles in LN<sub>2</sub> between plane-plane inclined electrode with an angle of 21°. Some bubble motion and coalescence phenomena have been observed using a high-speed camera and compared. To better understand these results, the forces experienced by the bubbles are analysed and presented. Chapter 5 describes experiments to investigate the effect of a dc uniform electric field on the behaviour of bubbles in LN<sub>2</sub> such as their growth, deformation and departure frequency. The experiment was performed using a stainless steel mesh-plate electrode. In order to explain obtained phenomena and results, the electric field distribution around a bubble has been simulated using the finite element analysis (FEA) method and the electric force acting on bubble calculated numerically. In addition, the effects of changes to thermal bubble behaviour on boiling heat transfer are discussed. Chapter 6 reports on an experimental investigation into the effects of a dc uniform electric field on boiling heat transfer of liquid nitrogen. A copper block electrode system with temperature measurement and vacuum heat insulation has been designed and manufactured. A heat transfer model based on this electrode geometry has been developed in order to provide some useful data for the electrode design and assist

temperature calculations. The boiling curves of LN<sub>2</sub> have been obtained with and without electric fields, the effect of electric field on onset of nucleate boiling (ONB), nucleate boiling enhancement, boiling hysteresis and critical heat flux (CHF) has been analysed and discussed. Finally, the conclusions of this research and recommendations for further study are presented in Chapter 7.

## 1.6 Summary

This chapter has introduced some general information regarding the study of thermal bubble behaviour under electric fields in liquid nitrogen. Basic knowledge and concepts on superconductivity and the properties of LN<sub>2</sub> are described. Initial study motivation and aims and objectives for this study have been defined.

## Chapter 2

# Literature Review

### 2.1 Introduction

Bubble behaviour in LN<sub>2</sub> in the presence of electric fields is of great interest within the study of electric insulation level of superconducting equipment and involves the consideration of prebreakdown as well as breakdown phenomena. Another widely accepted area of interest concerns Electrohydrodynamic (EHD) enhanced boiling heat transfer which is also concerned with bubble behaviour under electric fields. For real superconductor apparatus applications, bubbles caused by extra heat input or a quenching state are occasionally unavoidable, so it is also necessary to consider the change of heat stability and cooling ability due to bubble behaviour in these apparatus. With respect to these phenomena, a brief literature review is given according to three main viewpoints – electrical insulation, thermal stability and EHD enhancement heat transfer.

### 2.2 Electrical insulation

It has been known for some time that bubbles formed in a dielectric liquid such as liquid nitrogen can lower the electrical strength of the insulating system, including the liquid itself, and therefore result in a serious hazard. That is mainly because the insulation level of liquid state lowers to the gas state in the presence of bubbles, partial discharges can occur inside bubbles and both situations can co-exist.

### **2.2.1 Bubble generation mechanisms**

In cryogenic liquids, bubbles can be easily formed by heating, due to their narrow liquid temperature range and low latent heat of vaporization. Researchers have summarized and proposed the following mechanism for the bubble generation in dielectric liquids: Kao [21] summarized the generation mechanism of bubbles as: release of gas from microscopic cavities and hollows on an electrode surface; generation of low pressure in the liquid due to the electrical Maxwell stress; and local vaporization of liquid due to the action of electrical current, e.g. an electron beam from a microscopic protrusion on the electrode. Hara pointed out that motion of solid impurities [22, 23] and a local hot spot on the conductor [11, 24, 25] might cause bubble generation and reduced breakdown voltage of cryogenic liquids in superconducting and cryogenic devices.

### **2.2.2 Thermal bubble behaviour under uniform fields**

#### **2.2.2.1 Parallel plane electrode**

Before 1990, Hara et al.[11, 24-26] had studied dc, ac and lighting impulse breakdown strengths of liquid nitrogen in the presence of thermal bubbles and bubble behaviour under uniform electric fields. These studies were conducted with a pair of parallel plane electrodes, one of which had an electric heater to produce the thermal bubbles. With this arrangement the parallel plane electrode can provide a uniform or quasi-uniform electric field and the heater simulates a local hot spot. The schematic diagram of the typical experimental setup and electrode system is shown in Figure 2.1. Usually, the parallel electrode arrangements are defined as one of two main types: vertical channel or horizontal channel, and the horizontal channel is classed as: with upward heater surface or with downward heater surface. The following is a review of Hara et al's work [11, 24-27] in this area.

Within a vertical channel arrangement of Figure 2.1, with dc voltage, when an electric field of  $\sim 3$  kV/mm is applied, nucleate boiling turns into film boiling in the cryogenic liquid and a vapour column occurs and then bridges the gap at higher electric fields before breakdown, as shown in Figure 2.2. It also can be seen from Figure 2.2 that the sequential stages of bubble deformation depends on heat input and applied voltage [11]. A higher applied voltage can result in a locked vapour which is fixed tightly across the

gap. Consequently, the breakdown strength of both liquid nitrogen and helium decreases suddenly from about 30 kV/mm to that for each saturation gas when the heat transfer at a hot spot on the electrode changes from natural convection to nucleate boiling, as shown in Figure 2.3.

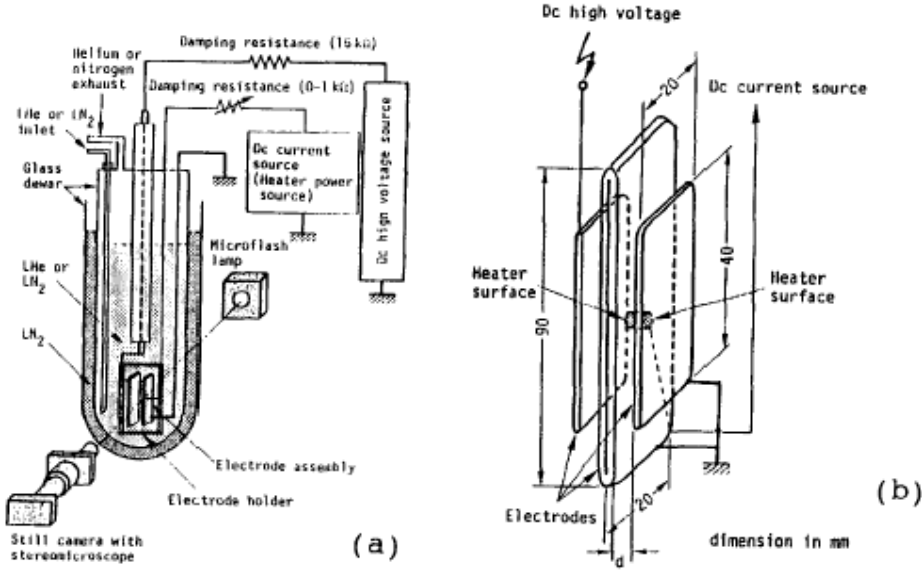


Figure 2.1 Schematic diagram of experimental setup and a pair of parallel electrode system [11]

(a) Experimental setup    (b) Electrode system (vertical channel)

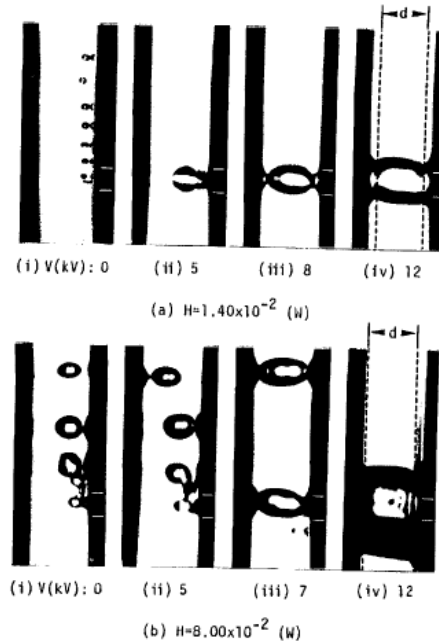


Figure 2.2 Sequential stages of bubble deformation in liquid nitrogen with applied voltage,  $d=1\text{mm}$  [11]

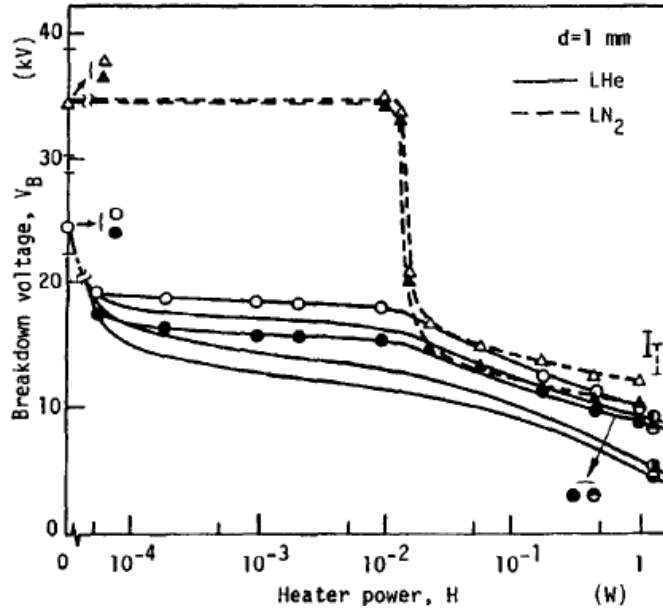


Figure 2.3 Breakdown voltage as a function of heater power,  $d=1\text{ mm}$  [11]

(in  $\text{LN}_2$ :  $\Delta$ : positive heater electrode,  $\blacktriangle$ : negative heater electrode; in  $\text{LHe}$ :  $\circ$ : positive heater electrode,  $\bullet$ : negative heater electrode; ---: estimated value from Paschen curve for nitrogen gas (79 K), —: estimated value from Paschen curve for helium gas (4.4 K)).

Generally speaking, bubble behaviour observed under various experimental conditions are classified into five types when a dc voltage is applied to a quasi-uniform field gap in which one electrode has a heater to simulate a local hot spot, as shown in Figure 2.4. With reference to Figure 2.4, bubble structure changes with an increase of applied voltage from (a) to (e). Breakdown occurs through liquid, vapour or a composite of two phases of vapour and liquid, and is dependent on the combination of ambient pressure and heater power [18].

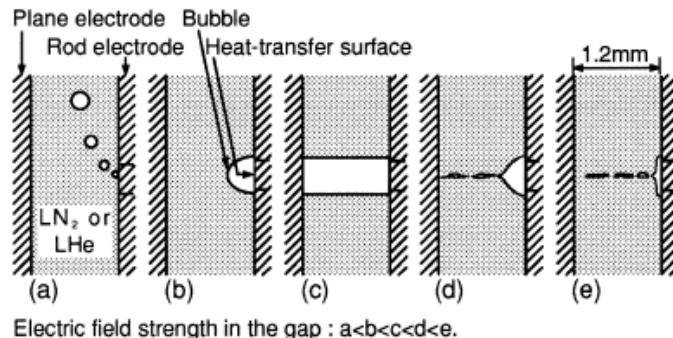


Figure 2.4 Vapour structure in the presence of dc uniform electric field [18].

(a) discrete bubbles; (b) fixed bubble; (c) locked vapour; (d) conical bubble with bubble stream; (e) vapour film with bubble stream

With ac voltage, the thermal bubble varies its shape according to the sinusoidal variation in voltage and the bubble vibrates violently [26], as shown in Figure 2.5. But the ac root mean square value for the onset voltage of vapour bridging is almost the same compared with that for dc voltage at gap lengths less than 2 mm. This suggests that the effective value of electric field determines the maximum bubble elongation. In addition, a significant reduction in ac breakdown voltage also occurs as in the case of dc voltage at a certain level of heat input corresponding to the onset of nucleate boiling,

When the standard lightning impulse ( $1.2/50\mu\text{s}$ ) voltage is applied to the gap, it was observed that the effect of electric field on the bubble deformation was negligible even though the applied voltage reached  $\approx 50\%$  flashover voltage. Therefore, breakdown occurs in a composite insulation system of bubbles and the surrounding liquid. The bubble size increases with heater power resulting in the breakdown voltage gradually reducing. The breakdown voltage can be estimated roughly as the required voltage for breakdown of a series composite of gas layer of  $2r$  thickness and liquid layer of  $(d - 2r)$  thickness where  $r$  and  $d$  are the bubble radius and the gap length respectively [26].

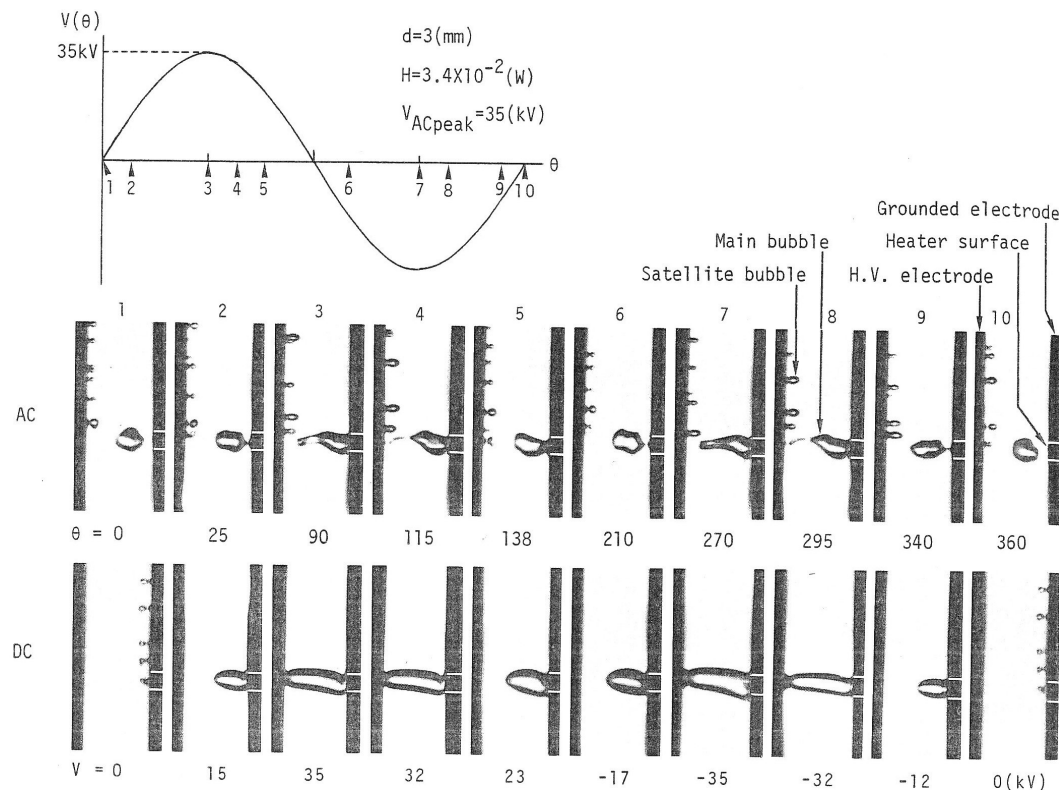


Figure 2.5 Comparison of bubble shapes under ac and dc electric fields [26]

### **2.2.3 V-t characteristics and breakdown mechanism**

Breakdown voltage versus time to breakdown (V-t) characteristics are very important as they define the breakdown characteristic of a given dielectric system. Studies [27, 28] into thermal bubble deformation and V-t characteristic have been made using different wave front pulse voltages in a parallel plane electrode system in order to get the electrical breakdown characteristics of liquid nitrogen in the presence of thermally induced bubbles to simulate the quenching state of superconducting magnets. The results suggest that the breakdown of liquid coolants depends not only on the bubble generation mechanism but also on the bubble deformation process. With a ramped voltage, the thermal-bubble breakdown mechanism in liquid nitrogen may be basically classified into three types [18] as shown in Figure 2.6.

- 1) Mechanism I: breakdown in locked vapour which is formed by growing of a bubble fixed on the heater surface. This appears with slower rising voltage,  $\sim 0.1$  kV/ms, and results in the “flat” region (see regions (III), (IV) and (V) in Figure 2.7) of the V-t curve. The time in the constant breakdown voltage region depends on the bubble growth velocity  $u$  and heat transfer rate  $q$  from the heater electrode to gas in the fixed bubble.
- 2) Mechanism II: breakdown in a composite insulation system of suspended and elongated bubbles and surrounding liquid. This appears with medium rising voltage,  $\sim 10$  kV/ms, and results in the increase of breakdown voltage of the V-t curve in a short time region (see regions (I) and (II) in Figure 2.7).
- 3) Mechanism III: breakdown in a composite insulation system of non-deformed bubbles and surrounding liquid at fast rising voltage such as the standard lightning impulse voltage. In this mechanism, the breakdown voltage is determined only by electrical phenomena and may be independent of thermal and mechanical effects such as bubble growth, condensation of gas in the bubble and bubble deformation. Unfortunately, the relevant data is not plotted in Figure 2.7.

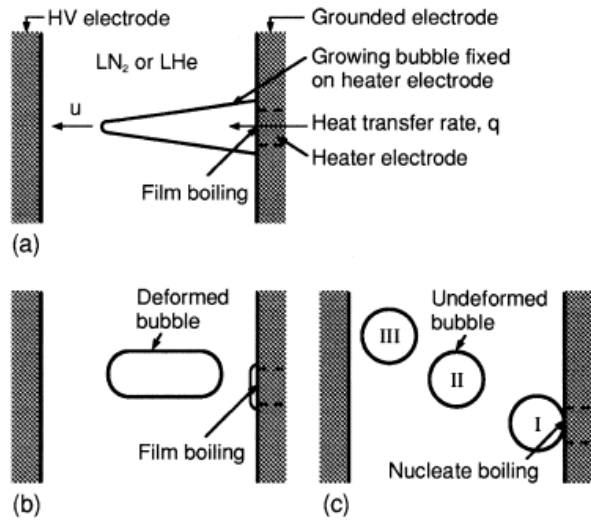


Figure 2.6 Summary of breakdown mechanism by ramped voltage in cryogenic liquid in the presence of nucleate boiling [18]

(a) Mechanism I; (b) Mechanism II; (c) Mechanism III.

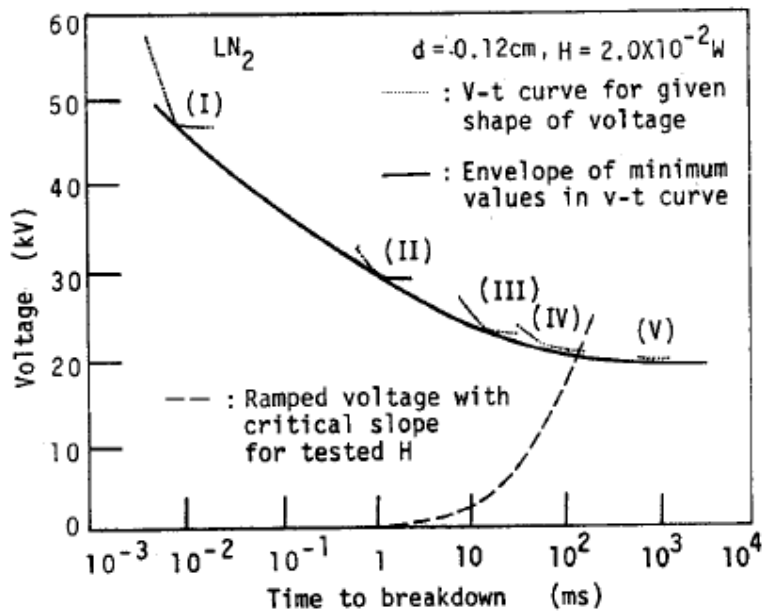


Figure 2.7 V-t curves of liquid nitrogen with different voltages [28]. Waveform of applied voltages: (I) 1.2/80  $\mu$ s, (II) 2.0/5.5ms, (III) 10/30 ms, (IV) 115/415 ms and (V) ramped voltage of  $\sim 2$  kV/s slope.

## **2.2.4 Thermal bubble behaviour under non-uniform fields**

Behaviour of bubbles in non-uniform fields is of great interest primarily to allow the study of electrically enhanced boiling heat transfer, prebreakdown phenomena in the presence of thermally induced bubbles and control of the shape of meniscus and the velocity of the liquid/vapour phase interface with electrostatic force in a microgravity environment [29].

Generally, there are three kinds of electrode systems used to study thermal bubble behaviour under the non-uniform electric fields. They are plane-to-cylinder, coil type structure, and conductor-to-plane electrode system.

### **2.2.4.1 Plane-to-cylinder electrodes**

Extensive research into bubble behaviour using a plane-to-cylinder electrode system has been undertaken [7, 30-33]. Some results on bubble behaviour under experimental conditions show, for example, the gradient force and Maxwell stress strongly affect the bubble dynamics and bubble shape in a plane-to-cylinder gap with/without fins. Also, bubble distribution and dielectric behaviour are affected by the cylinder electrode surface condition [30]. A study regarding the effect of voltage waveform on thermal bubble breakdown phenomena in liquid nitrogen using a plane-to-cylinder electrode shows that ac electric fields have less effect on bubble behaviour than dc electric fields [33]. In addition, a spherical bubble motion trajectory under dc fields was also described by using a set of differential equations and compared with experimental results [7]. The results show that the bubble agglomeration can occur in the period of quenching time of superconducting magnets and will affect the dielectric performance of liquid coolants.

### **2.2.4.2 Coil type structure electrodes**

The coil type electrode model winding structures can be seen in prototypes of either HTS transformers or HTS fault current limiters. In order to study thermal bubble behaviour and related electrical insulation performance with this kind of electrode system, experimental studies and theoretical analysis [34-37] have been carried out using a simulated electrode system of HTS coils. Obtained results show that bubble behaviour is affected by electric fields and pressure; the electric field drives bubbles into the lower field region before electric breakdown. Pressurizing liquid nitrogen was

found to be a very effective method of reducing the formation of large bubbles and increasing the partial breakdown inception voltage. In addition, different spacers also affect bubble behaviour and partial breakdown characteristics.

#### **2.2.4.3 Conductor-to-plane electrodes**

It has been assumed that a quasi-uniform field exists between a conductor and a plane when the gap between both electrodes is very small, with respect to the diameter of the conductor electrode, see for example the arrangement shown in Figure 2.4. It is assumed that a non-uniform field appears when this distance is larger and has been studied as part of this research [38], further details are presented in Chapter 3.

### **2.3 Thermal/cryogenic stability and heat transfer efficiency**

#### **2.3.1 Boiling phenomena**

When a surface is exposed to a liquid and is maintained at a temperature above the saturation temperature of the liquid, boiling may occur. Boiling is the process of vaporization when it occurs at a solid-liquid interface, this distinguishes it from the process of evaporation which occurs at a liquid-vapour boundary. Boiling is an extremely efficient process for heat removal and is utilized in various energy-conversion and heat-exchange systems and in the cooling of high-energy density components. Boiling is usually classified into two types: pool and forced-flow boiling. Pool boiling refers to boiling under natural convection conditions, whereas in forced-flow boiling, the liquid flow over the heater surface is imposed by external means.

#### **2.3.2 Pool boiling**

Pool boiling has two types: subcooled boiling and saturated boiling, this depending on the temperature of liquid. If the temperature of the liquid is below the saturation temperature, the process is called subcooled boiling. If the liquid is maintained at saturation temperature, the process is known as saturated boiling.

Figure 2.8 shows a typical pool boiling curve [39]. It is seen that the wall heat flux  $q$  is dependent on the wall superheat  $\Delta T$  (the difference between the wall temperature and the liquid's saturation temperature). The plotted curve is for a horizontal surface underlying a pool of liquid at its saturation temperature (the boiling point at a given

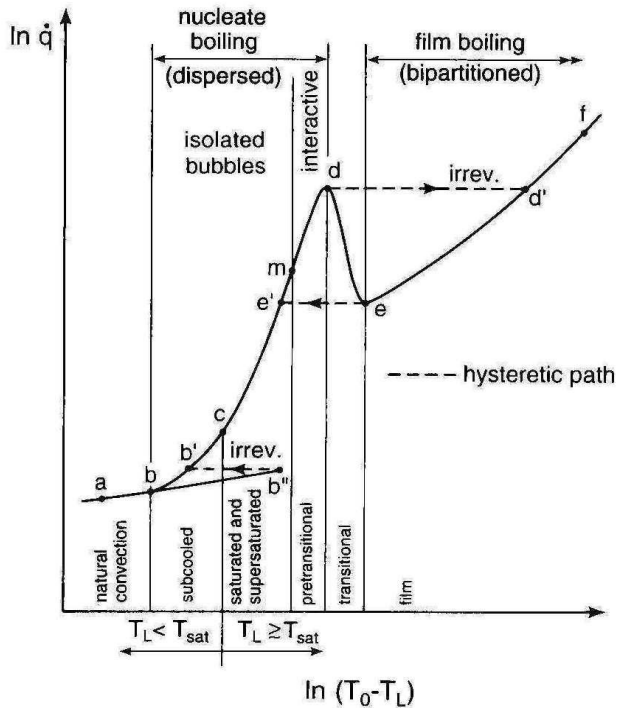


Figure 2.8 Typical pool boiling curve [39]

pressure). Several distinct heat transfer regimes can be identified on the boiling curve: single-phase natural convection, partial nucleate boiling, fully developed nucleate boiling, transition boiling, and film boiling. In the convection region ( $a-b$ ), single phase convection currents are responsible for motion of the fluid near the surface. The liquid near the heated surface is superheated slightly, and it subsequently evaporates when it rises to the surface. The heat transfer in this region can be calculated using the free-convection relations. At the beginning of nucleate boiling, for relatively low superheats, the larger microcavities of the heated surface are activated. Bubbles are isolated from each other and bubble interaction is minimal. Subcooled boiling (region  $b-c$ ) occurs and is preceded by natural convection with its characteristically low heat transfer rates. The effect of early bubble growth and detachment is therefore to increase the heat transfer rate through convection and evaporation. This effect continues progressively until the temperature of the enclosed liquid  $T_L$  has reached  $T_{sat}$  and saturated boiling begins. When the surface tension is large, and the liquid does not wet the microcavities of the surface, the transition from natural convection to subcooled boiling (at  $b$ ) and then to saturated boiling (at  $c$ ) is smooth, and is characterized by a reversible path; superheats are small. However, when the surface tension is small, the superheat required for

bubble initiation is much greater than required for repetitive bubbling. The boiling curve may then exhibit a reversible overshoot from the natural convection regime to the bubble initiation point  $b''$  before falling back irreversibly on to the subcooled boiling curve at  $b'$ . This can create a hysteresis effect. As the substrate temperature rises, smaller microcavities are also activated and the number of bubble sites increases. Once the bulk liquid temperature has reached  $T_{sat}$ , and saturated pool boiling begins, bubble behaviour becomes very important. The bubbles form more rapidly and bubble interaction is more violent. Eventually, bubbles are formed so rapidly that they blanket the heating surface and prevent the inflow of fresh liquid from taking their place. At this point the bubbles coalesce and form a vapour film which covers the surface. The process only occurs up to a point  $d$  called the critical heat flux in the figure. Beyond the critical heat flux two possibilities exist depending on the heating conditions. If the surface heat flux is controlled and increased beyond critical point, the surface temperature increases dramatically as shown by the dashed line from point  $d$  to  $d'$  in Figure 2.8. The temperature at  $d'$  is often higher than the maximum temperature that heater surface can maintain, and thus this heat flux is referred to as the burnout point. If the surface temperature is controlled and increased beyond the temperature at  $d$ , the insulating effect continues and the heat transfer rate decreases. This regime called transition boiling is characterized by the unstable vapour blanket that covers the surface. The vapour blanket collapses periodically and allows the fluid to contact the surface. This periodic motion results in large variations in surface temperature and a highly unstable flow. Stable film boiling is eventually encountered in region (e-f). Vapour bubbles are released regularly from the surface and the film is considered stable. Increasing the surface temperature results in a corresponding increase in heat transfer. However, the transport is generally governed by thermal radiation rather than the fluid motion due to the large temperature difference.

In industrial applications, the prediction of the heat transfer coefficient in various boiling regimes and the location of the peak heat flux in pool boiling are of practical interest. Nucleate boiling and film boiling regimes are important in several engineering applications where heat transfer is involved.

### **2.3.3 Heat transfer into liquid nitrogen**

Heat transfer into liquid nitrogen is of both fundamental and technical interest.

A. Sakurai *et al*, [40-42] have studied boiling phenomenon and heat transfer characteristics of LN<sub>2</sub> to quasi-steady and increasing heat inputs. For actual applications, LN<sub>2</sub> is an important coolant of HTS equipment because its boiling point is below the transition temperature of many high temperature superconductors. High current characterises in HTS equipment mean that the question of thermal stability and thermal control of LN<sub>2</sub> play a crucial role in the design of HTS equipment [19, 20]. For example, a superconducting a.c. magnet produces heat due to a.c. losses in its windings and other electrically conductive structure materials and the heat must be removed. Another example is the quench condition of a superconducting cable or the switching cycle of a fault-current limiter that causes energy dissipation into LN<sub>2</sub>. In these cases attention has to be paid to heat transfer characteristics of LN<sub>2</sub>. From these examples, it is clear that the heat transfer characteristics between the surface of superconductors and LN<sub>2</sub> are very important. Research has been undertaken to obtain experimental data on heat transfer characteristics of coolants. Generally, heat transfer characteristics change according to the following factors:

- 1) Heat source: wire [43-45], plane [46] and thin-film [47, 48]
- 2) Surface materials: metal [49], ceramic[46, 50, 51] and organic fibre [52]
- 3) Surface conditions: smooth surface or porous surface [53]; surface orientation and treatment [54].

It has been suggested that the features of HTS ceramics, which have different thermophysical properties and a more porous structure compared with metals, must be taken into account when calculating their thermal stability. In addition, according to the type of measurement, both transient heat transfer [47, 55, 56] and stationary heat transfer need to be assessed. Compared with stationary heat transfer, the transient heat transfer processes are more complex and can be influenced by many variables. For HTS power apparatus, the performance under over-current conditions also has a close relationship with heat transfer. Instability of some high temperature superconducting conductors due to over-current has been investigated [57-59].

### **2.3.4 Boiling curves of liquid nitrogen and its critical heat flux**

The boiling curve of fluids is a very important parameter in the design and application of heat exchange systems as well as the analysis of thermal stability. The major issues

include the thermal design and heat removal methods. In most cases of heat transfer applications, only work at natural convection and nucleate boiling region is allowable. So, a maximum heat flux in the nucleate boiling processes needs to be known. In addition, through a boiling curve, the heat transfer coefficient of different regions of heat transfer process can be obtained. Figure 2.9 shows a typical pool boiling curve (heat flux plotted as a function of the difference between the wall temperature and the saturation temperature of liquid) for liquid nitrogen, it is obtained by Merte and Clark [60] in an experimental investigation on nitrogen boiling using a 25.4 mm diameter copper sphere. Obviously, this curve consists of a single-phase natural convection region, a nucleate boiling region, a transition boiling region and a film boiling region. The nucleate boiling region can provide the most efficient heat transfer, and thereby those aspects related to this region cause special interest. These aspects are the onset of nucleate boiling (ONB), any superheat excursion phenomena accompanying boiling incipience, the rate of heat transfer by nucleate boiling and the maximum rate of heat transfer in nucleate boiling.

Brentari and Smith [61] plotted numerous experimental data on  $\text{LN}_2$  boiling heat transfer as shown in Figure 2.10. More boiling curves of  $\text{LN}_2$  can be found in [46, 62-64]. From these boiling curves, it is found that the critical heat flux (CHF) of liquid nitrogen is within a range of 13 to 22  $\text{W/cm}^2$  and occurs at a wall superheat of about 10K.

## 2.4 Electrohydrodynamic (EHD) principles

### 2.4.1 EHD phenomena

EHD phenomena were first reported in a UK patent over 90 years ago [65]. However, only in the last thirty years, has there been interest in its potential benefits for providing both economic and environmental advantage. EHD is the study of the dynamics of fluids in the presence of electric fields. That is, EHD phenomena involve the interaction of electric fields and flow fields in a dielectric fluid medium, this interaction can result in electrically induced fluid motion and interfacial instabilities which are caused by an electric body force. An excellent explanation and summary on EHD phenomenon and this electric body force has been given by Bryan [66, 67]. Based on this phenomenon, researchers have investigated EHD enhancement heat transfer in liquids since 1949.

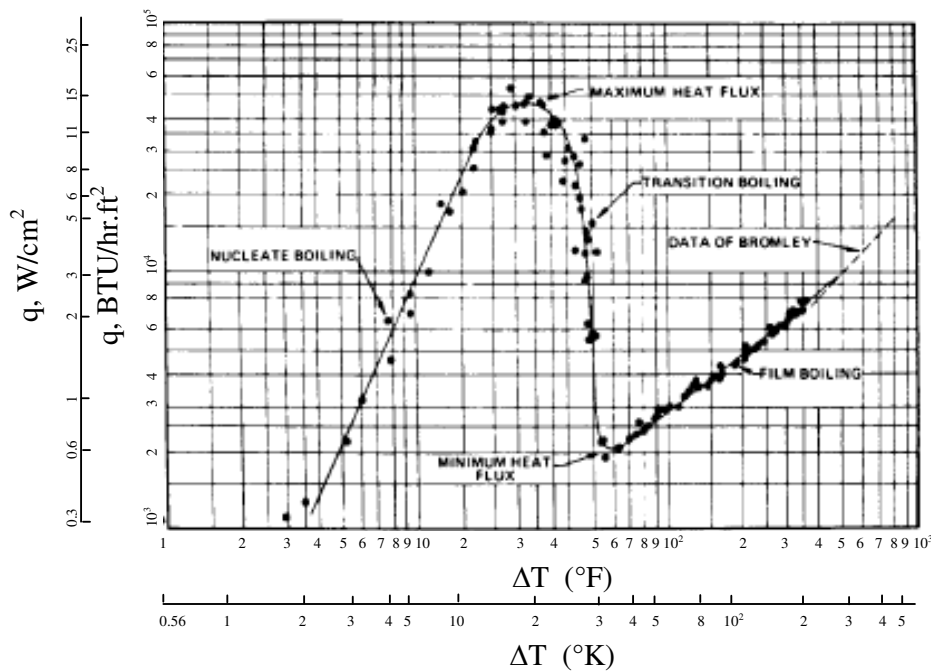


Figure 2.9 Typical pool boiling curve for liquid nitrogen [60]

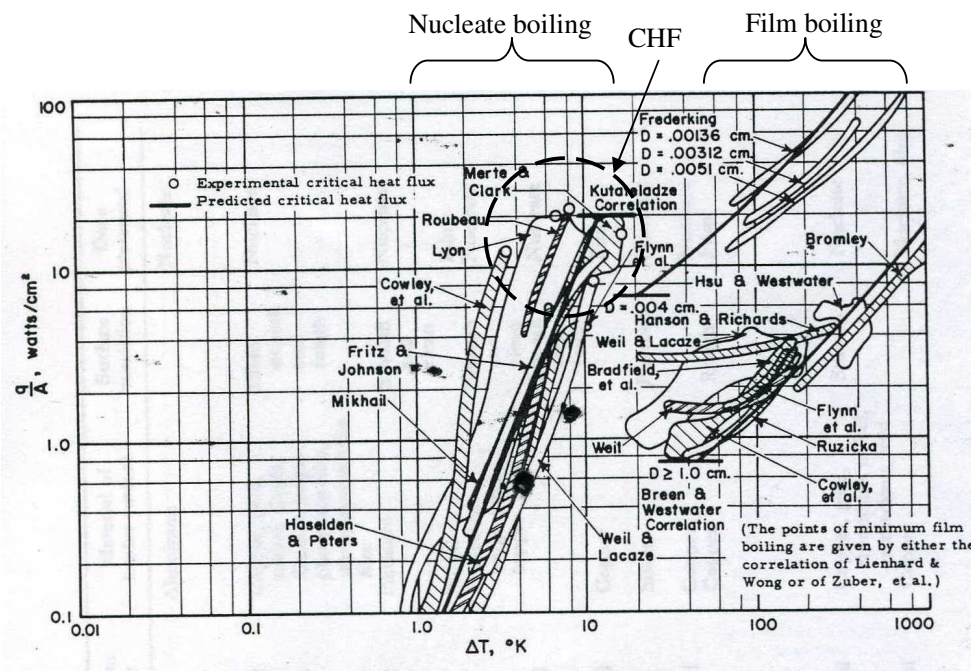


Figure 2.10 Experimental nucleate and film pool boiling of nitrogen at 1 atm [61].

some important review papers were presented by T.B.Jones in 1978 [68], P.H.G.Allen *et al.* in 1995 [69], I.W.Eames et al. in 1997 [70], and S.Laohalertdecha in 2007 [71] respectively. Electric field effects on pool boiling has received a lot of attention because experimental studies reveal an enhanced effect of an electric field on the boiling process; and its greater potential for practical applications such as refrigeration [72] and heat exchange [73]. EHD enhancement of boiling heat transfer has several distinct advantages over conventional passive methods. One is the ability to vary or control the boiling heat transfer coefficient by changing the applied voltage. Another is a significant enhancement in the boiling heat transfer that can be achieved with EHD. Furthermore, the EHD enhancement process contains no moving parts and the electric power assumption is usually negligible. In spite of some advantages obtained from the pool boiling heat transfer enhancement, the electric effect on boiling heat transfer is a complex phenomenon that depends on not only electrical parameters such as the electric field uniformity, the voltage waveshape and electric field polarity but also the thermophysical and electrical properties of liquid such as its dielectric permittivity and electrical conductivity.

In recent years, specific emphasis has been placed on two-phase boiling processes, especially on nucleate boiling processes [74-76], because it is believed that the change in the bubble behaviour in the presence of an electric field is one of the main reasons for the nucleate heat transfer enhancement. Several fundamental studies have been carried out in order to understand the phenomenon. These studies can be largely classified into two groups: studies on the freely suspended bubbles [77] and studies on bubbles attached to an electrode wall [78-80].

Though a lot of liquid materials [69] have been used in experimental studies to obtain more information about the EHD effect, there are few studies on the EHD effects on heat transfer of liquid nitrogen, and most of these are related to EHD pumping [81, 82] that utilizes polarization forces to generate pumping. Rutkowski [83, 84] carried out an experimental study on the influence of electric field on heat transfer of boiling nitrogen. Results have shown that an electric field greatly improves heat transfer in natural convection zone and at the start of nucleate boiling zone.

### **2.4.2 The EHD technique of heat transfer**

The heat transfer enhancement method utilizing an electric field is frequently called the EHD technique of heat transfer. To improve the performance of a heat exchanger for more efficient utilization of thermal energy, enhancing heat transfer and reducing power consumption for transporting a working fluid are two important issues to be considered. In various active techniques of enhancement heat transfer, the EHD technique utilizing an electric field, which is based on electrostatic force or polarization of dielectric fluid, is believed one of the most promising methods, especially applied to enhancement boiling processes, due to its several advantages. These include a reduction of the heat exchanger size for a given rating using only a small transformer and electrode, a smaller consumption of electric power, a significant increase in the heat transfer rate, a reduction of the temperature difference between the fluids and thereby greater thermal efficiency and a quick control of heat transport by easily varying the applied voltage. In real applications, evaporation processes enhanced with an EHD technique for refrigeration systems is expected to be the first large-scale industrial and commercial application.

In microgravity conditions, such as a space station, the EHD technique can provide some promise for thermal control system applications, as electric forces may be used as a replacement for gravity. For example, in a microgravity situation, a reduced gravity results in almost the same specific weights of vapour and liquid. This can cause deterioration of heat transfer due to hindered bubble departure and reduced convective motion. The addition of an electric force can remove bubbles generated during boiling and further enhance heat transfer [85].

### **2.4.3 EHD mechanism**

EHD enhancement of heat transfer refers to the coupling of an electric field with the fluid flow in a dielectric fluid medium. In general, it utilizes an electric field to destabilize or reduce the thermal boundary layer near the heat transfer surface, creating increased turbulence, bulk mixing flow or interfacial vaporization, thereby potentially leading to heat transfer coefficients higher than those achievable by conventional enhancement techniques. Lots of experimental and theoretical research suggests that EHD effects are due to the appearance of electrical body forces on the flow. For a dielectric fluid of electric permittivity  $\epsilon$  ( $\text{F}\cdot\text{m}^{-1}$ ), mass density  $\rho$  ( $\text{kg}\cdot\text{m}^{-3}$ ), and uniform

temperature  $T$ , when subjected to an electric field with strength  $E$  ( $\text{V}\cdot\text{m}^{-1}$ ), the body force per unit volume,  $f_e$  ( $\text{N}\cdot\text{m}^{-3}$ ), can be expressed as [75, 76]

$$\vec{f}_e = q_v \vec{E} - \frac{1}{2} E^2 \nabla \epsilon + \frac{1}{2} \nabla \left[ E^2 \rho \left( \frac{\partial \epsilon}{\partial \rho} \right)_T \right] \quad (2.1)$$

where  $q_v$  is the electric charge density ( $\text{C}\cdot\text{m}^{-3}$ ) in the fluid. The first term on the right side of above equation is the Coulomb force (known as the electrophoretic force) that results from net free charges or ions within the fluid or injected from the electrodes. This term is usually important in single-phase flows where the discharge of EHD current is predominantly responsible for the generation of electrically induced secondary motions and the resulting enhancement mechanism. For example, the generation of an ionic wind in gases from a wire electrode heat transfer surface propelled by the Coulomb force due to the space charge is a typical EHD phenomenon. The second term is the dielectrophoretic force that depends on the field strength and the spatial gradient of permittivity due to non-uniform electric fields, temperature gradients, and phase differences. The third term is the electrostrictive force that is caused by an inhomogeneous electric field strength and the change in dielectric permittivity with temperature and density. Note that these two terms are proportional to the square of the applied electric field and thus are independent of the sign of electric field. It becomes much more significant when the electric field is nonuniform and its intensity is strong. The second and third terms contribute substantially to the EHD body force in phase-change processes such as boiling and condensation where the EHD body force acts on the liquid-vapour interface due to  $\nabla \epsilon$  becoming singular at the liquid-vapour interface, which results in liquid-vapour surface instability. Obviously for higher dielectric permittivity differences between the two phases, the electric field force is greater. The dielectrophoretic force can be expanded as

$$-\frac{1}{2} E^2 \nabla \epsilon = -\frac{1}{2} E^2 \left( \left( \frac{\partial \epsilon}{\partial \rho} \right)_T \nabla \rho + \left( \frac{\partial \epsilon}{\partial T} \right)_\rho \nabla T \right) \quad (2.2)$$

The direction of the force depends on the direction of the increase of  $\epsilon$ . For non-polar fluids, the second term on the right-hand side is zero, and the above equation reduces to

$$-\frac{1}{2}E^2\nabla\epsilon = -\frac{1}{2}E^2\left(\frac{\partial\epsilon}{\partial\rho}\right)_T \nabla\rho \quad (2.3)$$

which indicates that the resultant component force is towards the heated surface. In the case of non-polar fluids, the electrostrictive force can be simplified by using the Clausius-Mossotti law:

$$\rho\left(\frac{\partial\epsilon}{\partial\rho}\right)_T = \frac{(\epsilon - \epsilon_0)(\epsilon + 2\epsilon_0)}{3\epsilon_0} \quad (2.4)$$

as follows:

$$\frac{1}{2}\nabla\left[E^2\rho\left(\frac{\partial\epsilon}{\partial\rho}\right)_T\right] = \nabla\left(E^2\frac{(\epsilon - \epsilon_0)(\epsilon + 2\epsilon_0)}{6\epsilon_0}\right) \quad (2.5)$$

However, in the case of polar fluids, since the electrical permittivity is a function of temperature and density, it is not easy to simplify the expression for the electrostrictive force. This force is a gradient force, thus it cannot produce any vorticity within the fluid and usually is neglected.

In most EHD systems, heating the fluid can cause electrical conductivity and dielectric permittivity gradients within the fluid. Thus, the Coulomb force becomes effective due to the generation of electric charges by the gradient of the electrical conductivity. Moreover, the dielectrophoretic and electrostriction forces become effective due to the variation of dielectric permittivity.

In two-phase fluids, dielectric forces arise from the difference in liquid-vapour dielectric constants. By using the Gauss theorem, the EHD body force can be transformed to the stress (Maxwell stress) as [77]

$$\mathbf{f}_{sj} = \epsilon_j(\mathbf{n} \cdot \mathbf{E})_j \cdot \mathbf{E}_j - \frac{\epsilon_j}{2} E_j^2 \left(1 - \frac{\rho}{\epsilon} \frac{d\epsilon}{d\rho}\right)_j \mathbf{n}_j \quad (2.6)$$

where  $j$  is the liquid or the vapour subscript and  $\mathbf{n}_j$  is the unit normal component in each phase. Equation (2.6) is very helpful for solving problems involving EHD surface instability. Recently, W.Dong [86] and F.Chen [87] used this function to give a full

explanation for their experimental studies on the behaviour of a single bubble in an electric field.

It should be noted that as the EHD phenomenon is a very complex process, the function of EHD body force in Eq. (2.1) is a simplified expression, and it has been generally accepted that it may not represent all forces involved in the EHD effect.

#### 2.4.4 Phase change processes

Phase change processes refer to the boiling or condensation processes. The effect of an electric field on phase change heat transfer enhancement was first observed by Bochirol et al. [88] in an experiment within pool boiling. Several similar studies were also performed by others [68, 89]. Generally, in the applications of EHD to boiling or condensation, an electrode is often placed within the liquid or vapour phases. The electrode is of either positive or negative polarity, while the heat transfer surface is generally electrically grounded, or held at the reverse polarity. This arrangement exposes the fluid to an electrical field, and can significantly enhance the heat transfer effect. The geometry of the electrodes and their spatial arrangement can be of many types, depending on the process and other parameters such as the working fluid properties.

In phase-change processes, the difference between the dielectric constant of the two phases is a contributing factor as mentioned above. Pohl [90] suggested the dielectrophoretic force acting on an insulating sphere of radius  $R$  and permittivity  $\varepsilon_2$  in a surrounding medium with the permittivity of  $\varepsilon_1$  can be given as:

$$f_e = 2\pi R^3 \varepsilon_1 \left( \frac{\varepsilon_2 - \varepsilon_1}{\varepsilon_2 + 2\varepsilon_1} \right) \nabla E^2 \quad (2.7)$$

If  $\varepsilon_2 > \varepsilon_1$ , the sphere is attracted to regions with the highest electric field intensity. If  $\varepsilon_2 < \varepsilon_1$ , the sphere is expelled, which is the case of a vapour bubble in a liquid. For example, in boiling, that means a vapour bubble in a liquid pool will move to the region with lower electric field intensity since the dielectric constant of vapour is always less than that of liquid. However, a drop of liquid in the vapour phase will move to the region of higher electric field intensity. This equation also shows that the direction of the dielectrophoretic force is independent of the sign of the applied field. The

application of a nonuniform electric field during boiling can increase agitation due to bubble motion by the imposition of an effective body force on the bubble. Since boiling is one of the most common phase-change processes, the EHD enhancement mechanism of boiling processes is further described in the following section.

#### **2.4.5 Mechanism of EHD Enhancement boiling heat transfer**

In many experimental studies [72, 73, 75, 76, 91-93] on bubble dynamics and EHD boiling heat transfer, a great enhancement has been obtained by using an applied electric field. At the same time, visual observation also suggests that EHD enhancement is due to the electroconvection effect on fluids and bubble behaviour changing under high fields. Further detailed phenomena can be described such as a reduction in thermal boundary layer, increased convection, bubble deformation and migration and interfacial instabilities. These factors result in heat transfer enhancement. Hence, the mechanism depends not only on electrical properties of the liquid itself such as dielectric permittivity and electrical conductivity but also on other electrical parameters such as the electric field strength, the electric field uniformity, the voltage period and polarity [94-96].

The most important liquid properties affecting the EHD boiling heat transfer are dielectric permittivity and the electric conductivity, and these two electric properties have been reviewed by Turnbull [97]. Essentially, the liquid electrical properties can be represented by the electric relaxation time,  $\tau_e$  defined as

$$\tau_e = \frac{\epsilon}{\lambda_e} \quad (2.8)$$

where  $\epsilon$  is the permittivity ( $F \cdot m^{-1}$ ) and  $\lambda_e$  is the electrical conductivity ( $\Omega^{-1} \cdot m^{-1}$ ) of the liquid. This is because when a fluid with a dielectric permittivity  $\epsilon$  and an electrical conductivity  $\lambda_e$  is excited by an electric field strength  $E$ , the generated electric charge density,  $q_v$ , can be expressed as [77]:

$$q_v = \frac{1}{\tau_e} \mathbf{D} \cdot \nabla \tau_e \quad (2.9)$$

It is resulted in charge accumulation on bubbles surface with surface charge density,  $q_s$  ( $C \cdot m^{-2}$ ), given by [92]:

$$q_s = \varepsilon E \left( 1 - \exp \left( -\frac{\lambda_e t}{\varepsilon} \right) \right) \quad (2.10)$$

This indicates that the effect of the electric field on a fluid depends on the relaxation time defined above. In boiling processes, the electric relaxation time represents the time needed by the free charge to relax from the bulk liquid to the liquid-vapour interface. By comparing  $\tau_e$  value to the characteristic time,  $\tau_c$ , which can be either the bubble detachment period or the period of the applied ac electric field whichever is shorter, the liquid can be determined if it behaves like an insulator or a conductor. If  $\tau_e \gg \tau_c$ , the liquid can be treated as insulator, and the electric field is distributed within both liquid and vapour. Thus, no electrical free charges appear within the liquid or the liquid-vapour interface and the electrical field effect is weak. In this case, the bubbles may detach from the heat transfer surface without being affected by the electric field. However, if  $\tau_e \ll \tau_c$ , the liquid can be considered as a conducting fluid. The electric field is totally excluded from the liquid and the entire voltage drop occurs at the liquid-vapour interface where electrical free charges exist. In this case, the electric field will influence the bubble movement and enhance significantly the boiling process. Some typical values of  $\tau_e$  for liquids boiling at atmospheric pressure taken from published papers are presented in Table 2.1. They are rarely measured in boiling experiments and only quoted from one reference to the next. The sensitivity of the electrical conductivity to contamination may account for some discrepancy between different values of  $\tau_e$ .

Karayianis [93] reported an experimental study on pool boiling of R123 and R11 on a 5-tube smooth tube bundle with rod electrodes under applied voltages up to 25 kV and heat fluxes up to 20 kW/m<sup>2</sup>. With R123, A significant enhancement ratio of up to 9.3 was obtained. While with R11, which has a long relaxation time, the enhancement by the electric field was only marginal due to negligible free charge effects. However, the enhancement increased (up to 8.5 times more than that without an electric field) with the addition of some ethanol to the R11 under a voltage of 25 kV and heat flux of  $5.8 \times 10^3$  W/m<sup>2</sup> condition was reported by Ogata and Yabe [91, 92], it is believed that ethanol is a conductive liquid which can change electrical conductivity of the mixture. This indicates there is a strong dependent relationship between the magnitude of EHD enhancement and electrical conductivity and, hence, the charge relaxation time. It

Table 2.1 Electrical properties of liquids boiling at 1 atm

Fluid	T <sub>sat</sub> (°C)	ε	λ <sub>e</sub> (Ω <sup>-1</sup> m <sup>-1</sup> )	τ <sub>e</sub> (s)	τ <sub>c</sub> (s)	Refs.
R11	25	2.28	1.6× 10 <sup>-11</sup>	1.3	0.02	[73, 92, 93]
R11+C2H5OH (2 wt%)	---	---	---	9.2× 10 <sup>-3</sup>		[92]
R113	47	2.40	1.0× 10 <sup>-11</sup>	2.12		[77]
			7.7× 10 <sup>-9</sup>	2.76× 10 <sup>-3</sup>	*a	[75]
			2.2× 10 <sup>-11</sup>	0.97		[73, 92]
R113+C2H5OH (4 wt%)	---	---	---	5.7× 10 <sup>-3</sup>		[92]
R123	28	3.42	3.4× 10 <sup>-8</sup>	0.9× 10 <sup>-3</sup>	*b	[75, 77]
					0.017	[93]
n-pentane	36	1.80	6.7× 10 <sup>-9</sup>	2.4× 10 <sup>-3</sup>		[77]
			4.7× 10 <sup>-9</sup>	3.4× 10 <sup>-3</sup>	*c	[75]
FC-72	56	1.75	1.0× 10 <sup>-13</sup>	155	0.02	[73]
Freon-113	---	---	---	10	0.01	[76]

---: no information given in relevant paper.

\*a,\*b,\*c: bubble detachment period is calculated and depends on the heat flux, detailed information can be found at corresponding references.

should be noted that a high conductivity value may limit the voltage applied to a liquid in order to avoid electrical breakdown even though it can increase the heat transfer. Oh and Kwak [73] investigated experimentally the effect of a dc electric field on nucleate boiling heat transfer for R11, R113 and FC72 using a single-tube shell/tube heat exchanger. A maximum heat transfer enhancements of 130% for R11 and 180% for R113 at a wall superheat of about 10 K were obtained and no electric field effect on the boiling heat transfer was observed for FC72, which has the longest relaxation time (see Table 2.1). Zaghdoudi and Lallemand [75] investigated the influence of a uniform electric field on the nucleate boiling heat transfer on a horizontal copper plate with a mesh electrode with n-pentane, R113 and R123. It was found the heat transfer enhancement depends on the property of the fluid and on the heat flux. For low heat flux, the enhancement ratio was large for all three fluids and decreased when the heat flux approached the critical condition, this is because a high heat flux can reduce the

bubble detachment period. For n-pentane and R-113, the bubble detachment period may be smaller than their corresponding relaxation time. Hence, the generated bubbles float to the free surface without being affected by the electric field. For R-123, the bubble detachment period is greater than the relaxation time of the electric charge whatever the heat flux, consequently, up to 500% enhancement is obtained. Kweon's study [76] on nucleate boiling enhancement and bubble dynamics using a nonuniform dc electric field has shown that the effect of the electric field on bubble behaviours in pool boiling of Freon-13 can be explained by the dielectrophoretic force rather than the Coulomb force due to Freon-13's relaxation time of 10 s that is much greater than the bubble detachment period of 0.01s.

In the boiling process, it is important to ensure a high degree of nonuniformity in electric field strengths in the vicinity of the heat transfer surface so that the resulting EHD force on the bubbles is comparable or higher than the gravitational force. The acceleration of the bubble due to EHD can cause agitation of the neighboring boundary layer liquid and thus improve heat transfer rates. In addition, the heat transfer rates can be greatly enhanced if the bubbles are made to slide along the heat transfer surface, leading to an increased evaporation rate from the thin superheated microlayer. This suggests that the heat transfer surface should be chosen to give a maximum degree of field nonuniformity. For example, the low fin tube is an excellent surface for EHD boiling enhancement. By using a coaxial cylindrical electrode [98] a nonuniform electric field can be introduced around the fin tube which can significantly enhance the heat transfer rate. This has been confirmed by Cooper's experiment [98] on the effect of an electric field applied to boiling of R114 on a finned tube.

In summary, the mechanism of EHD enhancement boiling heat transfer depends not only on electrical properties of the liquid itself but also on other electrical parameters. In addition, the combined effects of bubble deformation and the vigorous motion of bubbles along the heat transfer surface along with the effect of electroconvection on fluids also plays a role in enhancement boiling heat transfer. Besides, other effects that may enhance boiling heat transfer include:

- Instability of the vapour-liquid interface. This induces perturbations and waves at the surface of a boiling liquid, and destabilizes the thin micro-layer underneath the bubbles, which is able to increase the heat transfer [99].

- Suppression or elimination of boiling hysteresis, thereby decreasing the degree of superheat required to start nucleate boiling [69, 70, 94]. For nucleate boiling, the degree of superheat needed for bubble growth is believed to depend on the surface tension of the liquid-vapour interface, which has been reported to vary with electric field at reduced superheat [69]. Once boiling begins, initiated by an electric field at a low superheat, it still could continue without having to maintain the electric field.
- Increasing the number of bubbles by breaking up large bubbles and decreasing the bubble detachment diameter. This creates more turbulence [86, 91].
- Improvement of the wetting of heated surface due to the decrease of surface tension in the presence of an electric charge [100].

## 2.5 Summary

The bubble generation mechanism has been described, and studies on the thermal bubble behaviour in liquid nitrogen under electric fields reviewed according two different viewpoints, i.e. electric insulation and thermal stability, respectively. Bubble behaviour studies were discussed according to four kinds of electrode system arrangements under uniform and non-uniform electric fields. V-t characteristics of liquid nitrogen and thermal bubble breakdown have also been detailed. Heat transfer into liquids which cause boiling have been analysed and summarised. Finally, the EHD phenomenon has been described and fundamental equations governing the EHD body force and the mechanisms involved in heat transfer enhancement presented. From this review of the literature, it can be concluded that there have been very few studies regarding the effects of electric fields on boiling heat transfer of liquid nitrogen.

## Chapter 3

# **Thermal Bubble in a Non-uniform Electric Field: Conductor-Plane Electrode System**

### **3.1 Introduction**

It is well known that bubble behaviour in non-uniform fields is of great interest in the study of both electrically enhanced boiling heat transfer[72, 73, 76, 83, 84] as well as prebreakdown and breakdown phenomena [30, 33, 36, 37] in the presence of thermally induced bubbles. This chapter describes a theoretical and experimental study of the influence of a non-uniform electric field on bubble motion and behaviour in liquid nitrogen. The electric field effect on the bubble motion as it rises due to buoyancy within applied dc electric fields is quantitatively investigated by performing experiments over a range of electric stresses using a conductor-plane gap.

In this experiment, bubbles are thermally induced by a heater mounted below the electrode arrangement, and bubble behaviour and related characteristics in liquid nitrogen are recorded by a high-speed camera. Experimental observations and quantitative results are then presented and discussed.

## 3.2 Theoretical study of bubble behaviour

Investigations by other researchers into bubble trajectory in insulating dielectric liquids, such as liquid nitrogen, have been reported [7, 101, 102]. Bubble motion in liquid nitrogen under dc applied voltages was analyzed numerically with a cylinder-to-plane electrode system [7] and the inclined plane electrode system [101]. Fundamental motion equations and forces analysis have been presented and discussed. It can be hypothesised that in the presence of an electric field, the forces mainly exerted on a bubble are due to the electric field, the bubble drag and its buoyancy. Using suitable equations for these forces, it is possible to simulate the motion of a bubble in the presence of a non-uniform electric field.

### 3.2.1 Modelling of bubble motion

A model of thermally induced bubble motion in a conductor-plane gap is shown in Figure 3.1.

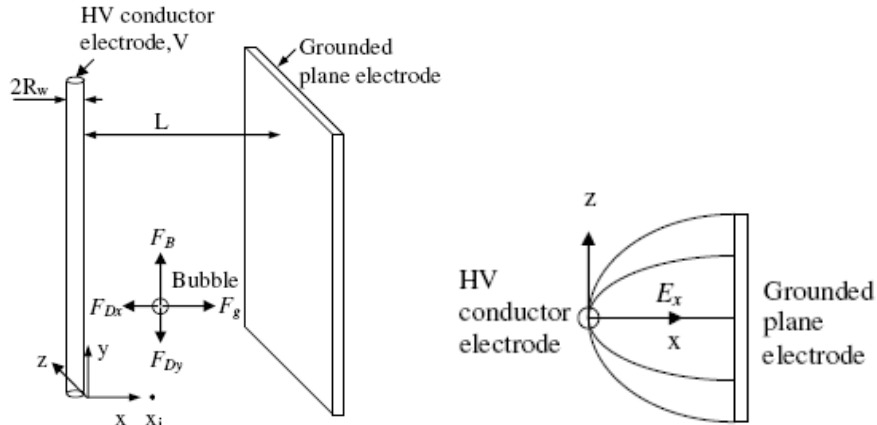


Figure 3.1 Electrode system and coordinates for analysis of bubble motion

In this 2-dimensional model,  $V$  is the applied voltage difference between two electrodes in V,  $L$  the electrode gap in m,  $R_w$  the radius of the conductor in m,  $R$  the bubble radius in m,  $x_i$  the initial location in m at which the bubble is released and  $x$  is the distance in m away from the conductor. Other parameters are detailed in section 3.2.3. Main electrode parameters on the basis of the experiment arrangement described in section 3.3.1 are shown in Table 3.1.

Table 3.1 Experimental electrode arrangement parameters

The distance between both electrodes	$L=16$ mm
The radius of the conductor	$R_w=0.75$ mm

### 3.2.2 Simulation of electric field distribution

The electric field distribution around a conductor electrode immersed in liquid nitrogen has been modelled using finite element analysis (FEA) simulation software. Figure 3.2(a) shows lines of equipotential between the conductor and plane electrode. 0 per unit (p.u.) is applied to the plate electrode represented by the bottom edge of the plane of the figure. The conductor electrode shown as a grey circle area is held at 1p.u.. The contours represent ten spaced gradations between 0 and 1p.u.. Due to the electric field concentration, the electric gradient in the vicinity of the conductor is greater and its electric field more non-uniform compared to the region closer to the plane electrode. The electric field is asymmetric around the conductor and is greatest where the conductor faces the plane electrode. Figure 3.2(b) shows that the normalized electric field strength perpendicular from the plane electrode to the conductor. Here,  $E_0$  is the average electric field strength defined as voltage divided by distance,  $E$  the electric field strength at distance  $x$  from the surface of the conductor,  $x$  the distance in mm to the conductor electrode. As shown in Figure 3.2(b), the electric field is concentrated near the conductor and its distribution is also highly non-uniform. At the conductor surface, the magnitude of the electric field is about 6 times greater than that of the average electric field strength. This large non-uniform electrical field may mean that bubbles experience significant force when passing between the two electrodes.

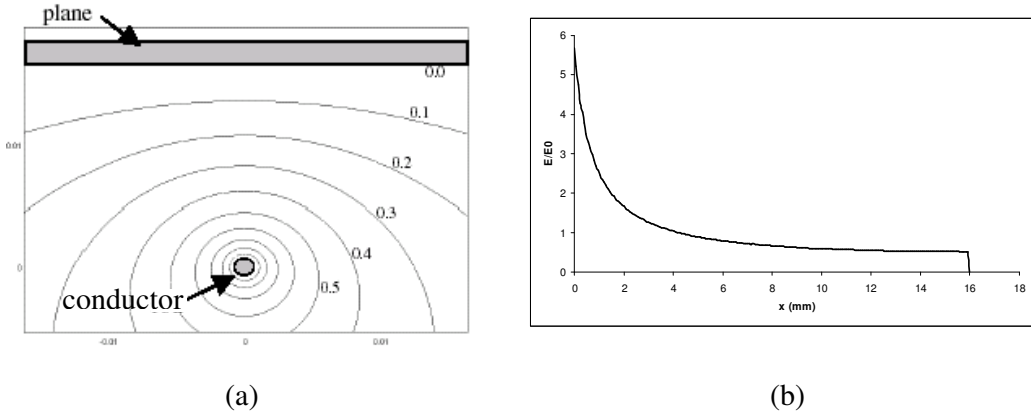


Figure 3.2 Electric field distribution on a conductor-plane electrode.

- (a) Distribution of equipotentials between the conductor and plane electrode
- (b) Electric field strength between conductor and plane electrode

### 3.2.3 Electric field force analysis

The effective electric field force,  $F_e$  (N), exerted on a dielectric liquid can be expressed as [75]:

$$\mathbf{F}_e = q_v \mathbf{E} - \frac{1}{2} \mathbf{E}^2 \nabla \epsilon + \frac{1}{2} \nabla \left[ \mathbf{E}^2 \left( \frac{\partial \epsilon}{\partial \rho} \right) \rho \right] \quad (3.1)$$

where  $q_v$  is the free charge density ( $\text{C}\cdot\text{m}^{-3}$ ),  $\epsilon$  is the permittivity ( $\text{F}\cdot\text{m}^{-1}$ ),  $\mathbf{E}$  is the electric field strength ( $\text{V}\cdot\text{m}^{-1}$ ) and  $\rho$  is the liquid density ( $\text{kg}\cdot\text{m}^{-3}$ ). This force is due to the electric free charge that contributes to conduction current, convection current and to the polarization of the medium. In (3.1), the first term is the Coulomb force exerted on the electric charges within the dielectric fluid. The second term is the dielectrophoretic force due to the spatial gradient of the dielectric permittivity in the fluid. Physically, this force acts on the polarization charges appearing in the dielectric medium under the application of an electric field. The third term is the electrostrictive force due to variation of dielectric permittivity with density and the non-uniformity of the electric field in the medium.

Since liquid nitrogen is a non-polar dielectric liquid with very low conductivity, the electric current through liquid nitrogen can be considered negligible. In addition, the relaxation time of liquid nitrogen, which is expressed as the ratio of the permittivity to electrical conductivity, is estimated to be several orders of magnitude greater than the time period of this dynamic process. In this case, it can be assumed that there are no appreciable free charges generated in the liquid nitrogen, and hence the Coulomb force effect is negligible. Thus, only the second and third terms of (3.1) contribute to the electric field force. When a bubble is in an electric field, the dielectrophoretic force dominates at the bubble interface, where the gradient of dielectric constant is a maximum.

In the case of the non-uniform field, the force  $\mathbf{F}_g$  (N) called the gradient (or dielectrophoretic) force acting on a suspended spherical bubble has been expressed by Pohl [90] as

$$\mathbf{F}_g = 2\pi R^3 \frac{\epsilon_l(\epsilon_g - \epsilon_l)}{(\epsilon_g + 2\epsilon_l)} \nabla \mathbf{E}^2 \quad (3.2)$$

where  $\epsilon_l$  is the dielectric permittivity of liquid nitrogen outside the bubble ( $\text{F}\cdot\text{m}^{-1}$ ),  $\epsilon_g$  is the dielectric permittivity of saturated gas in the bubble ( $\text{F}\cdot\text{m}^{-1}$ ),  $R$  is the bubble radius (m), and  $\mathbf{E}$  is the electric field intensity ( $\text{V}\cdot\text{m}^{-1}$ ) at the relevant bubble location. This

force is due to the combined effect of the different permittivities of liquid and bubble and the non-uniformity of the electric field. It is proportional to the square of the gradient of the electric field strength. Therefore, it becomes much more significant when the electric field is non-uniform and of high intensity. This force will act to drive bubbles towards the lower electric field region.

### 3.2.4 Equations of bubble motion

The fundamental equation of bubble motion is defined as [7]

$$M_{\text{eff}} \dot{\mathbf{v}} = \mathbf{F}_e + \mathbf{F}_D + \mathbf{F}_B \quad (3.3)$$

where  $M_{\text{eff}}$  the effective mass of the bubble in motion (kg),  $\dot{\mathbf{v}}$  the acceleration of the bubble ( $\text{m}\cdot\text{s}^{-2}$ ),  $\mathbf{v}$  the bubble vector velocity ( $\text{m}\cdot\text{s}^{-1}$ ),  $\mathbf{F}_e$  the electric field force (N),  $\mathbf{F}_D$  the drag force (N), and  $\mathbf{F}_B$  the buoyancy (N). At the prebreakdown stage in liquid nitrogen, there are no ionization events inside the bubble and the net charge on the bubble can be considered negligible. In this case, the predominant electric field force acting on the bubble is the gradient force  $\mathbf{F}_g$ , defined by Equation (3.2). Hence, the fundamental force equation of a suspended bubble is

$$M_{\text{eff}} \dot{\mathbf{v}} = \mathbf{F}_g + \mathbf{F}_D + \mathbf{F}_B \quad (3.4)$$

In the model represented by Figure 3.1, the effective mass of a spherical bubble and forces acting on the bubble are numerically determined using the following equation for effective mass [102]

$$M_{\text{eff}} = \frac{4}{3} \pi R^3 (\rho_g + \frac{1}{2} \rho_l) \quad (3.5)$$

where  $R$  is the bubble radius (m),  $\rho_l$  is the density of liquid nitrogen ( $\text{kg}\cdot\text{m}^{-3}$ ) and  $\rho_g$  the gas nitrogen density ( $\text{kg}\cdot\text{m}^{-3}$ ) at the saturation temperature. When the viscosity of the gas in the bubble is neglected, the drag force in the stationary liquid nitrogen is given by [7]

$$\mathbf{F}_D = 4\pi\mu R\mathbf{v} \quad (3.6)$$

where  $\mu$  is the dynamic viscosity of liquid nitrogen( $\text{kg}\cdot\text{m}^{-1}\cdot\text{s}^{-1}$ ). The buoyancy force,  $\mathbf{F}_B$ , is defined as [7]

$$\mathbf{F}_B = \frac{4}{3}\pi R^3 (\rho_l - \rho_g) \mathbf{g} \quad (3.7)$$

where  $\mathbf{g}$  is the gravitational acceleration ( $\text{m}\cdot\text{s}^{-2}$ ).

The gradient force,  $\mathbf{F}_g$ , requires the electric field intensity at the bubble location to be known. The electric field strength  $\mathbf{E}$  in  $x$ -directional of the conductor in Figure 3.1 can be determined using [76]

$$E_x = \frac{2V\sqrt{L^2 - R_w^2}}{(L^2 - R_w^2 - (L-x)^2) \ln[\frac{L + \sqrt{L^2 - R_w^2}}{R_w}]} \quad (3.8)$$

In order to determine  $\mathbf{F}_g$ , it is necessary to evaluate  $\nabla E_x^2$ , which for the experimental electrode arrangement is

$$\nabla E_x^2 \approx \frac{d}{dx}(E_x^2) = \frac{-16V^2(L^2 - R_w^2)}{\left(\ln[\frac{L + \sqrt{L^2 - R_w^2}}{R_w}]\right)^2 [(L^2 - R_w^2) - (L-x)^2]^3} \quad (3.9)$$

substituting this expression into Equation (3.2) yields:

$$F_{gx} = -32\pi R^3 V^2 \frac{\epsilon_l(\epsilon_g - \epsilon_l)}{(\epsilon_g + 2\epsilon_l)} \frac{L^2 - R_w^2}{\left(\ln[\frac{L + \sqrt{L^2 - R_w^2}}{R_w}]\right)^2 [(L^2 - R_w^2) - (L-x)^2]^3} \quad (3.10)$$

In order to simulate bubble trajectory, the following assumptions have to be made:  
Firstly, the bubble is released from position  $(x_i, 0)$  with  $y$ -direction initial velocity,  $v_{yi}$ .  
Secondly, the bubble radius is no more than 1 mm and any bubble deformation is negligible.  
Thirdly, the density of the gas,  $\rho_g$ , in the bubble is negligible compared to the density of liquid nitrogen  $\rho_l$ . Then, the dynamic equations of bubble motion can be rearranged in the  $x$  and  $y$ -directions as:

$$\left\{ \begin{array}{l} M_{eff} \dot{v}_x = F_{gx} - F_{Dx} \end{array} \right. \quad (3.11)$$

$$\left\{ \begin{array}{l} M_{eff} \dot{v}_y = F_B - F_{Dy} \end{array} \right. \quad (3.12)$$

where  $v_x$  is bubble velocity in the  $x$ -direction ( $\text{m}\cdot\text{s}^{-1}$ ) and  $v_y$  is bubble velocity in the  $y$ -direction ( $\text{m}\cdot\text{s}^{-1}$ ).  $F_{Dx}$  and  $F_{Dy}$  are the  $x$ -direction and  $y$ -direction components of the drag force (N), respectively. Equation (3.11) and (3.12) can be rewritten by substituting for the effective mass and the term for gradient, buoyancy and drag forces. In the  $y$ -direction, this yields

$$\ddot{y} + \frac{3\mu}{R^2(\rho_g + 0.5\rho_l)} \dot{y} = \left( \frac{\rho_l - \rho_g}{\rho_g + 0.5\rho_l} \right) \cdot g \quad (3.13)$$

This differential equation has a solution of the form

$$y = C_3 + C_4 e^{\left( -\frac{3\mu}{R^2(\rho_g + 0.5\rho_l)} t \right)} + \frac{R^2(\rho_l - \rho_g)g}{3\mu} t \quad (3.14)$$

where the coefficients  $C_3$  and  $C_4$  can be determined from known initial conditions. For the  $x$ -direction, the resulting differential equation is not as straightforward to solve.

Substitution yields

$$\begin{aligned} \ddot{x} + \frac{3\mu}{R^2(\rho_g + 0.5\rho_l)} \dot{x} + \frac{24}{(\rho_g + 0.5\rho_l)} \frac{\varepsilon_l(\varepsilon_g - \varepsilon_l)}{(\varepsilon_g + 2\varepsilon_l)} \\ \dots \times \frac{L^2 - R_w^2}{\left( \ln \left[ \frac{L + \sqrt{(L^2 - R_w^2)}}{R_w} \right] \right)^2} V^2 \frac{L - x}{((L^2 - R_w^2) - (L - x)^2)^3} = 0 \end{aligned} \quad (3.15)$$

In order to find a solution to (3.15), it is necessary to approximate its terms that are a function of the  $x$  variable. Using the values for  $R_w$  and  $L$  of the experiment described in Table 3.1, the value of

$$f(x) = \frac{L - x}{((L^2 - R_w^2) - (L - x)^2)^3} \quad (3.16)$$

as a function of  $x$  can be evaluated as shown in Figure 3.3.

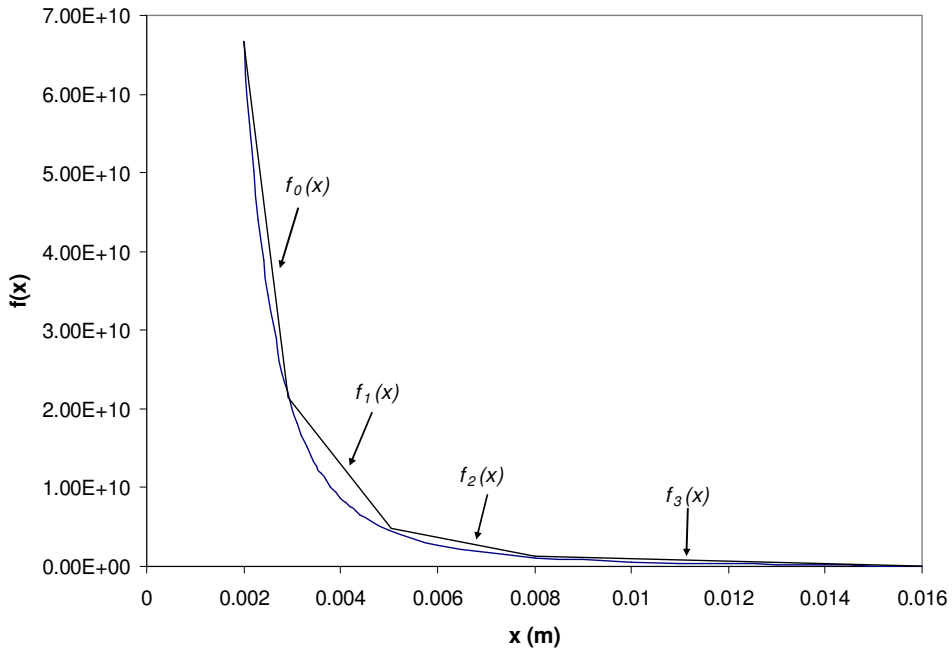


Figure 3.3 The function  $f(x)$  and linear approximations over the region  $0.002 \leq x \leq 0.016$

With reference to the Figure 3.3, it is necessary to evaluate (3.15) over the range  $0.002 \leq x \leq 0.016$ . This has been achieved using four straight line approximations defined as

$$\left. \begin{array}{l} f_0(x) = -4.660 \times 10^{13}x + 1.599 \times 10^{11} \quad 0.002 \leq x < 0.003 \\ f_1(x) = -7.785 \times 10^{12}x + 4.346 \times 10^{10} \quad 0.003 \leq x < 0.005 \\ f_2(x) = -1.130 \times 10^{12}x + 1.018 \times 10^{10} \quad 0.005 \leq x < 0.008 \\ f_3(x) = -1.425 \times 10^{11}x + 2.280 \times 10^9 \quad 0.008 \leq x \leq 0.016 \end{array} \right\} \quad (3.17)$$

Consequently (3.15) simplifies to

$$\left. \begin{array}{l} \ddot{x} + a\dot{x} - 4.660 \times 10^{13}bV^2x = -1.599 \times 10^{11}bV^2 \quad 0.002 \leq x < 0.003 \\ \ddot{x} + a\dot{x} - 7.785 \times 10^{12}bV^2x = -4.346 \times 10^{10}bV^2 \quad 0.003 \leq x < 0.005 \\ \ddot{x} + a\dot{x} - 1.130 \times 10^{12}bV^2x = -1.018 \times 10^{10}bV^2 \quad 0.005 \leq x < 0.008 \\ \ddot{x} + a\dot{x} - 1.425 \times 10^{11}bV^2x = -2.280 \times 10^9bV^2 \quad 0.008 \leq x \leq 0.016 \end{array} \right\} \quad (3.18)$$

where  $a = \frac{3\mu}{R^2(\rho_g + 0.5\rho_l)}$  (3.19)

$$b = \frac{24}{(\rho_g + 0.5\rho_l)} \frac{\varepsilon_i(\varepsilon_g - \varepsilon_l)}{(\varepsilon_g + 2\varepsilon_l)} \frac{L^2 - R_w^2}{\left( \ln \left[ \frac{L + \sqrt{(L^2 - R_w^2)}}{R_w} \right] \right)^2} \quad (3.20)$$

Equations (3.18) have solutions of the form

$$\left. \begin{array}{l} x = e^{-\frac{a}{2}t} (C_{01} \cos \beta_0 t + C_{02} \sin \beta_0 t) + 0.0034 \quad 0.002 \leq x < 0.003 \\ x = e^{-\frac{a}{2}t} (C_{11} \cos \beta_1 t + C_{12} \sin \beta_1 t) + 0.0056 \quad 0.003 \leq x < 0.005 \\ x = e^{-\frac{a}{2}t} (C_{21} \cos \beta_2 t + C_{22} \sin \beta_2 t) + 0.0090 \quad 0.005 \leq x < 0.008 \\ x = e^{-\frac{a}{2}t} (C_{31} \cos \beta_3 t + C_{32} \sin \beta_3 t) + 0.0160 \quad 0.008 \leq x \leq 0.016 \end{array} \right\} \quad (3.21)$$

$$\text{where } \left. \begin{array}{l} \beta_0 = 0.5\sqrt{-1.864 \times 10^{14} bV^2 - a^2} \\ \beta_1 = 0.5\sqrt{-3.114 \times 10^{13} bV^2 - a^2} \\ \beta_2 = 0.5\sqrt{-4.52 \times 10^{12} bV^2 - a^2} \\ \beta_3 = 0.5\sqrt{-5.70 \times 10^{11} bV^2 - a^2} \end{array} \right\} \quad (3.22)$$

and initial conditions can be used to determine the trajectory in the  $x$ -direction over the region  $0.002 \leq x < 0.003$  and then the terminal conditions evaluated to provide initial conditions for the trajectory over the region  $0.003 \leq x \leq 0.005$ , and so on for the complete range of  $x$ . In order to solve (3.14) and (3.21), the thermodynamic and electrical properties of nitrogen are required. The values used are given in Table 1.1 and Table 1.2.

### 3.2.5 Theoretical results

The theoretical results obtained for resultant bubble trajectory under different voltages are plotted in Figure 3.4. Here, the bubble radius is assumed to be 0.6 mm on the basis of preliminary experiments. Figure 3.4 shows simulation results for bubble trajectory as a function of release position and applied field at an initial bubble velocity of either 0.22 m/s (a-c) or 5 m/s (d-f) in the  $y$ -direction.

With reference to Figure 3.4, in general, the bubble trajectories are towards the plane electrode (positioned 16 mm away from the conductor), and the higher the applied voltage is, the more significant the electric field effect will be. Consequently, the lower will be the bubble collision height with the plane electrode. When the initial velocity in the  $y$ -direction is defined as a constant value, the release position has a significant

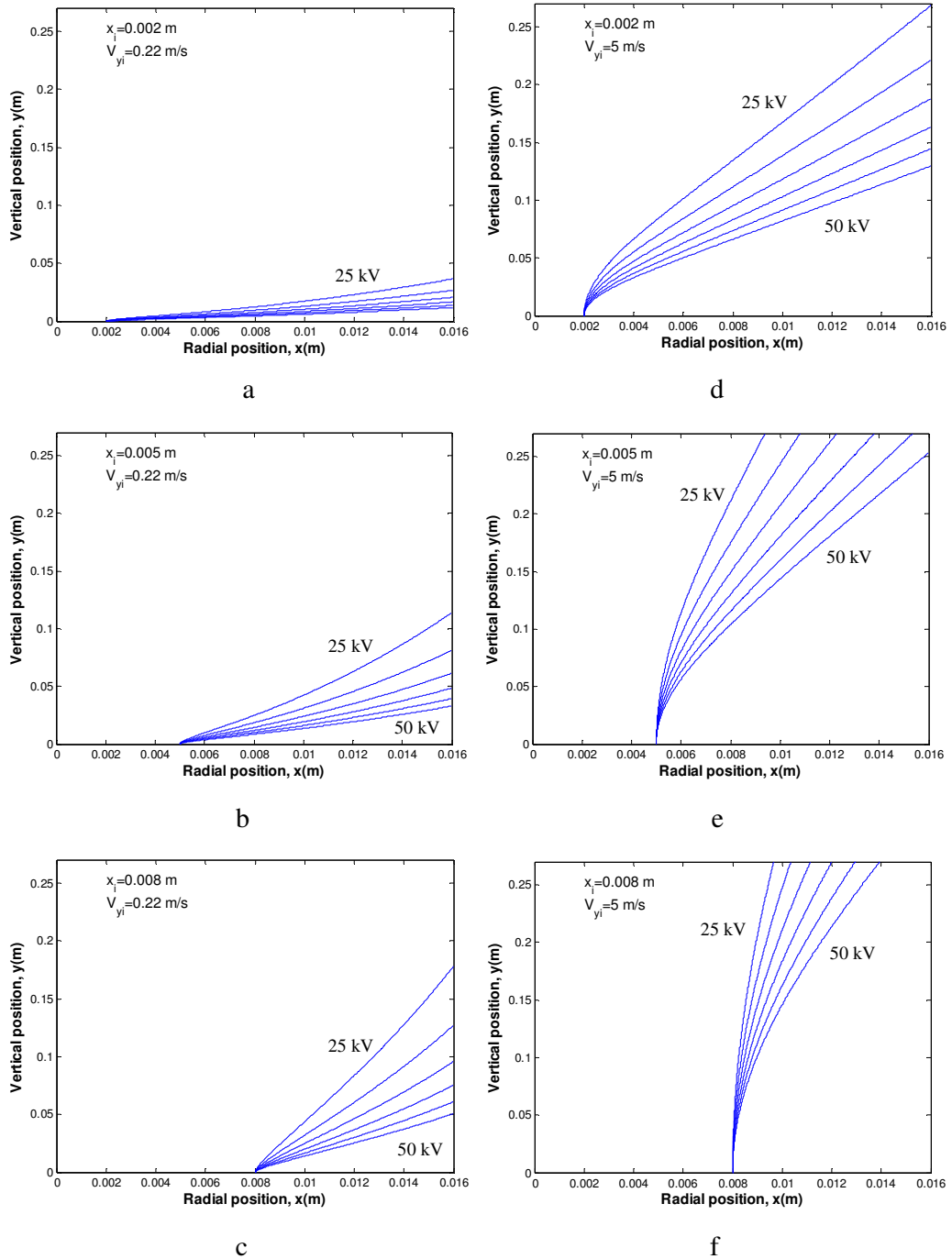


Figure 3.4 Bubble stream trajectories for six voltage values (25, 30, 35, 40, 45, 50 kV from top to bottom in each figure), Nitrogen bubble in LN<sub>2</sub> ( $R = 0.6 \text{ mm}$  on the basis of our preliminary experiments)

a:  $x_i=0.002 \text{ m}$ ,  $V_{yi}=0.22 \text{ m/s}$ , b:  $x_i=0.005 \text{ m}$ ,  $V_{yi}=0.22 \text{ m/s}$ , c:  $x_i=0.008 \text{ m}$ ,  $V_{yi}=0.22 \text{ m/s}$ ,  
d:  $x_i=0.002 \text{ m}$ ,  $V_{yi}=5 \text{ m/s}$ , e:  $x_i=0.005 \text{ m}$ ,  $V_{yi}=5 \text{ m/s}$ , f:  $x_i=0.008 \text{ m}$ ,  $V_{yi}=5 \text{ m/s}$ ,

effect on bubble trajectory. The closer the release position to the conductor, the more significant the electric field effect. This is because the electric field strength is very high near to the conductor (Figure 3.2). Comparing the bubble trajectory for the same release position, the initial velocity of bubble in y-direction,  $V_{yi}$  has also an obvious effect on bubble trajectory. For example, the bubble trajectories in Figure 3.4e are completely different to those in Figure 3.4b although the bubble is released at the same position (5mm away from the conductor). The main reason is the initial velocity (5m/s) of bubble in Figure 3.4e is much larger than (0.22m/s) of bubble in Figure 3.4b.

With reference to the detailed experimental arrangement (see 3.3.1), the bubbles are thermally generated 10 mm below the electrodes, and the nucleation point is positioned 5 mm across from the conductor. The gradient force acts to move the bubble away from the conductor, and consequently it can be assumed that the generated bubbles cannot be closer than 5 mm to the conductor when they enter the space between the two electrodes. With reference to Figure 3.3, it is only necessary to evaluate (3.15) over the range  $0.005 \leq x \leq 0.016$ . Consequently, the theoretical results obtained for the resultant bubble trajectory under different voltages are plotted in Figure 3.4b. With reference to Figure 3.4b, the initial bubble position is assumed to be 5 mm distant from the conductor electrode (at 0 mm). In this case, the initial velocity in the y-direction is assumed to be  $0.22 \text{ m}\cdot\text{s}^{-1}$ . The bubble trajectories are towards the plane electrode (positioned 16 mm away from the conductor). The results also indicate that the higher the applied voltage is, the more significant the electric field effect will be, and consequently, the lower will be the bubble collision height with the plane electrode. In addition, Figure 3.5 shows theoretical results of bubble trajectories for different release points under the same voltage of 35 kV. It is clear that the position of the bubble when it enters the electrode region has a significant effect on how far it travels in the y-direction before colliding with the plane electrode. Due to eddy shedding effect (bubbles rise in oscillating columns), the bubbles enter the electrode area over a range of distances from the conductor electrode. It is highly unlikely for any bubble to be closer than 5 mm away from the conductor. Consequently, when analyzing bubble image data, in order to validate the bubble motion model, it is important to carefully assess the minimum collision height on the plane electrode as a function of the applied voltage.

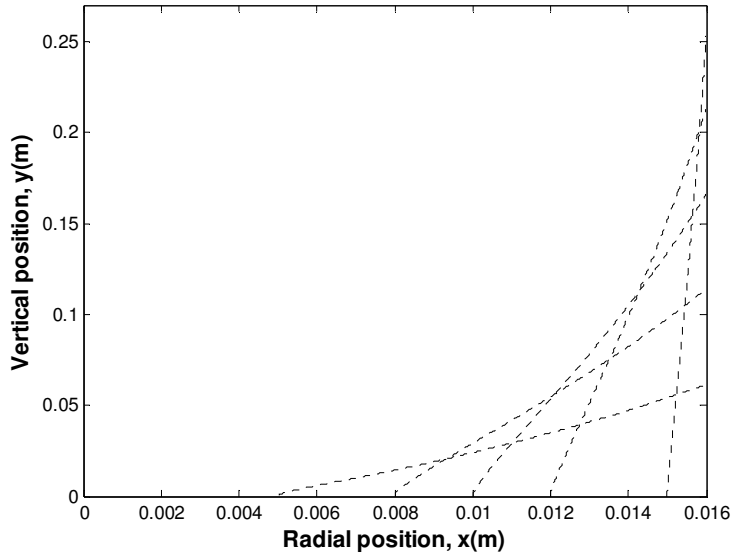


Figure 3.5 Bubble stream trajectories for five different release points under the same voltage value of 35 kV. Nitrogen bubble in LN<sub>2</sub> ( $R = 0.6$  mm and  $v_{yi} = 0.22$  m·s<sup>-1</sup> on the basis of preliminary experiments)

### 3.3 Experimental study of bubble behaviour

#### 3.3.1 Experiment setup and procedure

A schematic diagram of the experimental apparatus is shown in Figure 3.6. The apparatus consisted of a cryostat, a high voltage power supply, a polished single cylinder with a heater, a camera, and a conductor-to-plane electrode system.

The cryostat used in the experiment is made of two LN<sub>2</sub> glass vessels: the inner one is used for the test and the outer one provides thermal stability. The vessels were silver coated to limit radiant heat loss and contain observation windows. Through the windows, bubble behaviour was observed and digital images obtained. The outer cylindrical glass vessel is around 1.24 m tall with a 200 mm inner diameter. The inner cylindrical glass vessel is 1.24 m tall with a 124 mm inner diameter. The electric field is applied by means of a high-voltage dc power supply that provides voltages of up to 50 kV. In order to create a non-uniform electric field, a conductor-plane electrode configuration is used. The conductor electrode is connected to the high voltage dc supply and is made of copper (1.5 mm diameter and 270 mm long). The plane electrode is electrically grounded and is made of aluminium (270 mm high, 72 mm wide and 2 mm thick). The distance between the two electrodes is 16 mm. The single cylinder

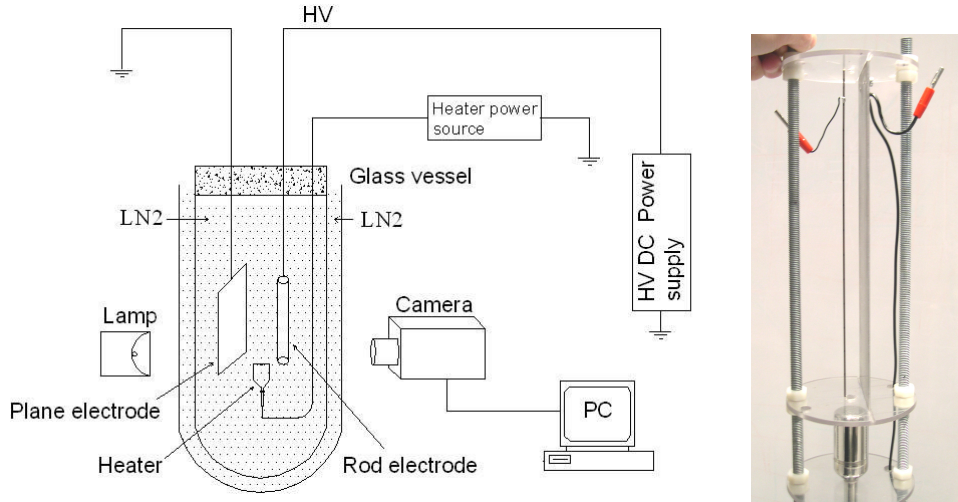


Figure 3.6 Schematic diagram of the experiment

(with a heater inside) polished stainless steel surface of diameter 30 mm was manufactured with a blind hole of 100  $\mu\text{m}$  diameter in the centre of the top surface. Behind this artificial cavity, a heater is mounted to provide a controllable heat source. The heater power was set to 0.36 W in order to produce successive streams of bubbles. That is, the generation of vapour bubbles takes place in a cavity on the heater surface, below the electrode arrangement. The top of the heater was positioned 10 mm below the bottom of the electrode arrangement with the bubble cavity 5 mm from the conductor and directly between the conductor-plane electrodes. A high-speed digital camera (MotionXtra HG-100K) was used to observe the dynamic behaviour of the bubbles between electrodes. It is capable of a frame rate of up to 100000 fps. In this experiment, the frame rate is set to 1000 fps. A sequence of images of bubble motion was recorded by the camera, over a range of dc voltages from -50 kV to +50 kV.

### 3.3.2 Experimental results and discussion

Experimental tests have been carried out with saturated liquid nitrogen (commercial grade) at atmospheric pressure. The two open-top cryostat vessels were filled with liquid nitrogen. Data, including voltage measurements and images were recorded after steady state conditions within the cryostat were realised.

#### 3.3.2.1 Effect of applied voltage on bubble behaviour

With no field applied, bubbles rise in oscillating columns in the conductor-to-plane gap

due to the combination force produced by buoyancy and drag acting on the bubbles. Typical results are shown in Figure 3.7(a) and Figure 3.8(a).

### 3.3.2.1.1 Positive polarity

For these experiments, the polarity of the conductor electrode was positive and the plane electrode along with the heater cylinder was electrically grounded. For applied voltages lower than 20 kV, bubbles were weakly influenced by the electric field, and bubble motion was similar to that observed with no electric field. When the applied voltage was higher than 20 kV, bubbles tended to move closer to the plane electrode. The higher the voltage, the quicker the bubbles moved to the plane electrode, eventually colliding with it, and then continuing to rise colliding with the plane again. A comparison of bubble behaviour at different voltages is shown in Figure 3.7.

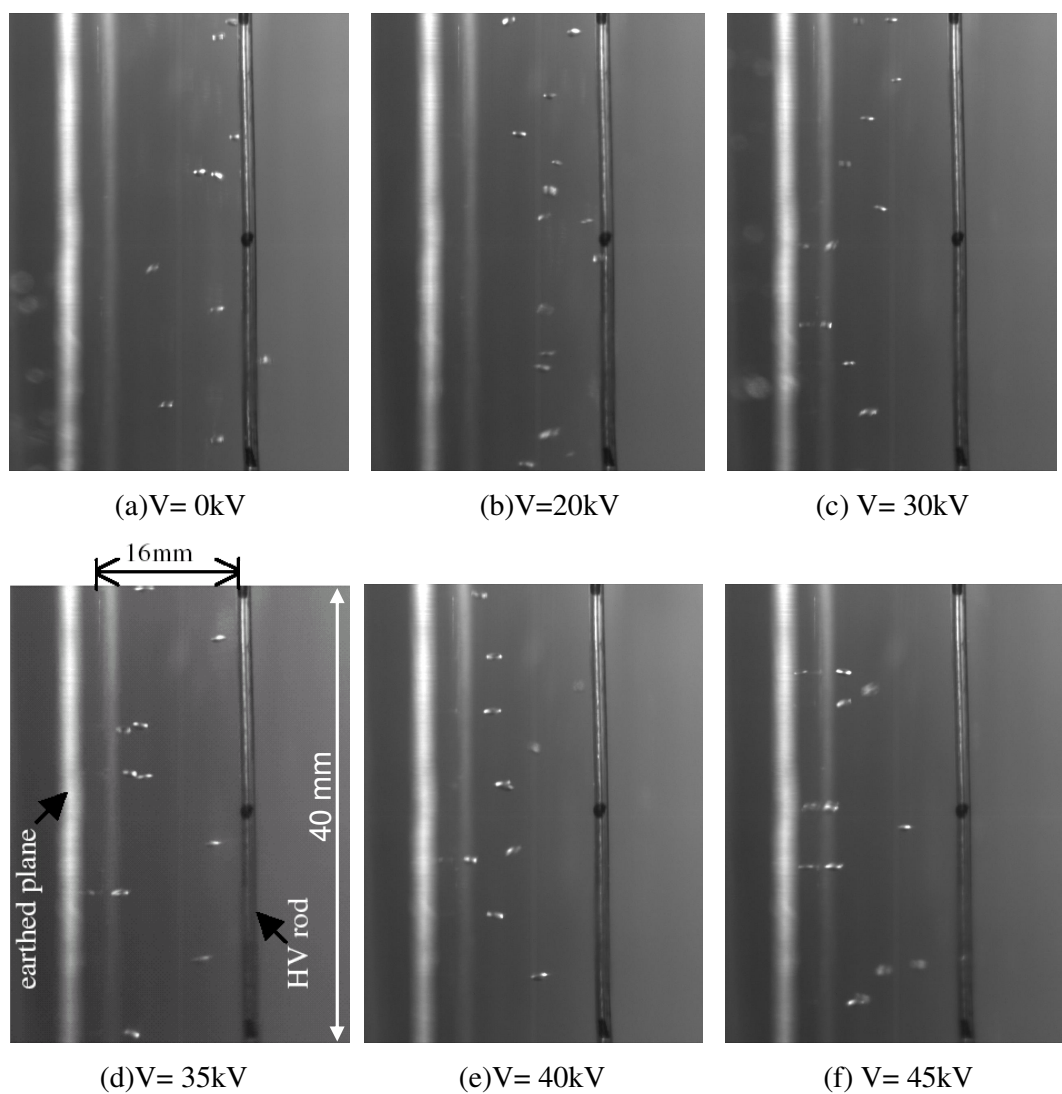


Figure 3.7 Bubble behaviour under positive voltage

### 3.3.2.1.2 Negative polarity

For the next sequence of tests, the plane electrode and the heater cylinder were still grounded but the conductor electrode was connected to a negative potential so that the electric field direction was reversed, being oriented from the plane to the conductor. Identical to the positive polarity condition, when applied voltages were higher than 20kV, bubbles moved towards the plane electrode. Again, very similar behaviour was observed, and typical results under negative polarity applied voltages are shown in Figure 3.8.

These experimental results confirm that dc non-uniform electric fields significantly affect bubble behaviour. Experimental evidence supports the theory that the gradient force greatly affects bubble dynamics in the presence of a non-uniform field and causes bubbles to move towards lower electric fields (a plane electrode in this case),

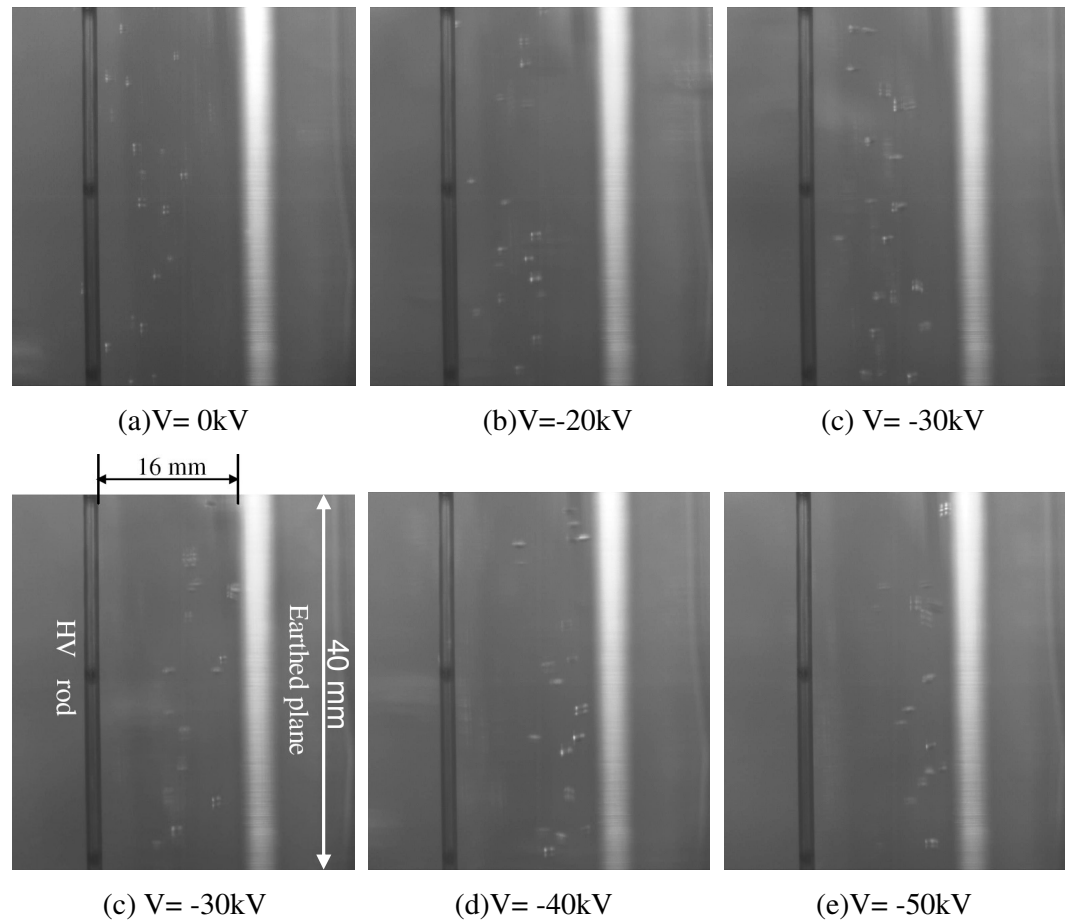


Figure 3.8 Bubble behaviour under negative voltage

irrespective of electric field direction. With increasing applied voltage the gradient force increases, thus, more bubbles move away from the conductor electrode.

### **3.3.2.1.3 Comparison between both polarities of applied field**

A method to study the effect of electric field on bubble motion quantitatively has been developed using an area map between the conductor and plane electrode as shown in Figure 3.9. There are 7 defined slices (A-G) from bottom to top, the height of each slice (except region G (30mm high)) is 40mm, the 40mm height is also a useful size for the camera to image at one instant. Each slice is divided into 2 areas of width 8 mm.  $K_h$  is defined as the half area bubble percentage, which is the ratio of the bubble numbers through one area (closest to the plane) to that through the whole slice. By analyzing captured images, data  $K_h$  can be obtained for different applied voltages. Figure 3.10 shows a comparison of the half area bubble percentage under both voltage polarities. These experimental results indicate that a negative polarity has a larger effect on bubble motion than a positive polarity of the same magnitude. The reasons for this result may be related to the presence of contamination in liquid nitrogen because a top-open glass vessel is used in this experiment. Another reason may be related to liquid convection because there is a heater under the bubbles. The net effects of these will be to increase the half area bubble percentage under negative polarity compared to the value obtained under positive polarity of the same magnitude.

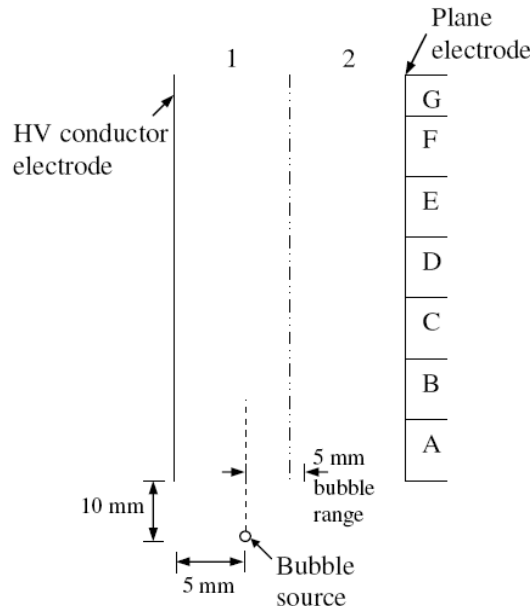


Figure 3.9 The conductor-plane electrode area map

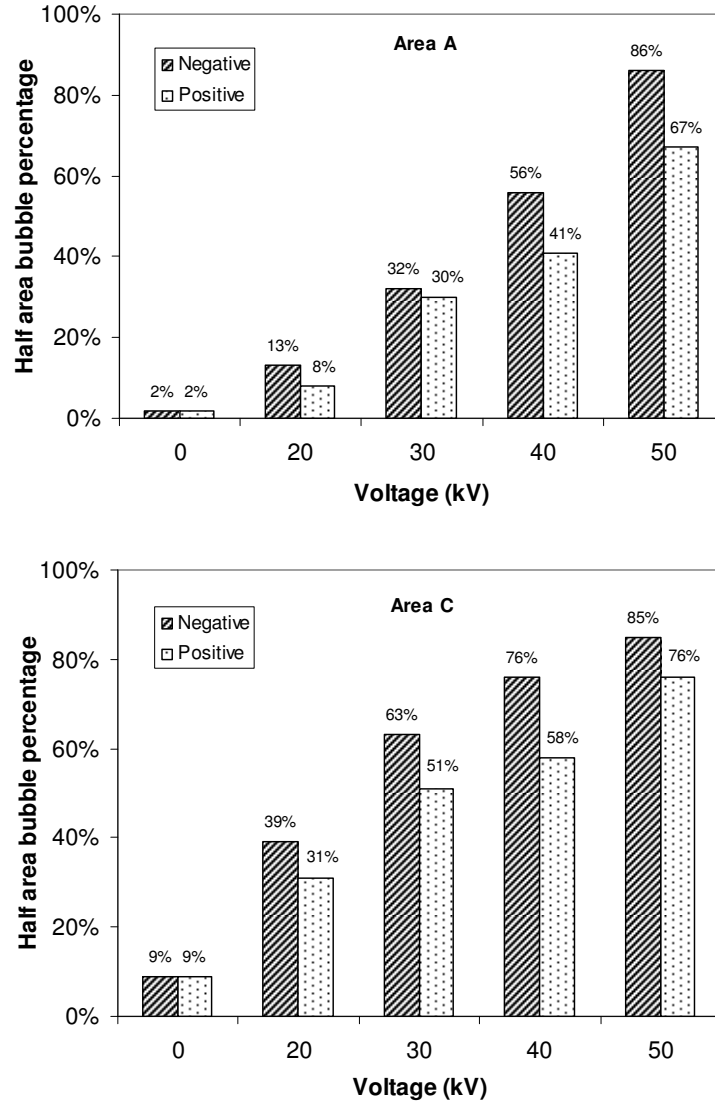


Figure 3.10 Comparison of half area bubble percentage under negative and positive polarity (Areas A and C)

### 3.3.2.2 Bubble trajectory

Analysis of recorded image data has allowed a comparison of experimental bubble crash point height on the plane electrode as a function of voltage with the model presented in 3.2.4. Obtained results are shown in Figure 3.11. The experimental values are compared with bounded theoretical values, based on the assumption that the actual bubble release position may vary from the 5 mm point to 10 mm point in  $x$ -direction. This is because the bubble source is 10 mm below the electrode area as shown in Figure 3.9. Therefore, from analysis of experimental data, the bubbles enter the

electrode area over a range of about 5 mm. Compared to the theoretical values, the experimental results are in good agreement for applied voltage up to 30 kV. For higher voltages, an increasing proportion of the bubbles collide with the plane electrode above the theoretical maximum value. This may be due to these reasons: 1) bubble recollisions with the plane electrode (not recognised due to limited camera frame size), 2) bubbles enter the field off centre line (i.e. not between the conductor-plane shortest path) due to convection currents in LN<sub>2</sub>, 3) eddy shedding effects; in this case, the bubble is not spherical but distorted into a ‘cap’ shape. The movement of the ‘cap’ is oscillatory because it is affected by turbulence caused by other caps above and beside it. Figure 3.12 shows a comparison of theoretical bubble collision minimum height and experimental results. The results show that measured bubbles trajectories are in reasonable agreement with those predicted by the theoretical model.

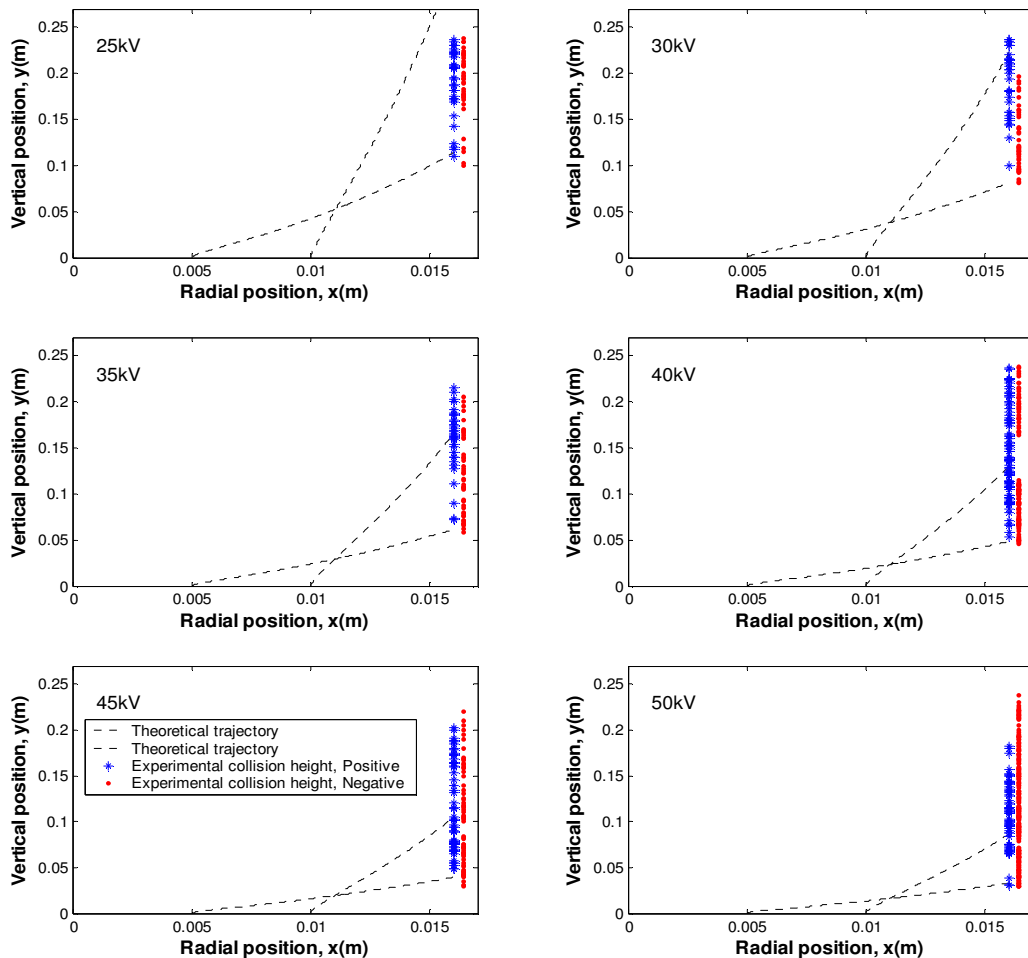


Figure 3.11 Bubble collision height as a function of voltage and comparison with theoretically modelled values

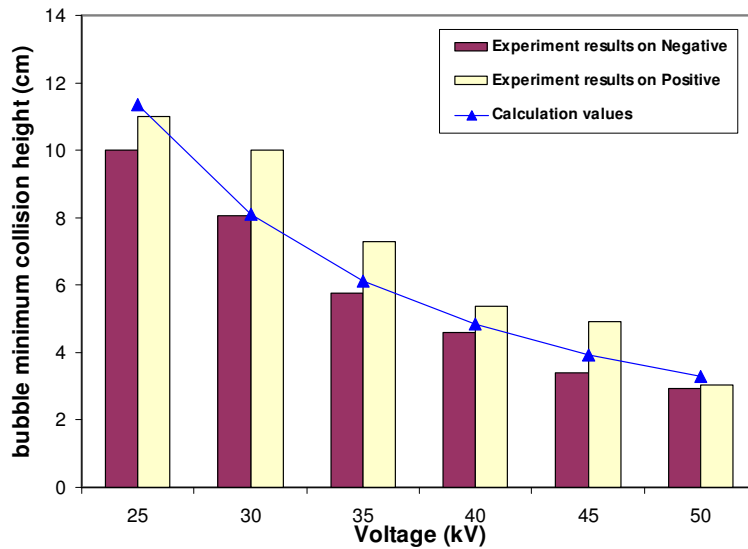


Figure 3.12 Comparison of minimum bubble collision height for theoretical and experimental results ( $x_i=5$  mm for theory calculation)

### 3.3.2.3 Percentage of moving bubble and collision bubbles distribution

Though bubbles can move to the plane electrode under applied voltages, experiments reveal that not all bubbles do this. Figure 3.13 details the relative number of bubbles that collide with the plane electrode as a percentage of the total number of bubbles. Only bubbles colliding with the electrode within the theoretically bounded region are considered. Even under very high electric stress no more than 40% of the total number of bubbles collide within the measurement region. Here, buoyancy plays an important role as the bubble moves towards the plane electrode. Figure 3.14 is a comparison of the magnitude of gradient force and buoyancy applied to a bubble of 0.6 mm radius under an applied voltage of 50 kV determined using (3.10) and (3.7). The gradient force acting in the horizontal direction has a larger magnitude than buoyancy (acting in the vertical direction) over the range 2-5 mm from the conductor electrode. For distances greater than 5 mm, the buoyancy force is of larger magnitude. Also, there are convection currents in the LN<sub>2</sub> due to the heater that produces the bubble stream, and this changes the entry position of bubbles and may also act to limit the number of bubbles that collide with the plane electrode.

Histograms of the distribution of bubble collision over the length of the plane electrode for each applied voltage are shown in Figure 3.15. In each case, the total number of

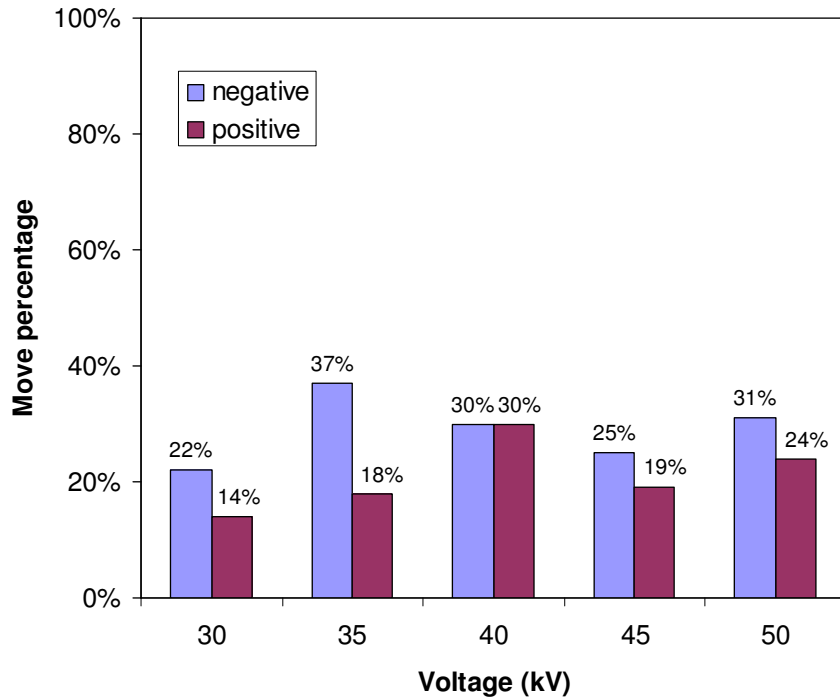


Figure 3.13 Bubbles collision percentage as a function of voltage

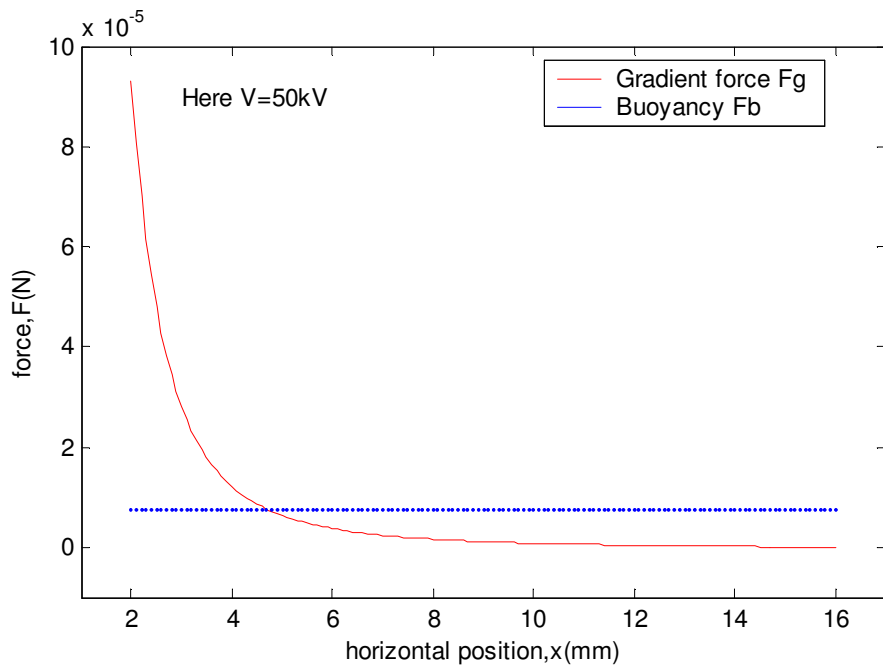


Figure 3.14 Comparison of the magnitude of gradient force and buoyancy applied to a bubble (here  $V=50\text{kV}$ ,  $R=0.6\text{ mm}$ )

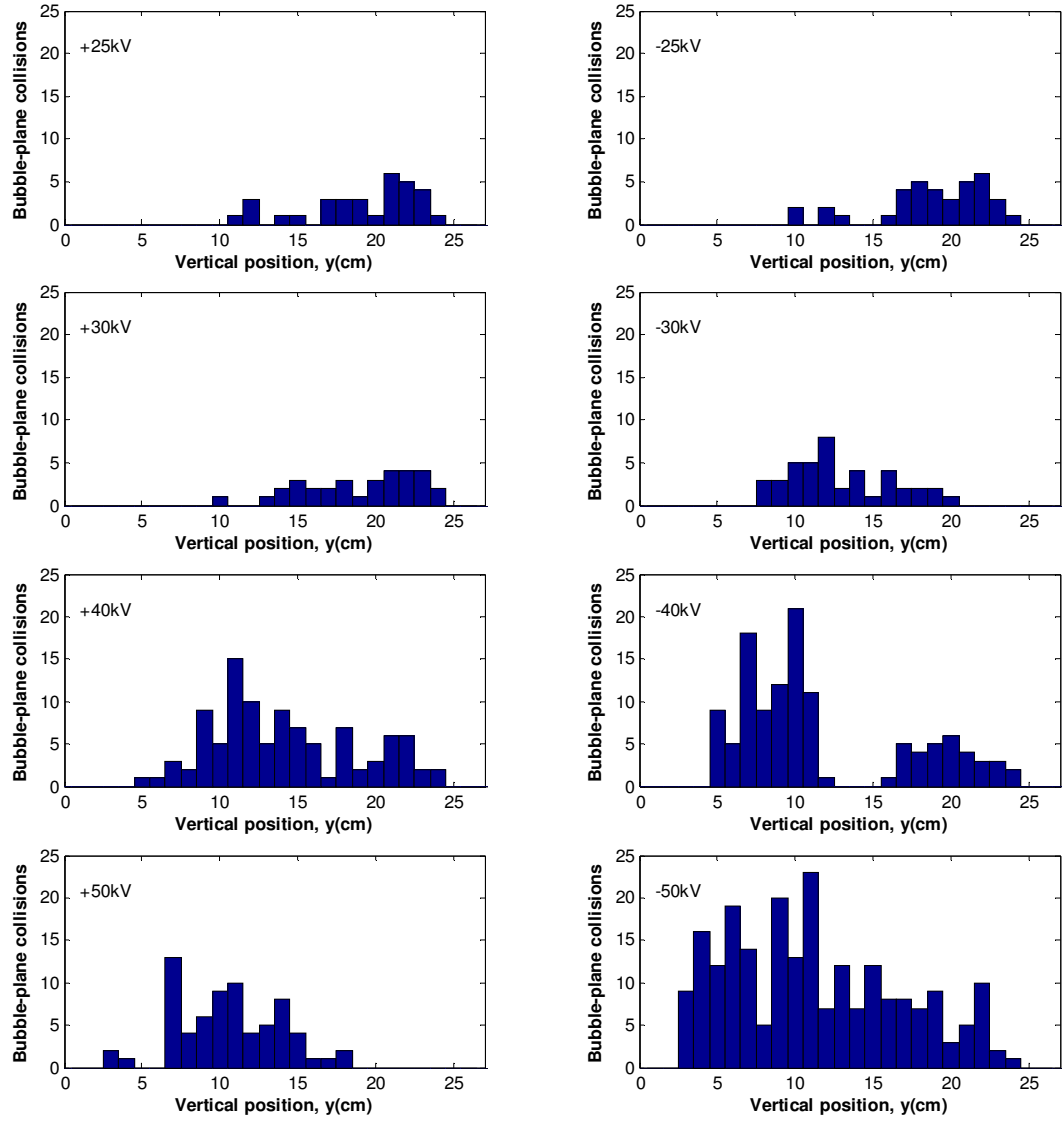


Figure 3.15 Histogram of bubble-plane collisions data (the interval is 10 mm, 2 groups of experimental data for each voltage situation)

bubbles analysed was approximately 240. With reference to Figure 3.15, increasing the gradient force increases the number of bubbles that collide with the plane electrode and broadens the horizontal range over which bubble collision occurs because the minimum collision height is reduced. The lowest collisions all occur under negative polarity.

### 3.4 Summary

The effect of non-uniform electric fields on thermally induced bubble motion in liquid nitrogen has been investigated theoretically and experimentally using a conductor-plane electrode system. Thermal bubble motion and bubble collision with the plane electrode

processes were observed in these experiments, the bubble dynamic mechanism has been analysed and explained by considering the electric field distribution and the electric field force and buoyancy. The obtained results are useful for understanding EHD phenomena influencing bubble behaviour in liquid nitrogen and may assist in the future development of a means of removing gas from cryostats of high temperature superconducting transformers or fault current limiters operating in a quench condition.

The obtained results can be summarized as follows:

- 1) DC non-uniform electric fields have an obvious effect on bubble behaviour, it is believed that the gradient force greatly affects bubble dynamics in the presence of a non-uniform field.
- 2) Bubbles tend to move closer to a lower field region (plane electrode), irrespective of electric field direction.
- 3) A non-uniform field of negative polarity has a larger effect on bubble motion than one of positive polarity. This maybe due to the presence of contamination causing the electric field distribution to be distorted or liquid convection because there is a heater under the bubbles.
- 4) Experimental results show that measured bubbles trajectories are in reasonable agreement with those predicted by the theoretical model.
- 5) No more than 40% of bubbles collide with the plane electrode, because buoyancy forces dominate bubble motion in the conductor-plane electrode geometry.

## Chapter 4

# **Thermal Bubbles in a Non-uniform Electric Field: Plane-Plane Inclined Electrode System**

### **4.1 Introduction**

A plane-plane electrode system is usually used to produce uniform or near uniform electric field. A series of studies on thermal bubble behaviour in liquid nitrogen under parallel plane-to-plane uniform electric fields have been made [11, 25-28]. However, bubble behaviour under a plane-to-plane non-uniform field electrode system has not been widely reported [101]; a situation which may exist in superconducting electric power applications. In addition, the control and positioning of bubbles may have potential implications in liquid-gas unit separation processes and in a zero-gravity environment where electric field forces are a promising replacement for gravity and the lack of buoyancy forces [101]. Thus, it is necessary to investigate the effect of a non-uniform electric field on bubble behaviour using a pair of plane-plane inclined electrode, having a non-uniform field geometry as shown in this study.

## 4.2 Electrode system and experimental apparatus

A plane-plane inclined non-uniform field electrode system as shown in Figure 4.1 was used for experiments. The arrangement consisted of two same-size rectangular aluminium plane electrodes with an angle of  $21^\circ$  between them, (here the choice of the  $21^\circ$  is due to geometry of the narrow channel and easy to setup the electrode system), each aluminium plane is 70 mm in width and 2 mm in thickness. There are two kinds of electrode arrangement (Type 1 and Type 2) for use in this study. Their common points are the same electrode material and same angle of  $21^\circ$ , the differences are different electrode plane length ( $L$ ) and different upper distance ( $D_1$ ) and lower distance ( $D_2$ ) between both plane electrodes. In addition, the size of the open hole in the upper polymer disk is also different. The detailed parameters are listed in Table 4.1. For each electrode arrangement, one of electrodes was connected to high voltage power supply, either positive polarity or negative polarity for dc electric field conditions; and the other was always grounded. Two round polymer disks of 100 mm in diameter were used to hold the plane electrodes. The lower round disk has a hole of 5 mm in radius in the centre for bubbles to pass through. The bubble source was 10 mm below the electrodes and at the centre line of the electrodes.

The glass cryostat and other equipment such as high voltage dc power supply, the high-speed camera, lamp, digital meter and the heater for thermal bubble source in this experiment were the same as those used in the previous study on thermal bubble behaviour under electric fields by using a conductor-plane electrode system described

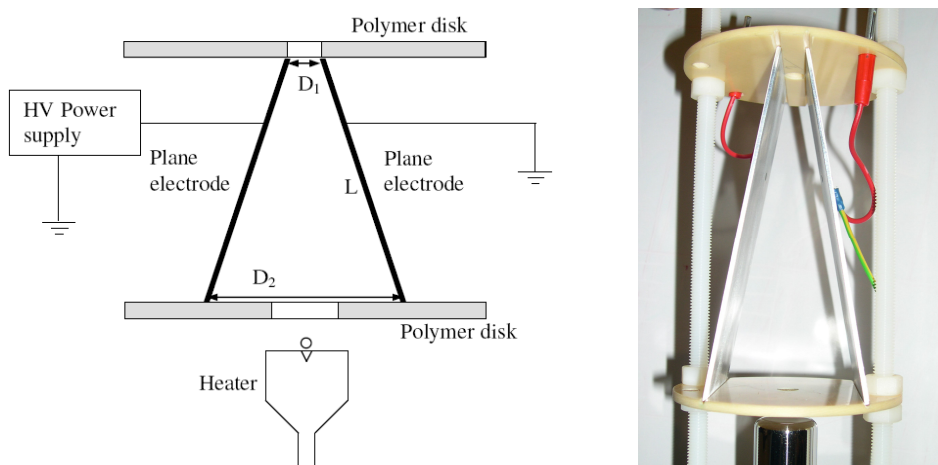


Figure 4.1 Plane-plane inclined non-uniform field electrode system. The angle between the electrodes is  $21^\circ$

Table 4.1 Parameters for the two electrode types

Parameter (unit:mm)	Type 1	Type 2
L	79	154
D <sub>1</sub>	5.5	11
D <sub>2</sub>	33	66
Open hole in upper disk	A slot of 5.5 × 20 mm	A round hole of 5 mm in radius

in Chapter 3. The input power of the heater for producing a regular train of bubbles of volume equal approximately 4 mm<sup>3</sup> was 0.36 W. A sequence of images of bubble behaviour were recorded with a high-speed digital camera, which was set to 1000 frames/s, this was performed for the following voltage magnitudes; 0, 10, 15, 20, 30 and 40 kV for both polarities. For each voltage situation, the detailed procedure was described as follows: Firstly power on the heater and wait for around 30 seconds to get stable bubble source, then the camera was set to ‘ready to record’ state, and then turn on the high voltage power supply and at the same time trigger the camera to record the images of 1 minute long and then turn off high voltage power supply. Finally take the 30<sup>th</sup> second image as the typical experimental result. 5 minutes waiting was introduced before moving to the next different voltage test.

### 4.3 Experimental results and analysis

All of experiments were performed at atmospheric pressure. The diameter of bubbles produced by the heater in this experiment was around 1 mm; bubble behaviour was compared at different voltages.

#### 4.3.1 Observation of bubble behaviour

##### 4.3.1.1 Bubbles coalescence

In the absence of electric fields, bubbles usually rise free and pass through the channel between electrodes due to buoyancy. Most of bubbles can pass through the slot (for Type 1 electrode system) in the centre of the top polymer disk, only a few bubbles may collect on the buffer side of the polymer disk as shown in Figure 4.2 (a). However, when a negative dc high voltage is applied to one of the plane electrodes, and once the voltage is set higher than 15 kV, small bubbles will gather at this location and become a

bubble chain and then coalesce to form a big bubble at the edge of the slot as shown in Figure 4.2 (c). The bubbles experience a gradient force in the top region of the electrodes (examined further in section 4.3.2.2) preventing them from rising through the hole until a sufficiently large bubble has grown by coalescence and overcomes this force by buoyancy, then passing up through the hole. The resultant large coalesced bubble can be seen for every test when the applied voltage is over 15 kV. This big bubble also prevents other small bubbles passing, collecting them to grow in volume. As shown in Figure 4.2 (c)-(f), the higher the voltage is the more obvious the bubble coalescence will be. In addition, it was observed that the higher the applied voltage is, the lower will be the time needed for formation of large bubbles. When a voltage higher than 40 kV is applied, a ‘bubble bridge’ was formed below the polymer disk which connects both electrodes as shown in Figure 4.2 (f). With reference to Figure 4.2 (f) at -40 kV the gradient force is sufficient to overcome buoyancy and the large bubble can be seen to have moved down away from the top of the electrodes. The same bubble coalescence phenomenon with increasing voltage is also seen when the Type 2 electrode arrangement was used, as shown in Figure 4.3 (a2)-(d2). An increase in

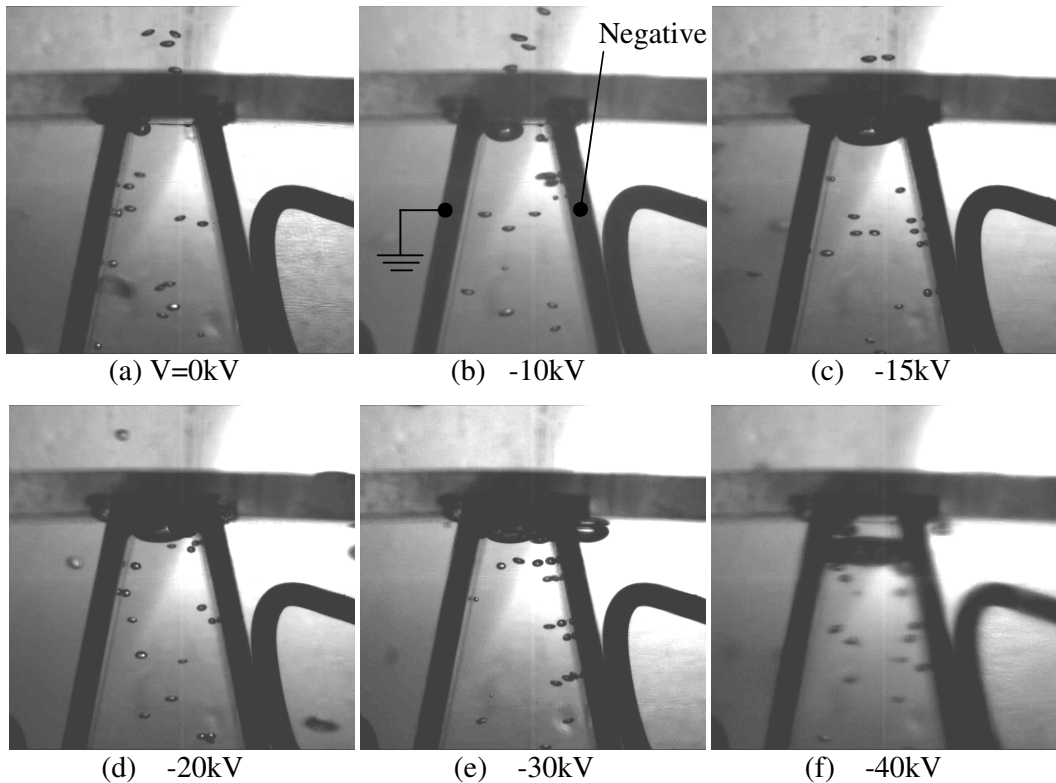


Figure 4.2 Bubble behaviour under plane-to-plane non-uniform negative fields (for Type 1 electrode arrangement)

vapour in the insulation gap has been known to reduce the breakdown voltage [11].

#### 4.3.1.2 Effect of electrode gaps

As mentioned above, two kinds of electrode arrangement are used in this experiment. The  $D_1$  of Type 2 is two times larger than the  $D_1$  of Type 1. The effect of electrode gap on bubble behaviour under different voltages is shown in Figure 4.3. The bubble coalescence activity with increasing voltage is similar in both electrode arrangements.

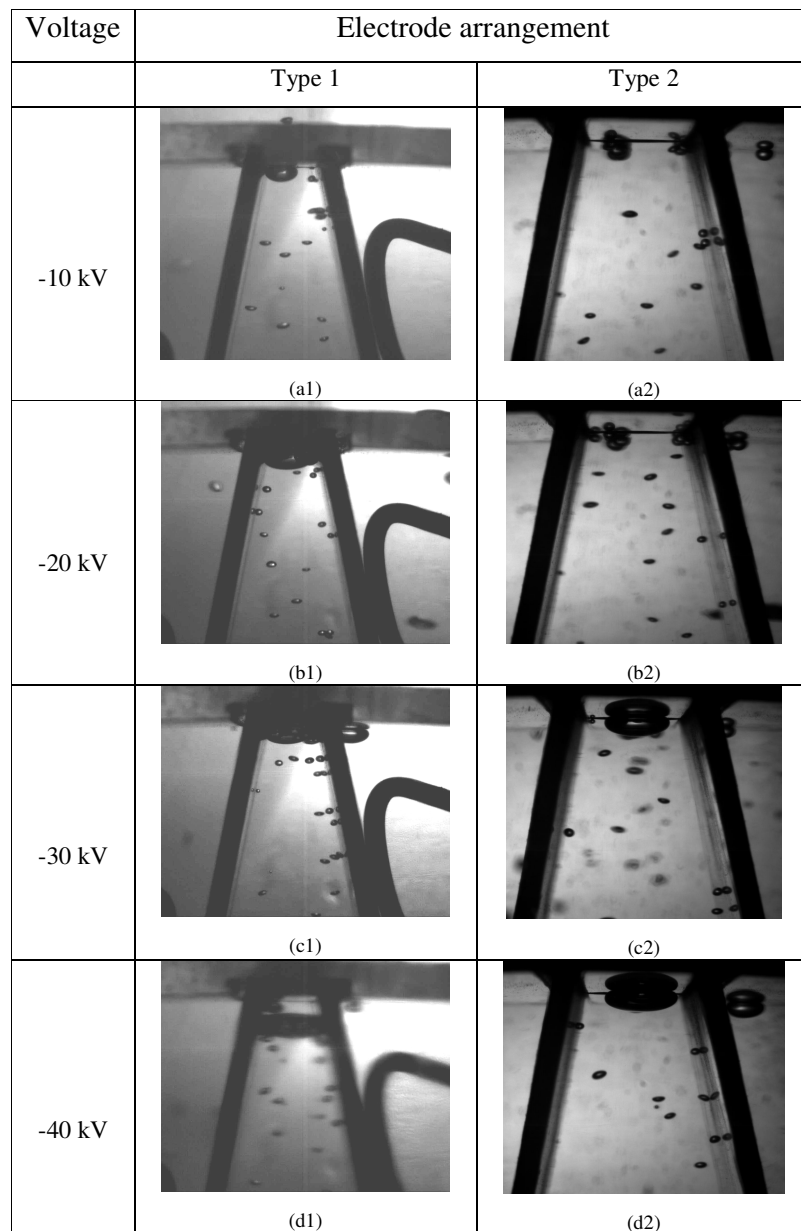


Figure 4.3 Comparison of bubble behaviour with different voltages for two kinds of electrode arrangements

The general difference is that bubble coalescence activity in Type 1 is more obvious than that in Type 2, this might be due to a higher electric force existing across a short distance when the same voltage is applied. In Type 2, the volume of bubbles is never sufficient to ‘bridge’ both electrodes up to an applied voltage of 50 kV while in Type 1, this phenomenon is very obvious. Especially, when the voltage is larger than 40 kV the large bubble chain can be pushed away from the upper disk. In addition, it can be noted that bubble coalescence activity is not obvious when the applied voltage is lower than 20 kV in Type 2.

#### 4.3.1.3 Effect of electric field polarity

The experimental results discussed above were obtained under negative applied voltages. Thermal bubble behaviour under a positive applied voltage has also been observed. Figure 4.4 shows the experimental images of thermal bubble behaviour at different positive voltages. Compared with results under a negative applied voltage, very similar phenomena and results were observed and obtained for both polarities of electric fields.

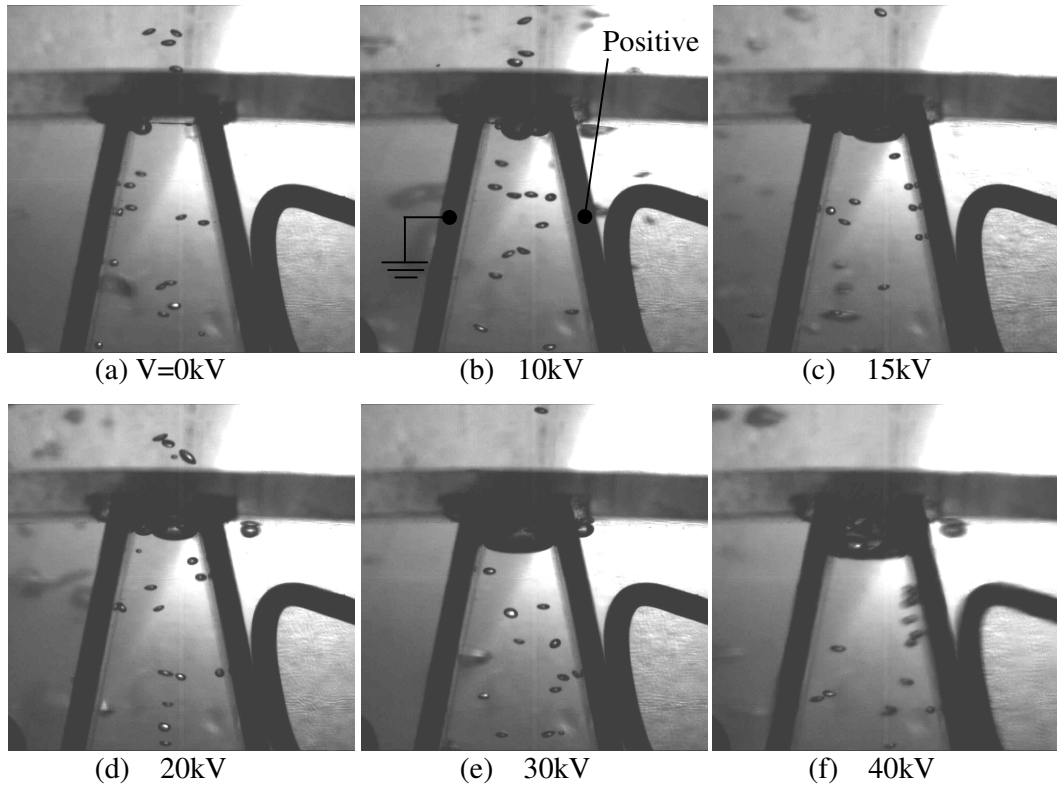


Figure 4.4 Bubble behaviour under plane-to-plane non-uniform positive fields (for Type 1 electrode arrangement)

### 4.3.2 Theoretical analysis of the bubble's behaviour

To understand the effect of electric fields on bubbles, the electric field distribution and the electric forces around a bubble are analysed.

#### 4.3.2.1 Electric field distribution

A non-uniform electric field could be generated using this electrode arrangement. The electric field distribution can be obtained by using FEA simulation software. Figure 4.5 and Figure 4.6 show electric field strength of the centre line position (see a-a' in Figure 4.7) between both plane electrodes and the horizontal position on the top of electrodes (see b-b' in Figure 4.7) when 40kV is applied (for Type 1 arrangement), respectively. It is noted that a significant non-uniformity at the top region (region A in Figure 4.5) of the electrode system. In addition, the electric field strength in the horizontal direction also shows certain non-uniformity. It is to be noted that the electric field strength is around 2 times greater near the top end of the plates compared to the centre line. This means electric force acting on the bubbles in the edge region is much larger than that on the centre position. Moreover, it is well known that bubbles (of lower permittivity than the bulk liquid) tend to move into a lower electric field region. So, the non-uniformity of the electric field is the main reason why bubbles are held against buoyancy force and gather on the top zone.

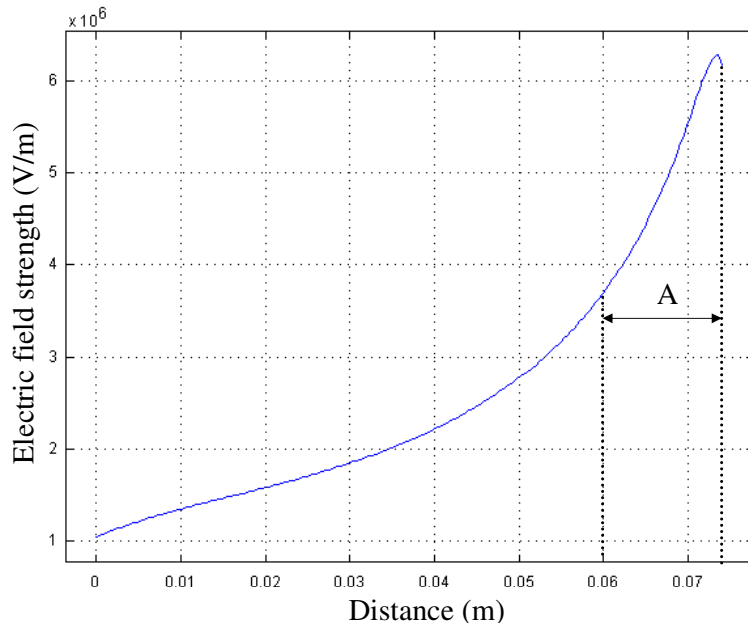


Figure 4.5 Electric field strength along centre line, bottom to top (a-a' with reference to Figure 4.7)

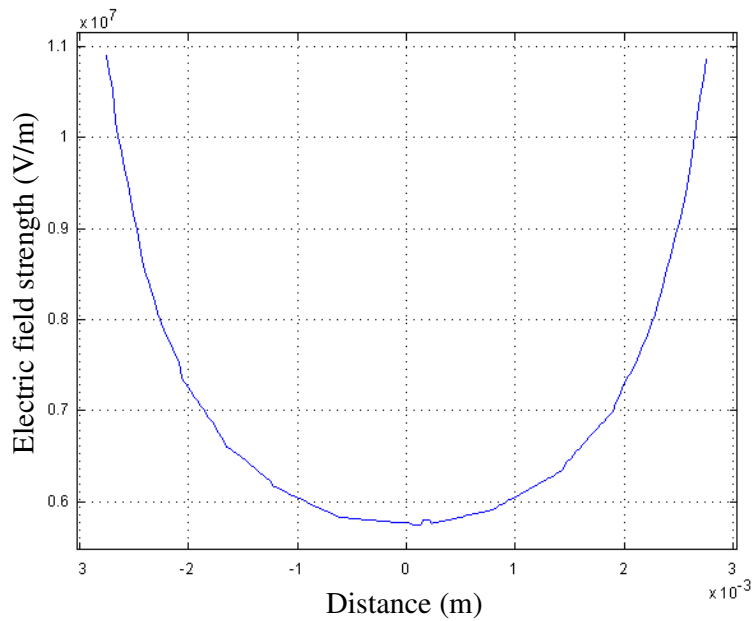


Figure 4.6 Electric field strength of the horizontal direction across the top of electrodes  
(b-b' with reference to Figure 4.7)

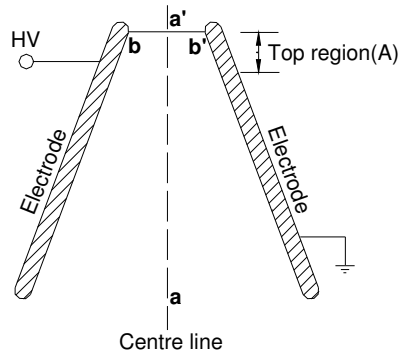


Figure 4.7 The centre line position and the horizontal position across the top of electrodes

Though the electric field strength is high at the top region of the electrode system, any breakdown events occurring in the bubbles were not observed. This is because the breakdown voltage of 20 kV/mm, given by the Paschen curve (see Figure 1.4), is greater than the value used in this experiment.

#### 4.3.2.2 Comparison of forces on a bubble

In this experiment, there are two main forces acting on a suspended spherical bubble, one is gradient force,  $F_g$ , which has been described and explained in Chapter 3. This force is due to the combined effect of the different permittivities of liquid and bubble

and the non-uniformity of the electric field. It is proportional to the square of the gradient of the electric field strength. Therefore, it becomes much more significant when the electric field is non-uniform and of high intensity. This force drives bubbles towards the lower electric field. For this experiment, it tends to force the bubble downwards. The other force is buoyancy,  $\mathbf{F}_B$ , that has been expressed as

$$\mathbf{F}_B = \frac{4}{3}\pi R^3(\rho_l - \rho_g)\mathbf{g} \quad (4.1)$$

where  $\mathbf{g}$  is the gravitational acceleration. Buoyancy always forces the bubble upwards. In order to calculate the gradient force  $\mathbf{F}_g$ , the electric field  $\mathbf{E}$  is needed. It was suggested in [102] to express vertical component of electric field as

$$\mathbf{E} = \frac{V}{r\theta_p} \hat{\theta}_p \quad (4.2)$$

where  $V$  is the applied voltage difference,  $\theta_p$  is the angle between the two electrodes and  $r$  is the position as shown in Figure 4.8 . With reference to Figure 4.8 position ‘0’ is taken as the crossing point of the two planes on which the electrodes lie. Considering the centre line (see Figure 4.7 a-a’), the distance  $r$  falls between the electrodes in the range 15 to 90 mm for the Type 1 electrode arrangement. Substituting in  $\mathbf{E}$  from (4.2) into Equation (3.2) the gradient force  $\mathbf{F}_g$  is

$$\mathbf{F}_g = \frac{4\pi R^3 \epsilon_l (\epsilon_l - \epsilon_g) V^2}{(\epsilon_g + 2\epsilon_l) r^3 \theta_p^2} \quad (4.3)$$

By using Equations (4.1) and (4.3) as well as relevant nitrogen parameters as listed in Table 4.1, Table 1.1 and Table 1.2,  $\mathbf{F}_B$  and  $\mathbf{F}_g$  can be calculated and compared along the centre line. Figure 4.9 shows a comparison of magnitude between  $\mathbf{F}_g$  and  $\mathbf{F}_B$  for a 40 kV applied voltage. It was noticed that  $\mathbf{F}_g$  was much more than  $\mathbf{F}_B$  at the top region of electrodes, Thus, this results in significant bubbles coalescence behaviour.

Especially,  $\mathbf{F}_g$  is equal to  $\mathbf{F}_B$  when the vertical position  $r$  is 18 mm, this is a good agreement with the experiment result shown in Figure 4.2f where bubble bridging is seen to occur. From the above discussion, when  $\theta_p$  and  $V$  are constant, to increase the electric field effect on bubble dynamics, to decrease gravitational acceleration  $\mathbf{g}$  (i.e. test in the microgravity environment) is a feasible method. In fact, some researchers

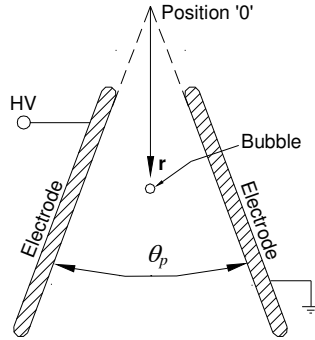


Figure 4.8 The sketch of plane-plane inclined electrode for non-uniform electric field calculation

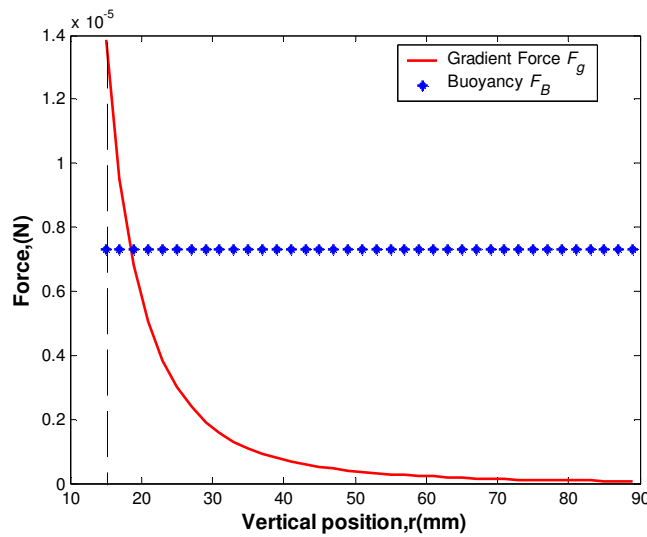


Figure 4.9 Comparison of buoyancy with gradient force applied to a bubble

$$(\theta_p = 21^\circ, V = 40 \text{ kV}, R = 0.6 \text{ mm}, g = 9.8 \text{ m} \cdot \text{s}^{-2})$$

have carried out similar studies on this situation. Y.Suda *et al* [8] observed the dynamic behaviour of bubbles in liquid nitrogen in a microgravity environment between plate electrodes with an angle of  $30^\circ$ . The value of  $F_g$  was found to be almost two orders of magnitude larger than  $F_B$ . So, even though gradient force has a generally low magnitude in a terrestrial environment, in the absence of buoyancy it might be an important tool for phase separation in space applications of HTS technology.

#### 4.4 Summary

Behaviour of thermal bubbles in liquid nitrogen between plane electrodes with an angle of  $21^\circ$  and applied dc fields was experimentally investigated. There were two types of electrode arrangement for use in this study. It has been observed that bubbles collect

near the top of the electrodes and only when of sufficient volume does the buoyancy force overcome the gradient force allowing the gas volume to rise from the electrode gap. Increasing the applied voltage led to a reduction in time for bubble collection and coalescence to begin. Both polarities were investigated and no polarity effect was obvious. Moreover, experimental results for two electrode arrangements were compared and discussed, and it was found that Type 1 has a more obvious effect on bubble behaviour than Type 2 (having a larger spacing and lower field for the same applied electric voltage). Analysis of the competing forces of the electric gradient and buoyancy show that for a fixed bubble size, the electric gradient force overcomes buoyancy near the top of the electrodes, consistent with the observed results. In addition, methods for increasing electric force effects on a bubble in a liquid have been discussed.

## Chapter 5

# The Effect of Uniform Electric Field Distribution on the Behaviour of Thermally Induced Bubbles in Liquid Nitrogen

### 5.1 Introduction

Electrohydrodynamic (EHD) enhancement of heat transfer in liquids is due to increased heat transfer efficiency from coupling the flow and temperature fields with a high-voltage, low-current electric field in the dielectric fluid medium. It is an active heat transfer enhancement method. An advantage of utilizing an EHD technique is that heat transfer performance can be easily controlled by varying the applied voltage. EHD boiling processes have been used in many industries such as in refrigeration units. So far, many liquid materials have been used in experimental studies to obtain more information about EHD effect on boiling heat transfer [68, 69], but there are fewer studies [84, 103, 104] on the EHD effects on heat transfer of liquid nitrogen. Moreover, the basic mechanisms for the EHD effect are still not completely understood.

In order to investigate the details of the mechanism of enhancement of boiling heat transfer of liquid nitrogen by the utilization of the EHD technique, basic experiments were initially performed and analysis of bubble behaviour in liquid nitrogen under uniform electric fields undertaken because it is believed that the change in bubble behaviour in the presence of an electric field is one of the main reasons for boiling heat transfer enhancement [74].

In this chapter, the effect of a dc uniform electric field on the behaviour of a single thermal nitrogen bubble in liquid nitrogen has been studied. For this purpose, the electric field distribution around a bubble and the electric force acting on the bubble were first determined numerically and then the bubble shape, the departure frequency and the departure volume were investigated experimentally. These results may provide an initial perspective on the effects of an electric field on the boiling heat transfer properties of liquid nitrogen.

## 5.2 Experimental setup and procedure

A schematic diagram of the experimental system used to observe thermal bubble behaviour in an electric field is shown in Figure 5.1. The system consists of a glass cryostat, a high voltage power supply, a high-speed camera, and a mesh-to-plate electrode. This system has been previously used to study thermal bubble dynamics in liquid nitrogen under non-uniform electric fields as described in Chapter 3 [38].

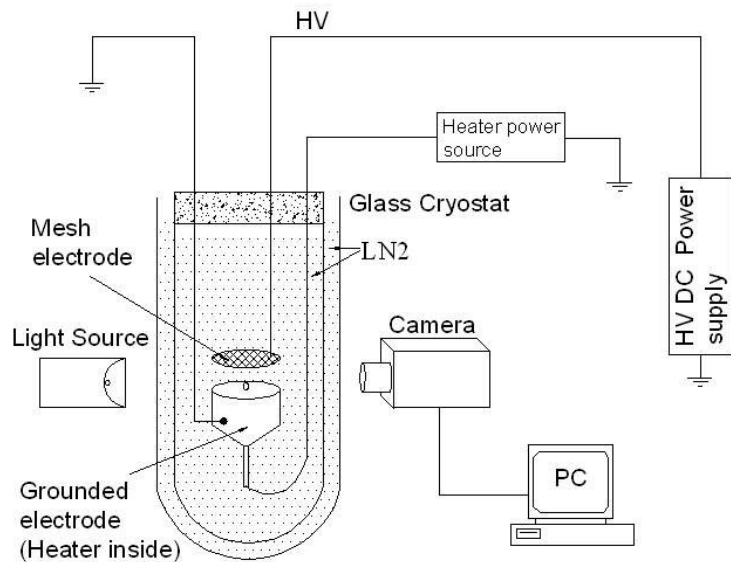


Figure 5.1 Schematic diagram of the experiment

In order to create a uniform electric field, a mesh-to-plate electrode configuration is used. The upper high voltage electrode of either positive or negative polarity is made of 1.8 mm aperture-size steel mesh (0.25mm wire diameter) to keep the bubble flow unrestricted. This steel mesh is 42 mm in diameter and has a void percentage of up to 75%. The lower grounded electrode is a single cylinder electrode with a polished stainless steel surface. This cylinder has a blind hole of 100  $\mu\text{m}$  diameter in the centre of the top surface (30mm diameter), and a heater is mounted behind this artificial cavity to provide a controllable heat source. The heater was set to provide a power of 0.36 W in order to produce successive bubbles. These electrodes generate a uniform electric field for the bubble. The gap between the mesh electrode and the lower grounded electrode is 6 mm. A sequence of images of bubble behaviour was recorded by a high-speed camera, over a range of dc voltages from 0 kV to 50 kV for both polarities. In this way, the process of bubble growth and deformation as a function of the electric field can be observed.

### **5.3 Electric field distribution and electric force acting on the bubble**

In order to provide an appreciation of the effect of electric fields on a bubble, the electric field distribution and the electric force around a spherical bubble were first analysed using a simulation model.

#### **5.3.1 The electric field distribution around a bubble**

The electric field distribution of an idealized bubble was obtained by using FEA modelling software. Figure 5.2 shows the potential contours around a single spherical bubble attached to the grounded electrode when 30 kV is applied. The potential contours curve near to the bubble surface and the electric field is distorted due to the presence of the bubble. Figure 5.3 shows the distribution of electric field strength around the bubble. The field is distorted greatly at the bubble interface and inside of the bubble. Compared with the uniform electric field strength of  $E_0 = 5\text{kV/mm}$  in the absence of the bubble, the electric field decrease (see Figure 5.4) at the top of the bubble, while around the sides of the bubble, the electric field increases (see Figure 5.5); Away from the bubble, the electric field is uniform (see Figure 5.6). The maximum gradient of the electric field occurs at the top of the bubble. Thus, it is seen that the

presence of a bubble destroys the uniformity of the electric field and results in the field distribution around the bubble being non-uniform.

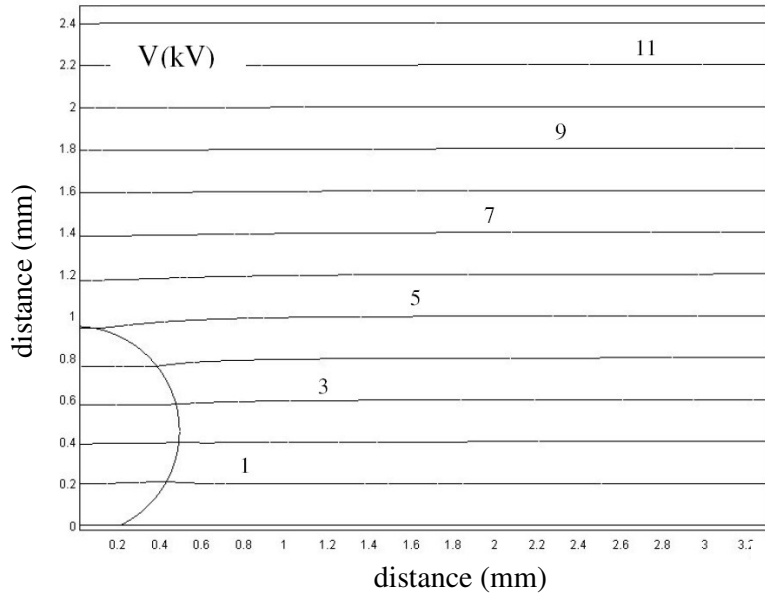


Figure 5.2 Potential contours around a bubble attached to grounded electrode (numbers close to potential lines corresponds to voltage in kV. bubble radius  $R=0.5\text{mm}$ , applied voltage  $V=30\text{kV}$ ,  $\epsilon_l=1.432$ ,  $\epsilon_g=1$ )

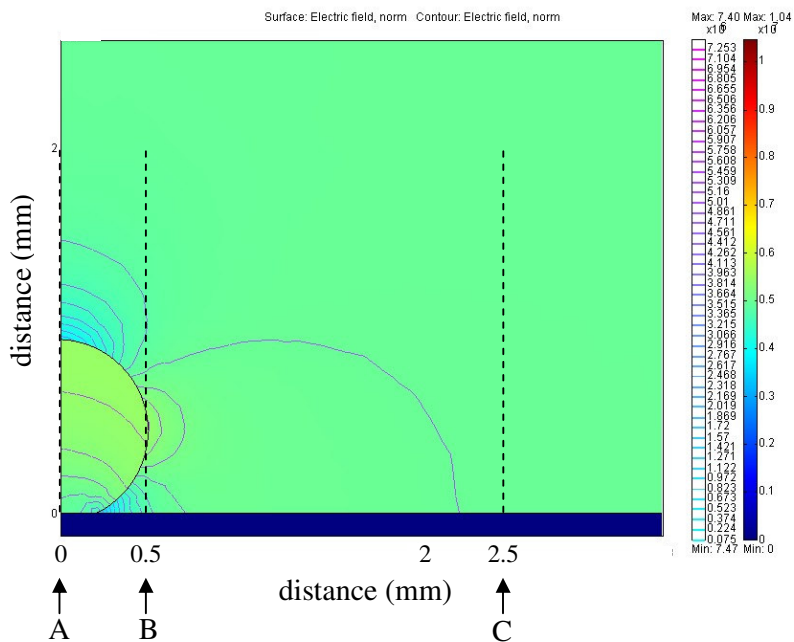


Figure 5.3 Distribution of the electric field around the bubble

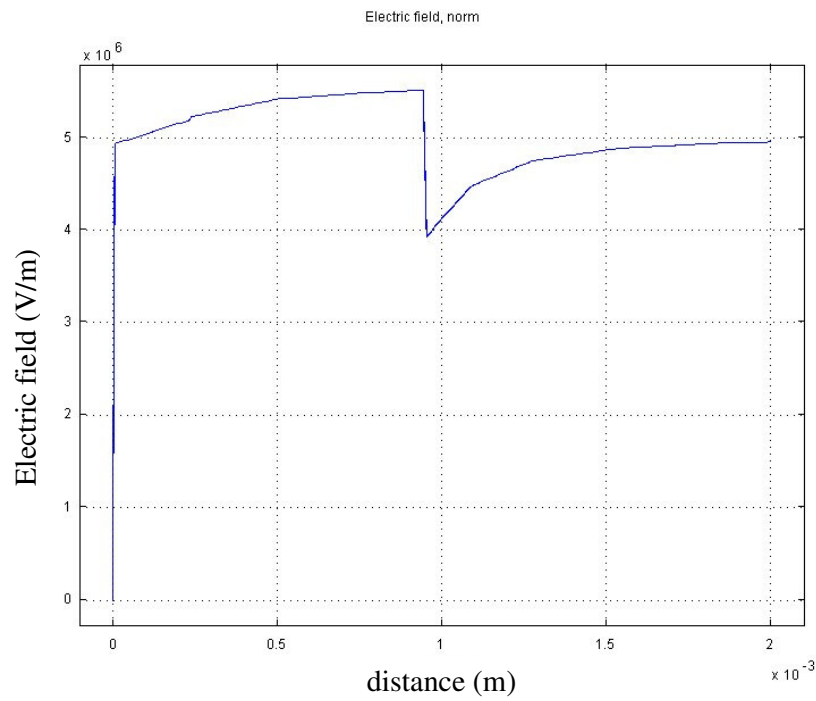


Figure 5.4 Distribution of the electric field in position A of Figure 5.3

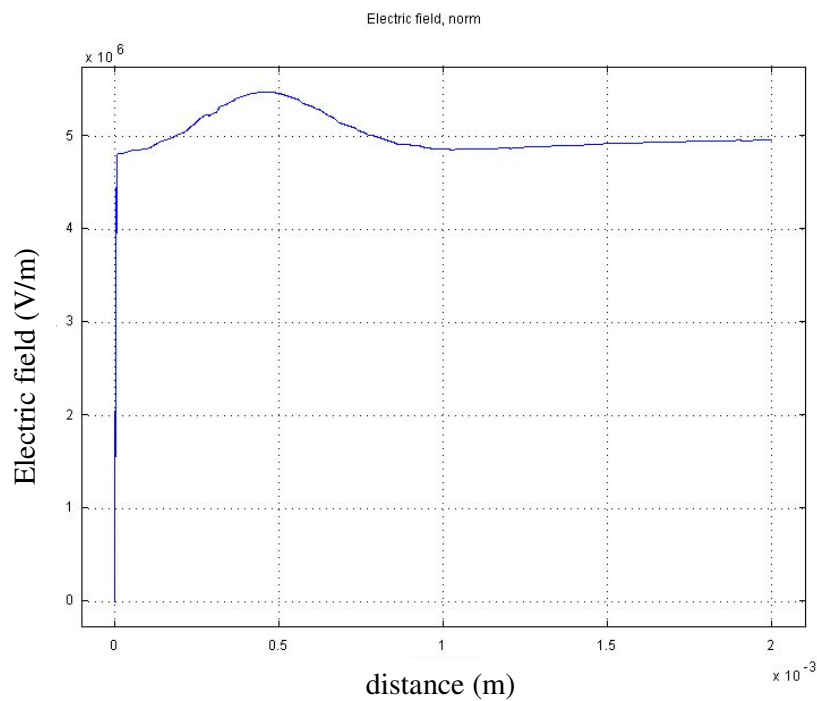


Figure 5.5 Distribution of the electric field in position B of Figure 5.3

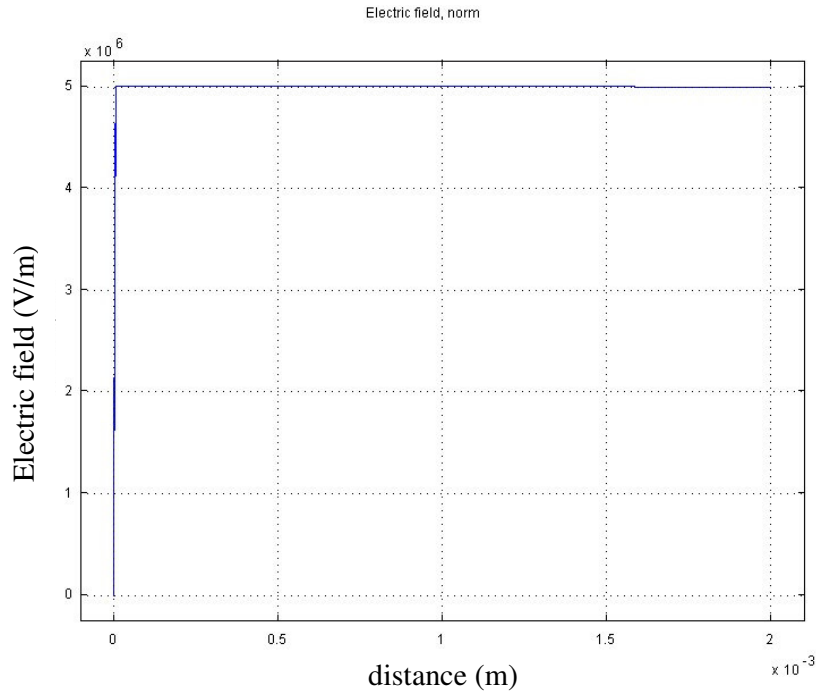


Figure 5.6 Distribution of the electric field in position C of Figure 5.3

### 5.3.2 Electric force acting on the bubble

As liquid nitrogen is a non-polar dielectric liquid with very low electrical conductivity ( $<1 \times 10^{-16} \text{ S}\cdot\text{m}^{-1}$ ), the electric current flowing through liquid nitrogen can be considered negligible. In addition, the relaxation time of liquid nitrogen, which is expressed as the ratio of the permittivity and electrical conductivity, is estimated to be several orders of magnitude greater than the detachment period of bubbles. As a result, it is assumed that no free charges appear within the liquid nitrogen or bubble interface during the experiment.

Zaghoudi and Lallemand [77] had carried out numerical analyses on the behaviour of a bubble in an insulating liquid while subjected to an electric field between parallel plate electrodes. A detailed analysis of the interfacial electric stresses acting on the liquid-vapour interface had been given. According to this analysis, the electric force acting at every point on gas bubble surface can be divided into normal and tangential components. The normal electric stress causes a distortion of the bubble, whereas the tangential electric stress, which is the Coulomb stress, acts if the bubble interface bears electrical free charges and it induces liquid movement around the bubble and vapour

movement within the bubble. As discussed above in this study, liquid nitrogen is considered as perfectly insulating with no free charge appearing on the bubble interface. So, only the normal component of the electric stress acts on the interface. That is, the shape of bubble is completely determined by the normal electric stress. The normal electric stress,  $f_{sn}$ , for a dielectric bubble (no electrical free charge density at the bubble interface) has been expressed as [77]

$$f_{sn} = \frac{9\epsilon_0 E_0^2}{2(2+1/Y)^2} (\alpha \cos^2 \theta - \beta) \quad (5.1)$$

where  $\alpha = \left(\frac{\epsilon_l^2 + 4\epsilon_l - 2}{3}\right)(1/Y)^2 - \left(\frac{\epsilon_l^2 - 2\epsilon_l + 4}{3}\right)$  (5.2)

$$\beta = -\frac{(\epsilon_l - 1)^2}{3} \quad (5.3)$$

$$Y = \epsilon_l / \epsilon_g \quad (5.4)$$

where  $\epsilon_0$  is the vacuum dielectric permittivity ( $\text{F}\cdot\text{m}^{-1}$ ),  $E_0$  is the uniform electric field strength far from the bubble ( $\text{V}\cdot\text{m}^{-1}$ ),  $\epsilon_l$  is the relative dielectric permittivity of the liquid,  $\epsilon_g$  is the relative dielectric permittivity of the gas in the bubble,  $\theta$  is the angular coordinate (see Figure 5.7).

The normal components,  $f_{sn}$ , acting on the bubble interface can be decomposed into horizontal and vertical ones,  $f_{snx}$  and  $f_{snz}$ , respectively. Figure 5.7 shows variations of  $f_{snx}$  and  $f_{snz}$  along the bubble interface as a function of the angular coordinate  $\theta$  (here  $E_0$  is  $5\text{kV}\cdot\text{mm}^{-1}$ , i.e. the applied voltage is  $30\text{kV}$ ;  $Y=1.432$ ). It is seen that the horizontal component strength is at its maximum of  $12.25\text{ N}\cdot\text{m}^{-2}$  at the bubble equator ( $\theta=90^\circ$ ) and is directed towards the gas phase and contributes to the compression of the bubble. The vertical component strength has the maximum value of  $11.73\text{ N}\cdot\text{m}^{-2}$  at the top of the bubble ( $\theta=0^\circ$ ) where it is directed towards the liquid phase and contributes to the bubble elongation in the electric field direction. Note that if the horizontal components in the two hemispheres of a bubble are not in balance, the bubble will move horizontally along the plate. This phenomenon was observed in the first experimental test, as shown in Figure 5.8, as the high-voltage mesh electrode has a slight inclination.

Such additional sliding movement of bubbles induced by the applied electric field may intensify the local flow and turbulence within the thermal boundary layer, reducing the thermal resistance, and enhancing heat transfer. Similar experimental phenomena have also been reported by other researchers [92].

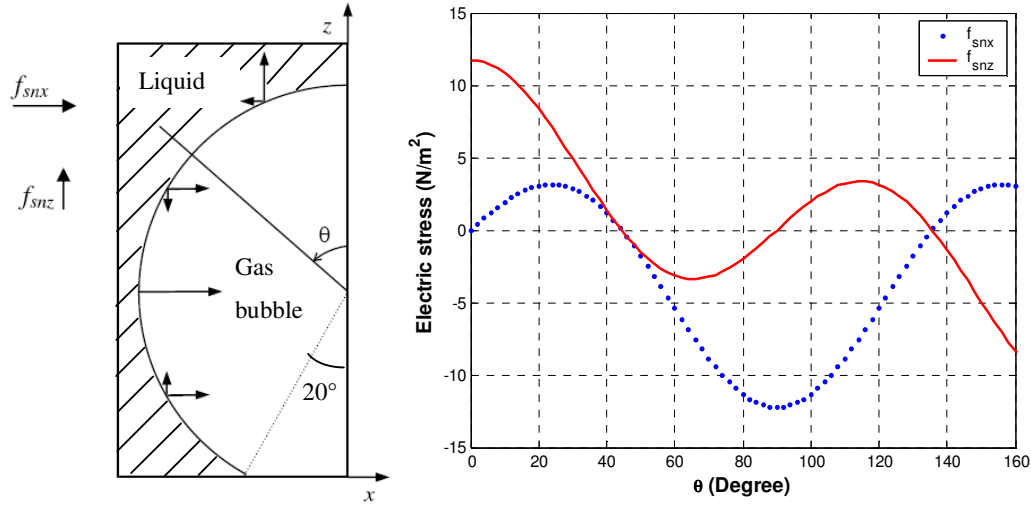


Figure 5.7 Horizontal and vertical components of the electric stresses acting on the bubble

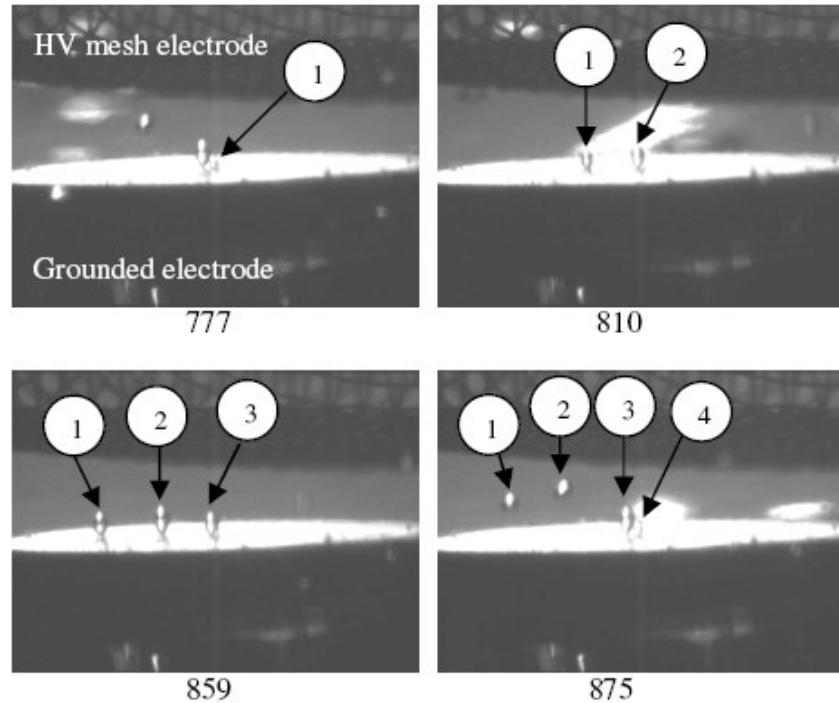


Figure 5.8 Bubble sliding phenomenon along the grounded electrode due to unbalanced horizontal forces acting on the bubble. Applied voltage is 50kV, camera speed is 1000fps. The frame number is included under each image.

## **5.4 Experimental results and discussion**

Experimental tests have been carried out with saturated liquid nitrogen (commercial grade) at atmospheric pressure.

### **5.4.1 Image processing**

During the experiments, original images are taken by using a high-speed camera. A filtering technique for image processing has been previously developed within the Tony Davies High Voltage Laboratory [105]. Using this technique, the original image can be converted to a suitable image to gain bubble's height, width and volume data. Before using this filtering technique to present image processing, image pre-processing is undertaken by firstly, magnifying the original image (Figure 5.9a) by a factor of 3 as shown in Figure 5.9b. Next, the electrode edge is detected based on the dynamic video record (experimental results); The particulate shadow around the bottom of the bubble is removed by identifying the bubble contour under this condition ensuring that no dimensional information is lost (see Figure 5.9c); reflected light is removed (Figure 5.9d) using a binary conversion). Finally, the filtering technique is applied to obtain useful images for dimensional calculations as shown in Figure 5.9e.

### **5.4.2 Thermal bubble growth and departure on the grounded electrode**

Typical bubble growth in the absence and presence of electric fields at 30, 40, and 50 kV is shown in Figure 5.10 a, b, c and d, respectively. It is seen that the thermal bubble grows uniformly like a sphere in the absence of electric field due to the combined effects of inertia forces and surface tension forces; in around 10 ms, the bubble is released into the bulk liquid nitrogen because the resultant forces of inertia and buoyancy exceed the surface tension force. However, when the electric field is applied, the bubble cannot retain its near spherical shape at the initial state of the growth, but is elongated to a prolate spheroid in the direction of the electric field, the time the bubble is attached on the plate increases with the applied voltage. As shown in Figure 5.10, at 30 kV, the bubble detaches into the liquid nitrogen in 18 ms; at 40 kV, in 34 ms and at 50 kV, in 69 ms. Accordingly, the bubble departure frequency also decreases with increasing applied voltage, as shown in Figure 5.11; This is very obvious when the applied voltage is greater than 30 kV. This decrease in frequency means that the bubble remains on the electrode surface for longer and is able to achieve greater growth before

departure. The result is a bubble of greater volume as shown in Figure 5.12. It can be seen that the rate of bubble volume increases almost exponentially with increasing voltage. At 50 kV, the departure volume of bubble can be up to around 11 times larger than that of the original case in the absence of an electric field.

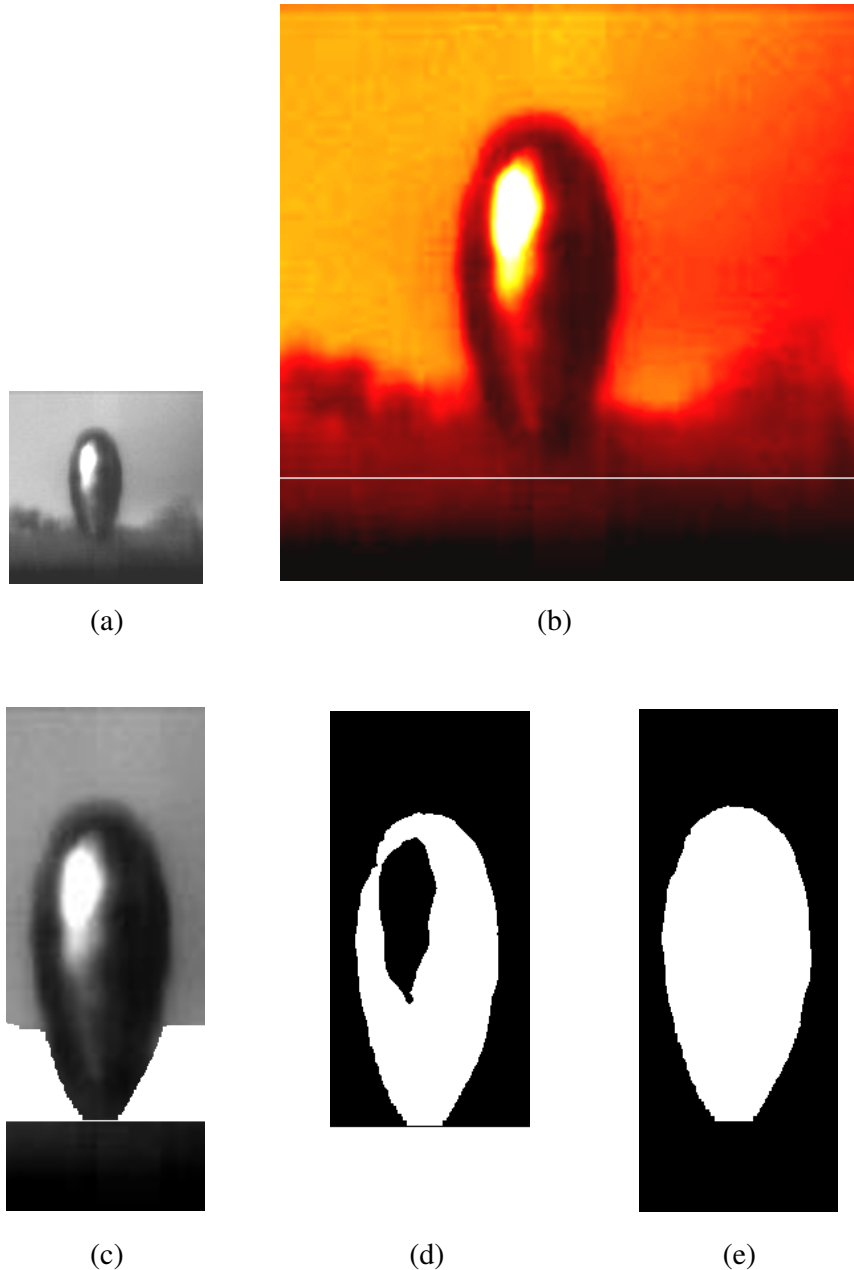


Figure 5.9 Image processing for a bubble at point of detachment

- a) original, b) original x 3 and find electrode edge, c) crop and clean particulate shadow,
- d) binary conversion by thresholding, e) output image for calculation.

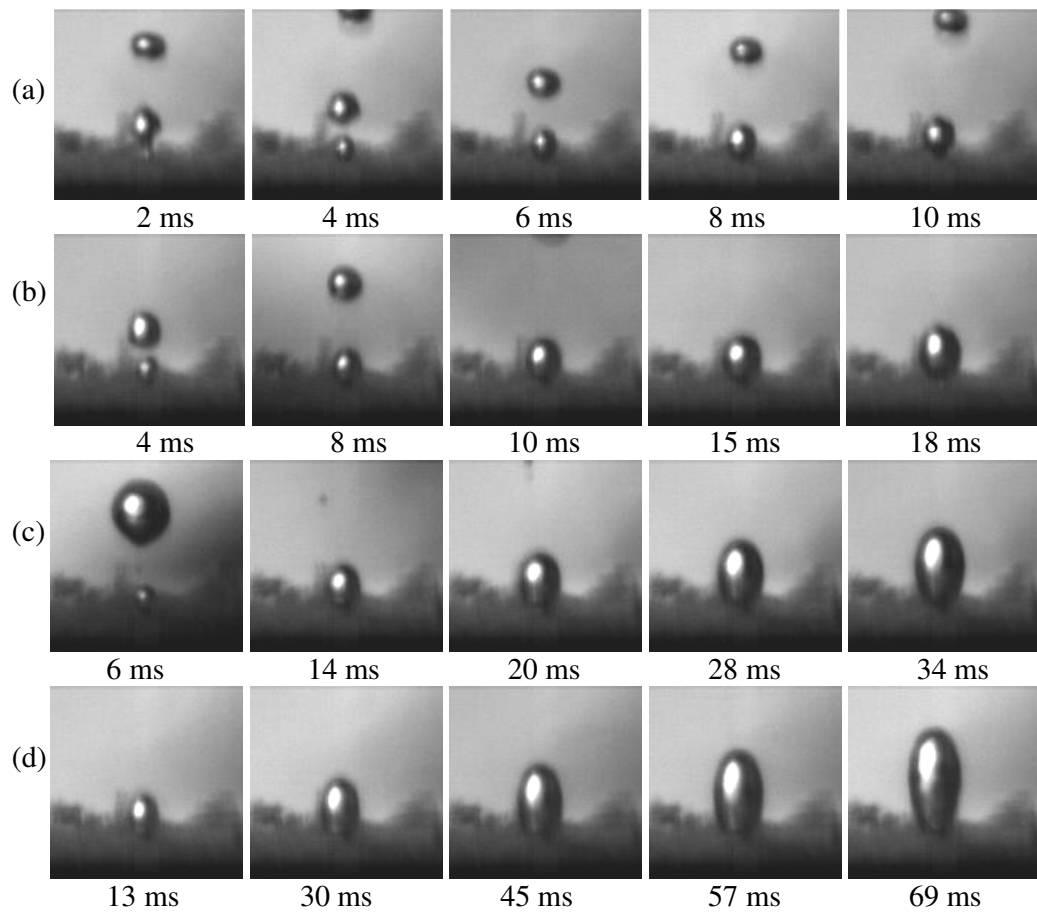


Figure 5.10 Bubble growth in the absence and presence of the electric field ( $V=0\text{kV}$ ,  $30\text{kV}$ ,  $40\text{kV}$  and  $50\text{kV}$  for (a)-(d)), the camera speed is  $5000\text{fps}$

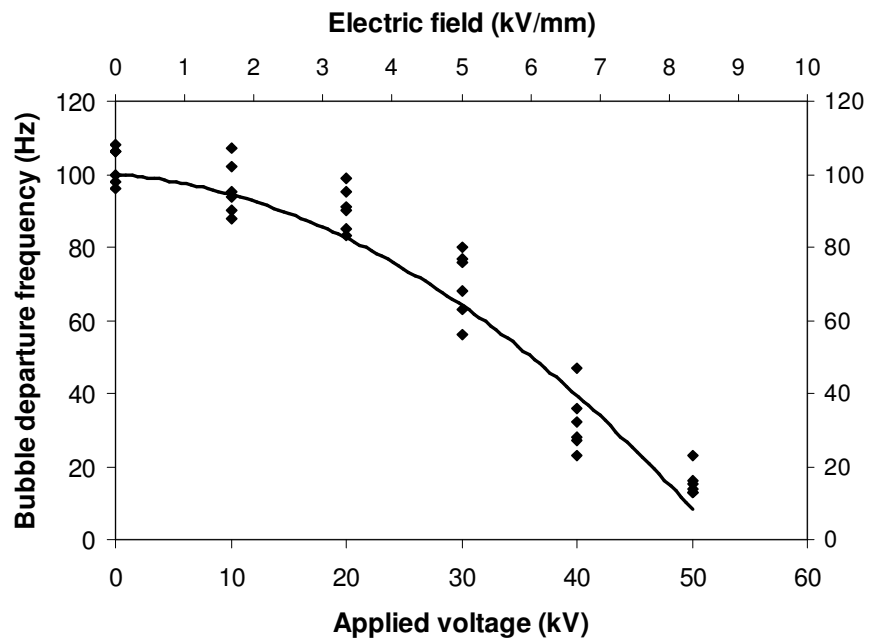


Figure 5.11 Bubble departure frequency as a function of applied voltage and electric field

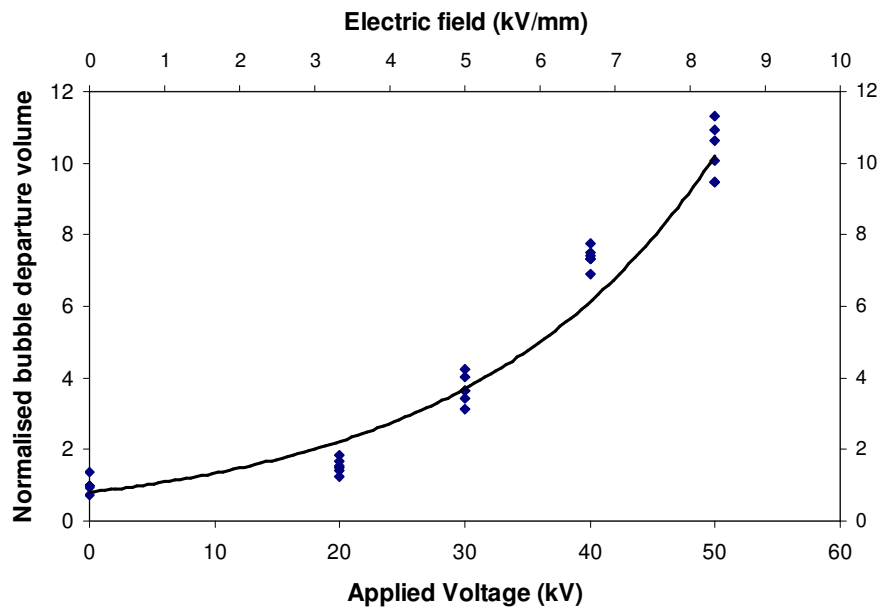


Figure 5.12 Normalized bubble departure volume versus applied voltage and electric field

### 5.4.3 Bubble deformation on the grounded electrode

The non-uniformity of the electric stress on the bubble surface deforms the bubble into a prolate spheroid in the direction of the electric field; this is shown in Figure 5.13. Here, a bubble is just about to detach from the grounded electrode under different positive applied voltages. To further study quantitatively bubble deformation under electric fields, the bubble aspect ratio (the ratio of height to width) as a function of applied voltages has been calculated and is shown in Figure 5.14. It can be seen that the rate of bubble deformation increases as shown in Figure 5.14 with increasing voltage; and the tendency of bubble deformation is particularly prominent at larger voltages. It can be seen that bubble height will reach up to 2.1 times greater than its width when the applied voltage is 50 kV.

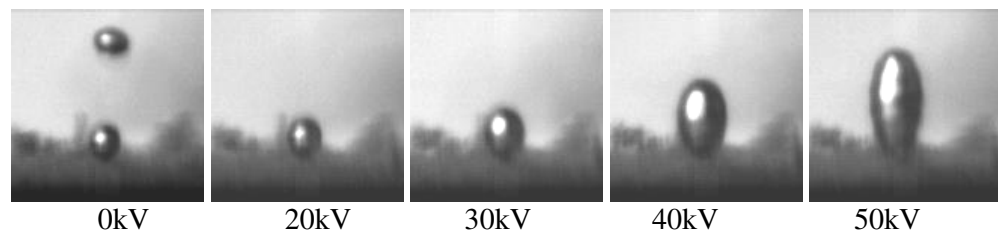


Figure 5.13 Experimental images of bubbles before departure recorded at 5000fps at different voltages

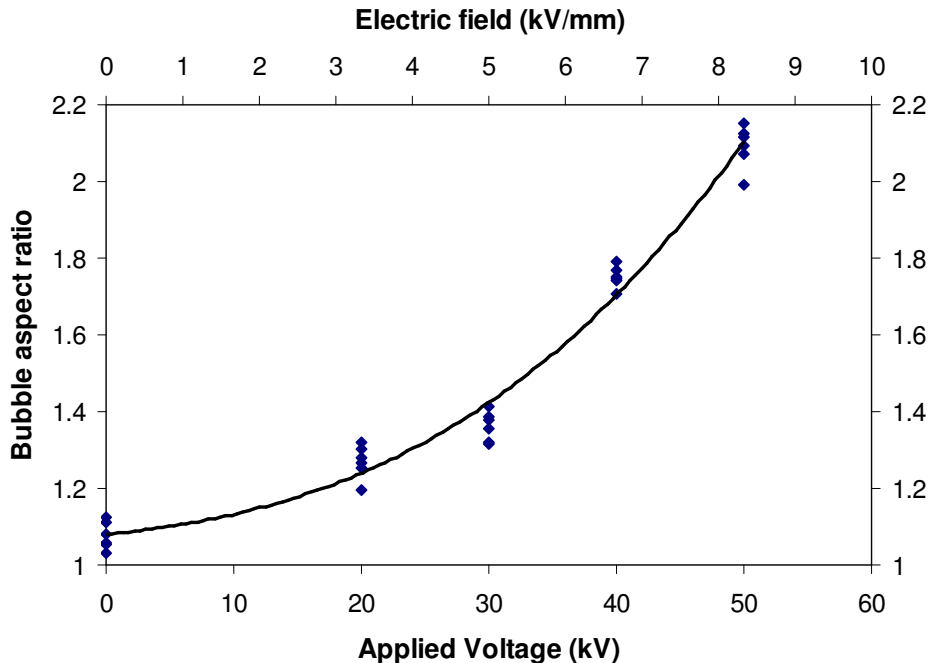


Figure 5.14 Bubble deformation versus applied voltage and electric field

The ratio of surface area to volume for a prolate spheroid bubble is always larger than that for a perfect spherical bubble. In EHD boiling conditions, the deformation of a bubble enlarges the interfacial area between the bubble and the surrounding liquid. Thus, the heat energy can be more effectively transferred from the surrounding superheated bulk liquid to the bubbles by evaporation; therefore, the growth rate of a bubble is higher. This phenomenon contributes to the enhancement of nucleate boiling heat transfer. In addition, due to the distinct differences in thermal properties, electric conductivities and permittivities between the gas phase and the bulk liquid, the bubble deformation will also cause the local electric field to become more non-uniform. These phenomena contribute to the enhancement of nucleate boiling heat transfer.

#### 5.4.4 Polarity effect

All of experimental results discussed above were obtained under positive applied voltages. Thermal bubble behaviour under negative polarity applied voltages has also been carried out. Figure 5.15 shows the experimental images of bubbles before departure at different negative voltages. Compared with those under the positive voltage, the results show that there is no noticeable polarity effect. Very similar phenomena and results were observed and obtained for both polarity electric fields.

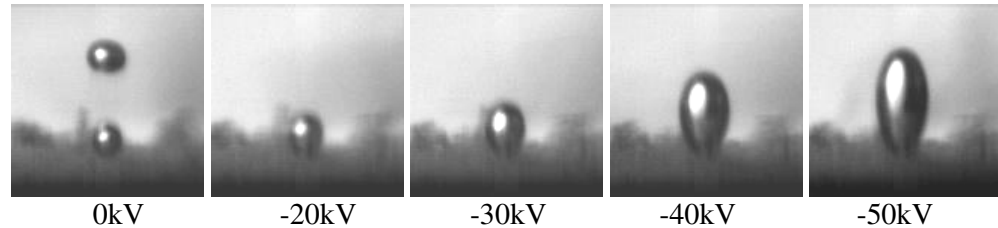


Figure 5.15 Experimental images of bubbles before departure recorded at 5000fps at different negative voltages

#### 5.4.5 Comparison with previous research results

Figure 5.16 shows experimental results of bubble departure frequency as a function of electric field strengths from a previous project within the Tony Davies High Voltage Laboratory [104] and from this investigation. With reference to this figure, it can be seen that the bubble departure frequency is a near linear relationship with electric field strength in the earlier study and is non-linear in the present study although in general the bubble departure frequency always tends to decrease with increasing electric field strength. This is because the experimental parameters for two the experiments are different. Table 5.1 summarizes the main parameters of the two experiments. One of most obvious differences is the maximum electric field strength applied to the HV electrode. It can be up to 8.333 kV/mm in the present study which is much higher than the 2.667 kV/mm in the earlier experiment. The present experiment provides results over a larger range of electric field strength. In addition, for no electric field conditions, the bubble departure frequency in the present experiment is about 4 times greater than that obtained in the earlier experiment. This is mainly due to different diameter of blind hole (bubble source) and heater input power between these two experiments. For the other two parameters, both sets of experimental data are in good agreement on bubble departure volume at a small range (0-2.667 kV/mm) as shown in Figure 5.17. However, the bubble aspect ratio is different (see Figure 5.18) and this maybe also related to these factors such as the diameter of blind hole and heater input power. In addition, the new laser cut 100  $\mu\text{m}$  hole is a much ‘cleaner’ cut compared to the mechanically cut hole previously which may also change some characteristics.

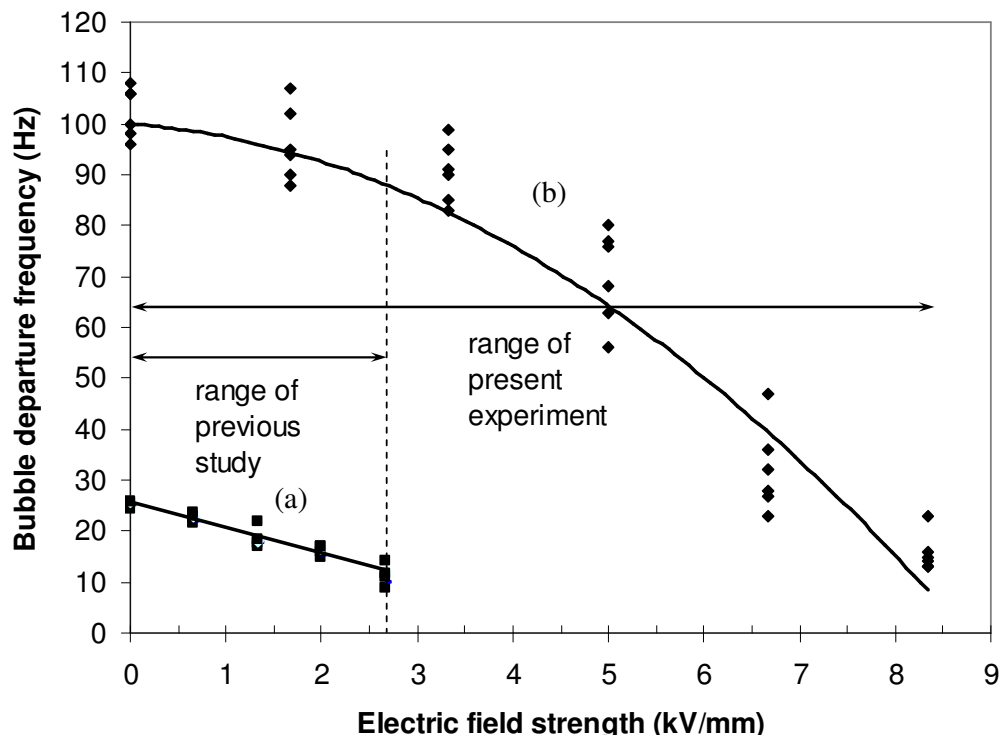


Figure 5.16 Comparison of experimental data on bubble departure frequency as a function of electric field strength for two experiments.

(a) previously obtained [104], (b) this study

Table 5.1 The comparison of parameters for the two experiments

Items	previous study [80, 104]	present experiment
Diameter of blind hole (thermal bubble source)	200 $\mu\text{m}$	100 $\mu\text{m}$
Heater input power	268.8 mW	360 mW
Distance between both electrodes	30 mm	6 mm
Applied maximum electric field strength	2.667 kV/mm	8.333 kV/mm
Electrode configuration	Plane-to-plane (uniform electric field)	Mesh-to-plane (uniform electric field)

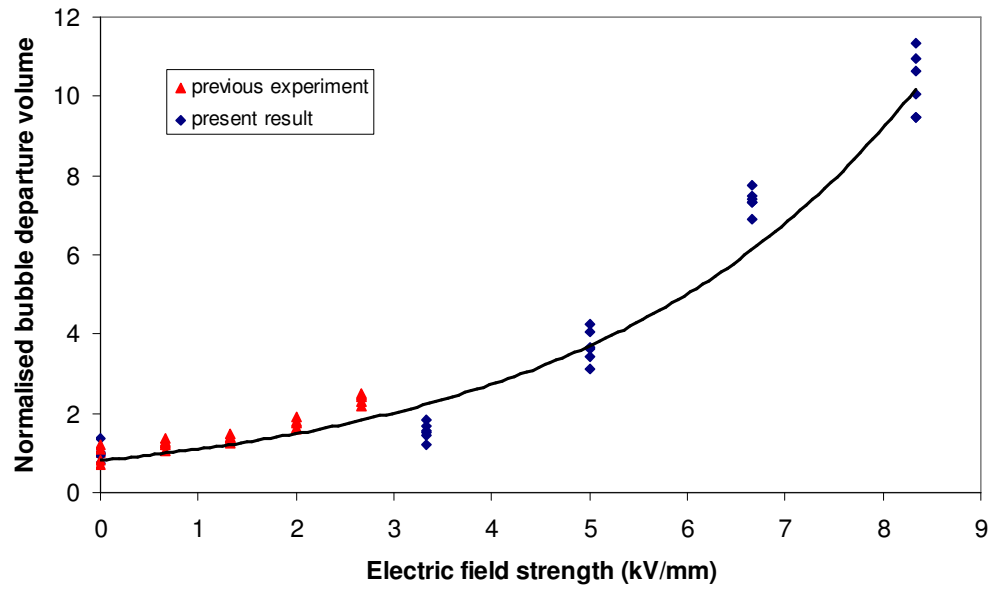


Figure 5.17 Comparison of experimental data on bubble departure volume as a function of electric field strength for two experiments.

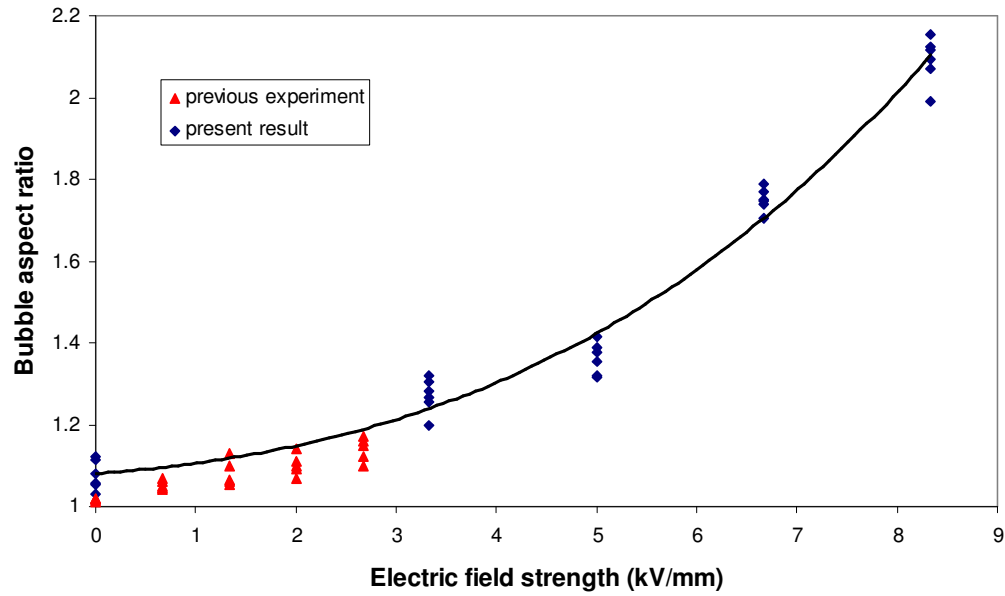


Figure 5.18 Comparison of experimental data on bubble aspect ratio as a function of electric field strength for two experiments.

## 5.5 Summary

Experimental investigations have been undertaken to study the effect of a uniform dc electric field on the behaviour of a thermally induced bubble in liquid nitrogen. The study has found that the behaviour of a bubble can be significantly influenced by an externally applied electric field. While attached to the electrode, the bubble is elongated in the direction of the electric field and grows as a prolate spheroid. The bubble departure frequency decreases and bubble departure volume increases with increasing applied voltage. The bubbles in the electric field are pushed against the grounded electrode, and will move horizontally along the plate if the horizontal components in the two hemispheres of bubble are not in balance. When the applied voltage is raised to a higher magnitude, this intensifies the local flow and turbulence within the thermal boundary layer, reduces thermal resistance and enhances heat transfer. In addition, the theoretical explanation of the bubble's shape has been studied through analysis of a FEA model of the electric potential distribution and the electric forces around a bubble. Finally, a comparison of experimental results obtained as part of this study with an earlier experiment has shown good agreement for bubble departure volume against electric field strength.

## Chapter 6

# The Effect of Electric Field on

## Boiling Heat Transfer of Liquid

### Nitrogen

#### 6.1 Introduction

Liquid nitrogen is used as the coolant for high temperature superconducting (HTS) devices, such as HTS cables. In such cases, heat transfer into the liquid nitrogen is an important issue, and interest is focused on the heat transfer characteristics of liquid nitrogen under electric fields due to two main reasons: Firstly, the heat transfer characteristic of liquid nitrogen is an important factor for HTS equipment design and operation processes, i.e. the equipment must maintain thermal stability. Secondly, the concept of enhanced boiling heat transfer by using an electric field (EHD technique) is also one of the methods used to increase the heat transfer coefficient in cryogenic cooling systems. In the cases of small scale and compact designs, heat transfer enhancement techniques should be considered because the heat needed to be removed per unit area will be increased.

To date, many experimental investigations have been carried out on the boiling heat transfer of liquid nitrogen by using a metallic surface [49, 53, 106] or superconductor surface [46, 50] under zero-fields. However, the effect of an electric field on heat transfer of liquid nitrogen has not been systematically studied. Only a few published results are available [83, 84, 103].

It is well known [68, 69, 71, 107] that the EHD enhancement technique is one of the most promising methods among various active techniques in practical boiling heat transfer applications. It has several advantages such as a quick response to control, a significant increase in heat transfer rate and a saving of energy. The EHD enhancing effect on boiling heat transfer rates on many refrigerating liquids [70] are also well documented. But no information directly concerning investigations of the EHD effect in cryogenic liquids is readily available. Therefore, there is the necessity for experimental investigation into the EHD effect on boiling heat transfer in liquid nitrogen.

In this chapter, the effect of a uniform dc electric field on liquid nitrogen pool boiling heat transfer is investigated by using a mesh-to-plane electrode system. Firstly, a copper block electrode, which has a heater and 3 temperature sensors embedded, with a ‘vacuum jacket’ was designed and manufactured. It was designed to ensure that EHD pool boiling will occur only on the heated copper block top surface. A heat transfer FEA model of the copper block and an electric field FEA model of the whole electrode system has been implemented and developed to obtain relevant simulation results in order to provide necessary information for the design of this experiment. Initial boiling heat transfer of liquid nitrogen was investigated with no applied electric field in order to obtain base values for further comparison. The obtained results demonstrate nucleate pool boiling and critical heat flux (CHF). Experiments were performed to investigate the effects of an electric field on the boiling heat transfer of liquid nitrogen including the behaviour of thermally generated bubbles. For this purpose, some key heat transfer characteristics such as the onset of nucleate boiling, nucleate boiling curve, and critical heat flux have been obtained under electric fields. In addition, since the hysteresis phenomenon affects pool boiling heat transfer, experimental tests are carried out to determine the EHD effect on this phenomenon. Finally, bubble behaviour under electric

fields has been visually recorded using a high speed camera and studied in order to propose possible explanations of the EHD effect.

In summary, detailed information on the EHD effect on boiling heat transfer of liquid nitrogen using a simple electrode system at atmospheric pressure has been obtained. The results may be helpful in the design of the liquid nitrogen related components for HTS device cooling. The obtained results provide an initial perspective on the possible improvements for cryogenic cooling of HTS equipment.

## 6.2 Experimental setup and procedures

### 6.2.1 Experiment apparatus

A schematic diagram of the experimental apparatus is shown in Figure 6.1. The apparatus consists of a large metal cryostat, a dc high voltage power supply, a high-speed digital camera, a light source and a electrode and temperature measurement system. Figure 6.2 shows a photograph of the whole experiment apparatus with additional components such as the helium cooling system. The metal cryostat used in the experiment has been described in detail in [108]. It was originally designed and developed for the study of the thermal and dielectric characterization of liquid nitrogen

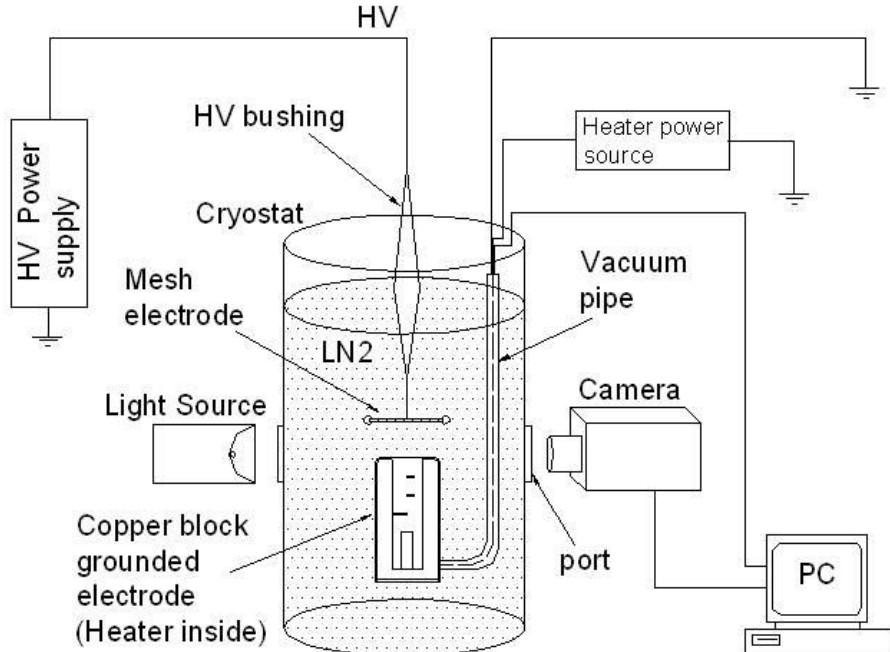


Figure 6.1 Schematic diagram of experimental setup for LN<sub>2</sub> boiling heat transfer study

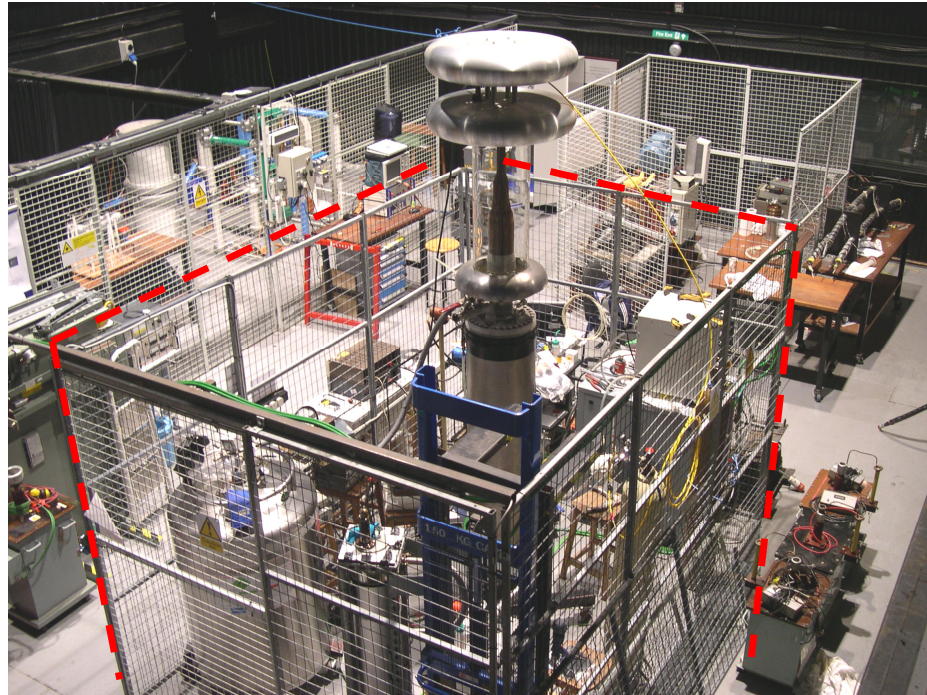


Figure 6.2 A photograph of the whole experimental apparatus

at temperatures between 64 and 125 K. Its inner vessel is rated to allow operation at elevated pressures up to 2 MPa. Through its observation ports, bubble behaviour between electrodes can be monitored and digital images obtained by the use of a high-speed camera and suitable light source. The high voltage is applied to the electrode via a custom-made filled-resin bushing. The HV bushing is able to supply voltages up to 76.2 kV rms at cryogenic temperatures and elevated pressures and is PD free for applied voltages up to 40 kV. Using this apparatus, studies on partial discharge behaviour and bubble dynamics in liquid nitrogen have been reported [80, 109-113].

In the present study, a mesh-plane electrode configuration is used to produce a uniform field. The electric field is applied by means of a high voltage dc power supply that provides voltages of up to 60 kV and has an accuracy  $\pm 1\%$ . The electrode design and temperature measurement are described in the following section.

### 6.2.2 Electrode design and arrangement

Figure 6.3 shows the experimental electrode arrangement. The upper high voltage electrode of either positive or negative polarity is made of a brass mesh (1 mm wire diameter, 2.36 mm width mesh) to keep the bubble flow unrestricted; its void percentage is about 47 percent. The gap between electrodes can be adjusted by moving

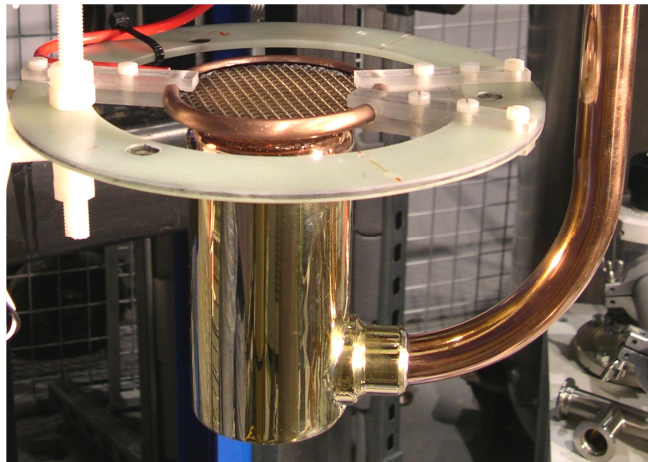


Figure 6.3 Electrode arrangement

the grid (80 mm diameter) up and down vertically before any test. The gap created varies from 5 mm to 50 mm so the electrical field strength can be adjusted for an applied voltage. For this experiment, it was set to 10 mm. In order to avoid surface edge effects, the HV mesh electrode edge and the grounded copper electrode edge are curved. The lower grounded electrode is a special cylindrical copper block with a heater and a ‘vacuum jacket’. A detail drawing of the copper block electrode is shown in Figure 6.4. It consists of two parts, a copper block and a brass tube with solid base. A photograph of the separate copper block and brass tube is shown in Figure 6.5. The top surface of the copper block also serves as the heating surface. Actually, the boiling process takes place at its centre circular surface (around 32mm in diameter), and the heat is supplied by a cartridge heater of 450 W (see Figure 6.4), which allows for heat fluxes of up to  $56 \text{ W/cm}^2$ . The power supply to the cartridge heaters is from the 240 V ac mains via a variac transformer. Two digital multimeters (TTi 1906 bench multimeter) are used to measure accurately both the voltage applied to the heater and the current through it. The copper block inside contains 3 pt100s at different depth locations along its central axis providing temperature measurements for the purpose of determining the top surface temperature. The pt100 locations from the top surface are 21mm, 41mm, and 61mm, respectively (see Figure 6.4) and are 120-degrees apart from each other to reduce their effect on heat transfer. The copper block top surface temperature is deduced by assuming a linear temperature gradient between the pt100 sensors and the heat transfer surface. The heat flux is obtained from the ratio of applied electrical power to heat transfer surface area. This extrapolation depends on a simulation result from a FEA model which shows that the temperature and heat flux are uniform on the

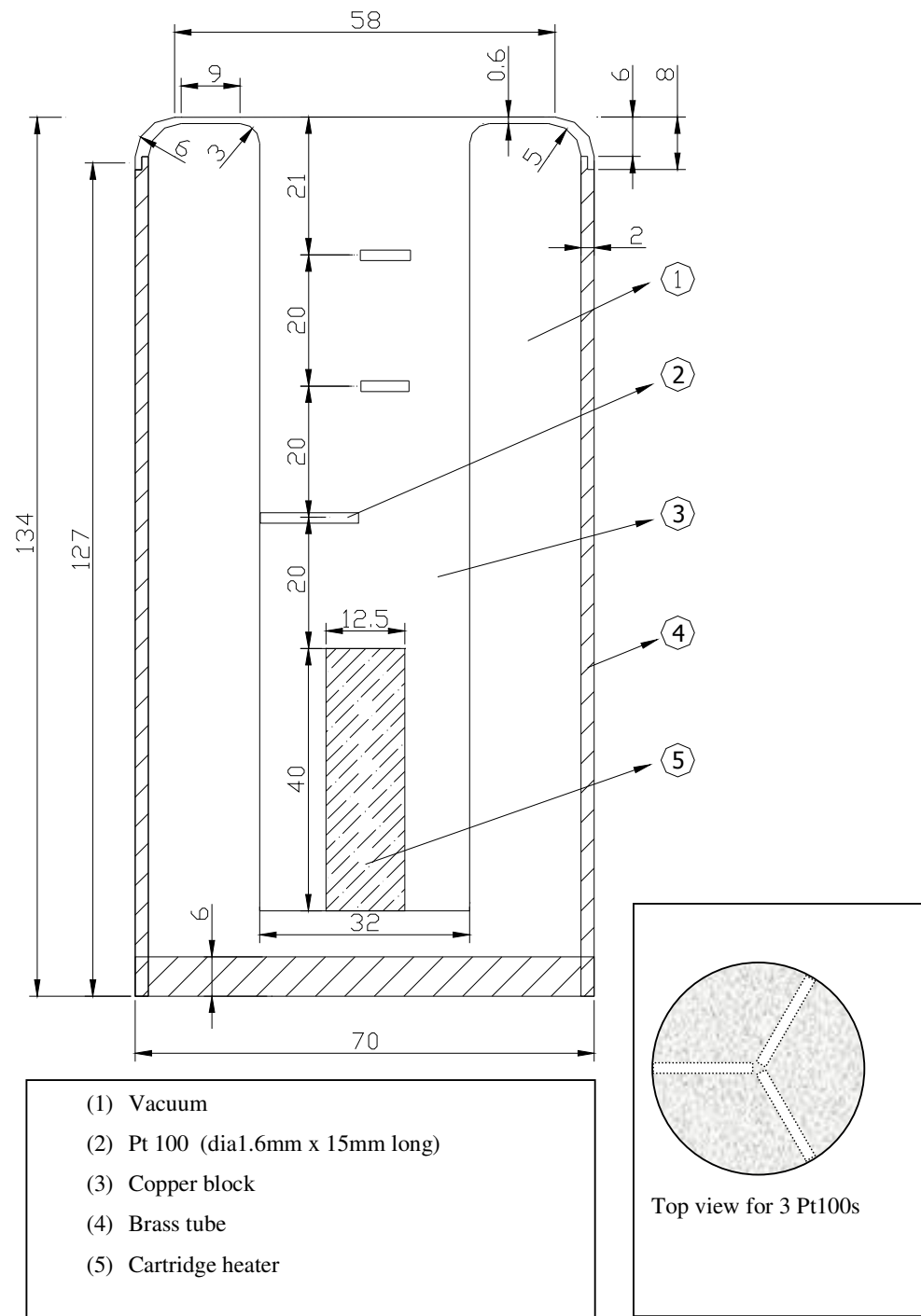


Figure 6.4 Cross section of the grounded electrode (unit in mm).



Figure 6.5 The copper block and brass tube

heated surface (further details in section 6.3). The copper block sides are insulated using a vacuum. In addition, aluminised mylar foil is wrapped around the cylindrical copper block to reduce heat radiation into the liquid nitrogen. The brass tube (70 mm in outer diameter, 2 mm wall thickness) with a base (6 mm thick) is used to support the copper block and form a vacuum jacket between them. The copper block and the brass tube are soldered together by pure indium (see Appendix C for technical details about indium solder). There is an opening of 22 mm in diameter on the side of the brass tube. A 22 mm-diameter copper pipe (see Figure 6.3) connects the side of the brass tube (which is also soldered using pure indium) and conveys electrical leads to the exterior of the cryostat for electrical connection. At the same time, it provides a means for evacuating the inside of the brass tube, thus, insulating the copper block from its surroundings. This is realized by soldering a one-way valve (ANVER CV38F38F) to the other end of the copper pipe to prevent air flowing back into the brass tube. Vacuum quality inside the brass tube is approximately  $1.2 \times 10^{-5}$  torr.

### 6.2.3 Heat transfer and temperature measurement system

A schematic diagram of the heat transfer and temperature measurement system is shown in Figure 6.6. The system consists mainly of a PC measurement card (National Instrument PCI-4351 high-precision temperature and voltage logger), 3 Pt100 sensors (TC direct 578-084) embedded in copper block electrodes, a cartridge heater of 450 W

power and 2 separate Pt100 sensors. A 4-wire connection is used for each Pt100 measurement in order to ensure good measurement accuracy. An ac power source is used to supply electric power to the heater. By changing the input voltage to obtain different electric power into the copper block, it is possible to control the heat developed at the heat transfer surface. The 3 pt100s embedded into the copper block measure the temperature at the different positions for a given heat input. From these measurements, the heat transfer surface temperature of the copper cylinder block can be inferred. The accuracy of the pt100s and the PC card are  $0.13^\circ$  and  $0.12^\circ$ , respectively. Two separate pt100s are placed at the top and bottom level of the electrode system to monitor the saturation temperature (bulk temperature) of liquid nitrogen. The TC1 and TC2 are the temperature indicators (Eurotherm 2132). Details of the electrical connection of this experiment are included in Appendix A.

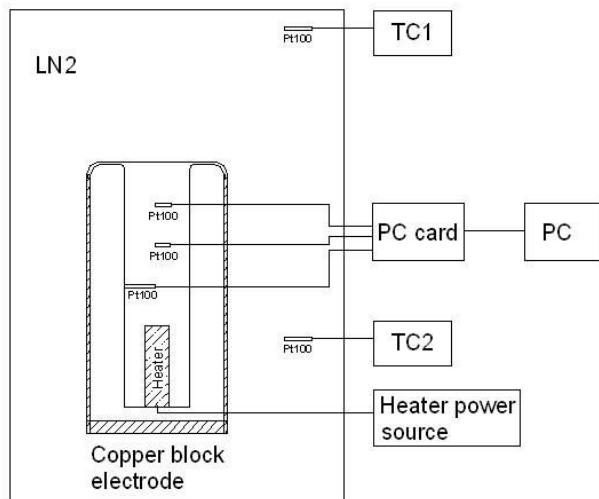


Figure 6.6 Schematic diagram of temperature measurement system

#### 6.2.4 Visual observation

A high-speed digital camera (MotionXtra HG-100K) is set up to examine the effects of an electric field on the behaviour of bubbles and any transitions in heat transfer behaviour. It is capable of a frame rate of up to 100000 fps. In this experiment, the frame rate is set to 500 fps and the resolution is  $640 \times 480$  pixels. A 250 W lamp is used as a light source. Using the camera, heat transfer process of liquid nitrogen such as nucleate boiling and film boiling can be easily identified and recorded. In addition, visual observation also confirms the vacuum heat insulation is functioning properly. As seen in Figure 6.7, boiling mainly occurs in the centre region of the top surface, even

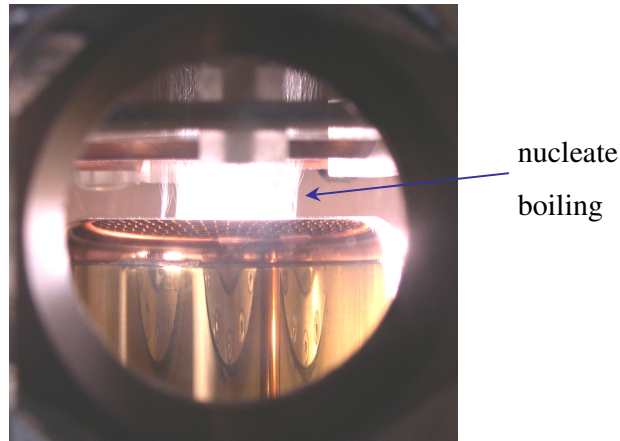


Figure 6.7 A photograph of boiling of liquid nitrogen

though occasionally the indium soldered regions also give rise to localized nucleate boiling at a lower heat flux than was required for nucleate boiling over the entire surface area of the copper block for high heat input conditions.

### 6.2.5 Experimental procedure

The experiments were conducted at atmospheric pressure. The vacuum jacket of the metal cryostat is pumped down in advance to a rough vacuum of about  $5.0 \times 10^{-6}$  torr to keep thermal stability and limit heat loss during the experiments. Before installation of the electrode system into the cryostat, the mesh electrode and heat transfer surfaces (copper block) are polished with a polishing compound and carefully cleaned with soft tissue saturated with ethyl alcohol to remove possible contamination that might affect electrical insulation and heat transfer. After installation of the electrode system and prior to an experiment, a vacuum is applied to the cryostat in order to eliminate non-condensable gases. The cryostat is pumped down to a vacuum of about  $3.4 \times 10^{-4}$  torr. Then, the cryostat is filled with commercial grade liquid nitrogen until the liquid-vapour interface was 0.5 m above the mesh plane electrode. Two level sensors are used to indicate the liquid nitrogen level (high level and low level). They are located in the 520 mm and 380 mm position away from the copper block surface (window centre), respectively. During experiments liquid nitrogen levels are kept between the two levels, i.e. the liquid nitrogen is renewed periodically after each test. The bulk temperature of liquid nitrogen is always held at saturation temperature of 77 K by using a pumped closed circuit helium cooling system. The pressure in the cryostat is maintained at 1 atmosphere using a one-way valve to vent nitrogen gas due to boil-off. This also

ensures that there is always a small positive pressure in the cryostat preventing contamination of LN<sub>2</sub>.

Before formal experiments, A few rough tests are first carried out to obtain some information on ONB and CHF point. In addition, it is necessary to ensure repeatable properties of the system after the boiling cycling process has been repeated many times.

The first experiments are performed under zero-fields. Due to a well-documented hysteresis phenomenon that exists, the complete boiling curves are obtained by gradually increasing the heat flux until the near to CHF, and then gradually decreasing the heat flux. Data including the heater voltage, current measurements and Pt100 readings are recorded after steady state conditions for each heater power level were attained. In addition, images of the heat transfer process and bubble behaviour are visually recorded. This is a time consuming exercise, for completion of one set of experiments, 5 hours or so are required.

Finally, boiling curves are obtained under applied dc voltages of 10, 20, 30 and 40 kV for both polarities. For each run, a constant high voltage is applied to the mesh electrode, the copper block electrode always grounded, the heating voltage is applied and then the same procedure, as used under zero-fields, was undertaken. In each case, experiments were repeated at least twice to ensure the validity of data obtained. The data are found reproducible.

### **6.2.6 Data processing and uncertainties analysis**

The input power,  $Q$ , is the electric power given to the cartridge heater, which is calculated from the measured voltage  $V$  and current  $I$ . i.e.

$$Q = VI \quad (6.1)$$

The average heat flux,  $q$ , is then calculated as:

$$q = \frac{Q}{A} \quad (6.2)$$

where  $A$  is the area of the heat transfer surface,  $A=\pi d^2/4$ ,  $d=32$  mm. The surface superheat,  $\Delta T$ , is defined by

$$\Delta T = T_w - T_{sat} \quad (6.3)$$

where  $T_w$  and  $T_{sat}$  are the heat transfer surface temperature (also called wall temperature) of the copper electrode and the saturation temperature of bulk liquid nitrogen, respectively. The heating surface temperature,  $T_w$ , is deduced from the three pt100 measurement values obtained under steady state conditions; it is assumed that a uniform radial temperature distribution exists along the copper block (discussed further in section 6.3) and then a method of least squares is used to obtain the surface temperature. For example, when a heat flux of  $7.54 \text{ W/cm}^2$  is applied to the copper block electrode and a steady state attained, the readings of  $T_1$ ,  $T_2$  and  $T_3$  are 90.144, 87.069 and 84.323 K, respectively. Then, the heat transfer surface temperature,  $T_w$ , can be obtained by using this method, it is 81.212 K as shown in Figure 6.8. As seen in this figure, the R-squared value of 0.9996 displays also a good linear agreement. The saturation temperature,  $T_{sat}$ , is maintained at 77 K, it is measured by two calibrated pt100s placed close to the bottom of the cryostat (140 mm away from the heat transfer surface of the copper block electrode).

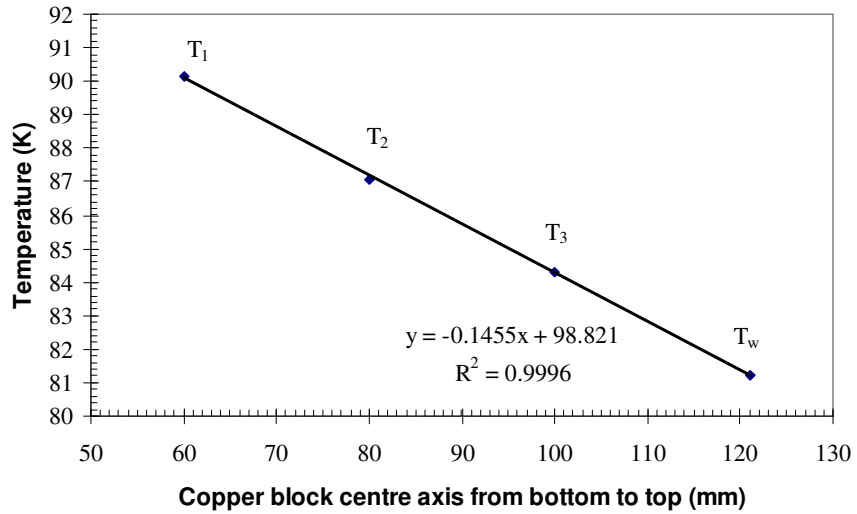


Figure 6.8 A sample to calculate the heating surface temperature

The heat transfer coefficient,  $h$ , is found from

$$h = \frac{q}{\Delta T} \quad (6.4)$$

A heat transfer enhancement ratio,  $f$ , which represents the efficiency of EHD augmentation of heat transfer directly, is subsequently calculated as

$$f = \frac{h(V)}{h(0)} \quad (6.5)$$

where  $h(V)$  is the heat transfer coefficient with an electric field, and  $h(0)$  is the heat transfer coefficient without an electric field.

A total uncertainty analysis is performed for all the measured data and calculated quantities based on methods described by Kline and McClintock [114]. Great care is taken to calibrate properly all instrumentation, which allowed for a complete uncertainty analysis to be performed with the lowest possible experimental uncertainties. The directly measured quantities are temperature, voltage, and current. The multimeter has accuracies of 0.2% and 0.37% for voltage and current readings, respectively. The 3 pt100s are calibrated with an accuracy of  $\pm 0.13$  K. the NI PC card has an accuracy of  $\pm 0.12$  K for RTDs. Thus, the relative error for the measurement of the temperature is about  $\pm 0.25$  K. The uncertainty on the bulk temperature of LN<sub>2</sub> is  $\pm 0.25$  K. The error on the calculated surface temperature is less than  $\pm 0.10$  K. The error in superheat  $\Delta T$  is estimated to be  $\pm 0.35$  K.

### **6.3 FEA model, simulation results and analysis**

It is necessary to simulate the real experiment by setting up an effective finite element analysis (FEA) model. The goals of the FEA simulation analysis are to aid the selection of the right measurement system for the real experiment. The FEA model also provides the opportunity to compare simulated results with experimental results.

#### **6.3.1 The heat transfer model and its input parameters**

Using the electrode geometry described in Figure 6.4, a 2-D copper block electrode heat transfer model has been developed using FEA software as shown in Figure 6.9. To minimise computational effort, the FEA model takes into account the symmetry of the electrode arrangement. A simple 2-D slice is taken through the centre line ( $r=0$ ) of the electrode arrangement and half is drawn into the FEA software. The axis of symmetry is the left hand edge for all plots obtained. The electrode outer boundary temperature is set to a constant value, for example, liquid nitrogen boiling temperature of 77 K; its inner boundary (heater location) is set as a heat source. Thermal conductivity of copper and brass are 400 W/m·K and 159 W/m·K, respectively.

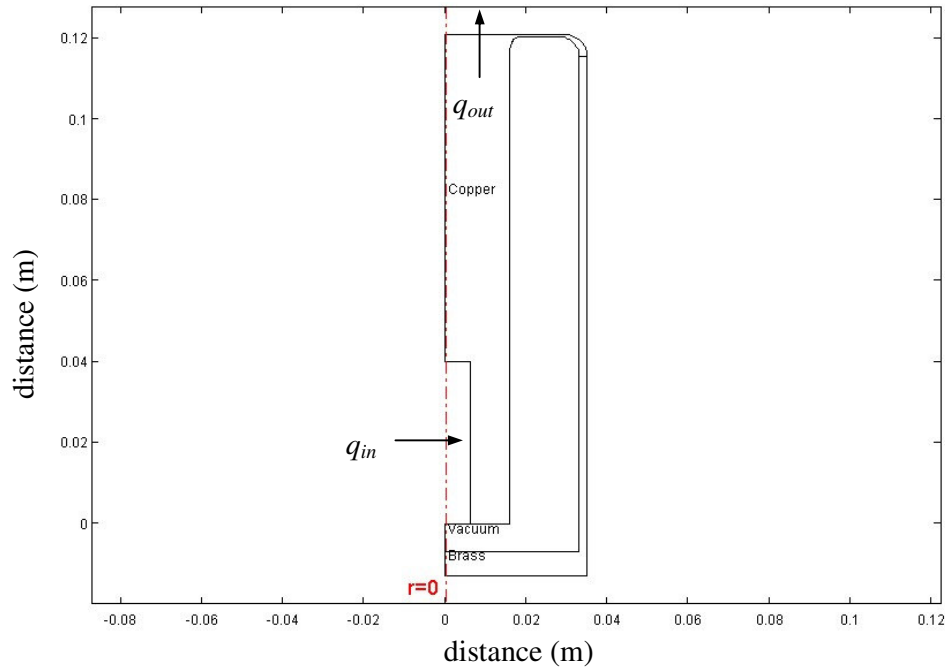


Figure 6.9 The 2-D axial symmetric copper block electrode FEA model

### 6.3.2 Simulation results and analysis

With regard to Figure 6.9, after setting an input heat flux  $q_{in}$  and outer boundary temperature  $T_{out}$ , the temperature distribution of the copper block and the heat flux  $q_{out}$  of the top surface of the copper block can be obtained using the model. Figure 6.10 shows a typical heat transfer simulation result. Here, the input power of the heater is 100 W (i.e.  $q_{in} = 63661.98 \text{ W/m}^2$ ) and outer boundary temperature  $T_{out}$  is set to 77 K. Figure 6.11 shows a close-up view of the electrode temperature contour. It can be seen clearly that the uniformity of temperature inside the copper block is very good. This will guarantee temperature measurement reliability from the horizontal Pt100 sensors fitted into the copper block. Figure 6.12 details the temperature value along the central axis of the copper block electrode. It is seen that there is good linear relationship between the temperature value and the distance in the vertical direction in the range 0.05 to 0.0121 m, which covers the 3 pt100s. This will help to calculate the temperature of the top surface of the copper block electrode after obtaining measured temperatures at 3 fixed positions by using pt100s. An example (see Figure 6.8) has been previously described in section 6.2.6.

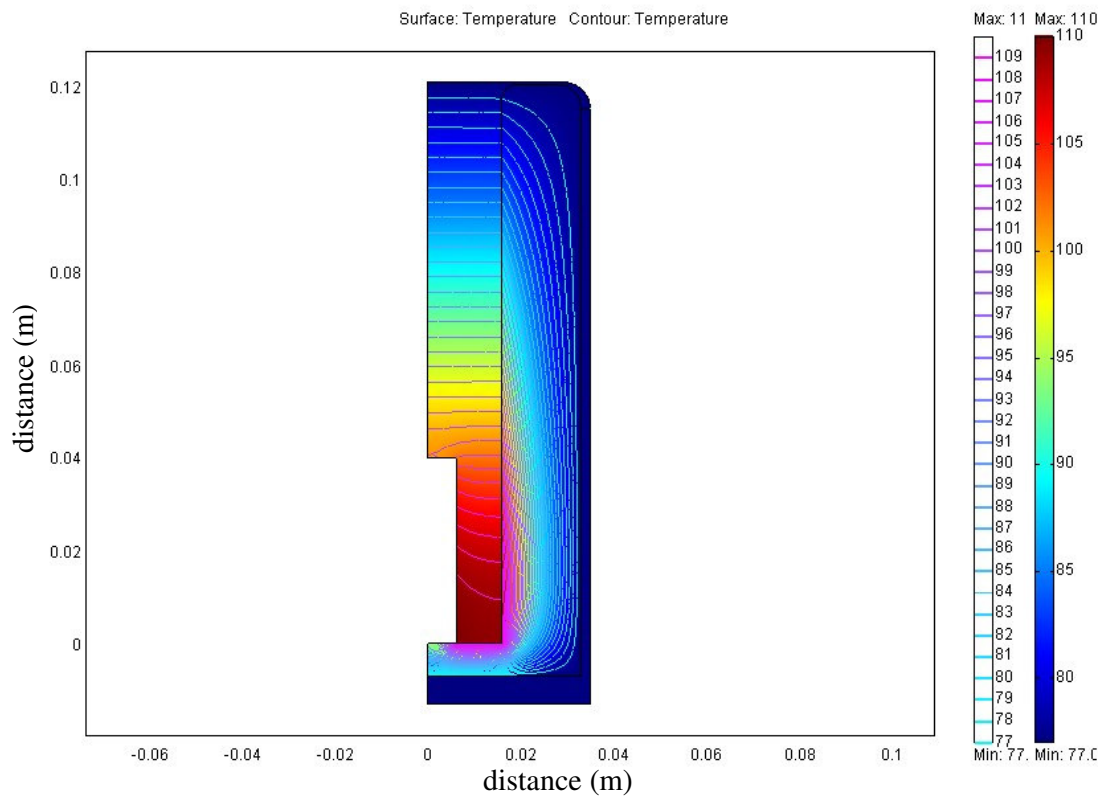


Figure 6.10 The 2-D axial symmetric surface plot, continuous plot of temperatures (input power is 100 W and outer boundary temperature is 77 K)

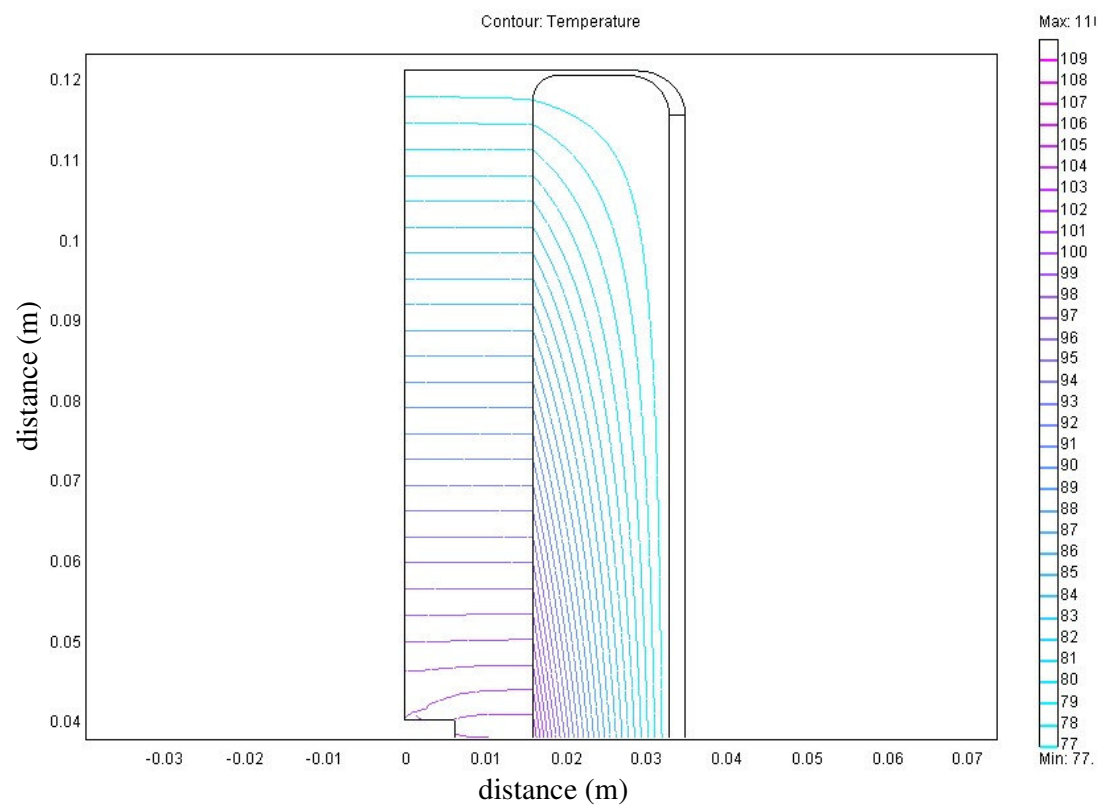


Figure 6.11 A close-up view of the electrode temperature contour

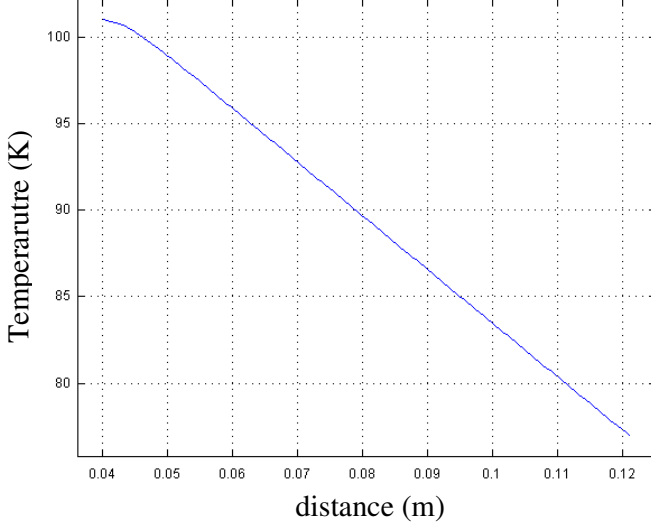


Figure 6.12 Temperature along the central axis, bottom to top

Through changing the heater power (equal to changing the input heat flux,  $q_{in}$ ) into the copper block, the temperatures of 3 pt100s and the heat flux through the top region of the copper block will change. Table 6.1 details the simulation results of these temperatures and temperature difference between them as well as the corresponding heat flux,  $q_{top}$ , through the top surface under different input power conditions. In this table, Q represents the heater power (W),  $q_{in}$  is the input heat flux into the copper block ( $\text{W/m}^2$ ),  $T_1$ ,  $T_2$ ,  $T_3$  are the temperature values (K) of test points where 3 pt100s are placed.  $T_{top}$  is the top surface temperature (K) of the copper block;  $q_{top}$  is the heat flux ( $\text{W/m}^2$ ) through the top surface of the copper block. From these simulation results, key information can be obtained; one is that high precision equipment is required for temperature measurement to be able to differentiate the low temperature differences at low heater powers, the other requirement is that a heater which provides more than 200W power is necessary to have enough heat flux to approach or exceed the CHF of liquid nitrogen. Published research [46, 60, 61, 63, 64] has shown that the CHF of nitrogen is about  $20 \text{ W/cm}^2$  depending on the experimental conditions (no electric field).

The choice of the thickness of the top copper cap of the heater electrode is also an important issue. The non-heat transfer area of the copper cap needs to be considered as it must not only withstand pressure from the  $\text{LN}_2$  above it but it is also required to reduce heat losses. Figure 6.13 shows a typical heat flux plot in the upper region of the

Table 6.1 The simulation results and analysis

## Temperature and temperature difference analysis

Heater power, Q (W)	Input heat flux, $q_{in}$ (W/m <sup>2</sup> )	T <sub>1</sub> ( K )	T <sub>2</sub> ( K )	T <sub>3</sub> ( K )	T <sub>top</sub> ( K )	T <sub>1</sub> - T <sub>2</sub>	T <sub>2</sub> - T <sub>3</sub>	T <sub>3</sub> -T <sub>top</sub>	T <sub>1</sub> -T <sub>top</sub>	$q_{out}$ (W/m <sup>2</sup> )	
10	6366.20	78.89	78.27	77.65	77	0.62	0.62	0.65	1.89	12150	
20	12732.40	80.78	79.53	78.29	77	1.25	1.24	1.29	3.78	24301	
30	19098.59	82.67	80.8	78.94	77	1.87	1.86	1.94	5.67	36451	
40	25464.79	84.55	82.07	79.59	77	2.48	2.48	2.59	7.55	48601	
50	31830.99	86.44	83.34	80.23	77	3.1	3.11	3.23	9.44	60752	
60	38197.19	88.33	84.6	80.88	77	3.73	3.72	3.88	11.33	72902	
70	44563.38	90.22	85.87	81.52	77	4.35	4.35	4.52	13.22	85052	
80	50929.58	92.11	87.14	82.17	77	4.97	4.97	5.17	15.11	97203	
90	57295.78	93.99	88.41	82.82	77	5.58	5.59	5.82	16.99	109353	
100	63661.98	95.88	89.67	83.46	77	6.21	6.21	6.46	18.88	121503	
110	70028.18	97.77	90.94	84.11	77	6.83	6.83	7.11	20.77	133654	
120	76394.37	99.66	92.21	84.76	77	7.45	7.45	7.76	22.66	145804	
130	82760.57	101.54	93.48	85.4	77	8.06	8.08	8.4	24.54	157954	
140	89126.77	103.44	94.75	86.05	77	8.69	8.7	9.05	26.44	170105	
150	95492.97	105.33	96.01	86.69	77	9.32	9.32	9.69	28.33	182255	
160	101859.17	107.21	97.28	87.34	77	9.93	9.94	10.34	30.21	194405	
170	108225.36	109.10	98.55	87.99	77	10.55	10.56	10.99	32.1	206556	
180	114591.56	110.99	99.82	88.63	77	11.17	11.19	11.63	33.99	218706	
190	120957.76	112.88	101.08	89.28	77	11.8	11.8	12.28	35.88	230856	
200	127323.96	114.78	102.35	89.93	77	12.43	12.42	12.93	37.78	243007	

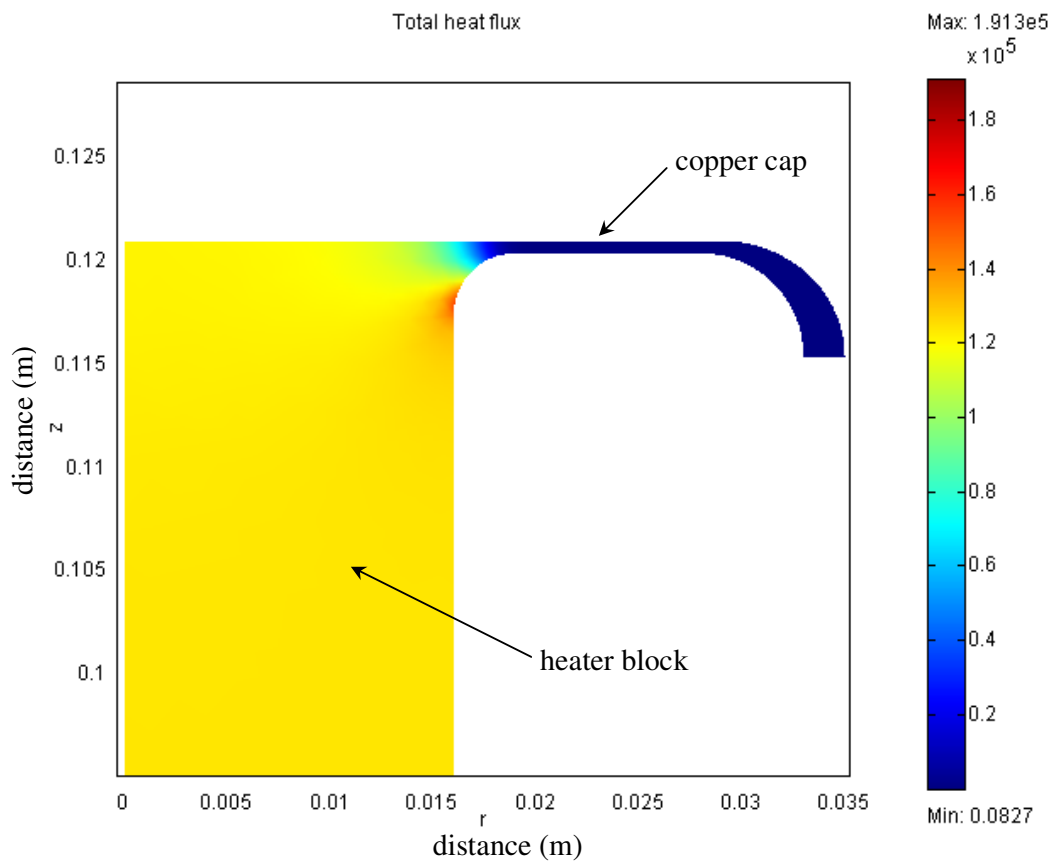


Figure 6.13 Heat flux in the upper region of the copper block electrode ( $Q=100 \text{ W}$ ,  $T_{\text{out}}=77 \text{ K}$ )

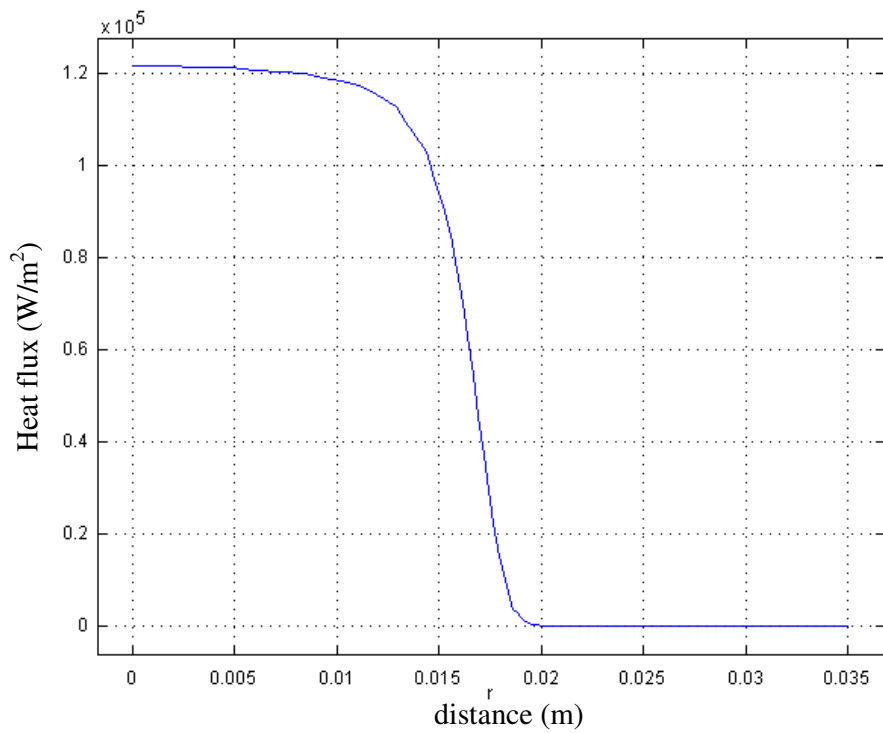


Figure 6.14 Heat flux along the top surface of the electrode

copper block electrode. It is seen that heat uniformity is very good with some enhancement at the point where the heater block joins the top cap. Figure 6.14 details the heat flux along the top surface of the copper electrode. It is seen that the heat flux reduces abruptly from  $1.215 \times 10^5 \text{ W/m}^2$  to zero at the joint area of the copper block and the cap, thus avoiding heat loss. In conclusion, a 0.6 mm top thickness is suitable for this experiment. Details of the pressure analysis are included in Appendix B.

## 6.4 Experimental results and discussion

Experimental tests were carried out with saturated liquid nitrogen (commercial grade, see Appendix D for details) at atmospheric pressure. The liquid nitrogen is renewed after all data for each boiling curve had been obtained.

### 6.4.1 Time to cool process

Cooling the electrode system must be completed before starting the experiments. For reliable performance, the copper block electrode cannot be placed into liquid nitrogen directly, it must be cooled slowly. Figure 6.15 shows a cooling process. T1 represents the temperature of one of 3 pt100s (closest to the heater) embedded in the copper block electrode (see Figure 6.6). In fact, all sensor measurements were nearly the same over this cooling process. It suggests the time needed to cool the electrode system from room temperature to LN<sub>2</sub> temperature (i.e. LN<sub>2</sub> cover the whole copper block electrode) is at least 45 minutes. This careful approach can avoid a rapid temperature drop that may cause the temperature sensors to fail or the electrode to leak at its solder joints.

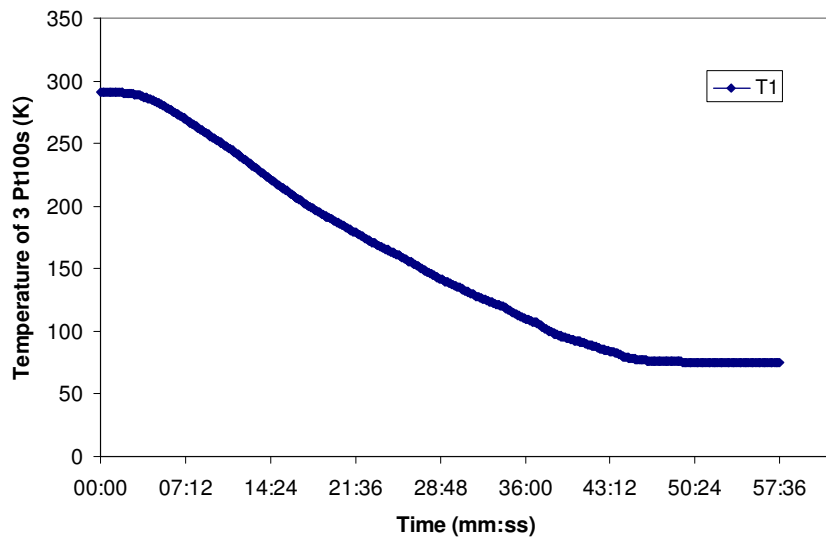


Figure 6.15 Time to cool for the electrode

### 6.4.2 Zero-field heat transfer and typical images

The first part of the experiment involves investigation of the heat transfer characteristic of liquid nitrogen under zero-field conditions. The heat flux ( $q$ ) as a function of surface superheat ( $\Delta T$ ) is shown in Figure 6.16. Even though tests were undertaken on different dates, there is good reproducibility. With regard to Figure 6.16, two observations can be made: (a) The results indicate typical trends of pool boiling for many fluids such as liquid nitrogen [49] [83], FC-72 [115] and R-11[72]. The “heating” curves obtained by increasing heat flux and the “cooling” curves by decreasing heat are different. The heating curves show temperature overshoot, while the cooling curves do not. This hysteresis phenomenon is due to the fact that the highly wetting fluid leaves only smaller imperfections to act as nucleation sites, which require a larger surface superheat to activate. Once the site is activated, the phase-change heat transfer causes the surface temperature to drop. Active sites tend to remain active without requiring higher temperatures. Therefore, no overshoot was observed along cooling curves. Moreover, visual observation also confirmed that this overshoot was due to nucleation with a sudden production of vapour which spread rapidly to cover the whole heat transfer surface; (b) The other fact is that the slope of the nucleate boiling heat transfer curve is much steeper than that of the natural convection heat transfer curve. This indicates more efficient heat transfer for nucleate boiling regimes, i.e. nucleate boiling plays a significant role in transferring heat from the heat transfer surface.

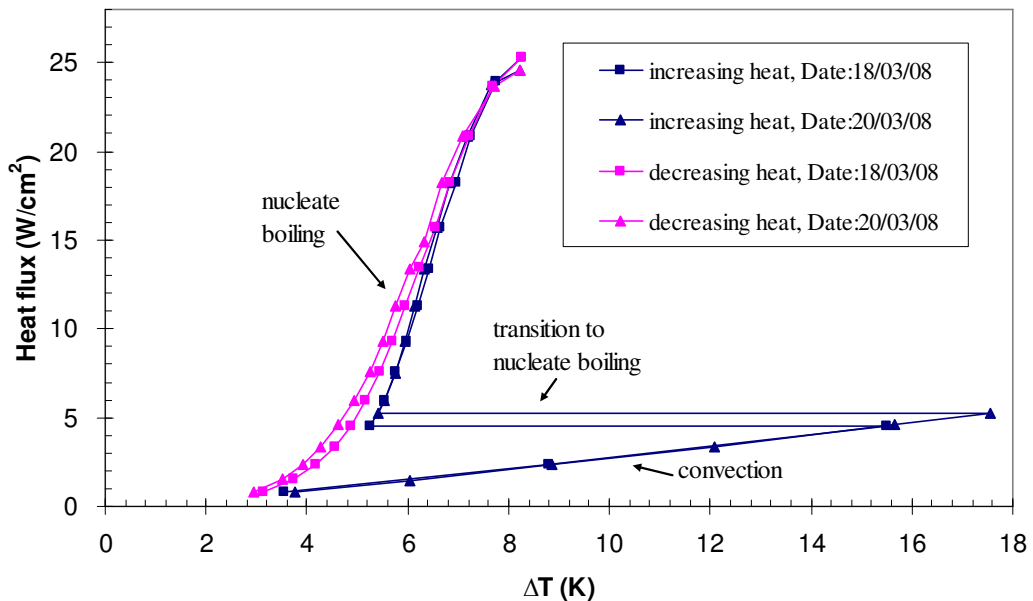


Figure 6.16 Heat flux as a function of surface superheat at zero-field conditions

In addition, visual observation of the whole boiling phenomenon allows identification of three typical heat transfer regimes according to the heat input as shown in Figure 6.17. Note that (b1) is obtained at decreasing heat flux conditions.

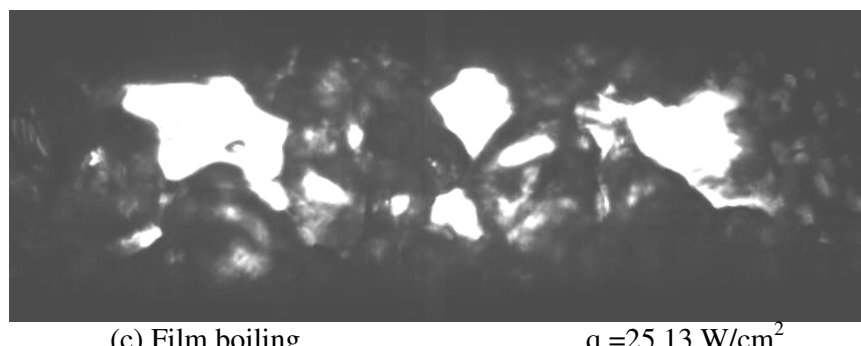
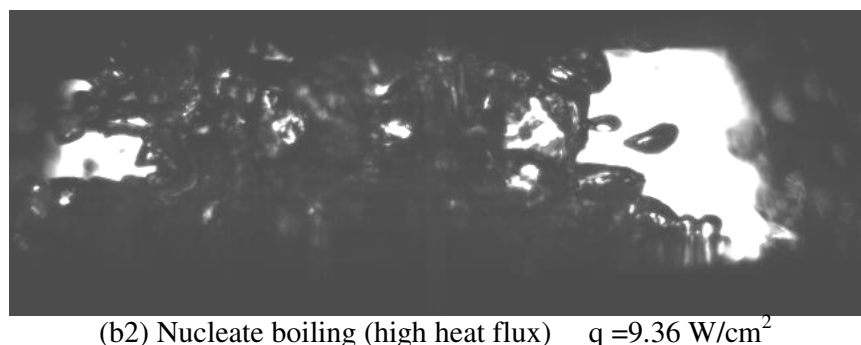
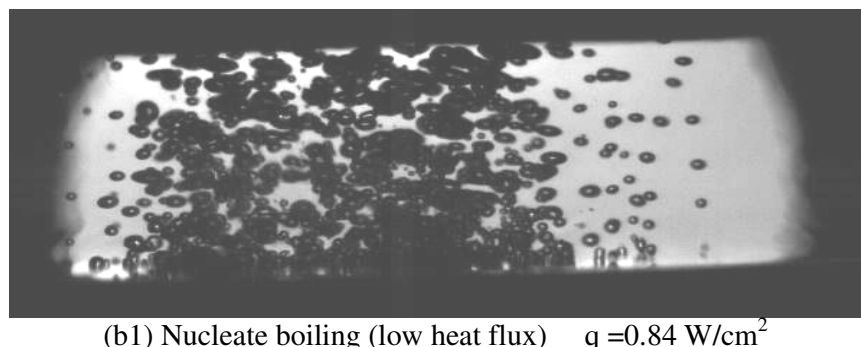
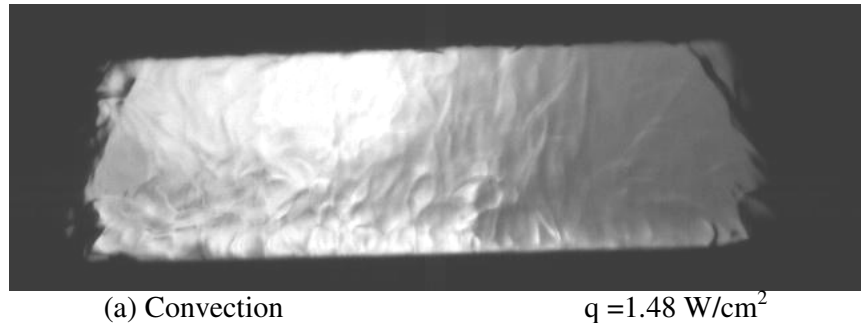
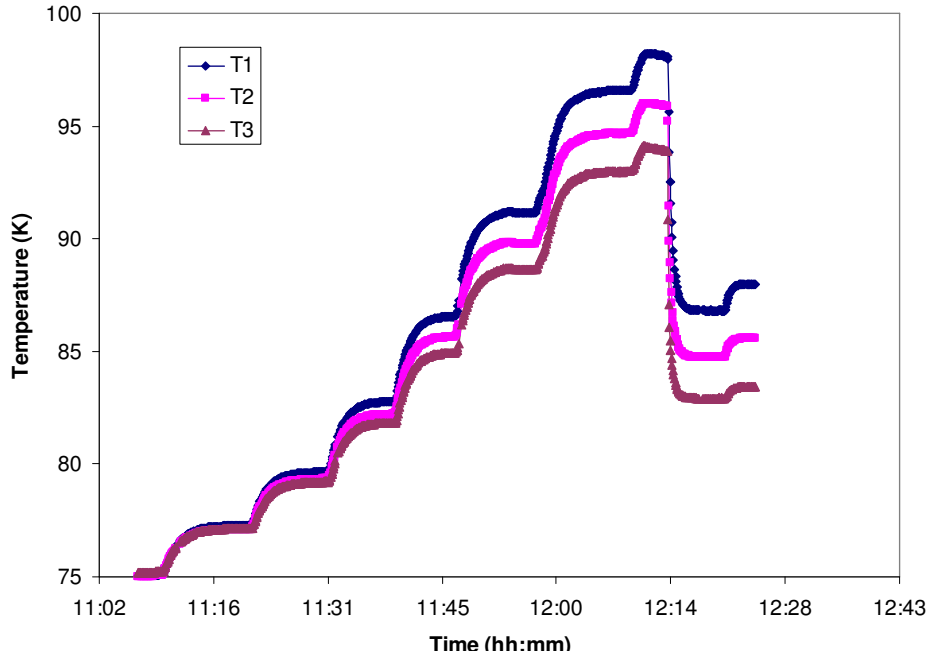


Figure 6.17 Typical images of three heat transfer regimes

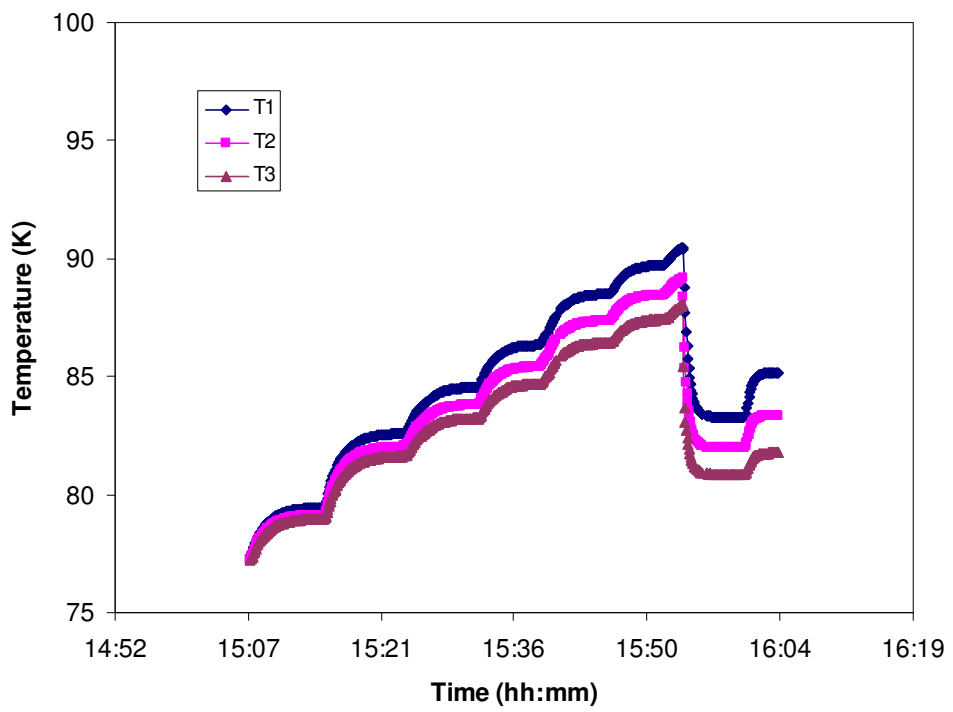
### **6.4.3 Effect of electric field on the ONB**

In order to obtain the ONB with and without high voltages, experiments are conducted at increasing heat flux values. The voltage of the heater power source (that generates heat flux) is raised from zero to the voltage value required to cause ONB in steps of 5V, while near the boiling point the incremental step is reduced to 2V. Each heat input change needs to be held for several minutes to meet the heat balance (see Figure 6.18) between the heat transfer surface and the bulk liquid nitrogen. Boiling incipience is easy to observe visually via the camera and can also be monitored through detection of a sudden drop in temperature (see Figure 6.18) of 3 pt100s embedded into the electrode. Figure 6.19 shows electric field effects on the ONB. Here, 3 test data points at each voltage value are plotted. It is noticed that under zero-field conditions, the ONB occurs at a highest heat flux of about  $5 \text{ W/cm}^2$  corresponding to about 17 K superheat. However, in the presence of an electric field for both polarities, the boiling begins at a lower heat flux and lower values of superheat. For a 40 kV applied voltage, only about  $2 \text{ W/cm}^2$  heat flux is required for ONB corresponding to a superheat of approximately 6 K. It can be concluded that ONB occurs at lower superheat and lower heat flux in the presence of an electric field. In other words, the presence of high voltages will cause nucleate boiling for lower heat inputs. The importance of this data cannot be underestimated as it informs the understanding of the complex transition phenomena (natural convection-nucleate boiling-film boiling) and provides useful references for the cooling stability design of HTS equipment cooled by liquid nitrogen.

It is well known that in pool boiling, a linear or near-linear relationship exists between heat flux and wall superheat, this persists to a high temperature during the increase in heat flux. Once boiling begins, the excess superheat is quickly released by vigorous boiling, resulting in an abrupt temperature drop. This phenomenon (transition of the natural convection to nucleate boiling) is usually called temperature overshoot. The temperature overshoot is a result of deactivation of large nucleation sites that are penetrated by the highly wetting liquid. In fact, it is disadvantageous in some engineering applications, such as the cooling of electric equipment. In the present experiments, the temperature overshoot is very pronounced under zero field conditions. While in the presence of electric fields, it becomes much reduced and will not be present if the electric field is high enough (Note that the overshoot did not disappear in



(a)



(b)

Figure 6.18 Temperature drop of 3 pt100s at onset of nucleate boiling  
 (a) 0 kV condition, (b) 30 kV positive dc voltage condition

the present study as only a maximum 40 kV voltage was applied to avoid breakdown between electrodes). Typical temperature overshoots for 0 kV and 30 kV positive dc high-voltage are shown in Figure 6.18a and b, respectively. With regard to this Figure, it is seen that temperature overshoot is more pronounced for that with no electric field than that with electric fields.

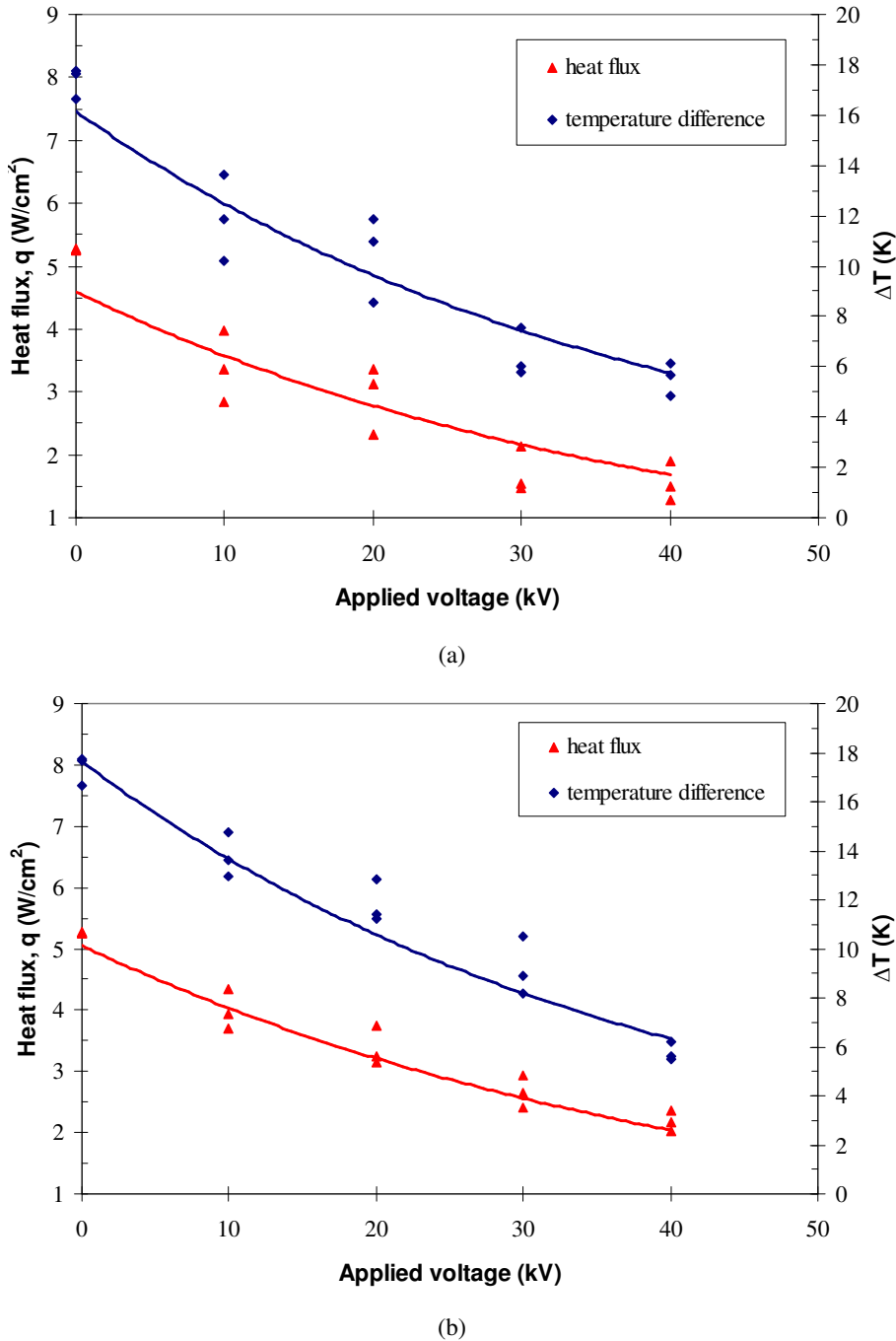


Figure 6.19 Electric field effect on ONB. (a) negative, (b) positive

#### 6.4.4 Effect of electric field on the boiling hysteresis

From previous boiling curve studies, two kinds of hysteresis are often observed as shown in Figure 6.20, the analysis and explanation on these two hysteresis are summarized as follows [75]: The first hysteresis is characterized by a sudden decrease of  $\Delta T$  (temperature overshoot) at boiling incipience and the end of the natural convection regime. This phenomenon corresponds to a change in the heat transfer mechanisms, i.e. from natural convection to nucleate boiling. At the beginning of nucleate boiling, in addition to the natural convection, the first bubbles emerge at some isolated nucleate sites on the heated surface. These nucleate sites correspond to cavities in which small residual quantities of noncondensable gas are accumulated. The liquid superheat needed for the generation of the first bubbles is large. After the departure of the first bubbles, the residual volume of gas inside each cavity is more important, so the superheat needed for the generation of following bubbles decreases. Moreover, the departure of the bubbles in the liquid increases the convective motion, which contributes to wall cooling. This type of hysteresis depends greatly on the presence of noncondensable gases, the wall roughness, and the liquid wettability. For a highly wetting fluid, numerous cavities are initially liquid filled, which increases the hysteresis. The second hysteresis, which remains for high heat fluxes, corresponds to the superheat difference between the two curves obtained at increasing and decreasing heat fluxes. At increasing heat flux conditions, after activation of the first sites, the nucleation in the cavities depends principally on the vapour propagation from one site to another. Indeed, after the growth of the first bubbles, the bubble interface spreads along the heated wall and the neighboring cavities are activated by propagation of the vapour with a weak superheat. For a wetting liquid, the liquid initially in the cavity can be separated from

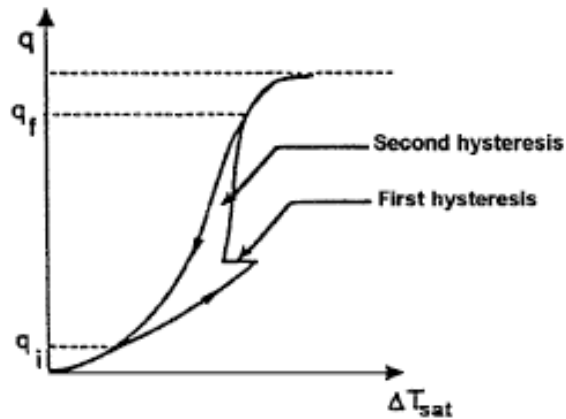


Figure 6.20 Two kinds of hysteresis phenomenon [75]

the main liquid pool. So, the activation of such a nucleate site requires a high superheat. At the decreasing heat flux, the sites stay active for a low superheat because they are already full of vapour.

These explanations above can be applied to the experimental results obtained during this study. The first hysteresis phenomenon for liquid nitrogen is very obvious, as shown in Figure 6.16. There are two main reasons for this result: (a) One is liquid nitrogen is highly wetting [116], the transition between natural convection and nucleate boiling is sudden, causing a temperature overshoot to occur which has been observed and discussed in section 6.4.3; (b) the other is the electrode geometry with heat transfer function used in our experiment. It is well known that the transition between natural convection and nucleate boiling depends on the size of the heating surfaces. For small surfaces such as wires, nucleation is generally homogeneous over the whole heating surface and the propagation of boiling is very fast so that almost no hysteresis effects are observed. For large surfaces, boiling appears at first from the zones where heat flux is locally higher. In that case, after boiling, the establishment of fully developed boiling is slow. The second hysteresis effect is observed in LN<sub>2</sub> for conditions of high heat fluxes near to the critical heat flux (see Figure 6.16).

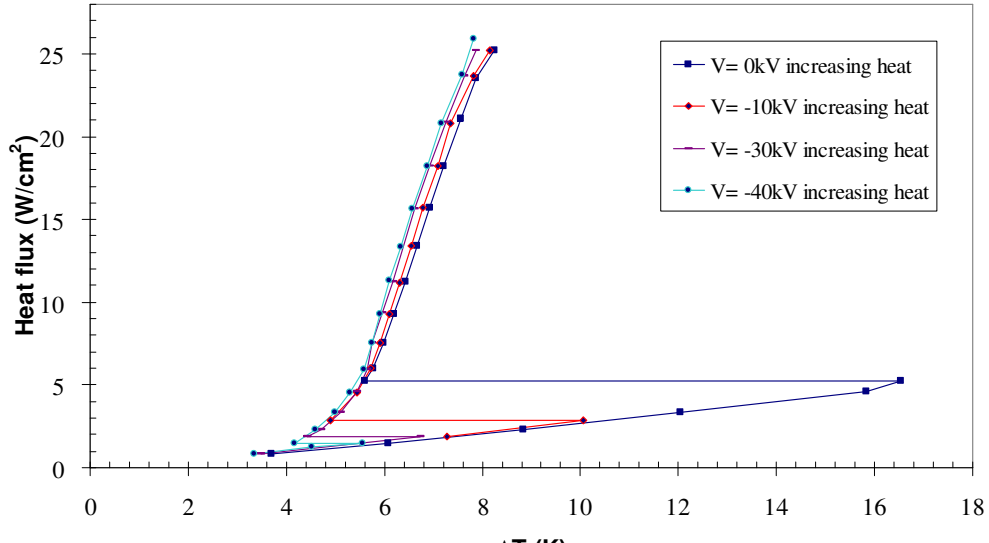
#### 6.4.4.1 First hysteresis in LN<sub>2</sub>

The effect of the electric field on the first hysteresis is shown in Figure 6.21. Here, only data for 0kV and 10, 30 and 40 kV of positive polarity are plotted for clarity. Indeed, it is another method of describing the effect of the electric field on the ONB, that has been previously described in section 6.4.3.

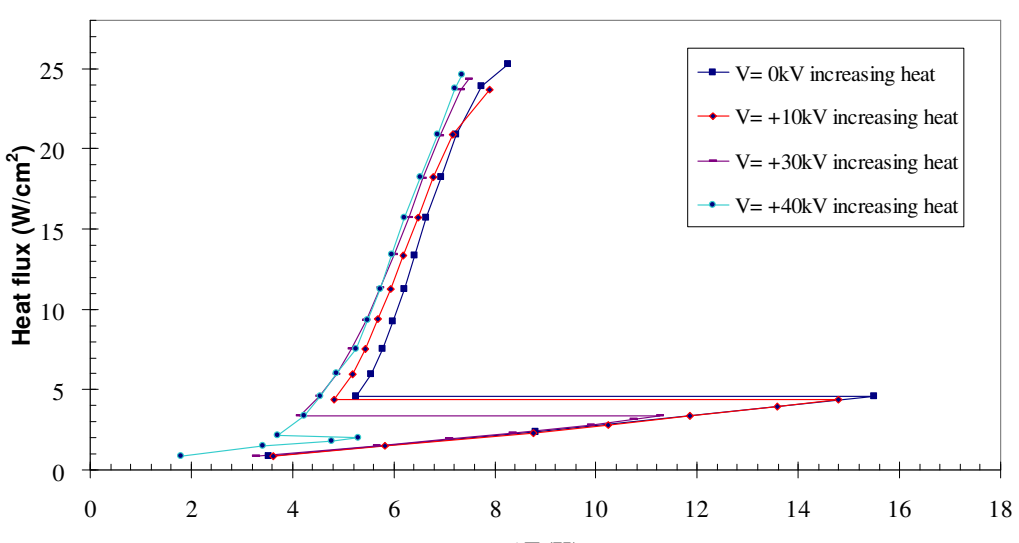
It can be seen that the magnitude of the first hysteresis reduces with increasing voltage. Thereby, decreasing the degree of the superheat required to start nucleate boiling. That means the EHD effect allows heat transfer enhancement. Once boiling begins, initiated by an electric field at a low superheat temperature, it can be maintained without having to maintain an electric field.

The reasons for the decrease or elimination of the first hysteresis under EHD conditions is due to the reduction of the thermal boundary layer caused by an electroconvective movement in the presence of electric fields and then the electrical activation of

nucleation sites. It may be related to the change of surface tensions at the liquid-vapour interface with electric field strength [69]. Visual observations show that an application of a modest electrode potential, results in very easy activation of boiling. Moreover, the number of nucleation sites decrease and bubble sizes become bigger under a higher voltage. This may be a factor which causes the hysteresis effect to decrease. Electrical stimulation of nucleation sites appears to be similar to thermal activation since sites remain active after removal of the activation energy source (i.e. the electric field).



(a)



(b)

Figure 6.21 First hysteresis of liquid nitrogen under high voltage

(a) negative, (b) positive

#### 6.4.4.2 Second hysteresis in LN<sub>2</sub>

Tests with increasing and decreasing heat flux reveal the second boiling hysteresis phenomenon at zero-field conditions as shown in Figure 6.22a. The effect of electric field for an applied dc voltage of 10, 20 and 30 kV is shown in Figure 6.22b, c and d, respectively. It is seen that application of an electric field can decrease the hysteresis when the applied high voltage increases, in particular the hysteresis disappears for high voltages in excess of 20 kV for this electrode arrangement.

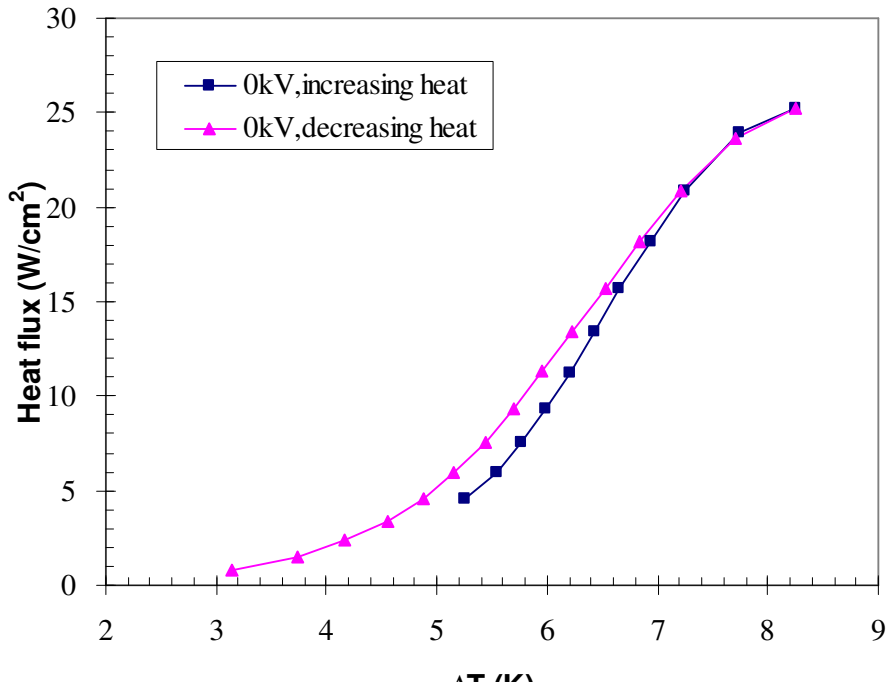
The following is an analysis of the EHD effect on the second hysteresis effect. In order to analyze the elimination of the hysteresis phenomenon with an electric field, it is necessary to consider the effect of the electric forces on the nucleation process.

Through analyzing the energy of a bubble formation in an electric field, the overpressure in the vapor phase as a function of the electric field can be expressed as [75]:

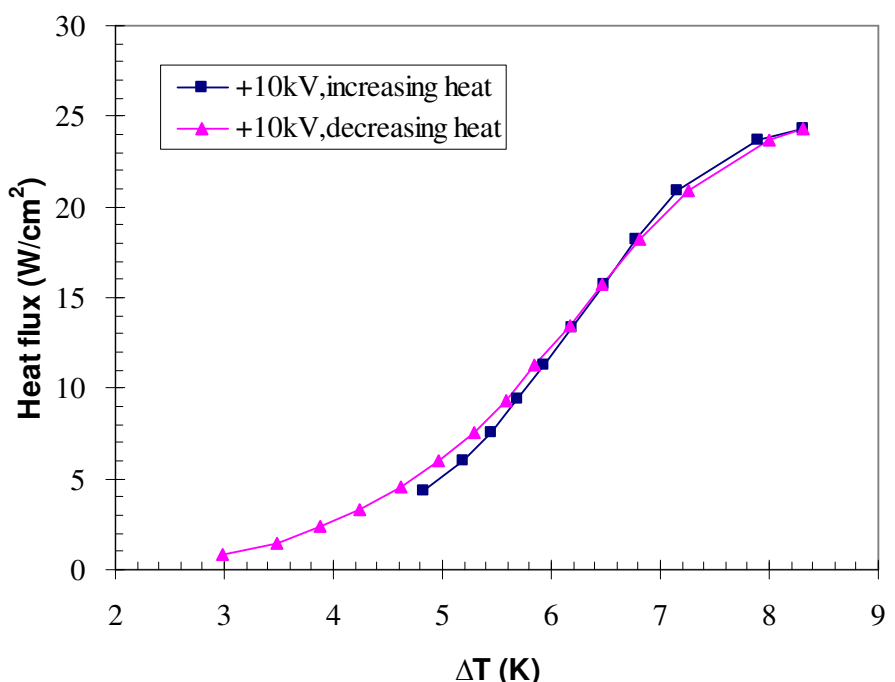
$$P_v - P_l = \frac{2}{r} \left[ \sigma + \frac{3\epsilon_0 \epsilon_l (\epsilon_l - \epsilon_v) E^2}{4(2\epsilon_l + \epsilon_v)} r \right] = \frac{2}{r} (\sigma + \sigma(E)) \quad (6.6)$$

where  $r$  is the equivalent radius of the deformed bubble for EHD boiling, the pressure  $P_v - P_l$  is the sum of capillary pressure, characterized by the fluid surface tension  $\sigma$ , and an electrostatic pressure characterized by an apparent surface tension  $\sigma(E)$ , which is proportional to the square of the electric field strength. The electric field modifies the surface tension so that the fluid has lower-wetting fluid behaviour. According to this analysis, for liquid nitrogen, the ratio  $\sigma(E)/\sigma$  is about 48% and 108% for 20 kV and 30 kV conditions, respectively. These calculations assume a bubble detachment radius of 1mm, and show that the pressure of the electric field on the bubble is substantial in comparison with the capillary pressure. The increase of apparent surface tension with electric field can give a reason for the reduction of the hysteresis phenomenon.

Consequently, at increasing heat fluxes, the activation of nucleation sites is easier and the hysteresis is reduced. Moreover, since bubbles are pressed close to the heated surface under the action of the electric field, gradual propagation of boiling on heat transfer is faster than that occurring in zero-field conditions.

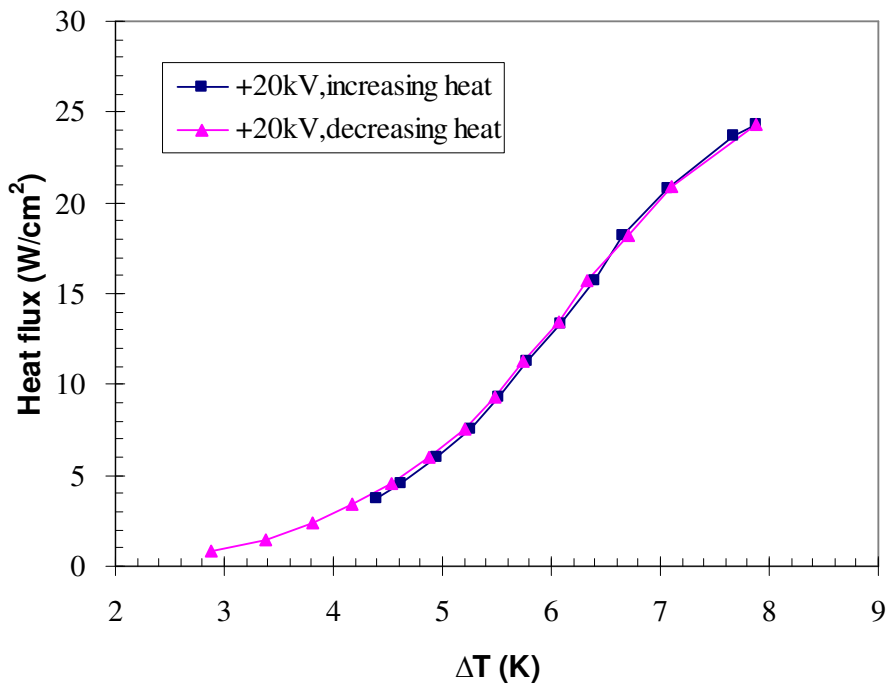


(a)

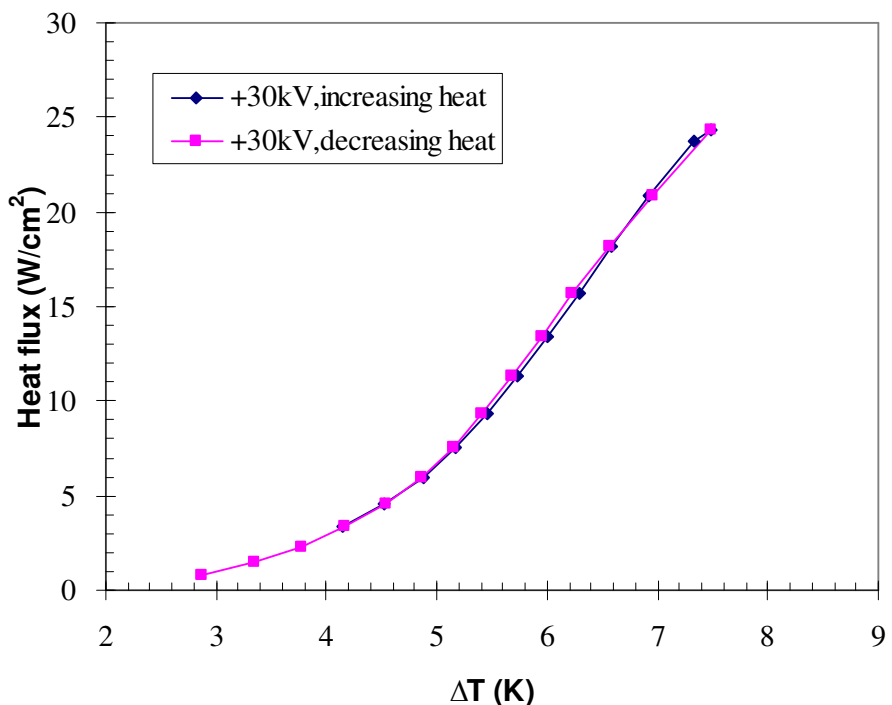


(b)

Figure continues on next page



(c)



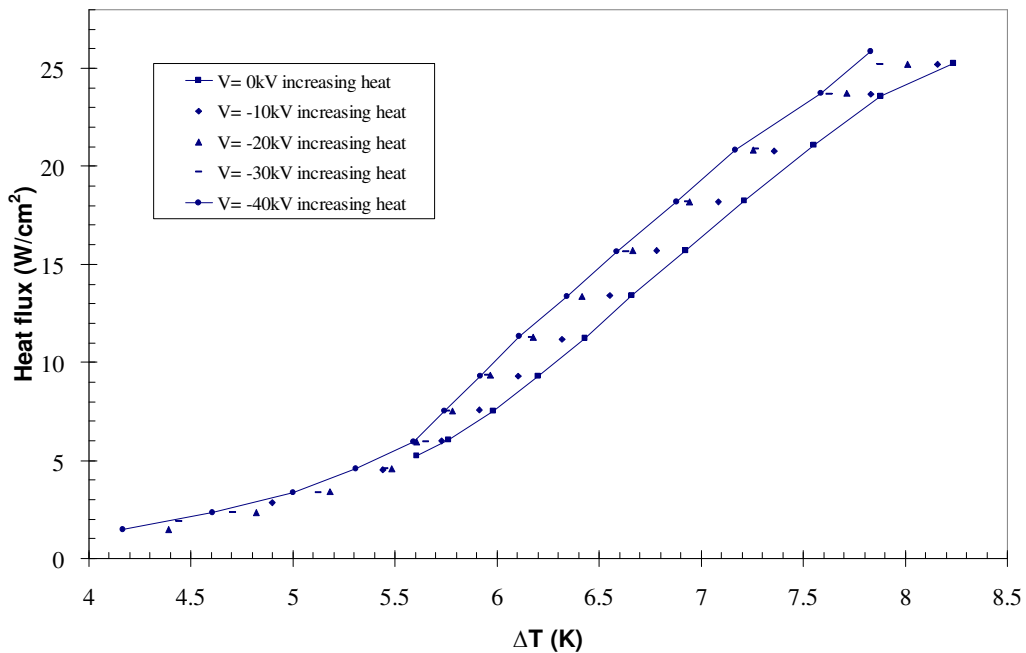
(d)

Figure 6.22 Hysteresis phenomenon: (a)  $0\text{kV}$ , (b)  $+10\text{kV}$  (c)  $+20\text{kV}$ , (d)  $+30\text{kV}$ .

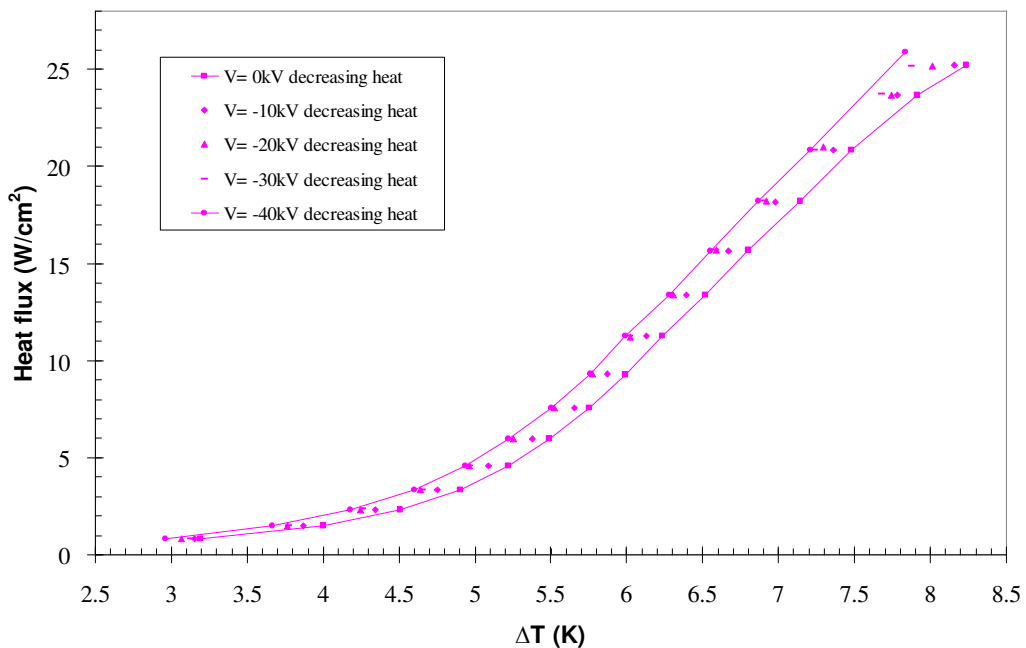
#### **6.4.5 Effect of electric field on nucleate boiling curves**

Nucleate boiling curves of liquid nitrogen (i.e. heat flux  $q$  as a function of temperature difference  $\Delta T$  between heat transfer surface of the copper electrode and liquid nitrogen bulk) have been obtained with both increasing and decreasing heat flux under different high voltages. The nucleate boiling curves are plotted in Figure 6.23 and Figure 6.24 for negative and positive voltage conditions, respectively. From an overall inspection of these two Figures, it is seen that the EHD effect allows a heat transfer enhancement, i.e. the heat flux  $q$  increases with increasing voltage for a given  $\Delta T$ . The influence of electric field strength on the heat transfer coefficient ratio  $h(V)/h(0)$  (i.e. ratio of the heat transfer coefficient with the electric field to that without the electric field) is shown in Figure 6.25. It can be seen that the EHD enhancement is greater for low heat fluxes than that obtained for high heat fluxes. The heat transfer coefficient  $h$  as a function of the heat flux,  $q$ , and the surface superheat,  $\Delta T$ , under different applied voltages are shown in Figure 6.26 and Figure 6.27, respectively. It can be seen that the heat transfer coefficient increases with increasing electric field strength and the EHD enhancement is very obvious for applied voltages over 20 kV during the nucleate boiling regime. For example, the heat transfer is increased by 30-50% when  $\Delta T = 6$  K. However, the heat transfer coefficient will not increase and may even decrease when near to CHF for each applied voltage value as shown in Figure 6.27.

The visual observation of the boiling phenomenon shows that for low heat flux, bubble behaviour is similar to that obtained from the previous study on EHD effect on single bubble behaviour presented in Chapter 5. Another observed experimental phenomenon is that the bubbles have a very rectilinear path when departing from the heat surface once the applied voltages exceed 20 kV in magnitude.



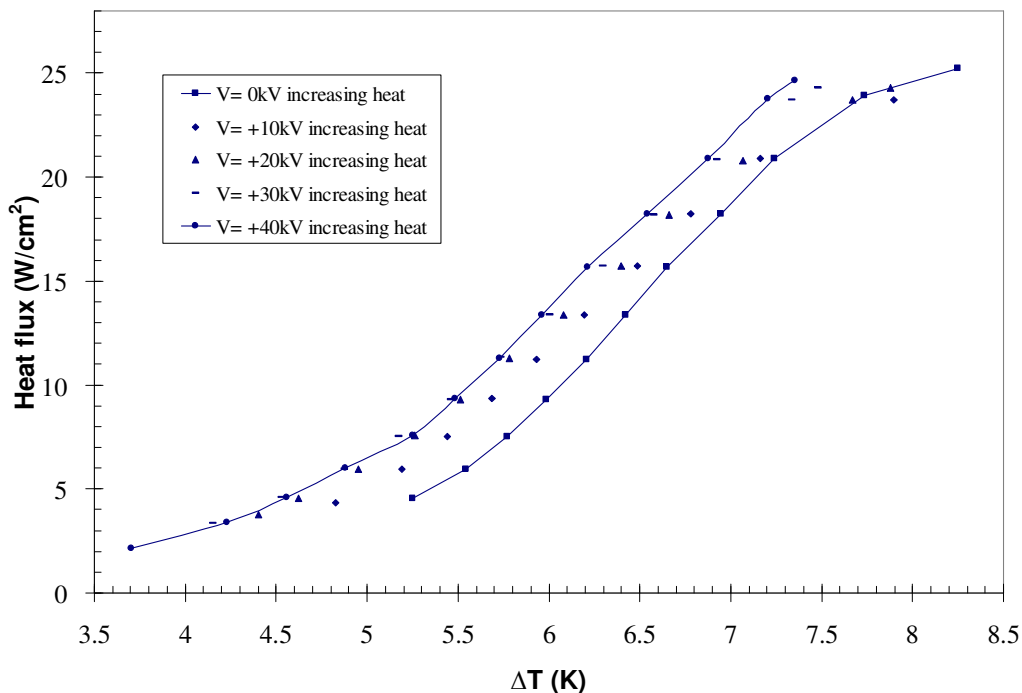
(a)



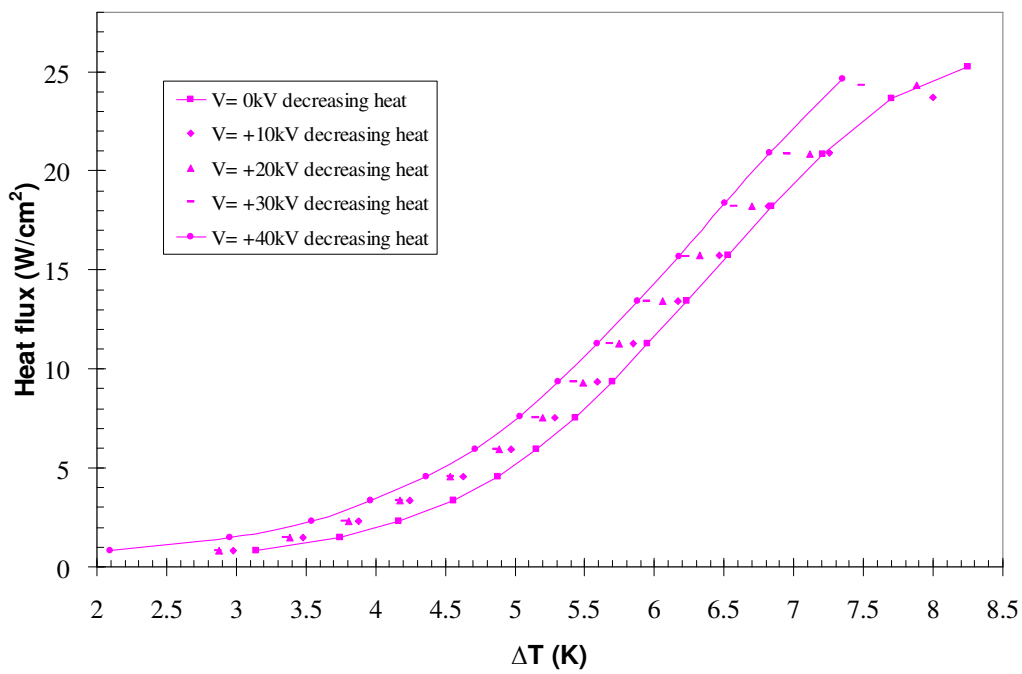
(b)

Figure 6.23 Nucleate boiling curve under different negative voltages

(a) increasing heat, (b) decreasing heat



(a)



(b)

Figure 6.24 Nucleate boiling curve under different positive voltages

(a) increasing heat, (b) decreasing heat

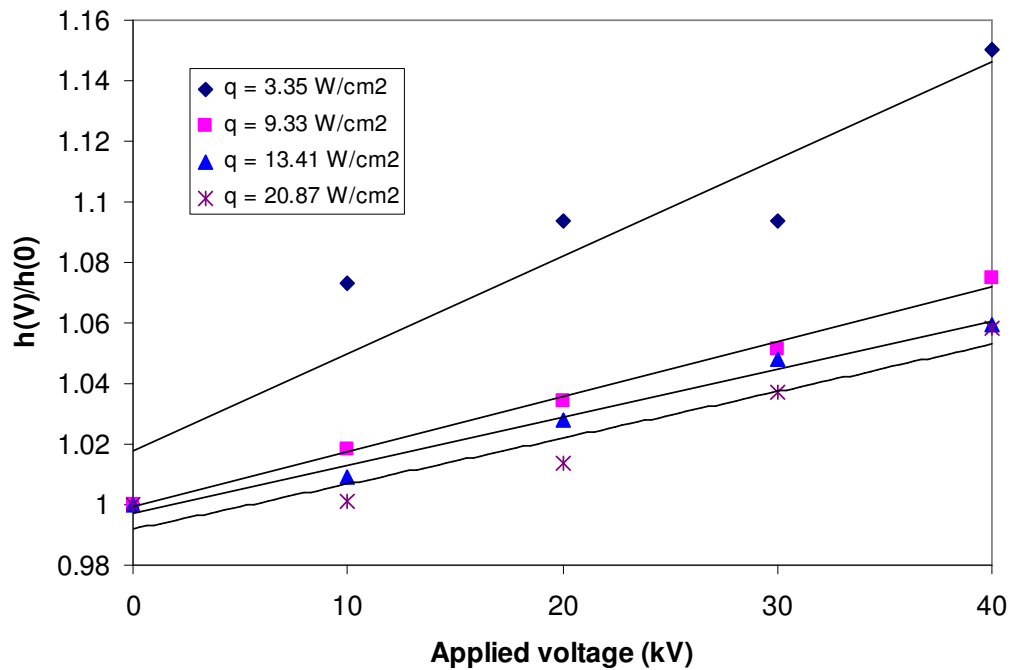


Figure 6.25 Heat transfer coefficients ratio versus applied voltage

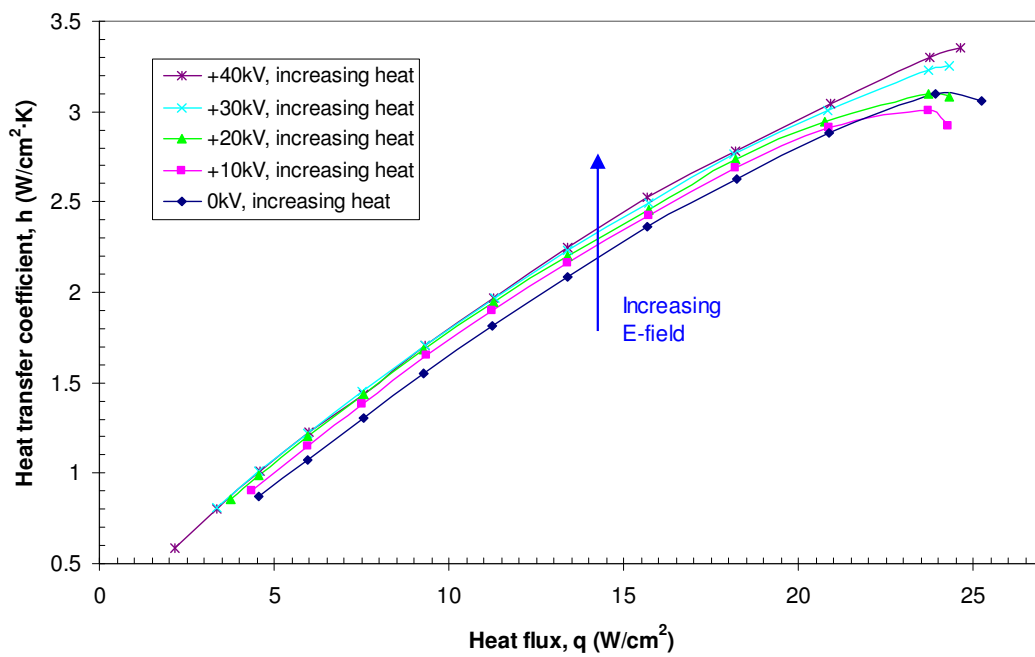


Figure 6.26 Heat transfer coefficient,  $h$ , vs heat flux,  $q$

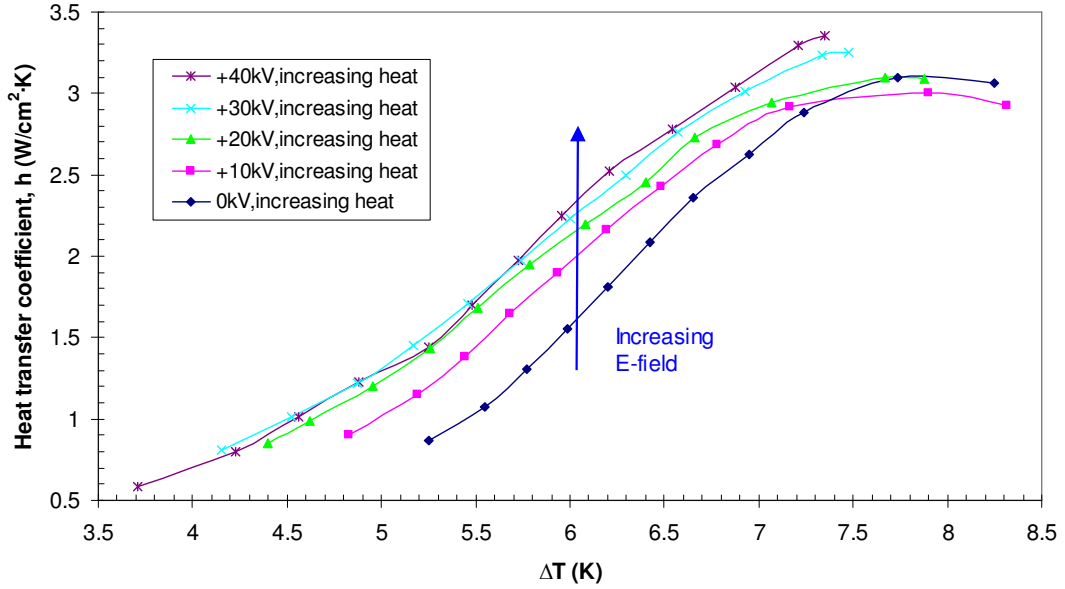


Figure 6.27 Heat transfer coefficient,  $h$ , vs surface superheat,  $\Delta T$

Two reasons for the enhancement of heat transfer utilizing the EHD technique need consideration: (a) One is the electroconvection effect on fluids due to the appearance of volume electric force on a continuous dielectric medium; (b) The other is the effect on the behaviour of the bubbles. The effect of the electric field on a vapor bubble is the interfacial EHD effect. Both effects are dependent on the electric field strength and the relaxation time of the electric charge.

At low heat fluxes and before any bubbles appear, the heat transfer mechanisms are governed by those of natural convection. Close to the heat transfer surface, a thermal boundary layer appears, and further away, the liquid is at the saturation temperature. Thermoconvection occurs within the liquid nitrogen. In the presence of an electric field, the electric force is within the thermal boundary layer due to the electric field and the temperature field become nonuniform. The forces reduce as the distance from the thermal boundary increases. The electric force induces an electroconvective movement inside the liquid nitrogen that is superimposed on the thermoconvective movement which has existed, thus the thermal boundary layer is decreased and, consequently, the superheat decreases too when heat flux is imposed. Under the nucleate boiling condition, the heat transfer mechanisms are governed by the following three factors [75]: (a) heat conduction through the macrolayer surrounding the bubble interface, (b) evaporation of the microlayer located between the heated surface and the bubble

bottom, and (c) convection within the liquid nitrogen adjacent to the bubble and the heated surface (see Figure 6.28a). Under EHD nucleate boiling conditions (see Figure 6.28b), as the electric field is not uniform in the liquid near the liquid-vapor interface, electrostrictive forces exist and electric forces within the liquid bulk are more important than those near the heated surface where the electric field is weaker. Thus, electroconvective movements are induced within the liquid region. Due to the electroconvective movements, the macrolayer thickness decreases and heat transfer within the macrolayer is increased.

The interfacial stresses acting on the bubbles involve a deformation of their shape. The bubble shape becomes elongated in the electric field direction and is very close to that of a prolate spheroid, this has been reported and discussed in Chapter 5. The resulting interfacial electric force tends to maintain the bubble against the heat transfer surface, causing intense vaporization of the microlayer between the bottom of the bubble and the heating surface. The heat transfer enhancement through both the macrolayer and the microlayer encourages rapid growth of bubbles, increasing their departure volume. More heat energy can be effectively transferred. Thus, convection currents are more important within the liquid nitrogen adjacent to the heating surface, which is more effectively cooled causing its temperature to decrease.

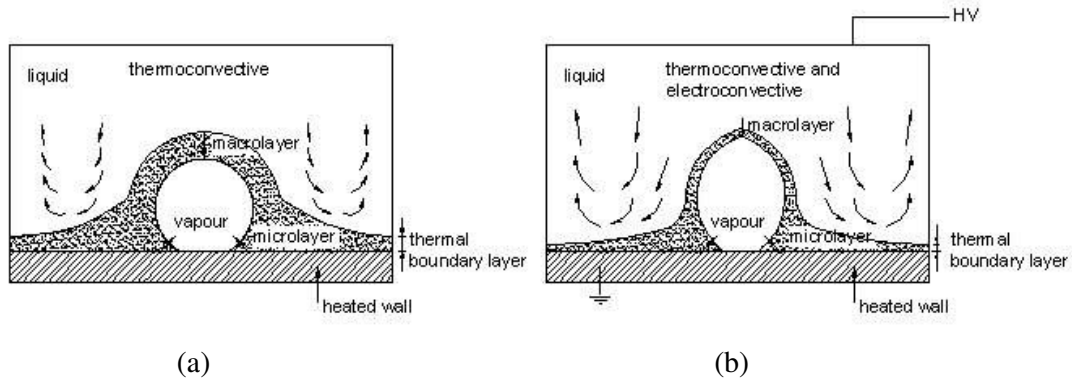


Figure 6.28 Nucleate boiling heat transfer mechanisms [75]

(a) under zero-field conditions, (b) under EHD conditions.

There is little information directly concerned with investigations of the EHD effect on liquid nitrogen boiling heat transfer, Rutkowski [83, 84] and Boyarintsev [103] have reported mainly on the EHD effect within the natural convection regime of liquid nitrogen. There are no previous experimental results readily available to compare with

results regarding the EHD effect on nucleate boiling of LN<sub>2</sub> obtained through the experiments conducted here.

However, there is a wealth of experimental studies that have been undertaken to evaluate the effect of electric fields on heat transfer of other refrigeration liquids such as R-114, R-123 and R-11. Results show that two important physical parameters of the fluids play a significant role in the EHD boiling heat transfer: electrical conductivity and dielectric constant. For example, Ogata and Yabe [91] obtained a huge heat transfer enhancement of up to 5000% using a mixture of R-11 and ethanol (to change electrical conductivity). Zaghodudi's study [75] gave an EHD enhancement comparison for three working fluids (n-pentane, R-113 and R-123) having different dielectric constants. A threefold increase in the heat transfer coefficient was obtained for R-123 with a higher dielectric constant, while only a near twofold increase was obtained for n-pentane and R-123 which both have a lower dielectric constant. In order to further understand LN<sub>2</sub> heat transfer properties, a comparison of the obtained LN<sub>2</sub> experimental results with those obtained by Zaghodudi in other liquids for a similar electrode configuration (parallel plate configuration) has been undertaken, as shown in Figure 6.29. It can be seen that the  $h(V)/h(0)$  is very small for LN<sub>2</sub>, compared with the other liquids under similar heat flux conditions. Comparison of the electrical properties of these working fluids plus that of LN<sub>2</sub> is shown in Table 6.2. Given that liquid nitrogen is a non-polar dielectric liquid with a quite low electrical conductivity of  $\sim 10^{-16} \Omega^{-1}m^{-1}$  and its relative dielectric constant is 1.432 (Table 1.2), may explain why the EHD enhancement on LN<sub>2</sub> nucleate boiling heat transfer is not significant even though the EHD effect has been shown to exist based on work completed in this study.

In conclusion, based on the discussion above and experimental results obtained, it can be seen that in terms of EHD enhanced heat transfer, liquid nitrogen does not perform as well as R-123, R-113 and n-pentane. It is suggested that the application of the EHD technique for liquid heat transfer is more effective when it is used in conjunction with an enhanced heat transfer surface such as a non-smooth electrode surface [117] rather than the smooth highly polished electrode used here.

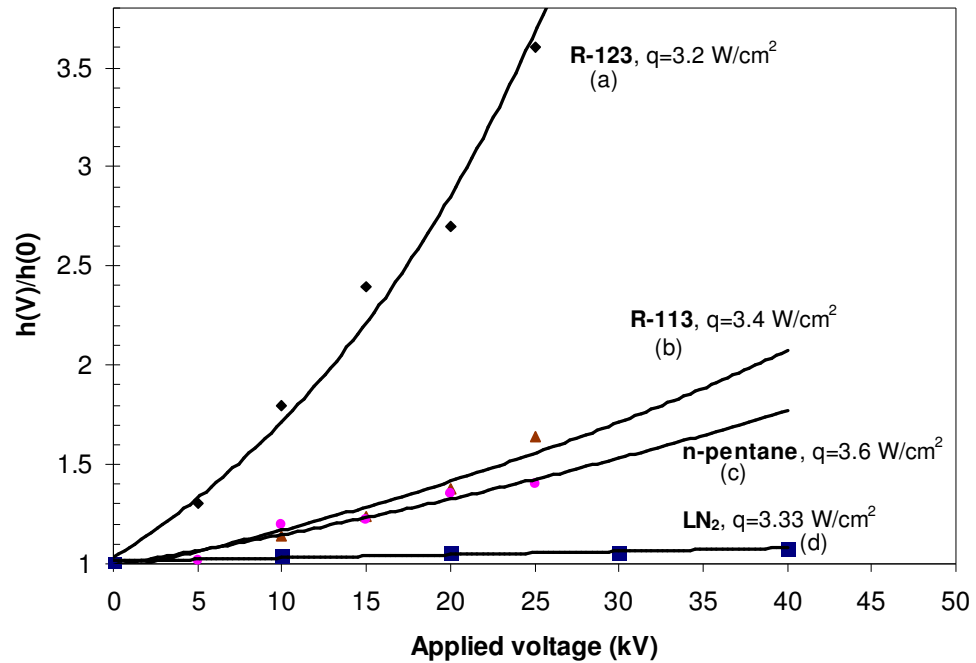


Figure 6.29 Comparison the heat transfer coefficients ratio of  $\text{LN}_2$  to those of other three fluids with similar heat flux conditions under electric fields (a, b, c from [75], d this study).

Table 6.2 Electrical properties of the other three working fluids and  $\text{LN}_2$

Fluid	$P$ (bar)	$T_{sat}$	$\varepsilon_{rl}$	$\lambda_e (\Omega^{-1}\text{m}^{-1})$	Refs.
$\text{LN}_2$	1	-196 °C	1.43	$\sim 10^{-16}$	[7] [8] [118]
n-pentane	1	36 °C	1.80	$4.7 \times 10^{-9}$	[75]
R-113	1	47 °C	2.40	$7.7 \times 10^{-8}$	[75]
R-123	1	28 °C	3.42	$3.4 \times 10^{-8}$	[75]

#### 6.4.6 Effect of electric field on the critical heat flux

CHF is one of the important parameters describing the heat transfer performance. Especially, in industrial cooling applications such as electronics, laser devices, nuclear power generation and nuclear fusion applications, it is a key parameter. If the mechanism to obtain critical heat transfer can be determined, it will be useful for improving the heat exchanger used in these applications. It will also be useful for achieving increased heat transfer efficiency by utilizing the near-critical boiling heat flux.

It is well known that the superheat increases greatly beyond CHF and the heat transfer will deteriorate when the boiling state enters film boiling. In order to determine the CHF experimentally, the sequence of operations is to preset the high voltage and incrementally increase the voltage of the heater power source in steps of approximately 10V, except in the vicinity of the critical heat flux, where steps are reduced to 2V. The critical heat flux is defined as the heat flux which causes the onset of film boiling, which is easy to observe using the high-speed camera (see Figure 6.17c), and detected through the sudden increase in the temperatures of the 3 pt100s embedded into the electrode (see Figure 6.30). An obvious temperature increase (about 20 K) is seen over a short duration (1 minute) as the onset of film boiling. This is because the vapour bubbles form groups and columns, and tend to coalesce forming an unstable vapour

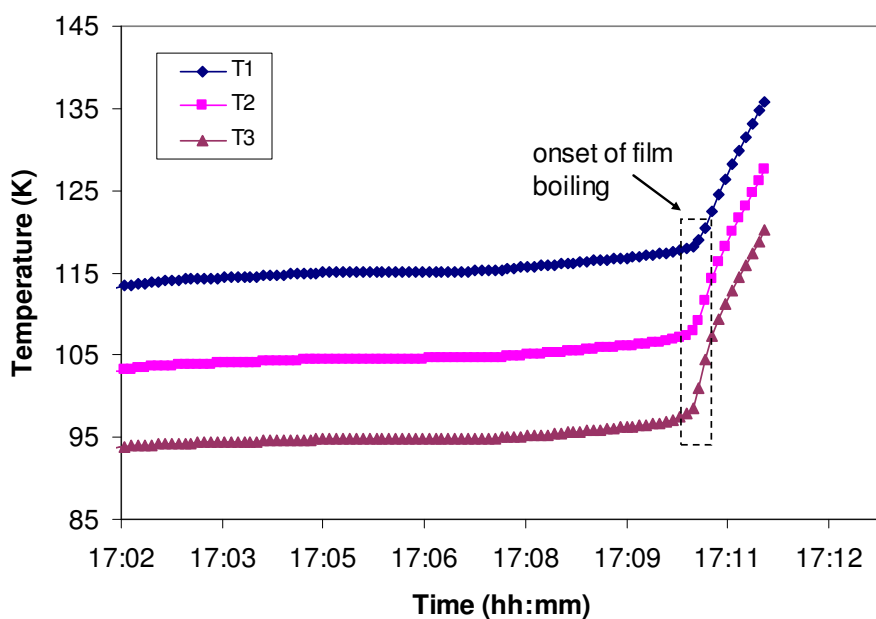


Figure 6.30 Temperature rise of the Pt100s at the onset of film boiling

film over the heat transfer surface at the critical point. Therefore, the vapour film increases the thermal resistance and insulates the surface and results in a rapid temperature rise inside and at the top of the electrode.

The visual observation of the bubble behaviour approaching CHF shows large individual bubbles (note these bubbles are already the results of the coalescence of many smaller bubbles) merge and form large mushroom-shaped bubbles, or vapour blankets (see Figure 6.17c), these hover over the heater surface. These vapour blankets are believed to be fed by the vaporizing liquid beneath them, causing them to grow in size. They might prevent the bulk fluid from reaching the heater surface while the liquid film beneath them evaporates, resulting in surface dryout. In EHD conditions, these mushroom-shaped bubbles or vapour blankets appear smaller than those obtained in zero-field condition.

The effect of applying negative high voltages on critical heat flux is shown in Figure 6.31. Here, each CHF is an average value from sets of test data at each corresponding voltage. It can be seen that the CHF increases with increasing voltage. CHF obtained without the electric field is about  $24.8 \text{ W/cm}^2$ , and for this experiment, a 13% increase can be obtained for a 40 kV high voltage, as shown in Figure 6.32. Very similar results have been obtained under positive high voltages as shown in Figure 6.31 and Figure 6.32. The electric field polarity effect is not obvious in this study.

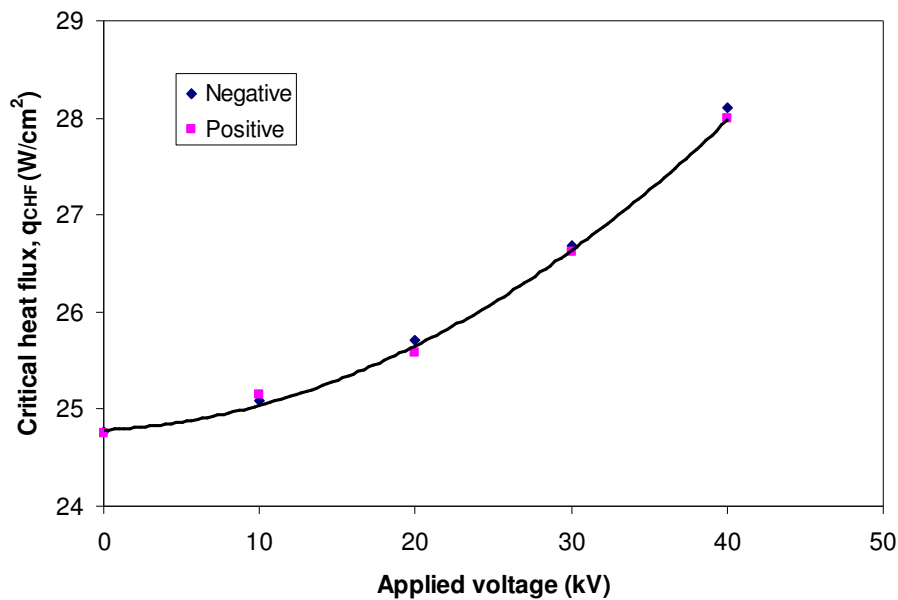


Figure 6.31 Critical heat flux,  $q_{CHF}$ , as a function of the voltage

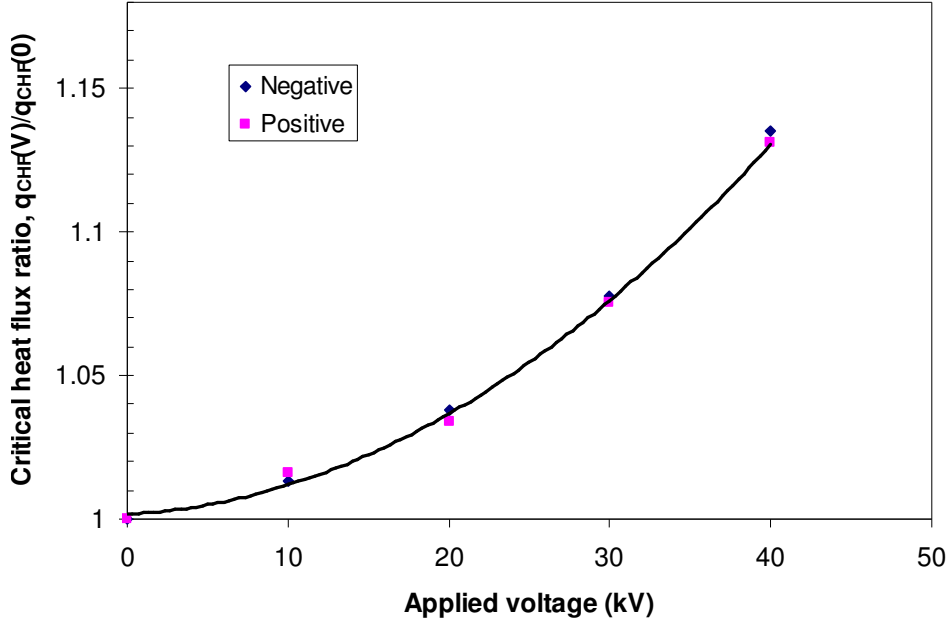


Figure 6.32  $q_{CHF}(V)/q_{CHF}(0)$  versus applied voltage

The increase of the CHF under electric fields has been explained by a model of the liquid-vapour interface stability [75]. Under a zero-field condition, near the CHF, the vapour columns flow adjacent to the liquid along an interface that is unstable under the action of inertia and surface tension forces (Helmoltz instability). A maximum relative vapour rate exists, above which a small disturbance is amplified and causes the distortion of the flow. The wavelength of the disturbance with the largest growth rate is called the most dangerous wavelength,  $\lambda_d$ . For a plate surface,  $\lambda_d$  is given as follows[75]:

$$\lambda_d = 2\sqrt{3}\pi \left[ \frac{\sigma}{(\rho_l - \rho_v)g} \right]^{1/2} \quad (6.7)$$

For LN<sub>2</sub>,  $\lambda_d$  is about 11mm in zero-field conditions. The presence of an electric field drastically modifies the liquid-vapour interface stability. In this case, the wavelength  $\lambda_d$  taking into account the electric field effects is given by [75]

$$\lambda_d = \frac{6\sqrt{2}\pi\delta}{(G^2 + (G^2 + 3B_o^2)^{1/2})} \quad (6.8)$$

Where  $\delta$  is the vapour film thickness that covers the heating surface. The bond number  $B_o$  and  $G$ , which represents the ratio of the electric forces to the surface tension forces, are given by

$$B_o^2 = \frac{\rho_l g \delta^2}{\sigma}, G^2 = \frac{\epsilon_v E^2 \delta}{\sigma} \quad (6.9)$$

For LN<sub>2</sub>,  $\lambda_d$  is about 3.1 mm for electric field strength of 20 kV/cm. The effect of the electric field is then to decrease the most critical wavelength, and consequently to break the vapour film that leads to an increase of the CHF.

## 6.5 Summary

The effects of a dc uniform electric field on boiling heat transfer of liquid nitrogen have been experimentally investigated. To achieve this, a copper block electrode system with temperature measurement and vacuum heat insulation was developed. Moreover, a heat transfer model based on this electrode geometry has been implemented in order to provide some useful data for electrode design and assist with temperature calculations. Most importantly boiling curves for liquid nitrogen have been obtained with and without electric fields, the effect of electric field on ONB, nucleate boiling enhancement, boiling hysteresis and CHF has been analysed and discussed. The conclusions drawn from the experimental results in this study are as follows:

1. A ‘temperature overshoot phenomenon’ happens on the heat transfer surface from convection state to nucleate boiling state due to a large number of bubbles generated within a short time, a higher electric field can reduce and even eliminate this temperature drop.
2. The higher the electric field is the easier to active nucleate boiling with a lower heat input will be.
3. Electric fields can enhance nucleate boiling heat transfer of LN<sub>2</sub>, and for this experiment, a 30-50% increase is obtained under an applied 40 kV high voltage.
4. A so called “second hysteresis” phenomenon exists for increasing heat and decreasing heat flux test conditions. A higher electric field is able to eliminate the hysteresis phenomenon.
5. The critical heat flux,  $q_{CHF}$ , can be augmented by the electric field, for this experiment a 13% increase is obtained under an applied 40 kV high voltage.
6. Any electric field polarity effect on boiling heat transfer was not observed.
7. In terms of EHD enhanced heat transfer, liquid nitrogen does not perform as well as R-123, R-113 and n-pentane due to its quite low electrical conductivity.

## Chapter 7

# Conclusions and Further work

### 7.1 Conclusions

The thesis describes how electric fields affect thermal bubble behaviour in liquid nitrogen. Research interests include single bubble behaviour and bubble column behaviour as well as boiling heat transfer enhancement due to bubble behaviour change. Using a conductor-plane electrode, plane-plane inclined electrode, and mesh-plane electrode geometries to generate non-uniform or uniform fields for experimental studies. Results have been obtained and, where appropriate, compared to theoretical values using either finite element analysis or analytical models.

Liquid nitrogen is a cheap and excellent cooling medium and also a good electrical insulator in many high temperature superconducting devices. However, bubbles are easily formed, even by moderate heating due to a narrow liquid temperature range and low latent heat of vaporization. It has been reported that bubbles generated thermally in the liquid coolant of superconducting and cryoresistive apparatus are considered to be one of the factors causing a reduction of the electrical insulation performance of these apparatus. In addition, it is well known that bubbles appear and change behaviour in a fluid under an electric field. This behaviour is one of the reasons for boiling heat transfer enhancement. EHD enhancement techniques applied to boiling heat transfer systems are a very promising development in the engineering of heat transfer, and will find wide application in the future.

Superconductivity and its development along with the physical, thermal and electrical properties of liquid nitrogen have been discussed and bubble generation mechanisms summarized. Past work on thermal bubble behaviour in liquid nitrogen under electric fields has been reviewed according to two viewpoints – electrical insulation and thermal stability. EHD phenomenon and its mechanism on boiling heat transfer have been explained.

A model for bubble motion in non-uniform electric fields has first been developed by analysis of the forces acting upon a bubble with conductor-plane electrode geometry. A set of differential equations that describes the motion of a spherical bubble in this gap has been proposed and solved numerically to find the bubble trajectory for a specified applied voltage. It was found that the bubble stream trajectory is really dependent on the initial position and velocity of the bubble and the magnitude of applied voltage. An experimental study on bubble behaviour under electric fields was investigated using a conductor-to-plane electrode system. Bubbles are thermally induced by a heater mounted below the conductor-to-plane electrode system. Thermal bubble motion and bubble collision with the plane electrode processes were observed in these experiments, the bubble dynamic mechanism has been analyzed and explained by considering the electric field distribution and the electric field force and buoyancy. The results show that dc non-uniform electric fields have an obvious effect on bubble behaviour. The bubbles tend to move closer to a lower field region (plane electrode), irrespective of electric field direction. It is postulated that the gradient force greatly affects bubble dynamics in the presence of a non-uniform field. It has also been found that negative polarity has a larger effect on bubble motion than positive polarity due to the presence of contamination or liquid convection. In addition, the percentage of bubbles moving to the plane electrode is no more than 40% and the bubble-electrode collision distributions also have been obtained and discussed. Experimental results show that measured bubbles trajectories are in reasonable agreement with the minimum collision height predicted by the presented theoretical model. These obtained results are useful for understanding electrohydrodynamic (EHD) phenomena influencing bubble behaviour in liquid nitrogen and for developing a practical method of removing gas from cryostats of high temperature superconducting transformers or fault current limiters operating under quench conditions.

A study on behaviour of thermal bubbles in liquid nitrogen between plane-plane inclined electrode with an angle of 21° has been experimentally investigated. Observation of the bubble motion captured using a high speed camera shows that a bubble's rising motion due to buoyancy is impeded by the application of a dc electric field and formation of a gradient force. Bubbles are observed to collect at the top of the plane-plane inclined electrode, the closest point. The gas vapour of successive bubbles coalesces forming a large volume bubble which totally bridges the electrode gap. Only when of sufficient volume does the buoyancy force overcome the gradient force allowing the gas volume to rise from the electrode gap. Increasing the applied voltage and, therefore, the gradient in electric field in the gap led to a reduction in time for bubble collection and coalescence to begin. Both polarities were investigated and no polarity effect was obvious. Moreover, experimental results for two electrode arrangements were compared and discussed and found that the Type 1 have more obvious effect on bubble behaviour than Type 2 having larger spacing and lower field for the same applied voltage. Analysis of the competing forces of the electric gradient and buoyancy show that for a fixed bubble size, the electric gradient force overcomes buoyancy near the top of the electrodes preventing the bubbles from rising, consistent with the observed results. In addition, the methods for increasing electric force effect on a bubble in liquid have been discussed. This experimental study using plane-plane inclined electrode also gives an opportunity to understand bubble behaviour in similar situations which may exist in superconducting electrical power applications, which has not been widely reported. Results are different to those obtained using a parallel plane electrode configuration as reported by other researchers. In addition, the control and positioning of bubbles may have potential implications in liquid-gas unit separation processes and in a zero-gravity environment where electric field forces are a promising replacement for gravity and the lack of buoyancy forces.

The effect of a dc uniform electric field on the behaviour of bubbles in liquid nitrogen such as their growth, deformation and departure frequency has been experimentally investigated using a stainless steel mesh-plane electrode. The experimental results show that (1) prolate spherical bubbles are formed in the direction of electric field and bubble deformation increases with increasing applied voltage, (2) the bubble departure frequency decreases and the departure volume increases with increasing electric field strength, (3) any effect of the electric field polarity is not obvious, (4) the bubbles in the

electric field are pushed against the grounded electrode and will move horizontally along the plane if the horizontal components in the two hemispheres of bubble are not in balance when the applied voltage is suitably large e.g. for an inclined plane. This behaviour intensifies the local flow and turbulence within the thermal boundary layer, reduces thermal resistance and enhances heat transfer. In order to clarify these phenomena, the electric field distribution around a bubble has been simulated using the FEA method and the electric force acting on a bubble calculated numerically. In addition, the effect of changes to thermal bubble behaviour on boiling heat transfer is also discussed. Obtained results may lay a foundation for exploring the mechanism of EHD enhancement of boiling heat transfer of liquid nitrogen.

An experiment to observe and measure the effect of a dc uniform electric field on boiling heat transfer of liquid nitrogen using a purpose-built mesh-plane electrode system has been conducted. A copper block electrode system with temperature measurement and vacuum heat insulation was designed and manufactured. A heat transfer model based on this electrode geometry has been developed in order to provide useful data for the electrode design and assist temperature calculations. Most importantly boiling curves for liquid nitrogen have been obtained with and without electric fields, the effect of electric field on ONB, nucleate boiling enhancement, boiling hysteresis and CHF has been analysed and discussed. Conclusions from this experiment are: 1) A ‘temperature overshoot phenomenon’ happens on the heat transfer surface from convection state to nucleate boiling state due to greater number of bubbles generated within a shorter time, a higher electric field can reduce and even eliminate this temperature drop. 2) The higher the electric field is, the easier it will be to active nucleate boiling with a lower heat input. 3) Electric fields can enhance nucleate boiling heat transfer of LN<sub>2</sub>, and for this experiment, a 30-50% increase is obtained under an applied 40 kV high voltage. 4) A hysteresis phenomenon exists in increasing heat and decreasing heat flux test conditions. A higher electric field is able to eliminate the hysteresis phenomenon. 5) The critical heat flux, q<sub>CHF</sub>, can be augmented by the electric field; for this experiment, a 13% increase is obtained under an applied voltage of 40 kV. 6) Any electric field polarity effect on boiling heat transfer was not observed. 7) In terms of EHD enhanced heat transfer, liquid nitrogen does not perform as well as R-123, R-113 and n-pentane due to its quite low electrical conductivity. These obtained results may be helpful in the design of the liquid nitrogen related components for HTS

device cooling and also provide an initial perspective on the possible improvements for cryogenic cooling of HTS equipment.

## 7.2 Further work

Further research is required in the following areas:

- ac field effects and partial discharge phenomena

In real electrical power applications, ac voltages are required, hence, the effect of ac electric fields on bubble behaviour under uniform and non-uniform fields and partial discharge phenomena due to thermal bubbles appearing between the electrodes need to be further investigated. Using developed conductor-plane electrode and plane-plane inclined electrode systems, the thermal bubble behaviour in liquid nitrogen can be studied using an ac non-uniform electric field and allow a comparison with results obtained under dc fields. In addition, partial discharge phenomena due to bubbles appearing in the plane-plane inclined electrode gap can also be investigated.

- Boiling curves of liquid nitrogen under different situations should be obtained.

More investigations into the EHD effect on boiling heat transfer of liquid nitrogen using the copper block electrode under different situations should be undertaken. These aspects include liquid nitrogen boiling curves at subcooled temperatures (63-77K) without and with electric fields, the effects of pressure on boiling curves without and with electric fields, the effects of electrode surface roughness on boiling curves without and with electric fields as well as ac electric field effects on boiling curves. In addition, power consumption under EHD conditions and the boiling phenomena comparison for steady state and fast-increasing transient heat input conditions could be further researched.

- A study of bubble behaviour and heat transfer characteristics using a coaxial cylinder electrode system should be considered.

In superconductor magnet applications, the cylinder cable structure is very common. A coaxial cylinder electrode system may be more similar to these situations. Thus, development of a new coaxial cylinder electrode system is another good choice to study bubble behaviour under electric fields. The heat transfer process of liquid nitrogen such as transitions from non-boiling to nucleate boiling regime and film boiling with and

without electric fields can be observed using this kind of electrode system. At the same time, the relevant heat transfer characteristics of liquid nitrogen such as boiling curves, boiling hysteresis and the critical heat flux can be conducted under a different electric field. Then, the heat transfer coefficient can also be investigated; the effect of applied voltage polarity on boiling heat transfer and the influence of the surface roughness on heat transfer into liquid nitrogen can also be studied.

- A modelling study on the boiling curve and CHF of liquid nitrogen can be implemented.

To date, many theoretical studies have been carried out on the EHD boiling heat transfer of non-cryogenic liquids. Especially, the CHF of fluid can be calculated and experimental results obtained are in close agreement. Theoretical models and mechanisms may be developed to allow a numerical study on EHD enhancement of boiling heat transfer of liquid nitrogen and obtained results compared with experimental values.

# Appendices

## A Electrical connection

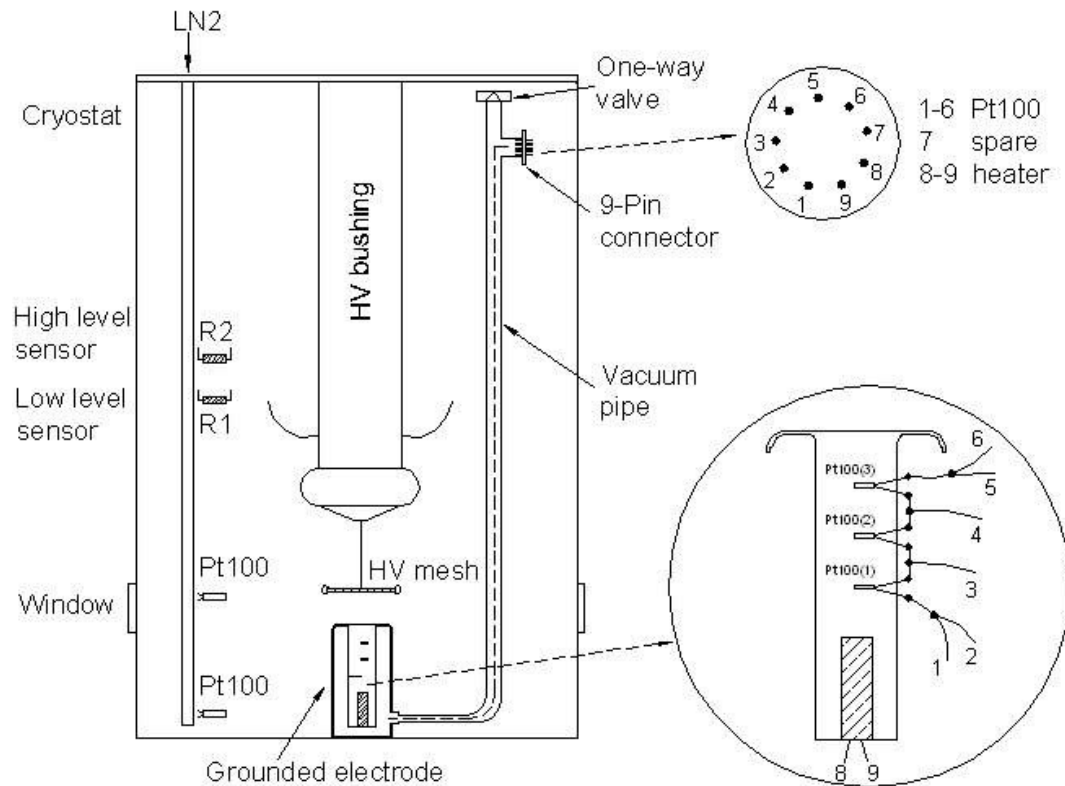


Figure A.1 General assembly schematic showing electrical components

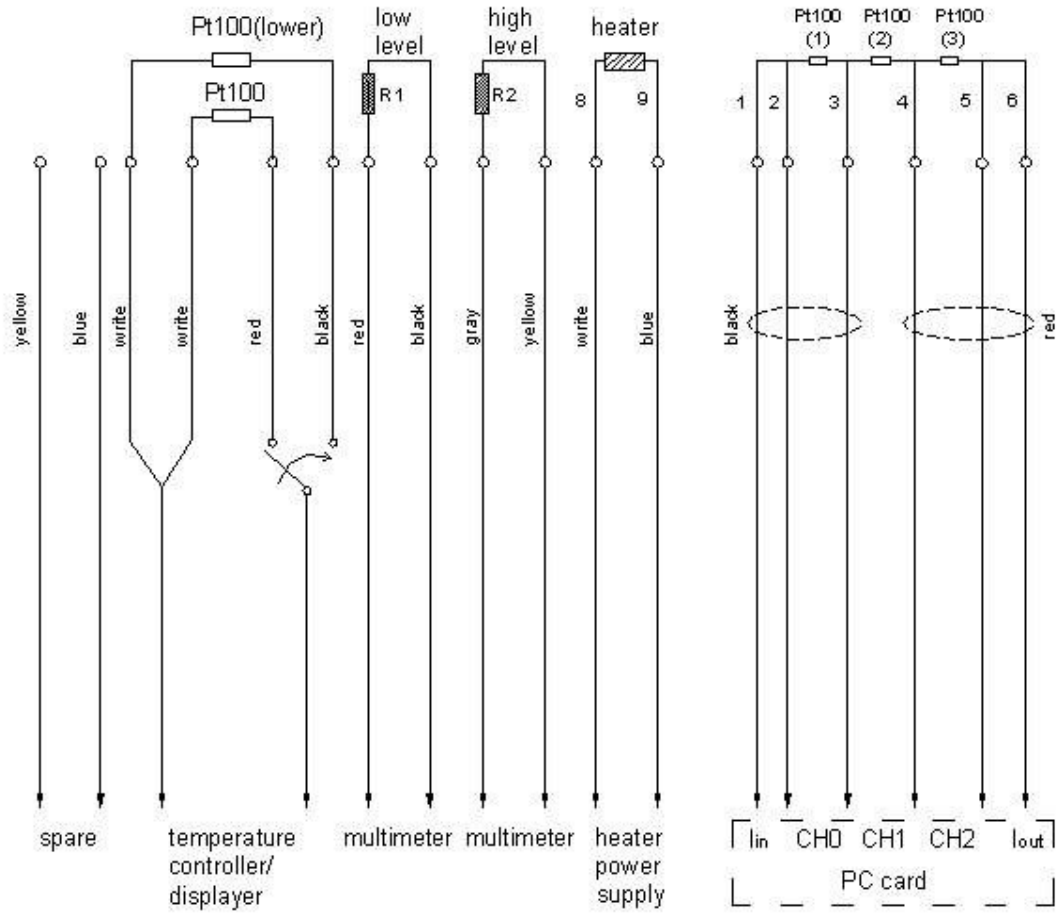


Figure A.2 Electrical feed through connections within the LN<sub>2</sub> cryostat

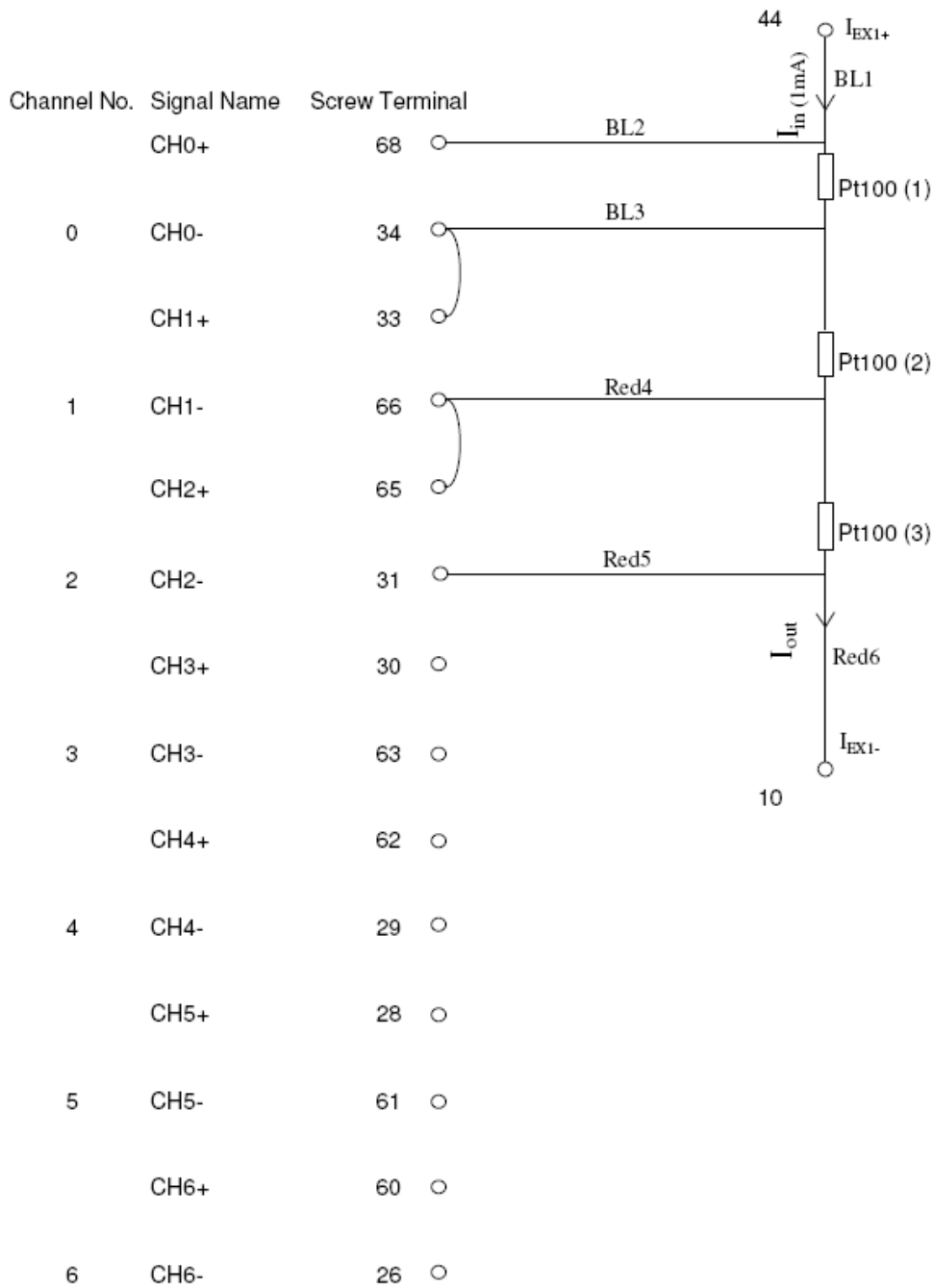


Figure A.3 Connection 3 Pt100s to the PC card terminal (TBX-68)

Note:

4-wire measurement connection for Pt100s

Use the 1 mA current source

Chose the DIN43760 standard

Terminal part no. :TBX-68

## B Force analysis for thickness of the copper cap

It is necessary to carry out a force analysis for the cap of the copper block, as it must withstand the pressure when the grounded electrode is vacuumed to a high vacuum quality and this may cause deflection of the cap. Although a thick cap can avoid this, it will result in greater heat losses. A suitable thickness for the cap needs to be considered from the prospective both its mechanical and thermal properties.

For a plate of radius  $a$  subjected to uniform pressure under a clamped periphery condition as shown in Figure B.1, the maximum deflection occurs at its centre. The deflection curve,  $w_{max}$ , is expressed as [119]:

$$w_{max} = \frac{pa^4}{64D} \quad (\text{B.1})$$

where  $p$  is pressure,  $D$  is flexural rigidity. The  $D$  can be calculated according to:

$$D = \frac{Eh^3}{12(1-\nu^2)} \quad (\text{B.2})$$

where  $E$  is young's modulus of elasticity (GPa) which is 120 GPa for copper,  $\nu$  is poisson's ratio which is 0.33 for copper,  $h$  is plate thickness. In this study, the pressure  $p$  applied to the copper cap includes the atmosphere pressure,  $p_{air}$ , and the pressure,  $p_b$ , caused by the copper block gravity. The  $p_b$  is defined as

$$p_b = \frac{G_b}{\pi a^2} \quad (\text{B.3})$$

where  $G_b$  is the gravity of the copper block, which can be calculated using

$$G_b = \rho_{cu} g V_b \quad (\text{B.4})$$

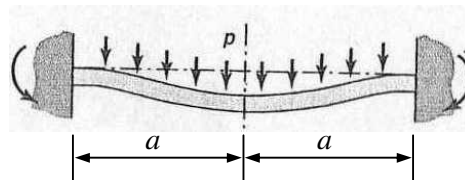


Figure B.1 A plate subjected to uniform pressure [119]

where  $\rho_{cu}$  is the density of copper which is  $8920 \text{ kg/m}^3$ ,  $g$  is the gravitational acceleration which is  $9.8 \text{ m/s}^2$ ,  $V_b$  is the volume of the cylinder copper block which can be calculated as

$$V_b = \pi R^2 L \quad (\text{B.5})$$

where  $R$  is the radius of the copper block which is 16 mm,  $L$  is its length which is 120 mm. Using these Equations (B.1-B.5) given above, the maximum deflection of a copper plate ( $a=26 \text{ mm}$  from real electrode data),  $w_{max}$ , as a function of the plate thickness,  $h$ , can be calculated and plotted as shown in Figure B.2. Obviously it is seen that the greater the maximum deflection, the thinner the copper plate. In this study a 0.6 mm thickness is chosen for the copper cap which may cause a 0.4 mm maximum deflection at the centre from this theoretical analysis. However, the actual deflection occurred at the circular edge between the block and the cap and was not very obvious. This perhaps is because the copper block and the cap are machined from a single piece of metal, see Figure 6.5.

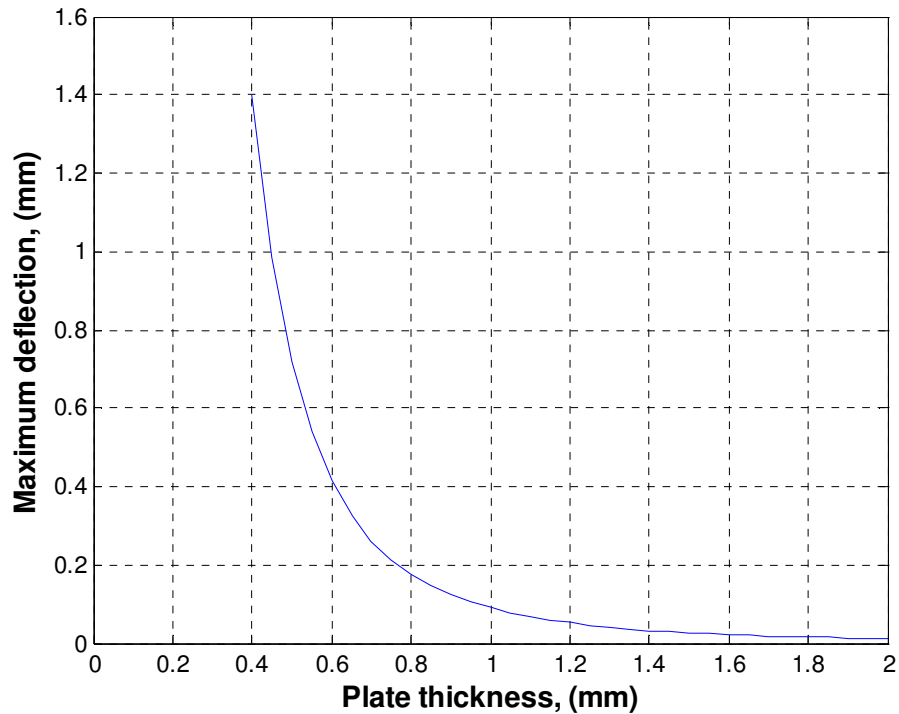


Figure B.2 The maximum deflection as a function of the plate thickness

## C Indium soldering of electrodes

Pure indium was selected to solder key parts of the electrode system in this study because of some of its significant characteristics. Indium is a semiprecious, nonferrous metal with a lustrous silver-white colour and softer than lead. It is very malleable and ductile and can easily fill voids between two surfaces, even at cryogenic temperature. Its ductility allows some materials with different coefficients of thermal expansion to be joined together and avoid crack propagation. It is, therefore, an ideal material to create a compression seal for cryogenic pumps, high vacuum systems and other unique joining and sealing applications.

There are two key joints where warm welding with indium is used in this copper block electrode system. One is between the cap of the copper block electrode and the brass tube (joint 1 in Figure C.1), the other is between the vacuum pipe (copper) and the brass tube (joint 2 in Figure C.1). In this Figure, other two joints (3 and 4) were soldered by using lead because they are near the top of the cryostat and will not be immersed in liquid nitrogen.

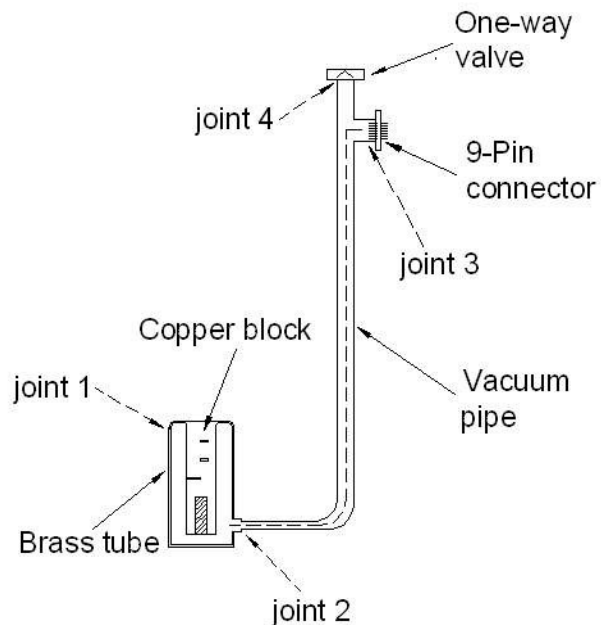


Figure C.1 Joints of the electrode (indium solder for joint 1 and 2, lead solder for 3 and 4)

Indium is self-passivating and can form 80-100 Angstroms of oxide on its surface. Prior to using indium in a sealing or welding application, it is recommended to remove the oxide because it may provide a leakage path if it gets compressed into the seal. The oxide can be easily removed according to the following procedure:

1. Degrease the indium with an acetone to remove any organic contaminants that may be on the surface.
2. Etch the indium surfaces in a solution of 5-10% hydrochloric acid (by volume) at room temperature for 1 to 4 minutes, depending on oxide thickness, until surface appears bright. This will remove the 80-100 Angstroms of oxide that form on the surface.
3. Thoroughly rinse twice in deionised water.
4. Rinse off the water with acetone or isopropyl alcohol.
5. Blow-dry with dry nitrogen.

It is should be noted that this procedure should be performed only if the indium is going to be used immediately because it slightly etches the metallic surface, exposing a larger surface area to oxidation. In addition, return any unused, etched indium to storage under nitrogen or argon.

The joints 2, 3 and 4 were warm soldered directly at suitable temperature. The joint 1 was welded by connecting the electrode to a vacuum pump via the copper pipe and one-way valve during the solder period. The welded seal can support a high vacuum of up to  $1.2 \times 10^{-5}$  torr.

It is important that for applications using indium seals that the welding temperature does not exceed its melting point of 156.6 °C, because that will cause leaks or cracking.

## D Data sheet of liquid nitrogen from BOC Gases

---

### 1. IDENTIFICATION OF THE SUBSTANCE AND OF THE COMPANY

Product name                    Liquid Nitrogen

Chemical formula                N<sub>2</sub>

Company identification        BOC Gases

---

### 2. HAZARDS IDENTIFICATION

Hazards identification         Refrigerated liquefied gas. Contact with product may cause cold burns or frostbite. In high concentrations may cause asphyxiation.

---

### 3. EXPOSURE CONTROLS/PERSONAL PROTECTION

Personal protection            Ensure adequate ventilation. Protect eyes, face and skin from liquid splashes.

---

### 4. HANDLING AND STORAGE

Handing and storage          Suck back of water into the container must be prevented. Do not allow backfeed into the container. Use only properly specified equipment which is suitable for this product, its supply pressure and temperature. Keep container below 50° C in a well ventilated place.

---

### 5. STABILITY AND REACTIVITY

Stability and reactivity      Stable under normal conditions. Liquid spillages can cause embrittlement of structural materials

---

### 6. PHYSICAL AND CHEMICAL PROPERTIES

Molecular weight              28

Melting point                -210 ° C

Boiling point                -196 ° C

Critical temperature        -147 ° C

Relative density, gas        0.97 (air=1)

Relative density, liquid    0.8 (water=1)

Solubility mg/l water      20 mg/l

Appearance/colour           Colourless liquid

Odour                        No odour warning properties

---

---

## 7. PRODUCT SPECIFICATION

	Specification	Typical Analysis
Nitrogen	99.999%	99.999%
Oxygen	< 5 vpm	< 2 vpm
Moisture	< 2 vpm	< 1 vpm
Carbon Monoxide		< 1 vpm
Carbon Dioxide		< 0.5 vpm
Hydrocarbons		< 1 vpm
Hydrogen		< 1 vpm
Neon		< 3 vpm
Helium		< 1 vpm
Argon	is include in the nitrogen	

---

## **E List of publications from this research**

### Conference

- (1) Wang, P., Swaffield, D. J., Lewin, P. L. and Chen, G. (2005) *Thermal Bubble Dynamics in Cryogenic Liquids under Non-Uniform Electric Fields on Superconducting Power Apparatus*. In: 2005 IEEE Conference on Electrical Insulation and Dielectric Phenomena (CEIDP), 16 - 19 October 2005, Nashville, Tennessee, USA
- (2) Wang, P., Swaffield, D. J., Lewin, P. L. and Chen, G. (2007) *Thermal Bubble Motion in Liquid Nitrogen under Non-Uniform Electric Fields*. In: 15th International Symposium on High Voltage Engineering (ISH), 27-31 August 2007, Ljubljana, Slovenia
- (3) Wang, P., Swaffield, D. J., Lewin, P. L. and Chen, G. (2007) *Thermal Bubble Behaviour in Liquid Nitrogen between Inclined Plane Electrodes*. In: Conference on Electrical Insulation and Dielectric Phenomena (CEIDP), 14-17 October 2007, Vancouver, British Columbia, Canada
- (4) Wang, P., Swaffield, D. J., Lewin, P. L. and Chen, G. (2008) *The Effect of an Electric Field on Behaviour of Thermally Induced Bubble in Liquid Nitrogen*. In: 16th IEEE Conference on Dielectric Liquid (ICDL), 30 June - 4 July 2008, Poitiers, France
- (5) Lewin, P. L., Wang, P., Swaffield, D. J. and Chen, G. (2008) *A Model for Bubble Motion in Non-uniform Electric Fields*. In: 16th IEEE Conference on Dielectric Liquid (ICDL), 30 June - 4 July 2008, Poitiers, France

### Journal

- (6) Wang, P., Swaffield, D. J., Lewin, P. L. and Chen, G. (2008) *Thermal Bubble Motion in Liquid Nitrogen under Non-uniform Electric Fields*. IEEE Transactions on Dielectrics and Electrical Insulation, 15 (3). pp. 626-634. ISSN 1070-9878
- (7) Wang, P., Lewin, P. L., Swaffield, D. J. and Chen, G. (2008) *Electric Field Effects on Boiling Heat Transfer of Liquid Nitrogen*. Cryogenics (submitted)

# References

- [1] "Superconductors history," in <http://www.superconductors.org/History.htm>.
- [2] C. H. Rosner, "Superconductivity: star technology for the 21st century," Applied Superconductivity, IEEE Transactions on, vol. 11, pp. 39-48, 2001.
- [3] "Highest T<sub>c</sub>," in [http://www.superconductors.org/150K\\_pat.htm](http://www.superconductors.org/150K_pat.htm).
- [4] J. Gerhold, "Cryogenic liquids - A prospective insulation basis for future power equipment," IEEE Transactions on Dielectrics and Electrical Insulation, vol. 9, pp. 68-74, 2002.
- [5] <http://www-safety.deas.harvard.edu/services/nitrogen.html>.
- [6] <http://en.wikipedia.org/wiki/Nitrogen>.
- [7] M. Hara and Z. C. Wang, "An analytical study of bubble motion in liquid nitrogen under DC nonuniform electric fields," presented at Proceedings of 4th International Conference on Properties and Applications of Dielectric Materials, Brisbane, Qld., Australia, vol. 2, pp. 459-462, 1994.
- [8] Y. Suda, M. Itoh, Y. Sakai, K. Matsuura, N. Honma, and T. Kimura, "Behaviour of liquid nitrogen between electrodes in a microgravity environment," Cryogenics, vol. 36, pp. 567-571, 1996.
- [9] H. Goshima, N. Hayakawa, M. Hikita, H. Okubo, and K. Uchida, "Area and volume effects on breakdown strength in liquid nitrogen," IEEE Transactions on Dielectrics and Electrical Insulation, vol. 2, pp. 376-384, 1995.
- [10] N. Hayakawa, H. Sakakibara, H. Goshima, M. Hikita, and H. Okubo, "Breakdown mechanism of liquid nitrogen viewed from area and volume effects," IEEE Transactions on Dielectrics and Electrical Insulation, vol. 4, pp. 127-134, 1997.
- [11] M. Hara, T. Kaneko, and K. Honda, "Thermal-bubble initiated breakdown characteristics of liquid helium and nitrogen at atmospheric pressure.," IEEE Transactions on Electrical Insulation, vol. 23, pp. 769-778, 1988.
- [12] J. Gerhold, "Properties of cryogenic insulants," Cryogenics, vol. 38, pp. 1063-1081, 1998.

- [13] J. R. Hull, "Applications of high-temperature superconductors in power technology," *Reports on Progress in Physics*, vol. 66, pp. 1865-1886, 2003.
- [14] O. Tsukamoto, "Ways for power applications of high temperature superconductors to go into the real world," *Superconductor Science and Technology*, vol. 17, pp. 185-190, 2004.
- [15] W. G. Garlick, "Power system applications of high temperature superconductors," *Cryogenics*, vol. 37, pp. 649-652, 1997.
- [16] M. Hara and J. Gerhold, "Electrical insulation specification and design method for superconducting power equipment," *Cryogenics*, vol. 38, pp. 1053-1061, 1998.
- [17] J. Gerhold, "Electrical insulation in superconducting power systems," *IEEE Electrical Insulation Magazine*, vol. 8, pp. 14-20, 1992.
- [18] M. Hara and H. Okubo, "Electrical insulation characteristics of superconducting power apparatus," *Cryogenics*, vol. 38, pp. 1083-1093, 1998.
- [19] A. Abeln, E. Klemt, and H. Reiss, "Stability considerations for design of a high temperature superconductor," *Cryogenics*, vol. 32, pp. 269-278, 1992.
- [20] J. Lehtonen, R. Mikkonen, and J. Paasi, "Stability considerations of a high-temperature superconductor tape at different operating temperatures," *Physica C: Superconductivity*, vol. 310, pp. 340-344, 1998.
- [21] K. C. Kao, "Deformation of Gas Bubbles and Liquid Drops in an Electrically Stressed Insulating Liquid," *Nature (London)*, vol. 208, pp. 279-280, 1965.
- [22] M. Hara, H. Nakagawa, T. Shinohara, and J. Suehiro, "Generation, growth and collapse of bubbles on collision of particle with electrode in DC electrically stressed liquid helium," *IEEE Transactions on Dielectrics and Electrical Insulation*, vol. 9, pp. 910-921, 2002.
- [23] M. Hara, J. Suehiro, H. Maeda, and H. Nakashima, "DC pre-breakdown phenomena and breakdown characteristics in the presence of conducting particles in liquid nitrogen," *IEEE Transactions on Dielectrics and Electrical Insulation*, vol. 9, pp. 23-30, 2002.
- [24] M. Hara, T. Kaneko, and K. Honda, "Electrical breakdown mechanism of liquid nitrogen in the presence of thermally induced bubbles," *Cryogenics*, vol. 27, pp. 93-101, 1987.

- [25] M. Hara, K. Honda, and T. Kaneko, "DC electrical breakdown of saturated liquid helium at 0.1 MPa in the presence of thermally induced bubbles," *Cryogenics*, vol. 27, pp. 567-576, 1987.
- [26] M. Hara, D. J. Kwak, and M. Kubuki, "Thermal bubble breakdown characteristics of LN<sub>2</sub> at 0.1 MPa under a.c. and impulse electric fields," *Cryogenics*, vol. 29, pp. 895-903, 1989.
- [27] M. Hara and M. Kubuki, "Effect of thermally induced bubbles on the electrical breakdown characteristics of liquid nitrogen," *IEE Proceedings, Part A: Physical Science, Measurement and Instrumentation, Management and Education, Reviews*, vol. 137, pp. 209-216, 1990.
- [28] M. Hara, H. Koishihara, and K. Saita, "Breakdown behavior of cryogenic liquids in the presence of thermal bubbles under ramped voltage," *IEEE Transactions on Electrical Insulation*, vol. 26, pp. 685-691, 1991.
- [29] U. E. Israelsson, H. W. Jackson, and D. Petrac, "Liquid/vapor phase separation in <sup>4</sup>He using electric fields.,," *Cryogenics*, vol. 28, pp. 120-125, 1988.
- [30] M. Hara, Z. C. Wang, and H. Saito, "Thermal bubble breakdown in liquid nitrogen under nonuniform fields," *IEEE Transactions on Dielectrics and Electrical Insulation*, vol. 1, pp. 709-715, 1994.
- [31] M. Hara, K. Takano, Z. C. Wang, H. Yoshizuka, and Y. Jiang, "Bubble motion and electrical breakdown in liquid helium under non-uniform fields," presented at 12th International Conference on Conduction and Breakdown in Dielectric Liquids, Roma, Italy, pp. 279-282, 1996.
- [32] K. Takano, S. Matsuura, J. Yan, J. Suehiro, and M. Hara, "Effect of a thin insulation film on thermal bubble-triggered breakdown phenomena in liquid nitrogen," *Electrical Engineering in Japan (English translation of Denki Gakkai Ronbunshi)*, vol. 127, pp. 18-28, 1999.
- [33] K. Takano, F. Shimokawa, and M. Hara, "Thermal bubble-triggered breakdown under DC, AC and impulse nonuniform electric fields in liquid nitrogen," presented at Proceedings of 11th International Symposium on High-Voltage Engineering, London, UK, vol. 3, pp. 128-131, 1999.

- [34] B. Y. Seok, N. Tamuro, and M. Hara, "A study of thermal bubble behavior in the simulated electrode system of HT superconducting coils," IEEE Transactions on Dielectrics and Electrical Insulation, vol. 6, pp. 109-116, 1999.
- [35] B. Y. Seok, H. Komatsu, J. Suehiro, and M. Hara, "Bubble behavior and PBD characteristics in the simulated electrode system of high temperature superconducting coils," presented at IEE Conference Publication Proceedings of the 11th International Symposium on High Voltage Engineering, London, UK, vol. 3, pp. 372-375, 1999.
- [36] B. Y. Seok, H. Komatsu, J. Suehiro, M. Hara, and H. Okamoto, "Partial and complete electrical breakdown in simulated high temperature superconducting coils," IEEE Transactions on Dielectrics and Electrical Insulation, vol. 7, pp. 78-86, 2000.
- [37] B. Y. Seok, H. Komatsu, M. Kushinaga, J. Suehiro, and M. Hara, "Pressurizing and sub-cooling effects on electrical breakdown of LN<sub>2</sub> in modeled HTS coils," IEEE Transactions on Dielectrics and Electrical Insulation, vol. 8, pp. 1016-1024, 2001.
- [38] P. Wang, D. J. Swaffield, P. L. Lewin, and G. Chen, "Thermal bubble dynamics in cryogenic liquids under non-uniform electric fields on superconducting power apparatus," presented at 2005 Annual Report Conference on Electrical Insulation and Dielectric Phenomena, Nashville, TN, USA, pp. 353-356, 2005.
- [39] G. S. H. Lock, Latent heat transfer : an introduction to fundamentals: Oxford university press, 1994.
- [40] A. Sakurai, M. Shiotsu, and K. Hata, "Boiling heat transfer characteristics for heat inputs with various increasing rates in liquid nitrogen," Cryogenics, vol. 32, pp. 421-429, 1992.
- [41] A. Sakurai, M. Shiotsu, and K. Hata, "Boiling phenomenon due to quasi-steadily and rapidly increasing heat inputs in LN<sub>2</sub> and LHe I," Cryogenics, vol. 36, pp. 189-196, 1996.
- [42] A. Sakurai, M. Shiotsu, K. Hata, and K. Fukuda, "Photographic study on transitions from non-boiling and nucleate boiling regime to film boiling due to increasing heat inputs in liquid nitrogen and water," Nuclear Engineering and Design, vol. 200, pp. 39-54, 2000.

- [43] L. Bewilogua, R. Kno[di]eresisner, and G. Wolf, "Heat transfer in boiling hydrogen, neon, nitrogen, and argon," *Cryogenics*, vol. 6, pp. 36-39, 1966.
- [44] P. Zhang, X. Ren, and R. Z. Wang, "Experimental investigation of the heat transfer characteristics of liquid nitrogen in the capillary tubes," *IEEE Transactions on Applied Superconductivity*, vol. 16, pp. 449-452, 2006.
- [45] K. Y. Yoon, D. K. Bae, H. Kang, M. C. Ahn, S.-J. Lee, H. M. Kim, Y. S. Yoon, and T. K. Ko, "Quench propagation characteristics of the liquid nitrogen cooled HTS wires by externally injected heat energy," *IEEE Transactions on Applied Superconductivity*, vol. 16, pp. 1015-1018, 2006.
- [46] Y. A. Kirichenko, S. M. Kozlov, K. V. Rusanov, and E. G. Tyurina, "Heat transfer crisis during liquid nitrogen cooling of high temperature superconductor," *Cryogenics*, vol. 31, pp. 979-984, 1991.
- [47] V. Drach and J. Fricke, "Transient heat transfer from smooth surfaces into liquid nitrogen," *Cryogenics*, vol. 36, pp. 263-269, 1996.
- [48] K. Nam, H. Kang, C. Lee, T. K. Ko, and B.-Y. Seok, "Visualization study on boiling of nitrogen during quench for fault current limiter applications," *IEEE Transactions on Applied Superconductivity*, vol. 16, pp. 727-730, 2006.
- [49] M. E. Bland, C. A. Bailey, and G. Davey, "Boiling from metal surfaces immersed in liquid nitrogen and liquid hydrogen," *Cryogenics*, vol. 13, pp. 651-657, 1973.
- [50] J. Mosqueira, O. Cabeza, M. X. Francois, C. Torron, and F. Vidal, "Measurements of pool boiling heat transfer from ceramic  $\text{Y}_1\text{Ba}_2\text{Cu}_3\text{O}_7$ -superconductors to liquid nitrogen," *Superconductor Science & Technology*, vol. 6, pp. 584-588, 1993.
- [51] V. I. Deev, K. V. Kutsenko, A. A. Lavrukhin, A. O. Komarov, and S. A. Voronkov, "Instability of heat transfer from HTSC-samples to liquid nitrogen," *Cryogenics*, vol. 38, pp. 715-719, 1998.
- [52] S. S. Ivanov and I. O. Shchegolev, "Boiling heat transfer to liquid nitrogen from structured surface with organic fibre net insulation in narrow channel," *Cryogenics*, vol. 38, pp. 707-713, 1998.
- [53] Y. Xiulin, X. Hongji, Z. Yuweng, and Q. Hongzhang, "Pool boiling heat transfer to liquid nitrogen from porous metallic coatings of tube bundles and

- experimental research of hysteresis phenomenon," *Cryogenics*, vol. 29, pp. 460-462, 1989.
- [54] A. Iwamoto, T. Mito, K. Takahata, N. Yanagi, and J. Yamamoto, "Dependence of heat transfer from a wide copper plate to liquid helium on heat transfer surface orientation and treatment," *Cryogenics*, vol. 36, pp. 139-143, 1996.
- [55] D. N. Sinha, L. C. Brodie, J. S. Semura, and F. M. Young, "Premature transition to stable film boiling initiated by power transients in liquid nitrogen," *Cryogenics*, vol. 19, pp. 225-230, 1979.
- [56] V. Drach, N. Sack, and J. Fricke, "Transient heat transfer from surfaces of defined roughness into liquid nitrogen," *International Journal of Heat and Mass Transfer*, vol. 39, pp. 1953-1961, 1996.
- [57] W. Bailey, E. A. Young, Y. Yang, and C. Beduz, "Boiling heat transfer to a liquid nitrogen pool from Ag sheathed BiPb2223 tapes carrying over-current," *Superconductor Science & Technology*, vol. 19, pp. 276-279, 2006.
- [58] F. Chovanec and P. Usak, "Instabilities above critical current region in Bi-2223/Ag superconducting coils cooled by liquid nitrogen," *Cryogenics*, vol. 42, pp. 543-546, 2002.
- [59] V. N. Skokov and V. P. Koverda, "Thermal multistability of thin YBCO films carrying direct current," *Cryogenics*, vol. 33, pp. 1072-1076, 1993.
- [60] R. J. Krane, J. R. Parsons, and A. Bar-Cohen, "Design of a candidate thermal control system for a cryogenically cooled computer," *IEEE Transactions on Components, Hybrids and Manufacturing Technology*, vol. 11, pp. 545-556, 1988.
- [61] E. G. Brentari and R. V. Smith, "Nucleate and film boiling design correlations for O<sub>2</sub>, N<sub>2</sub>, H<sub>2</sub>, and He," *Int. Advances in Cryogenic Engineering*, vol. 10, pp. 325-341, 1964.
- [62] C. W. Cowley, W. J. Timson, and J. A. Sawdye, "A Method for Improving Heat Transfer to a Boiling Fluid," *Ind. Eng. Chem. Proc. Des. Dev.*, vol. 1, pp. 81-84, 1962.
- [63] M. C. Duluc, M. X. Francois, and J. P. Brunet, "Liquid nitrogen boiling around a temperature controlled heated wire," *International Journal of Heat and Mass Transfer*, vol. 39, pp. 1758-1762, 1996.

- [64] M. C. Duluc and M. X. Francois, "Steady-state transition boiling on thin wires in liquid nitrogen. The role of Taylor wavelength," *Cryogenics*, vol. 38, pp. 631-638, 1998.
- [65] L. W. Chubb, "Improvements relating to methods and apparatus for heating liquids." UK patent No. 100796, 1916.
- [66] J. E. Bryan and J. Seyed-Yagoobi, "Electrohydrodynamically enhanced convective boiling: relationship between electrohydrodynamic pressure and momentum flux rate," *Transactions of the ASME. Journal of Heat Transfer*, vol. 122, pp. 266-277, 2000.
- [67] J. E. Bryan and J. Seyed-Yagoobi, "Influence of flow regime, heat flux, and mass flux on electrohydrodynamically enhanced convective boiling," *Journal of Heat Transfer*, vol. 123, pp. 355-367, 2001.
- [68] T. B. Jones, "Electrohydrodynamically enhanced heat transfer in liquids - A review," *Advances in heat transfer*, vol. 14, pp. 107-148, 1978.
- [69] P. H. G. Allen and T. G. Karayiannis, "Electrohydrodynamic enhancement of heat transfer and fluid flow," *Heat Recovery Systems and CHP*, vol. 15, pp. 389-423, 1995.
- [70] I. W. Eames and H. M. Sabir, "Potential benefits of electrohydrodynamic enhancement of two-phase heat transfer in the design of refrigeration systems," *Applied Thermal Engineering*, vol. 17, pp. 79-92, 1997.
- [71] S. Laohalertdecha, P. Naphon, and S. Wongwises, "A review of electrohydrodynamic enhancement of heat transfer," *Renewable and Sustainable Energy Reviews*, vol. 11, pp. 858-876, 2007.
- [72] H. Kawahira, Y. Kubo, T. Yokoyama, and J. Ogata, "The effect of an electric field on boiling heat transfer of refrigerant-11 - Boiling on a single tube," *IEEE Transactions on Industry Applications*, vol. 26, pp. 359-365, 1990.
- [73] S. D. Oh and H. Y. Kwak, "A Study of Bubble Behavior and Boiling Heat Transfer Enhancement under Electric Field," *Heat Transfer Engineering*, vol. 21, pp. 33-45, 2000.
- [74] M. C. Zaghdoudi and M. Lallemand, "Nucleate pool boiling under DC electric field," *Experimental Heat Transfer*, vol. 14, pp. 157-180, 2001.

- [75] M. C. Zaghdoudi and M. Lallemand, "Electric field effects on pool boiling," *Journal of Enhanced Heat Transfer*, vol. 9, pp. 187-208, 2002.
- [76] Y. C. Kweon and M. H. Kim, "Experimental study on nucleate boiling enhancement and bubble dynamic behavior in saturated pool boiling using a nonuniform dc electric field," *International Journal of Multiphase Flow*, vol. 26, pp. 1351-1368, 2000.
- [77] M. C. Zaghdoudi and M. Lallemand, "Study of the behaviour of a bubble in an electric field: steady shape and local fluid motion," *International Journal of Thermal Sciences*, vol. 39, pp. 39-52, 2000.
- [78] Y. C. Kweon, M. H. Kim, H. J. Cho, and I. S. Kang, "Study on the deformation and departure of a bubble attached to a wall in d.c./a.c. electric fields," *International Journal of Multiphase Flow*, vol. 24, pp. 145-162, 1998.
- [79] H. J. Cho, I. S. Kang, Y. C. Kweon, and M. H. Kim, "Study of the behavior of a bubble attached to a wall in a uniform electric field," *International Journal of Multiphase Flow*, vol. 22, pp. 909-922, 1996.
- [80] D. J. Swaffield, P. L. Lewin, G. Chen, and S. G. Swingler, "The influence of bubble dynamics in liquid nitrogen with applied electric fields on superconducting power apparatus," presented at The 13th International Symposium on High Voltage Engineering, pages CD-ROM 2003, Delft, Netherlands, 2003.
- [81] Y. Zhao, J. Lawler, P. Foroughi, and M. Ohadi, "Development of an electrohydrodynamic (EHD) micro pump for LN<sub>2</sub> spot cooling," presented at 2003 ASME International Mechanical Engineering Congress, Washington, DC, United States, pp. 113-118, 2003.
- [82] J. Darabi and H. Wang, "Development of an electrohydrodynamic injection micropump and its potential application in pumping fluids in cryogenic cooling systems," *Journal of Microelectromechanical Systems*, vol. 14, pp. 747-755, 2005.
- [83] J. Rutkowski, "The influence of electric field on heat transfer in boiling cryogenic liquid," *Cryogenics*, vol. 17, pp. 242-243, 1977.
- [84] J. Rutkowski, "The influence of electric field on heat transfer in a boiling cryogenic liquid," *Cryogenics*, vol. 20, pp. 75-78, 1980.

- [85] D. M. Pachosa and J. N. Chung, "Dielectrophoresis-driven nucleate boiling in a simulated microgravity environment," *Journal of Heat Transfer, Transactions ASME*, vol. 115, pp. 495-498, 1993.
- [86] W. Dong, R. Y. Li, H. L. Yu, and Y. Y. Yan, "An investigation of behaviours of a single bubble in a uniform electric field," *Experimental Thermal and Fluid Science*, vol. 30, pp. 579-586, 2006.
- [87] F. Chen, Y. Peng, Y. Z. Song, and M. Chen, "EHD behavior of nitrogen bubbles in DC electric fields," *Experimental Thermal and Fluid Science*, vol. 32, pp. 174-181, 2007.
- [88] L. Bochirol, E. Bonjour, and L. weil, "Exchanges thermiques-Etude de L' action de champs electriques sur les transferts de chaleur dans les liquides bouillants," *C. R. Hebd. Seances Acad. Sci.(Paris)*, vol. 250, 1960.
- [89] A. G. Zhorzholiani and I. G. Shekriladze, "Study of the effect of an electrostatic field on heat transfer with boiling dielectric fluids," *Heat Transfer - Soviet Research*, vol. 4, pp. 81-98, 1972.
- [90] H. A. Pohl, *Dielectrophoresis-The Behavior of Neutral Matter in Nonuniform Electric Field*. Cambridge, New York: Cambridge University Press, Ch.4, 1978.
- [91] J. Ogata and A. Yabe, "Augmentation of boiling heat transfer by utilizing the EHD effect - EHD behaviour of boiling bubbles and heat transfer characteristics," *International Journal of Heat and Mass Transfer*, vol. 36, pp. 783-791, 1993.
- [92] J. Ogata and A. Yabe, "Basic study on the enhancement of nucleate boiling heat transfer by applying electric fields," *International Journal of Heat and Mass Transfer*, vol. 36, pp. 775-782, 1993.
- [93] T. G. Karayiannis, "EHD boiling heat transfer enhancement of R123 and R11 on a tube bundle," *Applied Thermal Engineering*, vol. 18, pp. 809-817, 1998.
- [94] X. Huang, R. Y. Li, and H. L. Yu, "Enhancement of boiling heat transfer for R11 and R123 by appling uniform electric field," *Journal of Enhanced Heat Transfer*, vol. 11, pp. 299-306, 2004.
- [95] Y. Liu, R. Li, F. Wang, and H. Yu, "The effect of electrode polarity on EHD enhancement of boiling heat transfer in a vertical tube," *Experimental Thermal and Fluid Science*, vol. 29, pp. 601-608, 2005.

- [96] M. C. Zaghdoudi and M. Lallemand, "Analysis of the polarity influence on nucleate pool boiling under a DC electric field," *Transactions of the ASME. Journal of Heat Transfer*, vol. 12, pp. 856-864, 1999.
- [97] R. J. Turnbull, "Electroconvective Instability with a Stabilizing Temperature Gradient. I. Theory," *Physics of Fluids*, vol. 11, pp. 2588-2596, 1968.
- [98] P. Cooper, "EHD enhancement of nucleate boiling," *Transactions of the ASME. Journal of Heat Transfer*, vol. 112, pp. 458-464, 1990.
- [99] V. Penev, V. S. Krylov, C. Boyadjiev, and V. P. Vorotilin, "Wavy flow of thin liquid films," *International Journal of Heat and Mass Transfer*, vol. 15, pp. 1395-1406, 1972.
- [100] M. Markels and R. L. Durfee, "The effect of applied voltage on boiling heat transfer," *AIChE Journal*, vol. 10, pp. 106-110, 1964.
- [101] Y. Suda, K. Mutoh, Y. Sakai, K. Matsuura, and N. Honma, "Bubble motion in liquid nitrogen between electrodes in a microgravity environment," presented at 12th International Conference on Conduction and Breakdown in Dielectric Liquids, Roma, Italy, pp. 144-147, 1996.
- [102] T. B. Jones and G. W. Bliss, "Bubble dielectrophoresis," *Journal of Applied Physics*, vol. 48, pp. 1412-1417, 1977.
- [103] V. I. Boyarintsev, S. F. Kuznetsov, P. E. Molotov, and Y. V. Parinov, "Investigation of the EHD effect in liquid nitrogen," *Journal of Engineering Physics and Thermophysics*, vol. 63, pp. 959-964, 1992.
- [104] D. J. Swaffield, P. L. Lewin, G. Chen, and J. K. Sykulski, "Cryogenic dielectrics and HTS power apparatus: Research at the University of Southampton," *IEEE Electrical Insulation Magazine*, vol. 22, pp. 29-37, 2006.
- [105] D. J. Swaffield, "Effect of liquid nitrogen bubble dynamics on insulation performance for high temperature superconducting power apparatus." PhD Thesis: University of Southampton, 2005.
- [106] H. Ackermann, L. Bewilogua, and H. Vinzelberg, "Bubble boiling from heated surfaces of different material in liquid nitrogen," *Cryogenics*, vol. 15, pp. 677-678, 1975.
- [107] P. Di Marco and W. Grassi, "Saturated pool boiling enhancement by means of an electric field," *Journal of Enhanced Heat Transfer*, vol. 1, pp. 99-114, 1993.

- [108] D. J. Swaffield, P. L. Lewin, G. Chen, and S. G. Swingler, "Variable pressure and temperature liquid nitrogen cryostat for optical measurements with applied electric fields," *Measurement Science and Technology*, vol. 15, pp. 2325-2332, 2004.
- [109] D. J. Swaffield, P. L. Lewin, Y. Tian, G. Chen, and S. G. Swingler, "Characterisation of partial discharge behaviour in liquid nitrogen," presented at 2004 IEEE International Symposium on Electrical Insulation, Indianapolis, USA, pp. 135-138, 2004.
- [110] D. J. Swaffield, P. L. Lewin, Y. Tian, G. Chen, and S. G. Swingler, "Partial discharge characterisation in liquid nitrogen composite systems," presented at 2005 IEEE International Conference on Dielectric Liquids, Coimbra, Portugal, pp. 139-142, 2005.
- [111] D. J. Swaffield, P. L. Lewin, Y. Tian, G. Chen, and S. G. Swingler, "Characterisation of surface partial discharge behaviour in liquid nitrogen," presented at 2005 IEEE International Conference on Dielectric Liquids, Coimbra, Portugal, pp.143-146, 2005.
- [112] P. Wang, D. J. Swaffield, P. L. Lewin, and G. Chen, "Thermal bubble motion in liquid nitrogen under non-uniform electric fields," *IEEE Transactions on Dielectrics and Electrical Insulation*, vol. 15, pp. 626-634, 2008.
- [113] D. J. Swaffield, P. L. Lewin, G. Chen, and S. G. Swingler, "Partial discharge characterization of streamers in liquid nitrogen under applied AC voltages," *IEEE Transactions on Dielectrics and Electrical Insulation*, vol. 15, pp. 635-646, 2008.
- [114] S. J. Kline and F. A. McClintock, "Describing Uncertainties in Single Sample Experiments," *Mech.Eng.(Am.soc.Mech.Eng.)*, vol. 75, pp. 3-8, 1953.
- [115] D. P. Rini, R. H. Chen, and L. C. Chow, "Bubble behavior and heat transfer mechanism in FC-72 pool boiling," *Experimental Heat Transfer*, vol. 14, pp. 27-44, 2001.
- [116] A. Sakurai, "Mechanisms of transitions to film boiling at CHFs in subcooled and pressurized liquids due to steady and increasing heat inputs," *Nuclear Engineering and Design*, vol. 197, pp. 301-356, 2000.

- [117] M. Ohadi, J. Darabi, and B. Roget, "Electrode design, fabrication, and materials science for EHD-enhanced heat and mass transport," *Annual Reviews of Heat Transfer*, vol. 11, pp. 563-632, 2000.
- [118] B. Fallou, J. C. Bobo, E. Carvounas, and Z. Croitoru, "Insulation components for high voltage cryoelectric equipment," *American Machinist*, vol. 1, pp. 1-17, 1974.
- [119] P. P. Benham, R. J. Crawford, and C. G. Armstrong, *Mechanics of Engineering Materials* (2nd ed.), 1996.